Design and Characterisation of a Scale-Down Platform for the Recovery of Periplasmic Fab' From *E.coli*

Asma Ahmad

A thesis submitted for the degree of
Engineering Doctorate

The Advanced Centre for Biochemical Engineering
Department of Biochemical Engineering
University College London

UCL ENGINEERING
Change the world

I, Asma Ahmad, confirm that the work presented in this thesis is my own.
Where information has been derived from other sources, I confirm that this has been indicated in the thesis.

Abstract

The need to speed up bioprocessing and to enhance process understanding of the heat extraction process, for the recovery of periplasmic Fab' from *E.coli* cells, has led to the development of two workable scale-down models that are capable of predicting the performance of the lab scale and pilot scale process. In this work, a design of experiment (DoE) study was initially conducted at the 2L scale to identify the effect of key parameters such as heating duration (6-14 hours), heating temperature (55-65°C) and specific power input (0.05-0.41W L^{-1}) on the heat extraction process. The results showed that extraction temperature and duration had the most impact on the process whereas specific power input had no significant impact in the range studied. Fluid dynamic studies were conducted on the 2L vessel, and on a scale-down 20mL vessel and shaken 24-well deep square-well (DSW) plate, in order to assess mixing performance under various operating conditions. Mixing time studies were performed on all three models using the dual indicator system for mixing time (DISMT). The mixing time curves between the 2L and 20mL vessel were well matched over the same range of specific power input values and the results showed that mixing time stayed relatively constant for both scales above a specific power input value of 0.05W L^{-1}. Particle image velocimetry (PIV) experiments were also conducted on the 20mL vessel in order to visualise flow patterns and analyse fluid velocity. The data indicated that flow patterns were fully formed at 300rpm (9×10^{-4}W L^{-1}) and that velocity stabilised after 0.05W L^{-1}. Mixing time studies in the DSW plate showed that turbulent mixing was achieved above 500rpm. Process verification studies were performed between the two scale-down models and the 2L vessel, and the performance was compared using Fab' titre, total protein concentration, dsDNA concentration, HCP profiles and Fab' profiles. The results demonstrated that both models were capable of correctly mimicking the performance in the 2L vessel for a variety of different experimental conditions, using feed material from different batches and using different *E.coli* strains and Fab' types, provided that the heating profiles were matched and there was sufficient turbulent mixing at all scales. The results also agreed with data from the DoE and fluid dynamic studies, thus establishing the 20mL vessel and 24-well DSW plate as two feasible scale-down models for the periplasmic heat extraction process.

Impact Statement

The results obtained, from the work undertaken in this research project, may be used for informing decisions made by the sponsor company, UCB, when considering scale-down tools for their heat extraction process. The use of the microwell plate system, in particular, may be developed further to conduct experiments at the millilitre scale, in a high-throughput manner, thus reducing costs and improving process development timelines. The most advanced fluid dynamic techniques have been used to obtain characterisation information regarding the hydrodynamics in a miniature stirred and shaken system. This data can be used for modelling or to decide whether these systems would be feasible scale-down models for a variety of other processes before being used. By understanding the engineering and mixing environment in a system, ideal conditions can be selected to improve mixing and to significantly improve scaling.

The research has been presented in multiple national and international conferences, both in poster presentation and oral presentation formats, to hundreds of delegates over the course of the last 5 years, thus raising the profile of the sponsor company and the work that they do. Additionally the applicability of the fluid dynamic techniques to a number of emerging fields in the bioprocessing industry such as cell and gene therapy, means that further collaborations may be made between industry, who have the process knowledge, and academia, who have the engineering knowledge. More collaborations and sponsorships means that more students can have the opportunity to undertake further research in order to advance this area of science which will ultimately help improve the timelines for drug development. Additionally, through the efforts of the researcher, this work has been presented at a number of schools, fairs and events in order to inspire younger people to pursue Science and Engineering. During this EngD, two students were also taken for their masters research project, both of whom were inspired by the work and subsequently decided to pursue PhDs within this field.

Acknowledgements

I would like to thank a number of people who have provided me with the support, guidance and encouragement and without whom I would not have been able to complete this EngD. First and foremost, I would like to express my gratitude to Dr. Martina Micheletti, not only for her warmth, enthusiasm and constant supervision, but also for patiently helping me get through each stage of my research project during the difficult times. I would also like to thank my industrial supervisors, Dr. Geoff Brown and Dr. Richard Davies, for their unwavering support and for providing me with their expert knowledge and experience on the practical elements of the work. Additionally, my advisor, Prof. Eli Keshavarz-Moore, has been incredibly helpful whenever I have needed her assistance. I will always be grateful for every conversation I had with her during my time as an EngD researcher.

Having spent a third of my life in the Biochemical Engineering department at UCL, I can honestly say that I feel like it has been my second home. I have met some incredible people along this journey and I would like to thank each one for their time, laughter and friendship during my research; starting of course with Greg, for helping me through all the fluid dynamic studies in this work, and to Fatumina, for the hundreds of shared happy memories and for just being the most ridiculous, craziest girl I have ever met in my life! I would also like to thank the following people, including my new and old office colleagues, for all the fun times; Fernanda, Helmi, Dave, Lara, Roberto, Joe, Sarah, Mike, Thibault, Rachel, Carlotta, Nehal, Damiano and last but by no means least, Mike Sulu, for being an all round superstar! A huge thanks also goes to the whole upstream team at UCB, for making me feel so welcome and for helping me in the labs during experiments, particularly Jaroslava, Florian, Elena, Lenny, Raha, Camille and Zoe.

Finally, I would like to wholeheartedly thank Mel and Choby for being my absolute rocks, and my family; Anas, Nosheen, Shamyla and of course my Ami and Abu, for their unconditional love.

Table of Contents

Nomenclature

BOX	Bis(1,3-dibarbituric acid)-trimethine oxanol
CFD	Computational fluid dynamic
CPP	Critical process parameter
CQA	Critical quality attribute
DCW	Dry cell weight
DI	Deionised
DO	Dissolved oxygen
DSP	Downstream processing
DSW	Deep square-well
DoE	Design of experiment
E.*coli*	Escherichia coli
EDTA	Ethylenediaminetetraacetic acid
EMA	European medicines agency
Fab'	Antigen-binding fragment
FACS	Fluorescence assisted cell sorting
FDA	Food and Drug Administration
HCl	Hydrochloric acid
HCP	Host cell protein
HPLC	High performance liquid chromatography
IPTG	Isopropyl β-D-1-thiogalactopyranoside
kDa	Kilodaltons
LDA	Laser Doppler anemometry
LED	Light emitting diode

LPS	Lipopolysaccharide
MAb	Monoclonal antibodies
MFCS	Multi fermenter control system
OD	Optical density
ODf	Optical density of feed sample
ODs	Optical density of light phase sample
ODw	Optical density of well spun sample
OmpA	Outer membrane protein A
PE	Post extraction
PAP	Post acid precipitation
PBS	Phosphate buffered saline
PEG	Polyethylene glycol
PI	Propidium iodide
PIV	Particle image velocimetry
PLS	Partial least square
PPG	Polypropylene glycol
PrL	Protein L
PSD	Particle size distribution
PTM	Post translational modification
QbD	Quality by design
RGB	Red green blue
TNF	tumour necrosis factor
SDS-PAGE	Sodium dodecyl sulfate- polyacrylamide gel electrophoresis
SEM	Scanning electron microscopy
WCW	Wet cell weight

B_W	Baffle width
Di_{2L}	2L impeller diameter
Di_{20mL}	20mL impeller diameter
D_v	Internal vessel diameter
D_i	Impeller diameter
Fr	Froude number
H*	Maximum liquid height
H_L	Still liquid height
K_La	Volumetric mass transfer coefficient
N_{crit}	Critical shaking speed
N_{tm}	Dimensionless mixing time
P/V	Specific power input
P_g/V	Specific gassed power input
Ph	Phase number
Re	Reynolds number
rpm	Rotation per minute
t_m	Mixing time
V_{tip}	Impeller tip speed
ρ	Density
μ	Viscocity
μ_{max}	Maximum specific growth rate

List of Tables

List of Figures

Chapter 1

Introduction

1.1 Background

There have been great advancements in the biopharmaceutical industry since the 1970s, none more so than in perhaps the recombinant DNA technology sector. It is now possible to treat a number of diseases, by expressing a human gene that codes for a missing or defective protein in the human body, in a simple microorganism. This product can then be purified and given to a patient. A few decades ago, it would have been impossible to conceive the idea that microbial or mammalian cells could be used to produce fully functional proteins for therapeutic uses. When human insulin was first approved in 1982 by Eli Lilly (Birch and Onakunle 2000), it was considered no less than a miracle by the entire scientific community. Insulin no longer needed to be taken from the pancreas of pigs as it could be produced synthetically instead in bacterial cells using the cells own genetic system by transcribing human DNA. Continuous developments in science and manufacturing have made it possible to produce large quantities of this biotherapeutic in a short space of time, making the product significantly purer, cheaper and more efficacious. This protein product also lacked the side effects which were present in proteins originally sourced from natural sources (Birch and Onakunle 2000). The total number of recombinant biotherapeutics licensed in the USA and the EU by 2014 totalled 246 (Walsh 2014).

The discovery of human insulin opened the doors to a variety of other therapeutic proteins produced using recombinant technology. With the major breakthrough in decoding the human genome in 2003, the race to finding new therapeutic candidates was on, with a greater number of candidates being targeted for drug development. Depending on the size and complexity of the desired therapeutic molecule, different types of cells were used as an expression host. Monoclonal antibodies (mAbs), used to treat patients suffering from infectious diseases, immune disorders and cancer, for example, is a relatively large and

complex recombinant protein and therefore is typically expressed in mammalian cells because they have the necessary machinery to produce this protein. Small simple proteins, such as growth hormones or a fragment antigen-binding (Fab') that does not require post translation modifications can be expressed in microbial cells such as bacterial or yeast cells. Microbial cells have several advantages over alternative mammalian expression systems such as ease of gene manipulation, lower cost of goods, ease of fermentation and extensive regulatory experience for the expression of therapeutic protein products (Berlec and Strukelj 2013). These advantages make this expression system highly favourable in industry. In fact, about 30% of all recombinant protein products on the market were produced in *Escherichia coli* (*E.coli*) due their relatively high product titres (Huang *et al*., 2012).

Regardless of the therapeutic or the manufacturing process that is used to produce it, there is an ever increasing demand for greater volumes of the product due to an increasing and ageing population. This has put continuous pressure on companies to improve the process development and manufacturing aspect of drug development and to reduce timelines. An increase in the number of candidates in the product pipeline and a push by the FDA to use a quality by design (QbD) approach, for enhanced process knowledge, has acted as a driving factor for companies to invest in high-throughput technologies (Tai *et al*., 2014; Bhambure *et al*., 2011). The cost of research and development in Europe has almost doubled since the mid-90s and it is estimated that to bring a new biopharmaceutical product to market, it can take between 10 to 15 years, costing over €1 billion (European Commission 2009). The cost of producing a biopharmaceutical product can be 20 times greater than that of producing a traditional chemical (Walsh 2014) therefore it is important to improve the efficiency of processes in order to bring down these expenses. One of the main challenges associated with drug development is to find ways in which the process can be optimised as quickly as possible so that by the time a potential candidate is ready to go into clinical trials or ready to be manufactured, the process development work has already caught up to allow the therapeutic to be manufactured robustly, at a suitable scale, and in a cost-effective and reproducible manner, thus maximising on the patent life time.

Despite the costs and risks associated with developing a new drug product, there has been an increase in global biopharmaceutical sales from US $12 billion to US $30 billion between the years of 2000 and 2003 (Walsh 2000). By 2009, the sales of all global biopharmaceutical products totalled $99 billion (Walsh 2010), and by 2013, this value had reached $140 billion (Walsh 2014). One particularly lucrative area of the market is surrounding the treatment of autoimmune diseases, such as Crohn's disease and rheumatoid arthritis where the global market for therapeutics to treat these diseases is over $16 billion combined (Walsh 2010). There are therefore a number of companies that have focused on capturing this market and a variety of mAb based products have now been licenced for the treatment of these diseases (Walsh 2014).

1.2 Antibody Fragments

There has been a wave of new Fab' antibodies that have shown clinical promise for the treatment of a variety of indications, as an alternative to the traditional mAb product. The Food and Drug Administration (FDA) and European Medicines Agency (EMA) have both already approved three Fab' products for clot prevention, treatment of neovascular age-related macular degeneration and treatment of rheumatoid arthritis under the names of Reopro (abciximab), Lucentis® (ranibizumab) and Cimzia® (certolizumab pegol), respectively (Yoon *et al*., 2012). A Fab' based product called LeukoScan (sulesomab) has also been approved for use as a diagnostic tool.

The Fab' is the variable functioning part of a mAb that consists of one heavy chain and one light chain linked by a disulphide bond. It has just one binding site which allows it to bind very specifically with the target antigen, thus neutralising and suppressing its activity. The key advantage of producing a Fab' product is that it is able to maintain the high degree of specificity and selectivity of the whole mAb, whilst offering the benefit of production in a cheaper and faster manufacturing process (Nelson 2010). Cimzia® is currently the only PEGylated Fab' product on the market (Goel and Stephens 2010). This humanised Fab' is conjugated via a maleimide group to a polyethylene glycol (PEG) molecule to prevent the proteolytical degradation of the protein. The PEG essentially increases the half-life of the

Fab' by up to 80% (Andersen and Reilly 2004) as well as improving solubility, reducing immunogenicity and decreasing the rate of clearance from the body when administered into a patient (Walsh 2010). The molecular mass of the Fab' on its own is 49.5kDa but when it is attached to the PEG moiety as the final product, it is 90.5kDa (Therapeutic Goods Administration 2010). The fully formulated product is administered subcutaneously via injection to patients that suffer from rheumatoid arthritis.

Rheumatoid arthritis is a chronic inflammatory disease which occurs in roughly 1% of the global population (European Medicines Agency 2009). In patients who have this disease, human tumour necrosis factor (TNF-α) is over produced, which leads to synovial inflammation of the joints and ultimately in articular cartilage and bone degradation. Cimzia®, the Fab' product, is a TNF-α inhibitor that binds to the TNF-α in the body, thus suppressing its response and alleviating the symptoms of the disease. So far, Cimzia® has had strong commercial success, however increasing competition in the marketplace for the treatment of this disease has meant that more attention has been focused on improving process development and optimising the manufacturing process.

1.3 Fab' Production and Primary Recovery

The unique properties of the Fab' molecule, including its relatively simple structure and small size, has allowed it to be produced in the periplasm of *E.coli* cells. An outer membrane protein A (OmpA) is expressed with the Fab' to help direct it to the periplasmic space between the two cell walls. The oxidising environment in the periplasm facilitates correct Fab' folding and disulphide bond formation (Rouet *et al*., 2012). The periplasmic space also has less protease activity compared to the cytoplasm, because it only contains 7 of the 25 proteases that are typically found within an *E.coli* cell (Balasundaram *et al*., 2009) and protein aggregation and production of inclusion bodies is also prevented (Lee *et al*., 2005).

There have been a number of studies related to the production, capture and purification of the A33 Fab', expressed in the industrial *E.coli* strain W3110 (Ali *et al*., 2011; Barata *et al*., 2016; Humphries *et al*., 1996; Li *et al*., 2012; Li *et al*., 2013; Newton *et al*., 2016; Perez-Pardo

et al., 2011; Rayat *et al*., 2010; Tustian *et al*., 2007). For this particular strain, the lac promotor (lactose promotor-repressor-operator) system regulates the level of Fab' produced. To induce the production of Fab' a fragment, Isopropyl-β-D-1-thiogalactopyranoside (IPTG) is used. After the fermentation process is complete, the material is harvested, typically using centrifugation, and a method is selected for product release. A typical method used to release intracellular proteins at industrial scale is high pressure homogenisation or bead mills. Although these are effective for intracellular protein release, there are some significant drawbacks of using them for Fab' release. This includes an increase in viscosity, due to the release of host cell proteins and DNA, and also enhanced cell micronisation which makes subsequent filtration and centrifugation steps more challenging. Additionally, these mechanic techniques release cytoplasmic proteases which can cause degradation of the periplasmic Fab' due to proteolytic attack. One significant advantage of directing the Fab' into the periplasmic space is that, after fermentation is complete, it can be selectively released from the cell by removing just the outer membrane of the cell instead of using harsh mechanical disruption.

Heat extraction is a scalable process that removes the outer cell membrane by mixing the cells, at high temperatures, with tris and ethylene-diamine-tetra-acetic acid (EDTA) to release the Fab' from the periplasmic space. The cell wall of *E.coli* cells consists of an outer membrane and an inner membrane with space in between called the periplasmic space. This contains a cross linked peptidoglycan layer that provides rigidity to the cell wall. The outer membrane is made of a lipid bilayer which contains transmembrane proteins, phospholipids and lipopolysaccharide (LPS). The LPS molecules are non-covalently bound to divalent cations such as Mg^{2+} and Ca^{2+} and also to the peptidoglycan layer within the periplasmic space (Middelberg 1995). EDTA, which is a chelating agent, works by uncovering the mucopolypeptide layer either by removal of interfering ions such as magnesium, manganese and calcium or by changing the surface charge or configuration of the layer thus increasing membrane permeability (Goldschmidt and Wyss 1967) however it does not have any impact on the inner cell membrane. Tsuchido *et al*. (1985) found that when cells were heated to 55°C in a tris-hydrochloride buffer at pH 8.0, intracellular proteins were leaked from the cells. Middelberg (1995) also showed that thermochemical disruption of the cell

wall was achieved using temperatures of 50-55°C in the presence of EDTA in tris. An invention by Weir and Bailey (1997) showed that exposing *E.coli* cells to elevated temperatures between 34-60°C, for 10-18 hours, can help extract Fab'. Sehdev and Spitali (2006) published an invention regarding methods to increase the yield of Fab' during fermentation and to recover it using heat extraction. The data showed that agitating the cell suspension for up to 24 hours in tris and EDTA, at temperatures up to a maximum of 70°C, caused the yield of the functional Fab' to improve. At the elevated temperatures, the correctly folded Fab' fragment stayed stable whereas some of the other heat sensitive host cell proteins and Fab' fragments, such as free light and heavy chains aggregated together or formed precipitates. Thermal stability data, obtained by Millipore (2015), showed that when Fab' was exposed to 60°C for 5 hours, there was approximately a 15% reduction of titre in the first 15 minutes after which the Fab' titre became constant. This indicated that the loss in Fab' may have represented the incorrectly folded Fab' only and that the correctly folded Fab' was not affected by the elevated temperatures. These studies all demonstrate that it is possible to expose the cells to high temperatures, to release Fab' and to help improve the separation of the Fab' protein from other impurities, whilst retaining the integrity of the target product.

Once the Fab' has been released using heat extraction, an acid precipitation step can be used to precipitate out negatively charged impurities such as DNA, cell debris and some host cell proteins (Westoby *et al*., 2011). Under low pH conditions, DNA precipitates out as it is complexed with chromatin and some proteins precipitate out due to their low solubility in acidic solution (Roush and Lu 2008). Additionally, DNA, which has polyanionic charge characteristics, naturally binds to proteins of the opposite charge, thus causing a formation of a protein-nucleic acid complex (Singh *et al*., 2013) which also precipitates out. Lydersen *et al*. (1994) used a variety of acids, including phosphoric, sulphuric, citric and acetic acid, to precipitate out antibody producing hybridoma cells between a pH of 6.0 and 4.5. Acetic acid, which has a pKa of 4.7, was the preferred choice for acid precipitation compared to other acids. DNA was reduced from 20µg/mL to 1µg/mL and host cell proteins were also precipitated out, leaving the antibody as the predominant high molecular weight molecule in solution. The antibody activity was unaffected above pH 3.8 and the quality of the antibody, as observed using isoelectric focusing gels and hydrophobic interaction

chromatography, was also not affected. This acid precipitation process can also be applied to *E.coli* cells. Millipore (2015) used hydrochloric acid to adjust the pH of heat extracted *E.coli* cells to 4.5 and found that this step significantly reduced the relative total protein levels whilst preventing the loss of the Fab' product. Adjusting the pH of the cell mixture after the heat extraction step therefore aggregates different components of the cell which makes subsequent downstream processing (DSP) steps such as centrifugation, filtration and chromatography significantly easier and thus less expensive as well (Rayat 2011).

1.4 Scale-Up and Scale-Down

Process development and manufacturing costs can represent 40–60% of all development costs and can even equal or exceed clinical trial costs. The manufacturing costs alone typically represent up to 25% of the sales (Rosenberg 2000). Significant work has been done to improve Fab' titres during fermentation (Sehdev and Spitali 2006) which has lowered upstream costs, however, this has created a bottleneck at the primary recovery and downstream process stage therefore the cost of DSP in comparison to the total cost of Fab' production has increased. DSP costs typically contribute to 80% of the total manufacturing costs (Walsh 2010). It is therefore of utmost importance that the primary recovery stage for the Fab' protein is optimised in order to release the maximum amount of product and minimum amount of other intracellular components.

To reduce the research development work in this area, a high-throughput, scale-down approach is needed, which can screen and optimise extraction conditions quickly, and then translated to the pilot and manufacturing scale. There are a number of scale-down models, both stirred and shaken, which can potentially be used to mimic the large scale heat extraction and acid precipitation process. Miniature stirred tank vessels consume considerably less quantities of raw materials and if multiple vessels are set up and controlled by one controller they also have the advantage of being able to work in parallel and can therefore be considered as a high-throughput system (Weuster-Botz 2005). Gill *et al*. (2008a) described the design of a 100mL miniature stirred bioreactor system which enabled automated parallel operation of 4-16 microbial fermentations controlled using a

custom piece of PC based software. Shaken deep well microplates are also typically used as scale-down tools for achieving high throughput. They are typically designed for use with absorbance, fluorescence, or luminescence testing and their small size, flexibility and capability to be automated using robotic systems has made them favourable for use as scale-down models for the stirred tank vessel (Fernandes and Cabral 2006).

Efforts to move towards miniaturisation and parallelisation during process development means working with small volumes which inherently makes the experiments more prone to human error. Small differences in process handling and sampling can therefore result in error accumulations. It is therefore highly desirable to not only develop accurate small scale models, but to work towards automation of these systems where possible too, to minimise human error.

The heat extraction and acid precipitation process are both mixing dependent processes, performed in industrial scale stirred tank vessels, which may be scaled using bioprocess engineering principles. The best method to use for scaling depends on the process characteristics and on the critical factors, which control the reaction on a molecular scale, for that particular process. The choice of scaling also depends on whether the process is scaled between stirred systems or between stirred and shaken systems. When scaling down from a large scale stirred tank vessel to a miniature stirred tank vessel, it is important to use a geometrically similar vessel and impeller system, and to maintain key ratios such as aspect ratio, impeller diameter to tank diameter ratio and impeller positioning. The most common methods, for scaling a mixing related process, are specific power input (P/V), impeller tip speed and mixing time. For scaling of a fermentation process, the volumetric mass transfer coefficient (k_La) is also a popular choice however as the heat extraction process does not require oxygen sparging, this parameter cannot be used for scaling of this process. Specific power input determines the energy flow transferred from the impeller to the liquid which is why it is the most recommended scaling parameter to choose if mixing and dispersion at turbulent conditions is required (Wernersson and Tragard 1999). When working with shear sensitive material, maintaining the impeller tip speed becomes more important. Mixing time is a measure of combined convective and turbulent distribution within a vessel so if a fast dilution reaction is needed, the circulation time or mixing time may need to be kept

constant (Wernersson and Tragard 1999). Some dimensionless numbers such as Reynolds (Re) number may also be used as a basis of scaling but often the results require unrealistic equipment and operating parameters which is why it is rarely used (Marques 2010).

When scaling down from a stirred system into a shaken system, the task for choosing an appropriate scaling parameter is still a challenge due to fundamental differences in heat transfer, mass transfer, mixing, specific power input and shear (Marques 2010). Mixing in microwell plates is usually achieved by pipette aspiration, magnetically agitated stirrer bars or by orbital shakers (Betts and Baganz 2006). Although there have been a number of studies that have attempted to scale-down a fermentation process into miniature vessels and into shaken plates using k_La and specific power input, there have been limited studies attempting to scale-down the periplasmic heat extraction process into such models. The principles for scale-down using specific power input however may be applicable to this process and therefore relevant studies have been summarised in this chapter.

1.4.1 Scale-Down into Miniature Vessels

Ali *et al*. (2011) scaled down a 20L *E.coli* fermentation process, for Fab' production, into a 25mL miniature stirred tank vessel. The vessel used three 6-bladed paddle impellers with the impeller diameter approximately one third of the tank diameter. The distance between impellers and the impeller clearance was close to 1 impeller diameter. The miniature vessel was characterised, in terms of specific gassed power input (P_g/V), K_La and hydrodynamic conditions, and P_g/V was chosen as the most appropriate parameter for scaling. A power number of 5.7 was assumed for each Rushton impeller in the 20L vessel and the calculated power number for each paddle impeller in the 25mL vessel was 1, during turbulent flow. The growth profiles during fermentation between the two vessels were comparable and the final dry cell weight was 39.2g L^{-1} and 38.9g L^{-1} for the 25mL vessel and the 20L vessel respectively. The total yield obtained in the 25mL and 20L vessel was 943µg mL^{-1} and 990µg mL^{-1}, respectively. Fab' concentration in cell free suspension was found to be similar as well for both fermenters at around 450µg mL^{-1}. The overall results from the study showed that the 25mL vessel was capable of mimicking the 20L fermentation process based on specific power input.

Lamping *et al*. (2003) investigated the use of a 10mL Plexiglas miniature bioreactor as a scale-down model of a 20L bioreactor, for a batch fermentation process using *E.coli* DH5α cells. The miniature bioreactor had a diameter of 16mm, equal to a 24-well microwell plate, and three 6-bladed flat-turbine impellers with a diameter of almost half of the tank diameter. The impeller spacing and clearance was 1 impeller diameter. Power input measurements were difficult to obtain due to the small size of the bioreactor however computational fluid dynamics (CFD) was used to predict the power number of the impellers in both vessel. This value was 4.0 for the miniature turbine impeller and 6.0 for the Rushton impeller in the 20L bioreactor, during turbulent flow. The 10mL bioreactor was agitated and aerated so that it could mimic the flow conditions of the 20L bioreactor. The k_La was measured during the *E.coli* fermentation and was found to be comparable to the large scale bioreactor.

Betts *et al*. (2006) carried out further characterisation work on this miniature bioreactor and used it to scale up to a 7L bioreactor for an *E.coli* fermentation process, using matching P_g/V. The impellers in this paper are referred to as paddle impellers instead of flat-turbine impellers, as mentioned by Lamping *et al*. (2003), but the images from the two papers show that they are likely to be the same vessel and impeller system. Betts *et al*. (2006) measured the power number of the paddle impeller using a motion controller, under turbulent conditions, and obtained a value of 0.7 for each impeller. They assumed a power number of 5.0 for the Rushton impellers in the 7L bioreactor. A suggestion for why the power number of the paddle impeller was particularly low was due to the higher impeller thickness to impeller diameter ratio. This was found to be 0.115 in the miniature system and 0.027 for the 7L system. Additionally, the blade depth to impeller diameter ratio was lower, at 0.14, in the miniature system compared to 0.2 in the 7L system.

Mununga *et al*. (2003) found that a lower relative blade depth was responsible for a reduced power number. They found that thicker impellers reduced the amount of fluid between the blades thus reducing the work required to move the impeller. Rutherford *et al*. (1996b) suggested that high relative impeller thickness resulted in lower power numbers as they were less efficient at breaking up bubbles. The fermentation results from the

fermentation showed that growth and product kinetics were similar at both scales. The maximum specific growth rate (μ_{max}) and DNA product yield on biomass were almost equivalent at both scales. The μ_{max} values were 0.47 hr^{-1} and 0.44 hr^{-1} for the 10mL and 7L bioreactor, respectively, and the yield values were comparable between 20-25mg L^{-1}.

The design of a 100mL miniature stirred tank bioreactor, driven using a magnetically stirred 6-blade paddle impeller, has been described by Gill *et al*. (2008a). Each bioreactor was made of borosilicate glass with a stainless steel head plate. The tank diameter was 60mm and the impeller diameter was one third of the tank diameter. This bioreactor system was used to scale up microbial fermentation processes at the 2L vessel, using matched K_La, and the results showed comparable growth kinetics. In a further study, Gill *et al*. (2008b) characterised the same bioreactor system in terms of mixing and oxygen mass transfer. The power number for the miniature impeller was found to be 3.5, at turbulent flow. The low power number in the bioreactor was thought to be due to the relatively small size and high impeller thickness to impeller diameter ratio. The miniature bioreactor was then used to scale up an *E.coli* TOP10 pQR239 fermentation process using matched P_g/V. The results showed comparable growth performance at both scales above a P_g/V value of 1000W m^{-3}. These studies using miniature stirred tank vessels demonstrate that performance of a lab scale fermentation can be scaled down with good accuracy using specific gassed power input values.

1.4.2 Scale-Down into Microwell Plates

There are many different sizes and types of plates available to choose from when scaling down a lab scale process into microwell plates. The choice depends on the process requirements, however for most fermentation processes; squared plates are preferred due to the enhanced mixing performance caused by the corners of the well acting as baffles (Hermann *et al*., 2002). Zhang *et al*. (2008) conducted characterisation studies on a 96-well deep square-well (DSW) plate and a 24-well DSW plate. An orbital shaker with orbital shaking amplitude of 3mm was used to mix the liquid in the plate and CFD was used to obtain energy dissipation rate in both plates. They found that mixing performance was more intensive in the 96-well plate in comparison to the 24-well plate. The average power

consumption values, obtained from calculations based on shear rate predictions, in the 24-well DSW plate was estimated to be 0.07-0.1W L^{-1} between a shaking speed of 500-1500rpm. The energy dissipation rate was found to be at their highest near the walls of the well. At a 1000rpm, small vortices were seen at the gas-liquid interface but the liquid at the base of the well was not affected. Liquid velocities at the base of the well increased with increasing shaker speed.

Barret *et al*. (2010) characterised a 24-well ultra-low attachment microtitre plate in terms of energy dissipation at varying liquid volumes and shaken speed by using predictions from CFD. The predicted energy dissipation rate ranged between 0.005-0.035W L^{-1}. Hybridoma cells were grown in the 24-well plate and scaled to the 250mL Erlenmayer shake flask based on a constant average energy dissipation rate of 0.04W L^{-1}. Data was also compared to a 5L stirred tank bioreactor however due to process limitations, it was not possible to scale based on the specific energy dissipation rate and therefore a value of 0.008W L^{-1} was selected for the 5L scale. Cells were first cultured in the microwell plate at different speeds, between 120-250rpm. The results showed that viable cell concentration and μ_{max} were better at the lower speeds, whereas antibody titre was unaffected by speed. Additionally, optimum growth was achieved in the micro-well plate at a fill volume of 0.8mL compared to 2mL. Comparison of the growth kinetics between the microwell and shake flask system showed excellent comparability and comparison to the 5L scale also showed reasonable compatibility. The final antibody titres for all systems were well matched. The titre for the 24-well plate, 250mL shake flask and 5L bioreactor were 40mg L^{-1}, 34mg L^{-1} and 44mg L^{-1}, respectively, indicating that despite differences in mean energy dissipation rates between stirred and shaken systems, it is possible to scale a cell culture process with reasonable accuracy. The data offers an engineering basis upon which further development work may be done, in order to use a microwell system as a cell culture platform for fed-batch growth of industrially relevant cell lines.

Dürauer *et al*. (2016) obtained specific power input values for 6-well and 96-well microtitre plate using calorimetry, on an Eppendorf Thermomixer Comfort shaker, with orbital shaking amplitude of 3mm. The values obtained were of similar magnitudes between the two

microtitre plates and a 90mL stirred tank bioreactor but they differed significantly when compared to a 5L stirred tank bioreactor. The shaker speeds tested in both plates were between 300-1300rpm and the Re in the 9mL bioreactor was between 4000-8500rpm. The specific power input values for 6-well, 96-well and 90mL bioreactor were comparable at 0.04-0.08W L^{-1}, 0.04-0.14W L^{-1}, and 0.03-0.05W L^{-1}, respectively. The specific power input values for the 5L bioreactor however were significantly higher at 0.45-2.1W L^{-1}.

The data from this study showed that for these particular plate types, the hydrodynamic conditions differed slightly between the different shaken systems but the turbulent mixing and hydrodynamic conditions achieved in the lab scale bioreactor could not be achieved in microtitre plates. In stirred tank bioreactors, impellers are used to distribute energy throughout the liquid and therefore the power drawn is significantly higher close to the impeller region compared to the bulk of the liquid thus varying the specific power input values significantly across the vessel. Although specific power input values obtained in microwell plates tend to fall on the lower end of the spectrum for the values typically used in stirred tank vessels, the energy is more evenly distributed throughout the well due to its small size which therefore results in a more homogenous environment quickly compared to the stirred vessel Dürauer *et al*. (2016). Therefore higher specific power input values are not needed to achieve the same level of mixing.

In order to understand the engineering performance in orbital shaken cylindrical vessels better, Büchs *et al*. (2000) introduced the out-of-phase mixing phenomenon which was used to describe the rotation of the liquid in the vessel under certain operating conditions. The Phase number (Ph) and Froude (Fr) number help to determine if the liquid in the orbital wells followed an in-phase motion or the out-of-phase motion. They found that the desirable in-phase motion occurs at Fr>0.4 and Ph>1.26, which is achieved at higher shaking speeds. In contrast, at lower shaking speeds, the fluid is considered to be out-of-phase because a significant proportion of the liquid remains stationary in the middle of well and does not follow the motion of the shaking platform. In out-of-phase, the power consumption is found to be reduced which then reduces mixing and gas liquid mass transfer. The critical shaking frequency (N_{crit}) was initially used by Hermann *et al*. (2002) to describe the speed above which there was noticeable fluid flow. Once this speed is

exceeded in a shaken platform, the surface tension of the liquid breaks due to the increased centrifugal force at higher speeds.

Weheliye *et al*. (2012), conducted an in-depth analysis of in-phase and out-of-phase conditions and proposed a scaling law for shaken vessels using Fr and non-dimensional fluid height. Although there has been characterisation of liquid-phase hydrodynamics in orbitally shaken vessels, this work has not been extended to other plate formats, including square-well plates.

1.5 Fluid Dynamics

Fluid dynamic studies can be conducting using mixing time and particle image velocimetry (PIV) experiments in order to increase understanding of the engineering characteristics in small scale systems and to improve scale-up or scale-down, particularly between stirred and shaken systems, which to date have not been the focus of engineering studies (You *et al*., 2014).

1.5.1 Mixing Time

Matching the geometry and specific power input values between scales is not always possible due to physical and practical limitations. Old equipment is usually installed in companies which may no longer be fit for purpose and therefore rather than scrapping these equipment, adjustments are made to focus on mass and heat transfer to improve mixing (Oosterhuis 1984). A key parameter used to identify problems in mixing is mixing time (Tanguy *et al*., 2015). Macroscale mixing can be assessed by conducting mixing time experiments, using a number of different techniques, however each one falls into one of two categories. Either this value is obtained using a transducer technique, such as with the use of a probe, or it is measured using a global technique, which uses no intrusive probes and allows the user to visualise a colour change within a transparent vessel after adding a tracer (Lee and Yianneskis 1997). Each method used to measure mixing time has its

advantages and disadvantages but in both cases, the mixing time is typically calculated when it is assumed that 95% homogeneity has been achieved.

Transducer techniques typically use conductivity, pH or temperature probes, to measure variation in these respective properties, inside the vessel. A passive scalar of different conductivity, pH or temperature is introduced into the vessel and the variation in the particular property is measured until fluctuations stabilise. The probe is placed into the vessel at a specific position and therefore measurements are only representative of the local point (Ascanio 2015), however, it is assumed that the reading obtained is representative of the whole vessel. This may be true for small sized vessels at turbulent flow but it is possible that at the industrial scale, there is compartmentalisation or dead zones in the fluid due to inefficient mixing thus not representing the bulk flow of liquid. The 3D flow distributions inside the entire vessel can be measured using multiple probes to overcome this issue (Lee and Yianneskis 1997) however these interfere too much with the actual flow and therefore in some cases may possibly be even less representative of the actual mixing environment during a process.

Global methods use a qualitative approach to measure mixing time in visually accessible vessels. A fast reaction that involves a colour change, such as acid-base or redox, is observed but this technique can also introduce large inaccuracies to the mixing time measurements due to the subjectivity of the method. An advantage is that the flow patterns can be visualised to help identify if there are any stagnant areas in the vessel. One example of a global technique is the decolourisation method, where the reaction between iodine and thiosulphate is observed (Barrett *et al*., 2015). Another method, called the Schlieren method, utilises a fluid with a different density to the bulk fluid, which when injected into the fluid causes the mixture to become cloudy. Once fully mixed, the liquid becomes transparent again and the light scattered by the liquid can be used to measure mixing time (Brown *et al*., 2004). Liquid crystal thermography is also a technique which can be used to obtain mixing time. This method looks at the time taken for thermo-chromic liquid crystals, which are suspended in the bulk fluid, to change colour when exposed to different

temperatures. The crystals reflect light at a specific wavelength at a given temperature, and the change in colour is rapid and can be measured (Lee and Yianneskis 1997). The thermography method is very useful but one of the drawbacks of this method is that the liquid being measured must be of the same density as the liquid crystals in order for them to remain buoyant. Therefore if different fluids with different densities are to be studied, this method is not suitable.

There have been several studies published which have employed the dual indicator system for mixing time (DISMT) method, developed by Melton *et al*., (2002) to measure the macromixing time within stirred and shaken systems. This method is an advanced non-intrusive global technique which employs the chemistry of the acid-base reaction between NaOH and HCl in the presence of two pH indicators, thymol blue and methyl red, to calculate the mixing time. When these indicators are combined in liquid, the color is red if pH<6.3, blue if pH>8 and yellow if 6.3<pH<8. The addition of stoichiometric amounts of base to an acidic liquid starts the mixing time experiment. The DISMT method allows the user to work with liquids of different densities and unlike a single indicator method, it is possible to gain further insight into the types of fluid patterns that can be created.

Cabaret *et al*. (2007) developed a technique to remove the subjectivity of the naked eye when measuring the mixing time value using DISMT. This technique involved using a high speed camera to capture the images during the mixing time experiment and then to analyse them using a mathematical model written in Matlab software which analyses the evolution in colour change. The colour change can be quantified by analysing the individual red, green and blue (RGB) pixels within a given area of the vessel, over the duration of the experiment. The mixing time can be calculated by comparing the pixel values and was measured when the set threshold of 90% homogeneity is achieved after addition of base. This method is found to provide accurate mixing time measurements and is highly repeatable and reliable. To compare the macromixing performance of two different vessel systems, the dimensionless mixing time constant (K) can be obtained from the mixing time curves. This

value is the product of the mixing time and the impeller speed, during turbulent flow and it depends on the impeller power number and on impeller spacing (Magelli *et al*., 2013).

There is an extensive body of literature focusing on studying the effect of vessel geometry, impeller geometry, vessel size, impeller type and number of impellers on mixing time in a stirred tank vessel. One key mixing time study was conducted in a 10mL miniature bioreactor and a 7L bioreactor using an acid pH tracer response technique (Betts *et al*., 2006). HCl was used as the tracer of choice and change in the pH was recorded using a pH probe which was positioned near the edge of the vessel in line with the bottom impeller. Mixing times were measured over a range of specific power input values and were found to be lower in the miniature vessel.

Tissot *et al*. (2010) measured mixing times in shaken cylindrical vessels using a calorimetric method. The effect of vessel diameter, liquid height, shaking diameter and shaking speed on mixing time were evaluated. The results showed thst as speed increased, the mixing time decreased however increasing the liquid volume, had minimal effect on mixing time. Increasing the vessel diameter and reducing the shaking diameter also increased mixing times slightly. The areas closest to the walls were the first to be fully mixed but the bulk fluid took longer. Scale-up based on equal inner-to-shaking diameter and equal Froude numbers allowed the mixing regime between a 1500L vessel and 30L bioreactor to be mimicked

1.5.2 Particle Image Velocimetry

Other aspects of fluid dynamics, such as instantaneous velocity, vorticity, turbulence and shear in a system, can be assessed using particle image velocimetry (PIV). This is a non-invasive laser optical technique which can be used to visualise flow patterns and quantify fluid dynamic properties within a system under different operating conditions (Jahanmiri 2011). PIV provides instantaneous velocity fields over global domains relatively quickly. Small tracer particles, of sufficient concentration and size, are introduced into the flow and mixing is initiated. A sheet of light is omitted from a double pulsed laser, over the area of

interest, twice, over set time interval. The particles scatter light into a photographic lens located at 90° to the laser sheet (Adrian 1991). The displacement of the particles between the image pairs can be used to calculate the distance that the particle has travelled in the set interval time, thus calculating the fluid velocity. A computer digitises the images over a series of small interrogation spots in order to build up the whole flow field image thus providing information on the flow patterns and velocities in different parts of the system. The PIV system is able to detect 3D flow even though the recording is made in 2D. In order to be able to capture and analyse thousands of images quickly, high level sophisticated software is needed for processing images post capture. The ability of PIV to take non-intrusive and indirect measurements, using high spatial resolution over a whole flow field, makes this a highly attractive technique for obtaining fluid velocity measurements. Although the practical experiments can be done relatively quickly once everything is set up, image processing can be lengthy due to the high quantity of images collected. Selecting the right tracer particle for the particular system can be challenging and choosing the seeding density of the tracer is also important in order to avoid speckling or poor mixing patterns.

Laser Doppler anemometry (LDA) is another good technique used to visualise flow and obtain fluid velocity. It works in a similar way to the PIV technique however it measures only a single point in the fluid at one time rather than the whole field, unlike PIV. The depth of information obtained by PIV is therefore superior to LDA. There is a body of literature on work describing fluid flow in a range of stirred and shaken vessels, which makes comparison of data between different studies a challenge. The key is to use the data obtained from fluid dynamic studies, such as mixing time and PIV, to understand the capabilities and limitations of that particular system for meeting certain critical process requirements. Ultimately the information can be used to understand how mixing performance may be improved and how the system can be best used for scale-up or scale-down.

1.6 Scale-Down of the Heat Extraction Process

There are some studies focusing on the periplasmic extraction process, however most of these have been conducted using simple periplasmic extraction procedures, typically in

Eppendorf tubes (Hsu 2013; Humphreys *et al*., 1996; Poppelwell *et al*., 2005; Rayat 2011; Spitali *et al*., 2008). There have been limited attempts to scale-down the Fab' extraction process from the stirred reactor into shaken systems (Rayat *et al*., 2010; Aucamp *et al*., 2014).

Rayat *et al*. (2010) conducted a 20L fermentation process, using the *E.coli* W3110 strain, to express the A33 Fab'. The cells were centrifuged and frozen at -20°C until needed for periplasmic extraction experiments, which were performed in 24-well DSW plates. The aim of the study was to see how different methods of disruption affected the subsequent DSP steps which in this case were periplasmic extraction and dead-end filtration. The cells were thawed, centrifuged in an Eppendorf centrifuge and treated either using a thermochemical method or a mechanical method. Mechanical methods, used by rayat et al. (2010), to release intracellular proteins at the small scale included sonication and homogenisation. Another technique which can be used to shear cells to release Fab', but that was not used in this study, is called focused acoustics. This method uses higher frequency compared to sonication and there is no protein degradation (Li *et al*., 2012). The viscosity, particle size distribution (PSD) of the disruptate and the quality of the Fab' product after shearing can be used to help compare the performance of a USD device to the pilot scale homogeniser. For this study however, the effect of sonication and homogenisation on dead-end filtration were studied only.

The thermochemical method consisted of re-suspending the cell pellet in extraction buffer, lowering the pH using HCl, and then heating the cells to 35°C or 50°C in an Eppendorf ThermomixerComfort for up to a maximum of 16 hours. An automated micro-scale membrane filtration device was set up to evaluate different feed streams in a parallel fashion on all samples. The data showed that samples which were treated using a thermochemical treatment gave a better filtration performance in terms of the quality of the feed stream compared to the mechanically treated samples. The PSD data showed that homogenised samples had a d_{90} of about 4µm compared to sonicated samples which had a d_{90} of 9µm, indicating that the quality of the material obtained at both scales was not the

same. The d_{90} diameter is the diameter at which 90% of a samples mass is below this diameter. Additionally, the thermochemically treated samples had a bimodal distribution due to the presence of both small and large debris particles which contributed to two populations with a d_{90} of 23µm. The data from the filtration experiments showed that the specific cake resistance was greatest for the samples which were homogenised and lowest for the samples undergoing thermochemical treatment. Interactions between the cells, proteins, solutes and contaminants released from cells during the upstream process impacted the cake porosity and level of packing during filtration which is why samples with the smaller debris particles, such as those found after homogenisation, caused a compact cake to form on the filter, thus increasing the specific cake resistance and causing the permeate to decrease two-fold compared to the thermochemically treated samples. The Fab' and host cell protein (HCP) content, after the extraction, were in agreement with the PSD data, demonstrating that the homogenisation process released the greatest levels of both Fab' and HCP, followed by sonication and then the thermochemical treatment.

A comparison of Fab' release between thermochemically treated cells at the two different temperatures and durations showed that at the higher temperature of 50°C and at longer incubation time of 16 hours, no more than 9% extra Fab' was released compared to the extraction at 35°C and 1 minute. The HCP content decreased with time due to heat denaturation which was confirmed by SDS-PAGE gel. The gel also confirmed that the homogenised and sonicated samples had higher level of impurities, hence significantly more bands were seen on the gels. The results from such a study indicated that thermochemical extraction was the preferred choice for Fab' release compared to mechanical methods such as homogenisation and sonication. Additionally sonication, which is done at the lab scale only, was found to be a poor model for a large scale high-pressure homogeniser. The thermochemical treatment, however, was found to be scalable between the micro-scale and a 10L scale stirred tank vessel (unpublished data, Alison Tang, UCL).

Aucamp *et al*. (2014) performed *E.coli* fermentations in a 20L vessel in order to produce different Fab' types. They then conducted a heat extraction process in a 5L and 20L vessel at

2W Kg^{-1} at 60°C, and in a 250mL shake flask, agitated at 300rpm, in a shaken heated incubator. The specific power input in the shake flask was estimated to be approximately 8-9W Kg^{-1}. The methodology used for the extraction process in the stirred tank vessels was the same as that used at industrial scale for the heat extraction process, using freshly harvest cells. Fab' titres, dsDNA concentrations and PSD measurements between the shaken flask and the stirred tank vessel were obtained and the values were found to be comparable between both scales. This data indicates the feasibility for scaling down a lab scale and pilot scale heat extraction process into a shaken flask. The overall aim of this thesis is to establish a miniature stirred tank vessel, and a shaken microwell plate system, as suitable scale-down models for the industrially relevant heat extraction processs. This is so that the heat extraction process can be characterised and optimised quickly, using less resources, thus speeding up process development.

Chapter 2

Materials and Methods

2.1 Strains and Chemicals

All chemicals used for fermentation and extraction were of analytical grade and purchased from VWR International (Merck Ltd., Lutterworth, UK) with the exception of glycerol and acetic acid which were purchased from Fisher Chemicals (Fisher Scientific UK Ltd., Loughborough, UK), and polypropylene glycol (PPG), nickel sulphate hexahydrate and IPTG which were purchased from Sigma (Sigma-Aldrich Company Ltd., Dorset, UK). Deionised water (DI water supply, Ajax Avenue, UCB, Slough) was used in all the experiments except where specified otherwise. For the fermentation process, the industrial *E.coli* strain W3110 containing plasmid pTT0D A33 IGS2 was used (UCB Ltd. Slough, UK). The plasmid expresses a humanised Fab' fragment under the control of the *tac* promoter which is then directed towards the periplasm of the cell (Rayat *et al*., 2010). The master and working cell bank were prepared in 80% (v/v) glycerol and stored at -80°C. In some experiments, commercial Fab' variants were used and data obtained using these Fab's have been normalised in the thesis.

2.2 *E.coli* Fermentation

A very special acknowledgement goes to the upstream team at UCB who exclusively conducted fermentations at the 20L and 200L scale and disc stack centrifugation. In most cases, 5L fermentations were also conducted by the UCB upstream team. With their help and guidance, I was able to collect material from the upstream processes and use for my own scale-down experiments. Analytical data from the large scale upstream processes was used to gain insight of how raw material variability could impact the heat extraction process.

2.2.1 Shake Flask Experiments

For the seed train, 6xPY complex media (containing 48g L^{-1} phytone, 30g L^{-1} yeast extract and 5g L^{-1} NaCl) was prepared in a 2L baffled shake flasks and autoclaved at 121°C for 20 minutes. 10µg mL^{-1} of tetracycline and 1ml working cell bank vial, thawed for 10 minutes, was then added to the shake flasks and then incubated at 37°C, 230rpm in a shaken incubator until the cells reached an OD_{600} between 2 and 3. The culture was then transferred into inoculum flasks and used to inoculate the subsequent fermentation step.

2.2.2 Fermentation

2.2.2.1 Equipment for Fermentation

Fermentations were conducted at the 5L, 20L and 200L scale. 5L fermentations were conducted in the Sartorius UniVessel, an autoclaveable jacketed glass vessel with a stainless steel head plate and a top driven motor. The 20L fermentations were conducted in the stainless steel Sartorius Biostat Cplus Sterilisable-In-Place fermenters with a top driven motor and the 200L fermentations were conducted in stainless steel Sartorius Sterilisable-In-Place fermenters with a bottom driven motor. All three fermenter sizes used three 6-bladed Rushton impellers, a ring sparger and 4 equally spaced baffles inside the vessel. The vessels were equipped with a temperature probe, a Broadley James pH probe (Bedford, UK) and a Mettler Toledo DO probe (Leicester, UK). The pH probes were calibrated using pH 4.0 and pH 7.0 buffers and the DO probes were calibrated to 0% and 100% with nitrogen and air respectively. The fermentation protocol was controlled using the multi fermenter control system (MFCS) at each scale.

Because both the 20L and 200L reactors are constructed of stainless steel, they are sterilised in situ with all the relevant probes in place at 121°C for 20 minutes. To account for liquid lost due to evaporation at both scales, the media was topped up to the volume used prior to sterilisation, using sterile deionised (DI) water.

2.2.2.2 5L Fed-Batch Fermentation

For 5L fermentations, 2.75kg of MD5 defined media, containing 50g kg^{-1} of glycerol as the carbon source, was prepared and then added to the vessel and autoclaved at 121°C for 20 minutes. Following autoclaving, the vessel was connected to the Sartorius Biostat B plus unit and the temperature control loop was turned on and set to 30°C. Once at a stable temperature samples were taken for offline pH measurements and the pH probe was recalibrated to account for any drift during autoclaving. Following this recalibration the pH control loop was turned on and used to control the pH at 6.9 using 12.5% (v/v) ammonia and 10% (v/v) sulphuric acid. Dissolved oxygen (DO) was maintained above 30% using air and enriched oxygen via cascade control. Inoculum was transferred aseptically to the vessel once the cells were at the appropriate OD to achieve the required seeding density. Samples were taken regularly for offline OD_{600} readings. The fermentation was operated initially in batch mode and once the carbon source was depleted, 80% glycerol was added in fed-batch mode. A shot of 1M MgSO4.7H2O was added when the OD_{600} reached a value with the desired range. Foaming was controlled using the addition of PPG. Once the batched glycerol was depleted, a spike in the dissolved oxygen was observed and the exponential feed phase was initiated to allow a growth rate of 0.1 hr^{-1} using 80% glycerol for approximately 6.5 hours. At the end of the exponential feed phase, Fab' production was induced using IPTG. Samples were taken at different time points to measure % cell viability and dry cell weight (DCW) and for quantification of Fab', total protein and dsDNA content in the supernatant. Samples were also extracted using the 1mL extraction method described in section 2.4. The cells were aliquoted into an appropriate number of Eppendorf tubes and spun at 13,000rpm for 5 minutes. The supernatant was decanted into fresh Eppendorf tubes and frozen at -20°C till needed for analysis. After 40 hours, post induction, the broth was cooled to 18°C and harvested using a dead end centrifuge. Details on the condition of the cell, product and impurities for all experiments including % cell viability, Fab' titre, total protein and dsDNA concentration, at the end of the fermentation, are summarised in Table 5.1 in Chapter 5.

2.2.2.3 20L and 200L Fed-Batch Fermentation

The fed-batch fermentation protocol in the 20L vessel was conducted in a similar manner to the 5L fermentation as described in section 2.2.2.2 with the exception of the following differences. Depending on the type of Fab' used, the time taken to harvest cells post induction varied between 40 and 45 hours, after which the broth was cooled to 18°C and harvested using a disc stack centrifuge.

The fed-batch fermentation protocol in the 200L vessel was conducted in a similar manner to the 20L fermentation with the exception of the following differences. The seed train included an intermediate seed fermentation step in the 20L bioreactor. 10kg of MD5 defined media and 5µg mL^{-1} of tetracycline was prepared and added to the 20L vessel. A batch fermentation process was carried out in this 20L vessel at 30°C, maintaining a pH of 6.9, and a DO above 30%. Once the OD_{600} reached a value in the desired range, the cells were used to inoculate the 200L bioreactor. The culture was induced and harvested in the same way as for 20L scale.

2.3 Centrifugation

2.3.1 Pilot Scale Disc Stack Centrifugation

Following pilot scale fermentation, the cells were pooled together as necessary in a collection tank and then centrifuged using a continuous disc stack centrifuge (Westfalia PSC-5). The bowl speed was set to 10,500rpm and the feed flow was set to 54L hr^{-1}. The solids were collected using intermediate discharge. Samples were taken from the heavy phase and the light phase to determine the Fab', total protein and dsDNA concentrations after centrifugation. These samples were aliquoted into 2mL Eppendorf tubes and spun at 13,000rpm for 5 minutes. The supernatant was decanted into Eppendorf tubes and frozen at -20°C for subsequent analysis. The OD_{600} of the feed (OD_f), of the light phase sample (OD_s) and of a well spun sample (OD_w) were determined and used to calculate the % clarification

using Equation 2.1. The well spun OD was determined from the supernatant of a sample from the harvested material and spun in a bench top centrifuge at 13,000rpm for 30 minutes

$$\% \text{ Clarification} = \frac{OD_f - OD_s}{OD_f - OD_w} \times 100 \qquad \text{[Equation 2.1]}$$

The % dewatering level obtained by the disc stack centrifugation process was determined using Equation 2.2. This is a measure of how much of the light phase was removed from the heavy phase and consequently how concentrated the cells were.

$$\% \text{ Dewatering} = 1 - \left(\frac{Heavy\ Phase\ (kg)}{Feed\ (kg)}\right) \times 100 \qquad \text{[Equation 2.2]}$$

2.3.2 Cell Harvest by Dead End Centrifugation

The culture was harvested by centrifugation in 1L pots (Beckman Coulter J6-M1) operating at 4,200rpm and 4°C for 1 hour. The supernatant was decanted and then a calculated quantity was added back and mixed in order to achieve a dewatering level that is representative of the dewatering achieved using large scale disc stack centrifugation. Details of the centrifugation conditions including dewatering level, % clarification after centrifugation are summarised in Table 5.2 in Chapter 5.

2.4 Heat Extraction

2.4.1 Heat Extraction Buffers

Different strengths of extraction buffer were prepared in order to extract Fab' from within the periplasm of the cells after harvest centrifugation. 1x Extraction buffer was prepared for 1mL Eppendorf extractions using 2.43g L^{-1} of Tris base, 12.60g L^{-1} of Tris HCl and 3.72g L^{-1} of EDTA. 3x Extraction buffer was prepared for all other extractions in deep square well plates and for 20mL, 2L, 20L and 200L extractions using 7.28g L^{-1} of Tris base, 37.81g L^{-1} of Tris HCl and 11.17g L^{-1} of EDTA. All buffers were stored in the fridge at 4°C for up to a month. The 3x extraction buffer was mixed with DI water to make a pre-mix solution. The ratio of 3x extraction buffer to the DI water varied depending on the dewatering level achieved during the centrifugation step in each individual experiment such that once the cells were re-suspended the extraction buffer was at its 1x concentration. This was done in order to achieve the same concentration of cells at the end of fermentation. 30% acetic acid was prepared for the acid precipitation step after the completion of the heat extraction process using 30mL L^{-1} of 100% acetic acid solution in DI water. The solution was stored in the acids cupboard for up to 3 months.

2.4.2 Equipment for Heat Extraction

Heat extraction was performed at different scales in order to compare performance. Small scale extractions were performed on samples taken from harvested material after fermentation and used as a benchmark corresponding to 100% extraction efficiency. This was conducted in 2mL Eppendorf tubes using a shaken Eppendorf ThermomixerComfort (Eppendorf AG, Germany).

The 2L heat extractions were conducted in 2L Univessels using the Sartorius BioStat B Plus units. A schematic diagram of the 2L vessel showing the dimensions and key components is shown in Figure 2.1. The autoclave-able single jacketed glass vessel has a stainless steel head plate and a top driven motor. A triple Rushton impeller system was used, with a

diameter (Di_{2L}) of 5.3cm, an inter impeller spacing of $0.95Di_{2L}$ and an off-bottom clearance of Di_{2L}. A ring sparger and 4 equally spaced baffles were also present inside the vessel. The distance between the top impeller and liquid surface was $0.5Di_{2L}$. The vessel was equipped with a temperature probe, a Broadley James pH probe (Bedford, UK) and a Mettler Toledo DO probe . All other ports for sampling and addition were closed off to keep a sealed vessel. Temperature was controlled by passing water through the glass jacket. The pH probe was calibrated using pH 4.0 and pH 7.0 buffers and the DO probe was calibrated to 0% and 100% with nitrogen and air respectively. The extraction protocol was controlled using recipes created on MFCS.

Extraction experiments at the 20L and 200L scale were carried out in the 20L and 200L fermenters as described in section 2.2.2.1 and were conducted by the fermentation team at UCB. The analytical data subsequently obtained from these experiments were compared to the 2L, 20mL and the micro-well extractions in this study, as described in Chapters 5 and 6.

The 20mL heat extractions were conducted in a miniature stirred tank reactor. The initial design was created by Betts *et al*. (2006). The 20mL miniature vessel used in this study was a modified version and a schematic diagram, showing the dimensions and key components of the vessel for the purpose of microscale extraction experiments, is shown in Figure 2.2. The water jacket was constructed from borosilicate glass with an inner and outer diameter of 24.0mm and 36.2mm respectively, with a length of 82.2mm. A triple paddle impeller system was used, with a diameter (Di_{20mL}) of 0.85cm, an inter impeller spacing of $0.95Di_{20mL}$ and an off-bottom clearance of Di_{20mL}. The distance between the top impeller and liquid surface was $1.3Di_{20mL}$. This impeller system was used for all of the extraction experiments. The vessel was equipped with a 2.0mm Pt 100 stainless steel temperature probe (Process Parameters, Berkshire) and a 1.7mm wide MI-4146 micro pH probe (Microelectrodes Inc, USA). Four equally spaced baffles are also present in the vessel to minimise vortexing. A miniature stainless steel condenser, with a 0.22µm syringe filter on one end, was constructed and fitted onto the vessel to minimise evaporation during experiments. Plastic tubing was wrapped around the condenser and connected to the Sartorius B Plus unit to facilitate the flow of chilled water from the unit to cool the condenser. All other ports for

sampling and addition were closed off to keep a sealed vessel. The impeller speed was adjusted using an overhead Ika Eurostar digital motor with a speed range of 50 to 2000rpm.

Micro-well extractions were conducted in riplate® Polypropylene 24 x 10ml deep square well plates (Elkay Labs, Basingstoke, UK) with a diamond bottom. The dimensions of the micro-well plate are shown in Figure 2.3 including the height of the liquid at different fill volumes. An aluminium SEA-LPLT 100 foil (Elkay Labs, Basingstoke, UK) was used to seal the plate and prevent evaporation during the extraction process. An Eppendorf Thermomixer C v1.0.9 with a ThermoTop was used to heat and shake the plates during extraction. A YCT-747 hand held four channel data logger (Thermosense, Manchester UK) was connected to four fine wire type K thermocouples, PTFE 1m, and used to measure temperature in the different wells of the micro-well plate. To measure pH during the acid precipitation step, an InLab Micro pH probe (Mettler Toledo Leicester, UK) was used.

2.4.3 Heat Characterisation in the Scale-Down Models

To mimic the heating conditions of the lab or pilot scale extraction process, the miniature temperature probe and jacket lines were also connected to the Sartorius unit so that the same heating profiles could be used via MFCS. PID tuning was needed on the unit in order to achieve a smooth and accurate heating profile, using DI water as a sample fluid. Different heating profiles, with varying hold temperatures, durations and heat up and cool down rates were tested in the 20mL vessel to ensure that the PID settings were suitable for all conditions. The volume in the vessel was measured before and after completion of the heating profile to calculate % evaporation. Concentrations of Fab', total protein and dsDNA, obtained during analytics, were adjusted to compensate for the % evaporation during the heat extraction studies.

Temperature characterisation work in the 24-well DSW plate was conducted to ensure that the temperature was even across the plate. For this work, 2mL of DI water was added to each well. Four thermocouples were placed in the corners of the micro-well plate and taped

down using autoclave tape to prevent movement. Temperature measurements were made digitally every 7 seconds. The Thermomixer was set to 1000rpm which visually showed good mixing, and the aim was to create a programme which could accurately mimic the heating profiles as those used for extractions in the stirred tank. Different temperature settings were tested until the heating profile was satisfactory. The weight of the plate, containing the water, was weighed before and after completion of the heating profile in order to calculate the % evaporation. This work was repeated using different shaker speeds (300rpm, 500rpm, 800rpm and 1200rpm) and different fill volumes (2.5mL, 3.0mL, 3.5mL and 4.0mL) and across different wells, some close to the centre of the plate, to ensure that the heating profiles were running consistently under different operating conditions. Select conditions were also tested across different Thermomixers to confirm that they all worked in the same way

2.4.4 Process for Heat Extractions

For extractions in the Eppendorf tubes, 1mL of harvested cells were pipetted into multiple Eppendorf tubes and were centrifuged at 13,000rpm for 5 minutes. The supernatant was discarded and the pellet in each tube was re-suspended in 1mL of 1x extraction buffer. The tubes were then placed inside the thermoshaker and heated to 60°C for 10 hours at 1200rpm and then cooled to 18°C. The supernatant was poured into Eppendorf tubes and kept in the fridge at 4°C for subsequent analysis. The Fab', total protein and dsDNA results obtained from analytics were corrected for by a dilution factor based on wet cell weight (WCW) using Equation 2.3. The WCW was obtained as described in section 2.5.2.

$$\text{Dilution Factor} = Concentration\ in\ Extract \times (1 + harvest\ \%WCW) \quad \text{[Equation 2.3]}$$

For the 2L extraction process, material was taken after centrifugation and the required amount of heavy phase and premix were aliquoted into measuring jugs. The heavy phase was added to the 2L vessel and the temperature and impeller speed were set to 18°C and 200rpm respectively. Once the temperature reached 18°C, the pre-mix was added to the vessel and a pre-determined heating profile was initiated using MFCS. The total volume

used for extraction was 2L. Upon completion of the extraction process, the cell suspension was cooled to 18°C and held at that temperature until sampling. A 10mL sample was taken from the vessel after extraction the following morning, typically around 16 hours later, for analytics. The pH of the cell suspension was then adjusted to 4.5 by slowly adding 30% acetic acid to the vessel using a pipette gun. 5 minutes after pH was stable, another 10mL sample was taken for analytics. The samples taken, post extraction and post acid precipitation were pipetted into multiple 2mL Eppendorf tubes and centrifuged at 13,000rpm for 5 minutes. The supernatant was decanted into 2mL Eppendorf tubes and stored in the fridge at 4°C for subsequent analysis.

Heat extraction at the 2L scale were initially run for a design of experiment study (DoE) and then used as a benchmark comparison to verify small scale extraction results. Ten 2L scale extractions were conducted looking at the impact of specific power input, extraction hold duration and extraction temperature. Characteristics of the cell, product and impurities as well as fermentation and centrifugation conditions are provided in Table 5.1 and Table 5.2 in Chapter 5 respectively. The DoE experiment results are described in Chapter 3.

Heat extraction was performed in the 20mL vessel following a similar protocol to that used in the 2L vessel. The heavy phase and pre-mix were weighed out separately in 20mL syringes. The heavy phase was added to the vessel first and temperature and stirrer speed were set to 18°C and 1000rpm respectively. Once ready, the pre-mix was added, all open ports were sealed off, the heating profile was initiated using MFCS and the overhead stirrer was set to the required speed manually. The next morning, after completion of extraction, 4mL of the cells were taken for analytics. For some experiments, the cell suspension was then adjusted to pH 4.5 inside the vessel. For some experiments, the remaining cell suspension was removed from the vessel and placed inside a 60mL sterilin pot. A miniature magnetic bar was placed inside the pot, which was put on a magnetic stirrer and mixed, as the pH was adjusted to 4.5. For analytical measurements, 4mL was taken again. Both samples were pipetted into two Eppendorf tubes and centrifuged at 13,000rpm for 5 minutes. The supernatant was decanted into Eppendorf tubes and stored in the fridge at 4°C till required for analysis.

For the extractions in the micro-well plate, the Thermomixer was set to 18°C for pre-cooling. An empty micro-well plate was placed on top of a balance and the appropriate amount of heavy phase was weighed into each well using a pipette. The plate was placed onto the Thermomixer to be cooled and the appropriate amount of heavy phase, measured by weight, and pre-mix, measured by volume, were pipetted into each well. The plate was weighed and then sealed with 4 thermocouples placed into the four alternative wells in the plate. The heating programme and data logger were then started simultaneously in order to begin the extraction process and log the temperature profile. The next morning, once the extraction was complete, the seal and thermocouples were removed and the plate re-weighed to calculate % evaporation. Minimum volume of 2mL of sample was taken from alternative wells as shown in Figure 2.4 and pipetted into Eppendorf tubes. The shaker speed was reduced to 700rpm and the pH in the remaining wells was adjusted to 4.5 using a Mettler Toledo micro-pH probe, by adding 30% acetic acid using a pipette. After the acid precipitation step, samples were pipetted into 2mL Eppendorf tubes. All the post extraction and post acid precipitation samples were centrifuged at 13,000rpm for 5 minutes and the supernatant transferred into Eppendorf tubes to be stored in the fridge at 4°C until needed for analysis. The amount of heavy phase and pre-mix added to each well in a plate varied across experiments, depending on the total volume tested. This was calculated and adjusted for before each experiment. The total volume used for micro-well extraction experiments were 2.0mL, 2.5mL, 3.0mL and 3.5mL.

2.5 Analytic Techniques

2.5.1 Optical Density

Optical density measurements OD_{600} were taken throughout fermentation and also during the centrifugation unit operations, using the Thermo Genesys 10 UV spectrophotometer (Thermo Scientific, Leicestershire, UK). Samples were diluted as appropriate using Physio Saline to obtain readings between 0 and 0.4.

2.5.2 Dry Cell Weight

Empty 2mL Eppendorf tubes were dried in the oven, set at 112°C for a minimum of 16 hours, with the lids open. They were then placed into a desiccator for 2 hours to further cool dry before being weighed. Samples were taken during fermentation at different time points from induction onwards. 1mL of sample was aliquoted into the pre-weighed Eppendorf tubes and centrifuged at 13,000rpm for 5 minutes. The supernatant was then decanted and the tube re-weighed with just the wet pellet. The WCW was calculated by subtracting the weight of the tube with the wet pellet from the empty Eppendorf tube. These Eppendorf tubes were placed into a rack with their lids open and placed into the oven, for a minimum of 16 hours. The tubes were then placed in a desiccator for 2 hours to further dry and cool. The tubes were re-weighed one final time and the DCW was determined by subtracting the weight of the tube with the dry pellet from the empty Eppendorf tube. Triplicate measurements were taken for each sample and results presented in this work show the average ± 1 standard deviation.

2.5.3 Cell Viability

Cell viability was measured using the FACSCaliburTM flow cytometer (BD Biosciences, Oxford, UK). Bis(1,3-dibutylbarbituric acid)-trimethine oxanol (BOX) and propidium iodide (PI) were used to stain the cells. A 0.1 mg mL^{-1} solution of the BOX reagent was prepared in DMSO and stored in a foiled covered Eppendorf tube, in the fridge at 4°C, until needed. A 2mg mL^{-1} stock solution of PI was prepared in DI water and stored in a foiled covered Eppendorf tube, in the fridge at 4°C, until needed. Samples were taken during fermentation at different time points after induction. The samples were vortexed and then diluted in 50mL filtered physio saline solution. The volume of sample, in µL, needed for dilution was estimated by dividing 500 by the OD_{600} of the sample. Actual volumes were varied in some cases to ensure that approximately 1000 cells s^{-1} pass through the FACS laser. When ready, 1mL of the diluted sample was added to 5µL of BOX and 2.5µL of PI, vortexed and left for 5 minutes. The sample was then presented to the FACS and processed using the CellQuest Pro

software to measure the % viable cell count. Gated forward scatter and side scatter plots were obtained showing four quadrants reflecting BOX and PI signals. % cell viability was measured using the healthy cells present in the lower left quadrant where BOX and PI signals are at their lowest.

2.5.4 Chromatography

2.5.4.1 Protein G High Performance Liquid Chromatography

Fab' titre was quantified using a 1mL Hi-Trap protein G column (GE Healthcare, Chalfont, UK) on the Agilent HP1100 HPLC system (Agilent, USA) using the Empower2 software. Buffer A (20mM Sodium phosphate 50mM Sodium chloride buffer, adjusted to pH 7.4 using 12N NaOH and buffer B (50mM glycine, adjusted to pH 2.7 using 37% HCl) were used for equilibration and elution respectively. The column was stored in 20% ethanol when not in use. Samples taken after fermentation, centrifugation, extraction and acid precipitation were taken out from their place of storage and allowed to reach room temperature. Samples were vortexed and filtered using a 0.2µm syringe filter with low binding membrane and then injected onto the Hi-Trap protein G column on the HPLC machine. A standard curve, between 2µg and 100µg, was obtained using 1mg mL^{-1} of purified Fab'. A typical standard calibration curve for protein G HPLC can be seen in Appendix 2A. The Fab' component was measured by recording the absorbance at 280 nm. Each sample was analysed in duplicate and the results presented in this work show the average of the two values.

2.5.4.2 Protein L Chromatography

Fab' was purified on the TECAN Freedom EVO200 robotic system using the 600µL PreDictor RoboColumn Capto L columns. The EVOware standard software was used with the TECAN automated platform. Buffer A (20mM Sodium Phosphate buffer, adjusted to pH 7.4 using 30% H_3PO_4) and buffer B (0.1M glycine, adjusted to pH 2.7 using 37% HCl) were used for equilibration and elution respectively. The columns were stored in 20% ethanol. Protein L

chromatography was run on samples after extraction and acid precipitation. These samples were taken out of the fridge and allowed to reach room temperature. They were then vortexed and filtered using a 0.2µm syringe filter with low binding membrane and purified using the Capto L columns.

2.5.5 NanoDrop

The protein concentration in a protein L purified sample was determined using the NanoDrop2000 (Thermo Scientific, Leicestershire, UK) at a wavelength of A280nm. Phosphate buffered saline (PBS) was used as a blank and readings were taken in triplicates using an extinction coefficient of 1.78. The pH of the sample was adjusted to 7 using 2M Tris base and the sample stored in the fridge at 4°C until required for further analysis.

2.5.6 Total Protein Bradford Assay

The total protein concentration was measured using the Coomassie (Bradford) Protein Assay kit (Thermo Scientific, Leicestershire, UK). Samples taken after fermentation, centrifugation, extraction and acid precipitation were taken out from their place of storage and allowed to reach room temperature. All the samples were then vortexed and diluted 10 fold in sterile water. An appropriate amount of the coomasie reagent, that is included with the kit, is aliquoted into a 20mL sterilin pot, covered with aluminium foil and left to reach room temperature. The albumin standard was used with sterile water to prepare standards for a calibration curve between 100µg mL^{-1} and 700µg mL^{-1}. An example of the calibration curve for the total protein assay can be seen in Appendix 2B. Once ready, 10µL of the standards and the samples were pipetted into 96-well clear flat bottomed microtitre plates in triplicates. The coomasie reagent was poured into a suitable trough and a multichannel pipette was used to pipette 300µL of the reagent into each well. The plate was then shaken for 30 seconds and incubated for 10 minutes in the FLUOstar Optima plate reader (BMG LABTECH Ltd, Aylesbury, UK). Absorbance was read at 630nm in triplicates and the results presented in this work show the average ± 1 standard deviation

2.5.7 dsDNA PicoGreen Assay

To quantify dsDNA concentration, samples were analysed using the Quant-iT PicoGreen dsDNA Assay kit (Life Technologies, USA). Samples taken after fermentation, centrifugation, extraction and acid precipitation were taken out from their place of storage and allowed to reach room temperature. Tris-EDTA (TE) buffer was prepared by diluting the 20x TE buffer that is provided with the kit, 20 fold, with sterile water. Samples were vortexed and diluted with the 1x TE buffer. Typically, samples taken after fermentation and centrifugation were diluted 300 fold with the 1x TE buffer. Post extraction samples were diluted 3000 fold and post acid precipitation samples were diluted 100 fold. To prepare the reagent, the stock PicoGreen reagent that is supplied with the kit is diluted 200 fold in 1x TE buffer and stored in a 20mL sterilin covered with aluminium foil. To prepare the standards, the 20µL of the λDNA (100µg mL^{-1}), provided with the kit, is initially thawed and diluted 50 fold with the 1xTE buffer. This stock solution was then diluted furthermore to prepare the standards for the standard calibration curve between 0.1µg mL^{-1} and 2µg mL^{-1}. An example of the calibration curve for the PicoGreen assay can be seen in Appendix 2C. Once ready, 100µL of the standards and the samples were pipetted into low evaporation 96-well flat bottomed black microtitre plates in triplicates. The PicoGreen reagent was poured into a suitable trough and a multichannel pipette was used to pipette 100µL of the reagent into each well. The plate was placed in the FLUOstar Optima plate reader, shaken for 30 seconds and incubated for 5 minutes. The plate fluorescence reading was obtained by exciting at 485nm and reading absorbance at 520nm. The results presented in this work show the average ± 1 standard deviation.

2.5.8 SDS-PAGE

To look at the HCP profile in samples taken after fermentation, centrifugation, extraction and acid precipitation, SDS-PAGE gels were run. All samples were run on the non-reduced gels. Protein L purified extraction samples were also run on reduced gels in order to determine the quality of the Fab' product and to see if Fab' denaturation was affected by different extraction conditions. All chemicals were purchased from Thermo Scientific

(Leicestershire, UK) unless specified otherwise. The XCell SureLock Mini Cell Electrophoresis system was the system of choice for running the gels using Precast Novex 4-20% Tris-Glycine gels with 15 x 1.5mm wells. The sample buffer used in both sets of gels was the Invitrogen Novex Tris-glycine 2x SDS sample buffer. The reducing buffer used in the reduced gels was the NuPAGE 10x reducing buffer and the non-reducing buffer in the non-reduced gels was 100mM N-Ethylmaleimide (NEM).

All samples were vortexed and diluted with DI water, SDS PAGE buffer and a choice of either reducing buffer or NEM depending on whether reduced gels or non-reduced gels were being run respectively. The final amount of Fab' loaded into each well was 1µg. Mark 12 unstained standard was used for a protein ladder showing protein bands in the range of 2.5 to 200 kDa. Electrophoresis was conducted using Novex Tris-Glycine running buffer. Upon completion, the gels were washed with DI water and placed onto a rocking shaker in de-stain solution, which was prepared using 40% (v/v) methanol and 10 % (v/v) acetic acid in DI water. The gels were then washed with DI water and left in Sypro Ruby Protein gel stain overnight. In the morning, the gels were washed one last time and left in DI water for 1 hour before being imaged using the GeneSys (Syngene, Cambridge, UK) imaging system and software.

2.5.9 Scanning Electron Microscopy

A special thanks to Mark Turmaine, the Experimental Officer at the Biosciences department at UCL for his help in sample preparation of cells for scanning electron microscopy.

Fresh samples taken after fermentation, extraction and acid precipitation were aliquoted into 2mL Eppendorf tubes and centrifuged at 13,000rpm for 5 minutes, the supernatant was decanted and the pellet was re-suspended in 2% glutaraldehyde solution containing 0.1M sodium cacodylate buffer (pH 7.3) to primarily fix the cell and to coagulate any proteins present. To aid re-suspension, the cells were vortexed gently till none of the pellet could be visually observed on the Eppendorf wall. The samples were then stored in the fridge at 4°C for 24 hours. The suspension was spun down and the cells exchanged for osmium. The

material was post fixed with 1% osmium tetraoxide solution containing 0.1 M cacodylate buffer at 38°C for 1.5 hours. The osmium tetroxide fixes the lipids in the cell membrane. The cells were washed one more time with 0.1 M cacodylate buffer and then washed with dH2O. Next, they were dehydrated slowly in a graded ethanol-water series to 100% ethanol in order to stop shrinkage of the cells. To be able to visualise the specimen under a microscope, the sample needed to be dried out. This was achieved by substituting the ethanol in the sample with liquid CO2 and then using critical point drying to turn the liquid CO2 into gaseous CO2. Once dry, the samples were mounted onto aluminium stubs using adhesive carbon tabs and the specimen was coated with an approximately 2nm thick layer of Au/Pd using a Gatan ion beam coater. The stubs were then viewed under a JSM-7610F scanning electron microscope (Jeol, USA) and multiple images were recorded under different magnification settings.

2.6 Mixing Time

2.6.1 Introduction

Mixing time experiments were conducted using an adaptation of the dual pH indicator system for mixing time (DISMT) first developed by Melton *et al*. (2002). By adding stoichiometric ratios of acid and base in the presence of pH indicators, the visual change in colour could be quantified by taking a series of images using a high speed camera and then analysing it using a purposely developed code in Mathwork Matlab R2012b.

2.6.2 Chemicals and Equipment

All chemicals used for the mixing time experiments were purchased from Fisher Scientific (Pittsburgh, PA). Methyl Red and Thymol blue powders were used as indicators for the experiment. A replica of a single well in a 24-well deep square-well plate was constructed out of Pyrex glass at the UCL Biochemical Engineering Workshop which was fixed to a 96-well clear flat bottomed microtitre plate. Arms were constructed which extended from the

plate to provide a platform for the color NET iCube camera to be fixed onto in order to provide static images of the well during mixing time experiments. The camera was set up in front of the well and used to take images at a capture speed in the range of 40-1000ms, depending on the impeller or shaken speed chosen. An 8 LED OMC backlight panel with a homogenous 580 mcd white light was placed behind each vessel being studied to reduce background noise during image capture.

A stainless steel replica of the existing impeller shaft used in the 20mL vessel was constructed at the UCL Biochemical Engineering Workshop. The new impeller shaft allowed the impeller positions to be varied through the use of adjustable metallic sleeves and a bottom screw to hold the impellers and sleeves in place. It was therefore possible to observe the impact of inter impeller spacing and off bottom clearance on mixing time experiments. Schematic diagrams showing the setup of the mixing time experiments for the different models is shown in Figure 2.5. Data from these studies are presented in Chapter 4.

2.6.3 Mixing Time Methodology

50mL of thymol blue and methyl stock solutions were prepared in 70% ethanol to a concentration of 1.38g L^{-1} and 1.52g L^{-1} respectively. The stock solutions were then added to 2L sterile water achieving a final concentration of 6.5g L^{-1} for each indicator. 5M NaOH and 5M HCl were diluted in sterile water to make 0.75M NaoH and 0.75M HCl, used to adjust pH and initiate mixing time experiments. 110µL of 0.75M NaOH was added to the solution to make up the yellow coloured working DISMT reagent. This reagent was believed to be suitable as a mimic of an *E.coli* culture, which has water like properties (Tissot *et al*., 2010).

For the mixing time experiments in the 2L and 20mL stirred tank vessel, 0.1mL of 0.75M NaOH and 0.75M HCL was used per litre of DISMT reagent to start the mixing time experiments. For the 24-well deep square-well plate, 1mL of 0.075M NaOH and 0.075M HCL was used per litre of reagent to start the mixing time experiments. Experiments were conducted to determine how many times the reagent could be re-used without affecting the final colour by alternatively adding stoichiometric amounts of NaOH and HCl. Images

seen in Appendix 2D show that the reagent may be used up to three times without the need to exchange for fresh reagent. Each experimental condition was repeated minimum of 3 times.

2.6.3.1 Mixing Time Experiments in 2L Vessel

A 2L vessel was set up in the same way as for a 2L extraction experiment, with all the relevant probes in place. 2L of the DISMT reagent was added to the vessel, an LED light panel and the camera, fixed on a tripod, were placed behind and in front of the vessel respectively. The set up was enclosed inside a manually made cardboard housing to further minimise background noise during experimentation. An impeller speed was selected to develop a stable flow. 200µL of 0.75M HCl was added into the vessel to acidify the reagent and turn it red. This was added through an open port on the head plate using a 200µL pipette fixed in place approximately 20cm above the surface of the liquid using a clamp stand. Once ready, the camera was turned on to start recording high speed images and 200µL of 0.75M NaOH was added to initiate the mixing time experiment. Recording was suspended well after a color change was observed from red to yellow. The speeds tested for the mixing time experiments in the 2L vessel were in the range of 20-275rpm (1.2×10^{-4}W L^{-1} – 0.30W L^{-1}) as calculated in Appendix A.

2.6.3.2 Mixing Time Experiments in 20mL Vessel

Mixing time experiments in the 20mL vessel were conducted in a similar way to the 2L vessel. The 20mL vessel was set up in a same way as during an extraction experiment with all necessary probes in place inside the vessel, an LED light panel behind it and the camera fixed in front of the vessel on a stand, all enclosed inside a cardboard housing. 20mL of the DISMT reagent was added to the vessel through the sampling port using a 20mL syringe. To acidify the reagent and initiate the experiment, 2µL of 0.75M HCl and 2µL of 0.75M NaOH were added respectively. The impeller speed ranged between 50rpm and 2000rpm (4×10^{-6}W L^{-1} – 0.27W L^{-1}).

The impact of fill volume, impeller positioning and number of impellers on mixing time was also investigated over the same range of speeds. Using the same impeller positioning, a volume of 14mL and 12mL were tested. At 14mL the top impeller was sitting on the same level as the surface of the liquid. At 12mL, two impellers were submerged under the liquid level with the top impeller just above the surface. Additionally, keeping the fill volume at 20mL the new adjustable impeller shaft was used to adjust the positions of the three impellers to achieve a wider or narrower spacing. The middle impeller was kept in the same place and the top and bottom impeller were moved apart to achieve an inter impeller spacing of $1.5Di_{20mL}$ and $0.60\ Di_{20mL}$ respectively. Finally at a fill volume of 20mL, mixing time was measured using just one impeller that was positioned in place of where the bottom and middle impeller sat on the original impeller shaft.

2.6.3.3 Mixing Time Experiments in a 24-Well Deep Square-Well Plate

Mixing time experiments in the replica of a single 24-well deep square-well plate were conducted in a similar way to the 2L and 20mL vessel. The replica with the fixed camera attached to the plate, was placed onto a Thermomixer C shaker with an LED light panel behind it, all enclosed inside a cardboard housing. The well was filled with 2mL of the DISMT reagent and mixing time was measured over a shaken speed of 300rpm – 1200rpm. To acidify the reagent 2µL of 0.075M HCl was added to the well. To initiate the experiment 2µL of 0.075M NaOH was added. These experiments were repeated for a fill volume of 2.5mL, 3mL, 3.5mL and 4mL. The volume of HCl and NaOH used in the experiments was increased accordingly to 2.5µL, 3µL, 3.5µL and 4µL respectively.

2.6.4 Image Processing for Mixing Time

All images were processed using a Matlab code, developed by Rodriguez *et al*. (2014) which was modified to be able to crop out areas of the images not suitable for measurement. The red, blue and green (RGB) components of the pixels in the remaining selected area, representing the coloured liquid in the vessel only, was analysed using the modified script.

The pixel value of each of the RGB components, which ranges from 0 to 255, was measured and the standard deviation between the pixels in the area was calculated for each image over the course of the experiment. For this study, the green channel was selected to distinguish between mixed and non-mixed pixels and the final mixing time value was estimated as the time taken for the standard deviation between the green pixels to reach ±5% of the last standard deviation value, where upon complete mixing was assumed to have occurred. This approach to mixing time measurement helps to remove subjectivity of the naked eye.

2.7 Particle Image Velocimetry

2.7.1 PIV Introduction

2D Particle Image velocimetry (PIV) is a non-invasive laser optical technique typically used to assess fluid dynamic properties such as instantaneous velocity, vorticity, turbulence and shear within an environment. This technique was applied to the 20mL vessel where a whole field of view could be observed and the impact of different impeller speeds on the velocity, vorticity and flow patterns in the vessel could be investigated. To visualise the flow in a fluid, the fluid is first seeded with a suitable tracer and a laser is used to illuminate the suspension by pulsing a laser light twice over a short but measurable period of time. Two images are taken using a high speed camera which captures the trajectory of the light scattered by each tracer particle between the pulses and calculates the velocity of the fluid. The images are then processed using software which splits the captured image into several 'interrogation' areas in order to calculate the motion of the tracer particles. Each interrogation area should have a sufficient number of particles seeded, typically between 3-8 particles, in order to allow the software to produce reliable velocity vector images.

2.7.2 PIV Experimental Setup

The key components of the setup for PIV consisted of the 20mL vessel to be studied, a high speed intensified camera, which was positioned in front of the vessel and a continuous

green diode laser which was positioned perpendicular to the vessel and at 90° to the laser. A photographic image showing the setup of the PIV experiments for the 20mL vessel is shown in Figure 2.6. The 20mL vessel was filled with 20mL of sterile water and seeded using 50µm Rhodamine-coated Polymethyl methacrylate spheres particles (Dantec, Denmark). A wooden base, constructed at the UCL Biochemical Engineering Workshop, was fixed to the bottom of the vessel to secure it during movement of the impeller shaft. A rectangular glass trough was used to encase the base and the vessel and was filled with sterile water to surround the vessel and reach a level just above the height of the liquid in the vessel to avoid optical distortion caused by a curved surface. A 300 mW Nd:Yag diode laser with a 532 nm wavelength set up in front of the vessel, was aligned to the middle of the impeller shaft and a Dantec Dynamics camera was used to capture image pairs with a short time interval of 5µs. A 570 nm orange cut-off filter was used on the camera to minimise laser reflections caused by metallic components in the vessel. The motor used for the 20mL vessel was fixed in place above the glass trough and vessel. To obtain images with the impeller in the same position, a magnet was fixed to the rotating head, which holds the impeller shaft, and a magnetic Hall-effect encoder and timing box was synchronised with the camera to trigger the capture of images with each revolution of the impeller shaft. The Dantec Dynamic Studio software was used to view and digitise the acquired images. Velocity vector plots were obtained for each condition using the average of 1000 images to get an ensemble average image which was then processed using Matlab.

Phase-resolved PIV experiments were conducted on the 20mL vessel to determine the velocity characteristics at different impeller speeds, ranging between 50rpm and 2000rpm (4×10^{-6} W L^{-1} – 0.27W L^{-1}). Measurements of the vertical plane of the vessel were done both with and without the presence of baffles in order to compare flow dynamics in both cases. Experiments with the baffles are more representative of conditions during a heat extraction experiment however the experiments without the baffles allowed the laser to pass through the liquid without obtrusions thus providing full visualisation of the flow patterns in one half of the vessel. Both set of images will be compared and analysed in Chapter 4.

2.7.3 Image Processing for PIV

Prior to image capture during experimentation, a sample image was taken once the setup was ready. A mask was constructed over the sample image to eliminate areas without liquid and was subsequently applied to all images. These images were digitised over a series of small interrogation spots to provide vector related information which was then analysed by Matlab. The velocity vectors and vorticity profiles were normalised to tip speed.

2.8 Conclusive Remarks

In this chapter an overview of the upstream processes, scale-down models and fluid dynamic studies was provided. The 20mL vessel and 24-well deep square-well plate was characterised and used to mimic the heat extraction process at the 2L scale. The dimensions of the vessels have been provided and the methodology on fermentation, centrifugation and heat extraction at the different scales has been described. Details on the mixing time experiments conducted at all three scales have also been provided as well as PIV experiments on the 20mL vessel.

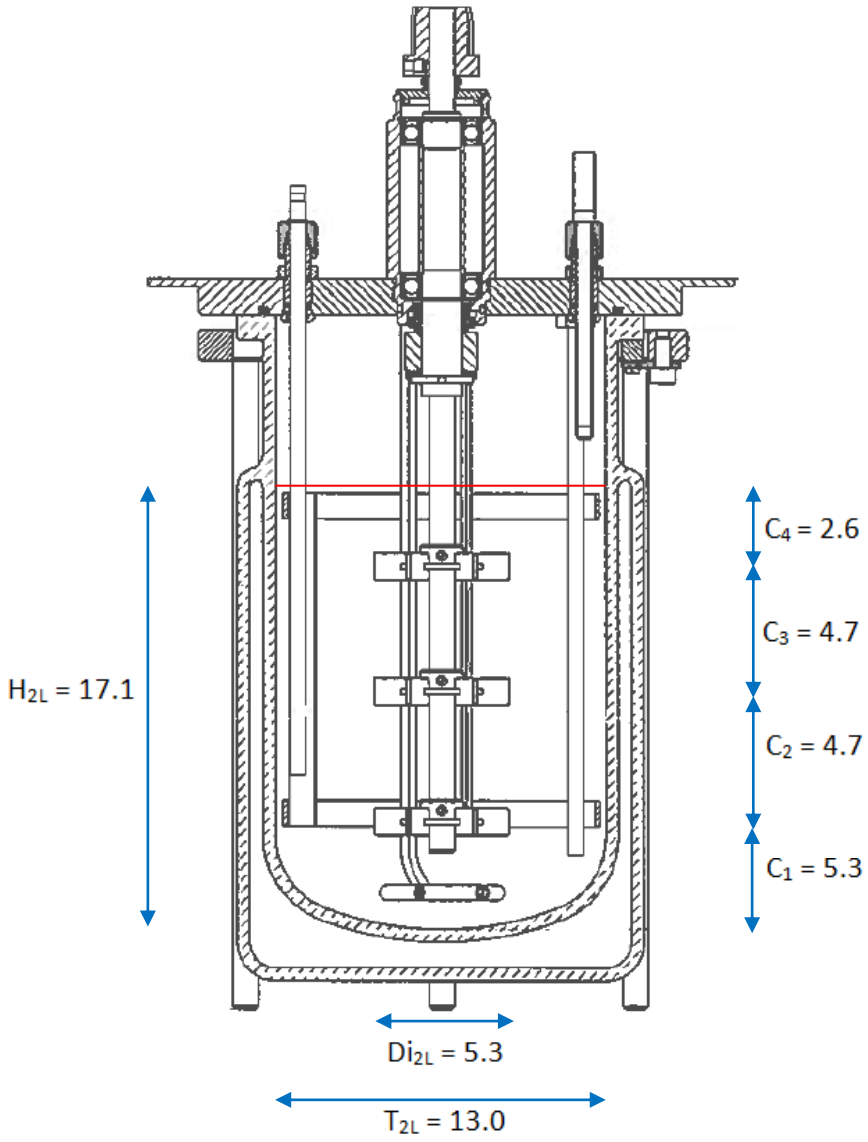

Figure 2.1: Mechanical drawing of the 2L extraction vessel showing the positioning of the impellers and the key dimensions (in cm). H_{2L} represents the height of the liquid. The red line indicates a fill volume of 2L.

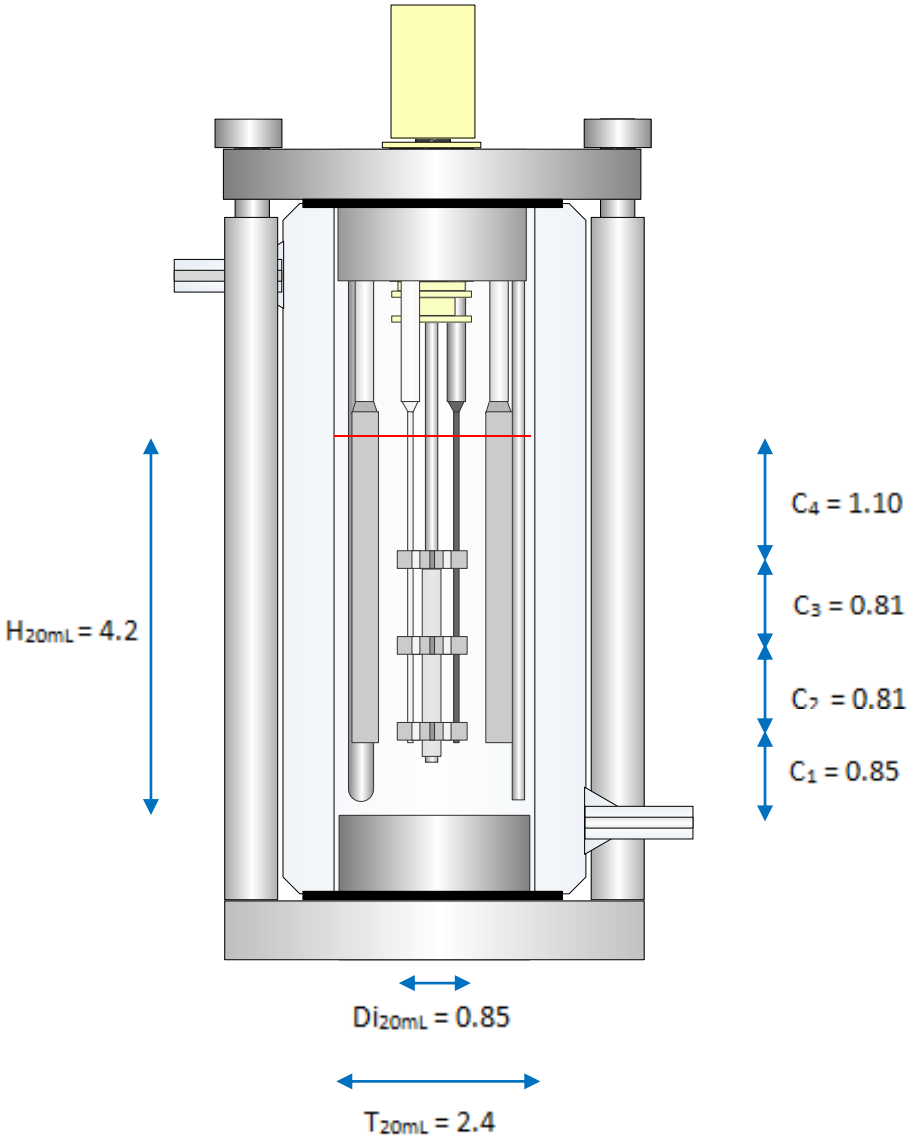

Figure 2.2: Schematic diagram of the 20mL extraction vessel designed on Microsoft Visio, showing the key dimensions (in cm) and the positioning of the impellers on the original impeller shaft. The red line indicates a fill volume of 20mL.

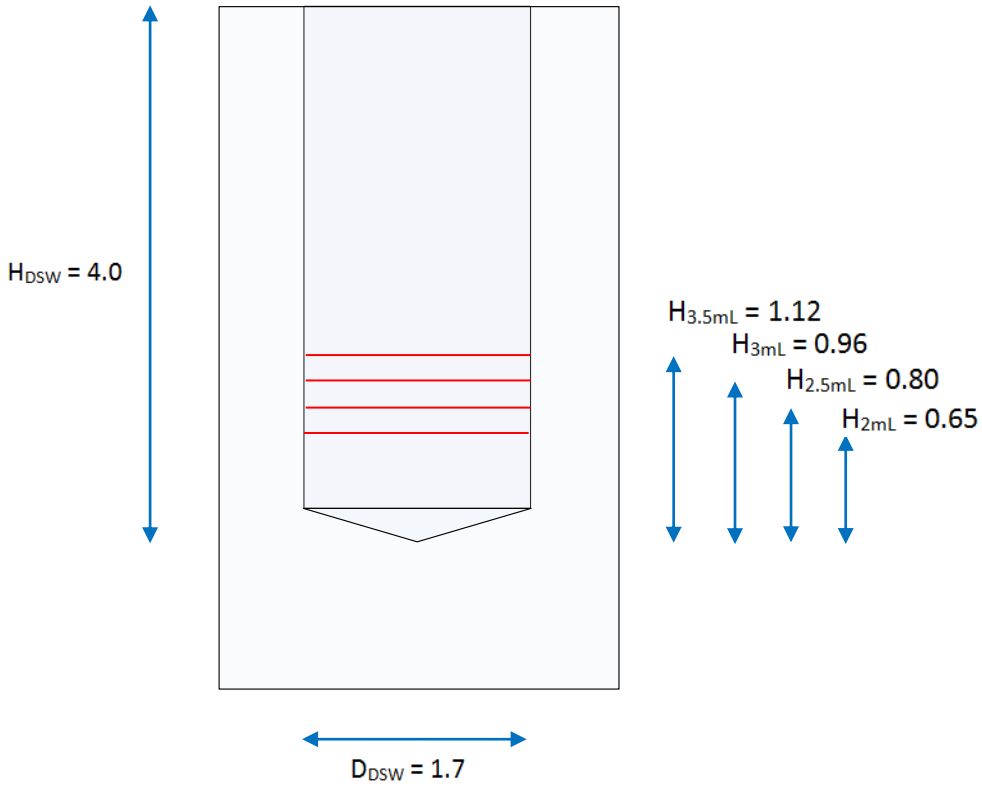

Figure 2.3: Schematic diagram of a single well in 24-well deep square-well plate, showing the key dimensions (in cm). H_{2mL} represents the height of the liquid at 2mL fill volume. Similarly $H_{2.5mL}$, H_{3mL}, and $H_{3.5mL}$ represent the height of the liquid at 2.5mL, 3mL and 3.5mL fill volume

A)

A1	A2			A5	A6
		B3	B4		
		C3	C4		
D1	D2			D5	D6

B)

A1	A2	A3	A4	A5	A6
B1	B2	B3	B4	B5	B6
C1	C2	C3	C4	C5	C6
D1	D2	D3	D4	D5	D6

post extraction

post acid precipitation

C)

A1					A6
		B3			
			C4		
D1					D6

Figure 2.4: Top view of the 24-well deep square-well plate indicating which wells were typically sampled from for **A)** Fab' quantification, **B)** total protein and dsDNA quantification and **C)** protein L purification for both post extraction and post acid precipitation

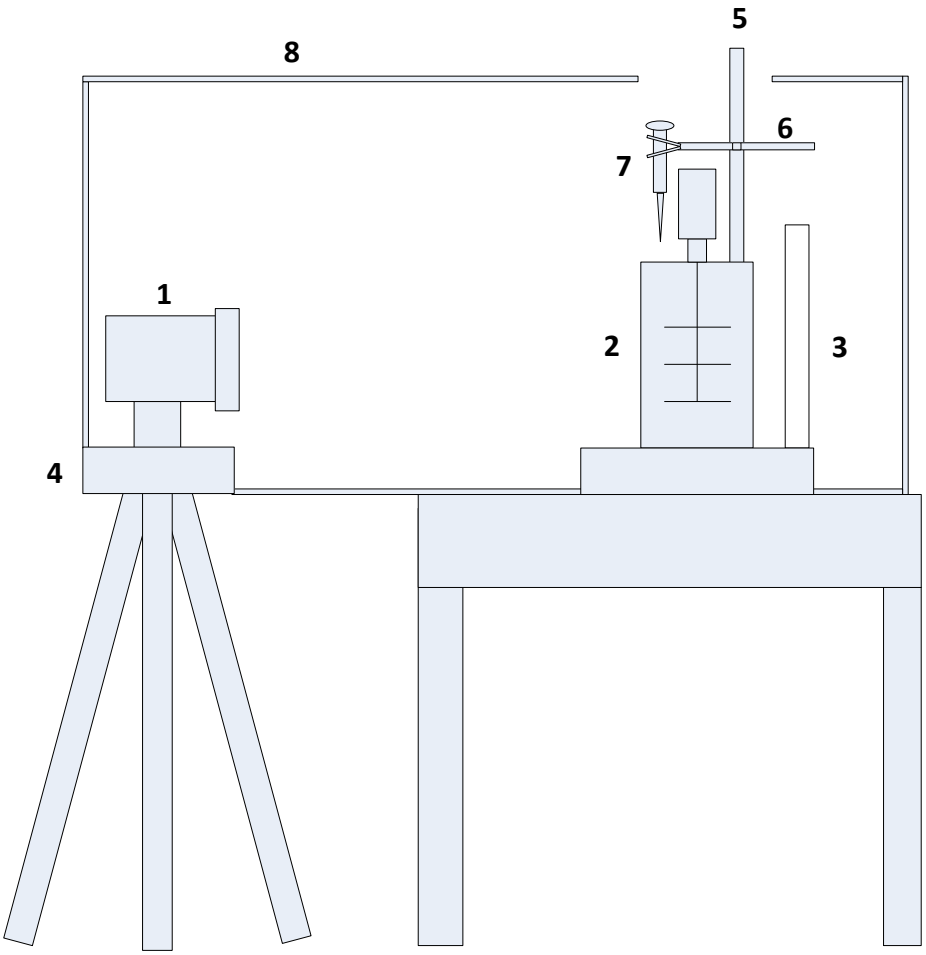

Figure 2.5: Schematic diagram of the setup for the mixing time experiments: **1)** high speed camera; **2)** mixing model (either 2L vessel, 20mL vessel or deep square well and shaker system); **3)** LED white light; **4)** tripod; **5)** clamp stand; **6)** clamp; **7)** pipette; **8)** cardboard housing

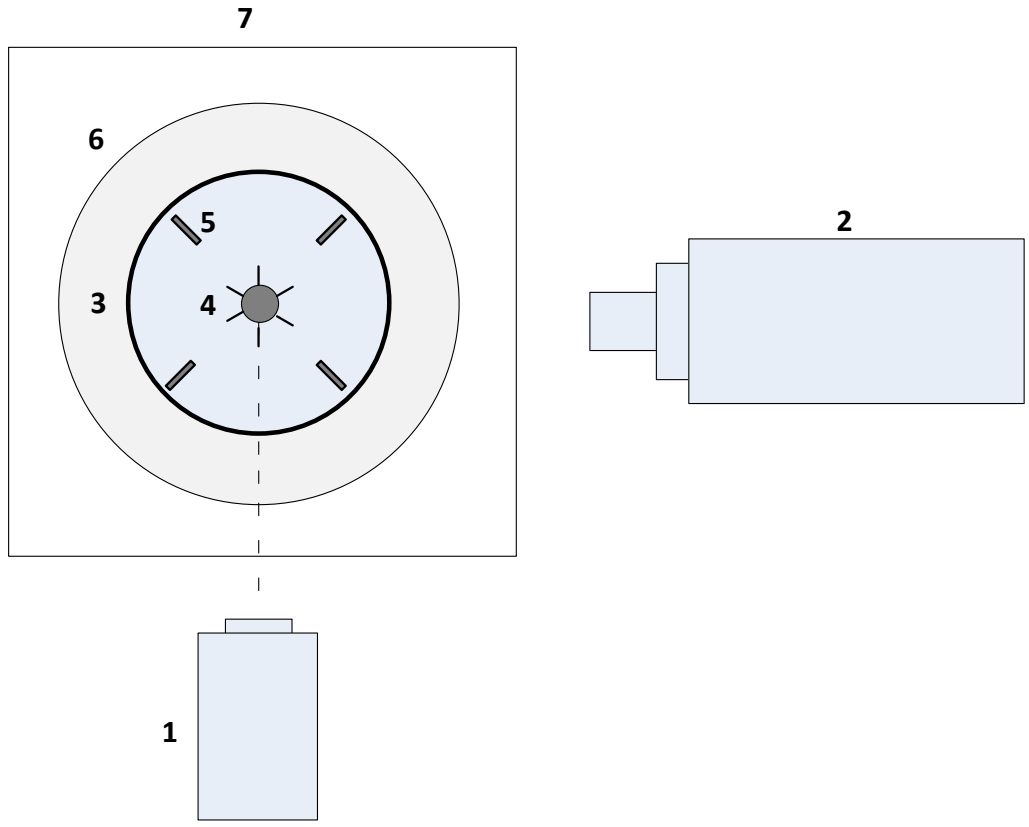

Figure 2.6: Schematic diagram showing a top view of the setup of the 20mL vessel for the PIV experiments: **1)** ND:Yag laser; **2)** high speed camera; **3)** 20mL vessel; **4)** impeller system; **5)** baffles; **6)** wooden base; **7)** glass trough

Chapter 3

Using a DoE Approach to Investigate the Effects of Different Operating Conditions on the Extraction Performance

3.1 Introduction and Aims

The benefits of the use of reliable scale-down models to predict the performance of a primary recovery process for a Fab' fragment has been discussed in Rayat *et al*. (2010) and Aucamp *et al*. (2014). Understanding the effect of and interactions between different process parameters on this unit operation at the lab scale is the first step in gaining a wider knowledge of which factors will have the most impact on the performance. This will ultimately help inform decisions when scaling down this process. The advantages of using a design of experiment (DoE) approach, which allows the study of multiple design elements on the process performance, have been summarised in Ellert and Vikström (2014) and have been applied to scale-down studies for bioprocesses such as Li *et al*. (2006), Islam *et al*. (2007) and Grant *et al*. (2012). The application of DoE is an efficient strategy to significantly reduce the time and resources needed to study the effect of individual factors one at a time and the knowledge that is gained from the experiments can then be used to select and focus on specific experimental conditions which may be replicated in a representative scale-down model.

This chapter aims to investigate the impact that different operating conditions have on the extraction performance at the 2L scale. The three parameters evaluated are specific power input (W/L), extraction hold duration (hours) and extraction hold temperature (°C). The heat extraction process is essentially a heating and mixing process where *E.coli* cells are suspended in tris-EDTA buffers and heated to an elevated temperature in order to permeabilise the outer membrane of the cell. The cells and the buffer components must be well mixed, with an even distribution of heat throughout the mixing vessel, to ensure a homogenous state. The DoE parameters were chosen in order to determine the importance of both heating and mixing on the process.

The specific objectives of this chapter are:

- To understand properties of material obtained from 20L scale fermentations using the *E.coli* W3110 containing plasmid A33 Fab'
- To investigate the impact of specific power input, extraction hold temperature and extraction hold duration on the 2L extraction process using a DoE approach
- To select the operating conditions which have the most impact where the Fab', total protein and dsDNA titres have been most affected and to use those conditions for scale-down studies.

3.2 Experimental Approach

For the fermentation process, the industrial *E.coli* strain W3110 containing plasmid pTT0D A33 IGS2 was kindly provided by UCB (Slough, UK). The seed train consisted of the pooling and splitting of 5 shake flask cultures which were used to inoculate three 20L vessels. The cells were induced using IPTG at the end of the exponential phase and then harvested 40 hours after induction as described fully in section 2.2.2. Samples were taken for DCW and cell viability measurements as well for Fab', total protein and dsDNA concentrations as described in section 2.5. Small scale extractions in Eppendorf tubes were performed on harvest samples as described in section 2.4.4.

After harvesting the cells, the pooled material was processed using a disc stack centrifuge according to section 2.3.1 and further samples were taken from the heavy and light phase obtained from centrifugation, to calculate % clarification and to observe the extent of shear on the cells during this unit operation. Fab', total protein and dsDNA concentrations were also determined. Following the fermentation and disc stack centrifugation operations, a DoE was performed. The heat extraction experiments were conducted in ten identical 2L glass vessels using equal amounts of heavy phase material and extraction buffer, as descried in section 2.4.4. Samples taken after heat extraction and acid precipitation were used to determine Fab', total protein and dsDNA concentrations. This data was then input into the DoE MODDE 9.1 software to see how the different factors interact with each other. Post

extraction samples were purified using protein L chromatography according to section 2.5.4.2 and ran on SDS-PAGE gels, according to section 2.5.8, to look at the purified Fab' profiles.

The impeller speed calculations (N), have been calculated for the 2L vessel for each specific power input (P/V), using equation 3.1.

$$N = \sqrt[3]{\frac{P}{Po.\rho.Di^5}} \qquad \text{[Equation 3.1]}$$

The power number (Po) was determined as 5 for a single Rushton impeller under turbulent conditions (Hewitt and Nienow, 2007), which was assumed for this study. The impeller has a diameter (D_i) of 0.053m, the total working volume was 2L and the density (ρ) of the liquid is 1000kg m^{-3}. For 0.23W L^{-1}, the calculated speed (N) was 250 rpm, for 0.05W L^{-1}, the calculated speed (N) was 150 rpm and for 0.41W L^{-1}, the calculated speed (N) was 305 rpm.

To get an indicator of the type of fluid flow in the vessel, the Reynolds number (Re) was calculated using equation 3.2.

$$Re = \frac{\rho.N.Di^2}{\mu} \qquad \text{[Equation 3.2]}$$

The viscosity (μ) of the liquid was assumed to be 0.001kg m Ns m^{-2}. The Re was calculated to be 7100, 11700 and 14300 for 0.05W L^{-1}, 0.23W L^{-1} and 0.41W L^{-1} respectively.

Table 3.1 summarises the design of the experiments and the operating conditions for each run. Ten experiments were conducted in a two level full factorial DoE design with 2 midpoint replicates as seen in Figure 3.1. The conditions for an extraction, run at the midpoint of the DoE, were at 60°C for 10 hours at a specific power input of 0.23W L^{-1}. This condition was chosen from baseline data used by industry (UCB). The other experimental conditions chosen in the design space were based on a number of factors including using some previous understanding of the sensitivity of the heating parameters by industry whilst

also taking into account a reasonable degree of difference in values suitable for characterisation purposes. Sehdev and Spitali (2006) have shown that the particular conditions chosen for heat extraction depend on the stability of the particular antibody in question. Heat treatments on *E.coli* cells during the extraction process are usually conducted between 30-70°C but the most preferable range is considered to be between 55-60°C. The length of the heat treatment can also be varied between 1-24 hours but a preferable range is between 10 and 14 hours. For specific power input in this DoE study, a relatively large range was chosen in order to assess the effect of mixing, as this aspect is still poorly understood.

3.3 Results and Discussion

3.3.1 Fermentation

OD_{600} and % cell viability measurements were taken at different time points during the 20L fermentations and the growth curve has been plotted in Figure 3.2. The batch, exponential fed-batch and linear phases are indicated on the curve with induction taking place using IPTG at the end of the exponential fed-batch phase. It can be observed that the growth curves follow the expected trend for a microbial fermentation process. There was an initial lag in the batch growth phase as the cells adapt their metabolism from the complex media in the shake flask to the defined media in the bioreactor. The batch phase lasted for approximately 21 hours and once the carbon source was depleted, the exponential fed batch phase was initiated using 80% glycerol feed, to achieve a specific growth rate of $0.1h^{-1}$. The exponential phase lasted approximately 6.5 hours after which the cells were induced and the feed rate was kept constant at 41.25g h^{-1} to achieve linear growth. This phase lasted 40 hours and the cells were then harvested. After harvest, the fermentation culture was pooled from the three bioreactors. The final OD_{600} of the cells was 132 corresponding to a biomass concentration of $57.05g_{DCW}$ L^{-1}. The growth kinetics obtained in these fermentations are in agreement with previously obtained results for similar 20L W3110 *E.coli* Fab' fermentation processes (Ali *et al*., 2011; Perez-Pardo *et al*., 2011). Final OD_{600} and g_{DCW} L^{-1} obtained by Ali *et al*. (2011) were 117.6 and $38.9g_{DCW}$ L^{-1} respectively. Similarly, final OD_{600} and g_{DCW} L^{-1} obtained by Perez-Padro *et al*. (2011) were 111 and 47 ± $2.2g_{DCW}$ L^{-1} respectively. The relatively lower OD_{600} and biomass concentration in both of these previous

studies could be due to small variations in the media composition or control strategy, such as dropping the temperature from 30°C to 25°C approximately 24 hours after the start of fermentation, in comparison to keeping a constant temperature of 30°C throughout for this study. Additionally, Perez-Padro *et al*. (2011) maintained dissolved oxygen at 40% instead of 30% which may also have impacted overall growth kinetics. As illustrated in Figure 3.2, good reproducibility was obtained for the three fermentation runs achieving average growth rates for the batch, exponential fed-batch and linear phases of 0.235 ± 0.002hr^{-1}, 0.114 ± 0.007hr^{-1} and 0.011 ± 0.001hr^{-1}, respectively. As expected, these growth rates are slightly higher overall than those obtained by Ali *et al*. (2011) at 0.2hr^{-1}, 0.13hr^{-1} and 0.0046hr^{-1} for all three phases, respectively and for Perez-Padro *et al*. (2011) at 0.19hr^{-1}, 0.12hr^{-1} and 0.0043hr^{-1} respectively.

The % cell viability measurements were taken post induction, as described in section 2.5.3. All measurements were reproducible in nature with a coefficient of variance less than 1.5%. The cell viability decreased at approximately 50 hours into the fermentation during the linear growth phase, as shown in Figure 3.2. This is expected at this late stage of fermentation and may be caused by several factors such as unbalanced cell growth, change in cell morphology or physiology, and toxic waste build up (Andersson *et al*., 1996; Hewitt and Nienow 2007; and Newton *et al*., 2016). According to Andersson *et al*. (1996), when the maximum specific growth rate falls below 0.2h^{-1}, *E.coli* cells enter a non culturable state where the cells stop dividing but still maintain their metabolic activity therefore causing significant cell death which is responsible for the decline in cell viability. The fermentation process in this study was terminated 40 hours after induction to allow a reasonable amount of time for sufficient expression of the Fab' product, whilst still maintaining relatively good cell viabilities of above 85%. At harvest, the final % cell viability values for the three fermenters were 87.5%, 88.7% and 86%. A cell viability greater than 80% is considered good for an *E.coli* fermentation process (Sehdev and Spitali 2006). Lower cell viabilities could result in product losses and in a build-up and release of intracellular impurities, leading to an increase in broth viscosity and subsequent downstream processing challenges. These % cell viability measurements are in agreement with previous studies for 20L Fab'

fermentations using the W3110 *E.coli* strain in similar fermentation conditions (Aucamp *et al*., 2014).

The average Fab', total protein and dsDNA concentrations measured in the supernatant of the harvested material were 0.249 ± 0.011g L^{-1}, 3.14 ± 0.03g L^{-1} and 44.76 ± 4.68g L^{-1}. These concentrations represent the Fab' titre, total protein concentration and dsDNA concentration, respectively, that have been released into the media over the course of the fermentation. The presence of Fab' in the supernatant throughout fermentation is not uncommon. Some cells lose their structural integrity with time and therefore periplasmic proteins leave the outer cell membrane and are released into the media (Bäcklund *et al*., 2008) causing some product leakage, while still maintaining protein producing functions. Equally, as the fermentation progresses, Fab' is released into the media due to whole cell lysis. Like % cell viability, the amount of total protein and dsDNA in the supernatant is a good indicator of whether cell lysis is occurring. The amount of total protein being measured includes Fab' as well as other periplasmic and cytoplasmic proteins. dsDNA is present only inside the cytoplasm and therefore is released if there is damage to the inner cell membrane which typically occurs when there is whole cell disruption.

The Fab' titre in the harvest sample, measured using the 1mL eppendorf tube extraction method, was 0.980g L^{-1}. This method was used to measure the quantity of Fab' inside the periplasmic space of the cell and it takes into account any dilution effects during the 1mL extraction process, and adjusts for them as described in equation 2.3. This titre is assumed to represent the maximum concentration of Fab' inside of the cells that is available for extraction in the lab scale heat extraction process. The total amount of Fab' produced by the cells during fermentation is the sum of the periplasmic Fab' and the supernatant Fab', giving a maximum productivity of 1.229g L^{-1}. These values for Fab' titres lie within ranges published in literature value, where expression levels of Fab' fragments can reach up to 2g L^{-1} in *E.coli* cells (Andersen and Reilly, 2004). This indicates that in this study, 20% of the Fab' was released into the media at the point of harvest and could not be recovered in subsequent steps. This is in agreement with Ellis and Humphreys (2011) who reported a Fab' loss of 22% when using the periplasmic extraction method to obtain Fab' titre. Ali *et al*.

(2011) obtained a 45% Fab' loss with a final total Fab' titre of 0.990 ± 0.03g L^{-1}. This significantly higher proportion of Fab' lost to the supernatant compared to the 20% in this study could be due to the method used to obtain total Fab' measurements. Ali *et al*. (2011) used adapted focused acoustics instead of the extraction method. This technique operates in the megahertz range (Wenger *et al*., 2008), to deliver highly focused acoustic energy into a sample to significantly disrupture the whole cell causing a greater release of Fab' compared to extraction methods, however it also creates micronized cell debris formation, making the Fab' more difficult to purify in the downstream processing steps. Focused acoustics has been used in other experiments (Li *et al*., 2012; Li *et al*., 2013; Perez-Pardo *et al*., 2011) to measure Fab' titre as it mimics high pressure homogenisation, a unit operation used at large scale to release Fab'. This study however focuses on using the heat extraction step and therefore uses small scale periplasmic extractions to mimic the large scale process.

3.3.2 Disc Stack Centrifugation

The disc stack centrifugation process achieved a dewatering level of 63.5%, calculated using the method described in section 2.2.3.4. Fab' concentration was found to be 0.282g L^{-1} in the light phase and 0.896g L^{-1} in the supernatant of the heavy phase. This 260% increase in the Fab' titre in the heavy phase supernatant compared to the 0.249 ± 0.011g L^{-1} in the harvest supernatant is partly due to the concentration effect of the dewatering process. However a significant reason for such an increase could be due to the unavoidable shear experienced by the cells during the discharge step in the disc stack centrifuge. The cells exit the centrifuge at high velocity and impact on collection surfaces, causing cell disrupture and release of intracellular components (Chan, 2006). The Fab' titre in the light phase increases by 13.3% compared to the harvest supernatant, which indicates that little shear occurs inside the feeding pump inlet. This is attributable to the presence of a hydro-hermetic seal in the feed zone of the disc stack centrifuge which was used in these experiments. This facilitates minimal disruption of the cell due to the flooding of the inlet area which allows the feed to be introduced beneath the level of the liquid so that it can reach the acceleration required without a significant release of energy. The flooded inlet therefore dissipates the energy generated inside the centrifuge and prevents applying significant

shear to the cells. The majority of the Fab' product is therefore present within the heavy phase component and is consequently available in the subsequent heat extraction step.

Total protein concentration in the light phase and in the supernatant of the heavy phase was found to be 3.98g L^{-1} and 15.06g L^{-1} respectively after centrifugation. This represents a 380% increase in total protein in the heavy phase supernatant compared to the harvest concentration of 3.14 ± 0.03g L^{-1} as well as a 26.8% increase in concentration in the light phase compared to at harvest. This follows the trend seen for Fab'. The concentration of dsDNA obtained in the light phase and in the supernatant of the heavy phase was 44.45g L^{-1} and 697g L^{-1} respectively. This indicates almost no change in dsDNA concentration in the light phase compared to the harvest concentration of 44.76 ± 4.68g L^{-1} but a significant increase of 1460% in the supernatant of the heavy phase compared to at harvest. The negligible release of dsDNA in the light phase, compared to Fab' and total protein content, indicates that only the outer cell membrane is weakened by the fermentation process and this is slightly further disrupted by the feed zone of the centrifuge with little damage to the inner cell membrane. The very large increase in dsDNA in the supernatant of the heavy phase also suggests that the inner cell membrane is kept relatively intact after harvest and is disrupted only by the shear exerted on the cells after discharge from the centrifuge.

3.3.3 Fab' Extraction using DoE

Examples of the heat profiles and impeller speed are shown in Figure 3.3 for experiments number 1, 5 and 8. The vessel was kept at 18°C before and after the extraction step is complete and the time taken to go from 18°C to the required temperature and back down to 18°C was kept constant at 1.5 hours for all experiments. Samples were taken after extraction and after acid precipitation and the data obtained from the analytical measurements were input into the MODDE software to estimate the coefficients of the model by applying a regression model using the partial least squares (PLS). Figure 3.4 shows the DoE summary plot which reviews the model in terms of summary of the fit, R^2, Q^2, model validity and reproducibility.

The R^2 component represents the model fit. The Q^2 component is an indicator of how well the model can predict new experiments and is a superior factor to determine the usefulness of the model compared to R^2. A model with a R^2 of 0.75 or above indicates a rough but stable and useful model and a Q^2 of 0.5 or above also indicates a good enough model to draw conclusions from (Eriksson *et al*., 2008). The model validity indicates if there are any statistically significant model problems and a low validity can occur despite a high Q^2 which may be as a result of high sensitivity in the test. The reproducibility is an indicator of the variation of the replicates compared to the overall variability and should ideally be higher than 5. Q^2 however is the most sensitive indicator for a good model and is therefore consulted first. Based on the summary statistics, the first five models for Fab', total protein and dsDNA after heat extraction and Fab' and total protein after acid precipitation are all considered to be good models overall and may be used for analysis.

The response 4D contour plots for the first three models are shown in Figure 3.5, Figure 3.6 and Figure 3.7 for Fab' titre, total protein concentration and dsDNA concentration, respectively. These plots display the effect of all three variables for the different responses. Figure 3.5 shows three individual contour plots, A, B and C which represent the three different specific power inputs of 0.05W L^{-1}, 0.23W L^{-1} and 0.41W L^{-1} respectively. The contour plots show that extraction temperature had the highest impact on Fab' extraction titres, followed by extraction hold duration and finally the specific power input. Figure 3.5A shows that at the lower end of the temperature range, at 55°C, the Fab' titre reaches a maximum of 1.1g L^{-1}. The total amount of Fab' produced by the cells was determined to be 1.229g L^{-1} which indicates that 90% of the Fab' that could be released from the periplasm has been extracted in the 2L extraction process within this DoE experiment. The extraction process therefore has the potential to be more efficient and as the trends in the contour plots suggest, higher titres may be achievable at an extraction temperature lower than 55°C. Considering the DoE data only, the optimal temperature needed for Fab' release, regardless of the duration of the extraction process is 55°C. At this temperature, there is sufficient heat available to significantly aid the disruption of the outer membrane of the *E.coli* cell to help release the Fab' (Katsui *et al*., 1982). The Fab' protein itself is undamaged by the heating process at 55°C due to its relatively high melting temperature of 79°C (Barata *et al*., 2016).

The duration of the extraction process therefore has very little effect on the Fab' titre at this low temperature. As the extraction temperature increases however, the effect of the extraction duration begins to have a significant impact on Fab' measurement. Titres are almost 30% higher when the extraction hold duration is 6 hours compared to 14 hours. This is because as the temperature is elevated, such as when it approaches 65°C, the Fab' begins to denature but only at a very slow pace. This is in agreement with studies conducted by Humphreys *et al*. (2007) which demonstrated the unfolding of the Fab' at 64°C. At these higher extraction temperatures, it is assumed that the heat combined with the tris-EDTA buffer facilitates an even greater permeabilisation of the outer cell membrane thereby releasing even more of the Fab' product from the periplasm. However, extended exposure of the Fab' to the elevated temperatures causes more of the Fab' to lose its structural integrity and therefore be damaged. It is possible that after unfolding, some Fab' binds to other proteins through hydrophobic interactions, and therefore the Fab' is not detectable by analytics. The shape of the contour lines further indicates that the higher the extraction temperature, the faster the denaturation process takes place. Therefore to ensure that significant amounts of Fab' product is not lost, a shorter extraction should be run at higher temperatures when not considering any other factor.

Comparison of Figure 3.5A, B and C shows that the specific power input has the least influence on the amount of Fab' released as there is minimal difference between the three plots. This suggests that there is no real advantage of running the extraction at a higher power input because increasing the power input does not appear to impact the Fab' release process. It is assumed that the degree of mixing and homogeneity of the cell suspension may therefore similar for all three conditions and the degree of heat and buffer distribution needed to lyse open the outer membrane of the cell can be sufficiently achieved at the lowest specific power input of 0.05W L^{-1}. The Reynolds number (Re) for each specific power input was found to be 7100, 11700 and 14300 for 0.05W L^{-1}, 0.23W L^{-1} and 0.41W L^{-1} respectively. Fluid flow is usually considered to be turbulent at a Re value above 10,000 (Hewitt and Nienow, 2007) however in practise, this must be determined experimentally on the individual bioreactor system and impeller configuration. Plotting a power curve with Re against mixing time or dimensionless mixing time can help to estimate the different flow regimes and identify when turbulence is achieved. Although 0.05W L^{-1} would be considered

to fall in the transitional regime, the data from Figure 3.5 suggests that perhaps a turbulent, or well mixed state is indeed achieved but further studies are needed to verify this. Varying the speed of the impeller therefore does not appear to impact extraction for the range studied in this DoE experiment.

Figure 3.6A, B and C show the contour plots that illustrate the effect of all the factors from the DoE experiment on the total protein concentrations post extraction obtained at the different specific power inputs of 0.05W L^{-1}, 0.23W L^{-1} and 0.41W L^{-1} respectively. The contour plots show a similar overall trend for the total protein concentrations as observed previously for Fab'. In this case however, the specific power input has a marginal impact on total protein concentration with protein concentration increasing as the specific power input increases. The highest concentration of total protein of 3.2g L^{-1} can be measured at the lowest temperatures of 55°C and at an extraction duration of 6 hours. This plot shows that the total protein concentration is more sensitive to extraction duration than Fab', especially at the lower temperatures tested. This difference in trend may be due to the fact that different proteins have different melting temperatures which are approached over a range of different temperatures. Therefore different proteins start to denature at different times, some sooner than others, throughout the course of the extraction, and therefore may no longer be detectable by the Bradford assay.

Comparison of Figure 3.6A to B and C indicates that specific power input, and hence higher speeds, may cause some level of further disruption to the cells during the extraction process because higher power inputs result in slightly higher total protein concentration overall. It is unclear why as the specific power input increases, the total protein concentrations increases overall, whereas it had negligible effect on Fab' titre as observed in Figure 3.5A, B and C. It may be that a significant proportion of the available Fab' in the periplasm has already been released from the cells, which occurs irrespective of the specific power input applied, and the differences in titre are dependent on the biochemical environment within the vessel only. At higher specific power inputs, the cells may well be sheared to a small extent, releasing more host cell proteins from within the cytoplasm, resulting in higher total protein concentrations overall. The dsDNA contour plots will help confirm if this is the case. The

optimum condition, where total protein concentration is lowest, is when the temperature is 65°C, the duration of the extraction is 14 hours and the specific power input is 0.05W L^{-1}. These conditions are on the opposite side of the contour plot to the optimum spot for achieving the highest Fab' titre.

Figure 3.7A, B and C shows the contour plots illustrating the effect of all the factors from the DoE experiment on the dsDNA concentrations post extraction for all three specific power inputs of 0.05W L^{-1}, 0.23W L^{-1} and 0.41W L^{-1} respectively. These contour plots show that similar to what was observed for Figure 3.6, all of the factors affect the amount of dsDNA measured. This is different to the trend observed for Fab' and total protein. It may be that at the higher temperatures, there is a greater disruption of the cytoplasmic membrane and therefore more dsDNA is released. The melting temperature for dsDNA is a lot higher than for Fab'. Mackey *et al*. (1988), reports that for an *E.coli* strain, the melting temperature of dsDNA was 94°C. This is significantly higher than for most proteins which may explain why the dsDNA is not as sensitive to temperature as shown in the contour plot in Figure 3.7. However, at most extraction temperatures, as the duration of the extraction increases, the amount of dsDNA obtained slowly decreases. This could either be the extended effect of the heat on the dsDNA but also could be due to extended effect of the extraction buffer on the dsDNA which causes denaturation of some kind. A comparison of the contour plots in Figure 3.7A, B and C show that as specific power input increases, the amount of dsDNA obtained also increases. Although the difference between the maximum or minimum dsDNA concentrations is not significant between the plots, it is still measurable and therefore might indicate a higher level of shear is affecting the cells at the higher speeds. It is clear that there is the least amount of dsDNA present at 55°C, for 14 hour extraction duration and a specific power input of 0.05W L^{-1} and so this is the optimum area to operate in with respect to this parameter.

The contour plots for samples taken after extraction therefore have shown that when considering just periplasmic Fab', the best condition for maximum titre is at temperatures below 55°C. It is possible to achieve relatively high titres at other temperatures too; however, a shorter duration is preferred which is an advantage as it means the overall

process cycle time can be shortened. For minimal dsDNA content, running an extraction at 55°C is also optimal, but a longer extraction duration is preferred. Finally, when considering obtaining minimal total protein, an extraction temperature of 65°C and a duration of 14 hours is preferred. Since a low temperature and high extraction duration suit most criteria, this area is best to run extractions in. Considering now the specific power input too, it is clear that specific power input had little or no impact on the three variables and the lowest setting was best for all three variables. From an economical and operational point of view, this may be valuable because it means that lower impeller speeds can be used to carry out the extraction process whilst still maintaining relatively high post extraction Fab' titres, thus potentially saving on energy costs.

Figure 3.8 and Figure 3.9 show the contour plots for Fab' titre and total protein concentration respectively for the same three specific power inputs after the acid precipitation step. Figures 3.8A, B and C show that the contour plots for Fab' titre are very similar to those plotted in Figure 3.5A, B and C, indicating that the acid precipitation step does not impact negatively on the quantity of the Fab' product. This shows that Fab' is stable at low pH. Similar trends are observed for total protein in Figure 3.9, however the acid precipitation step has caused a considerable reduction in the total protein content overall. Total protein concentration does not exceed 2g L^{-1} in Figure 3.9 whereas in Figure 3.6 a maximum of 3.2g L^{-1} was noted. From a processing point of view, this is desirable because it means some of the host cell proteins have been removed from the sample therefore reducing burden on the downstream processing steps. This may be due to a number of negatively charged proteins being precipitated out by the addition of the acid, thus causing the concentration to decrease. Increasing the specific power input appears to increase the amount of total protein present slightly. The reason for this may be due to the fact that when the acid was added, it formed cell aggregates and the higher impeller speeds may have created shearing forces large enough to break these aggregates up thus disrupting the inner cell contents thus releasing more proteins.

Figure 3.10A, B and C shows the contour plots from the DoE experiment on the dsDNA concentration after the acid precipitation step for the three specific power inputs.

Observing the statistical data for the dsDNA model in Figure 3.4, the graph clearly shows that the model predicting dsDNA results after acid precipitation is very poor in comparison to the others and should not be used to draw conclusions from. However, it is noteworthy to observe from the contour plots that the range of dsDNA concentration after acid precipitation goes from 1.6mg L^{-1} to 2.6mg L^{-1}. This is a significantly small range compared to the dsDNA range observed in the sample after extraction in Figure 3.7, which corresponded to values between 300mg L^{-1} and 550mg L^{-1}. This large drop in concentration after acid addition is due to the fact that the majority of the dsDNA is precipitated out by acetic acid and is therefore no longer being detected by the Picogreen assay. The dsDNA is aggregated together with cells, thus increasing the density difference between cells and the liquid, making the following downstream processing steps such as centrifugation and filtration more efficient. Since the majority of the dsDNA is removed from the acid precipitation and subsequent steps, the choice of operating conditions for the extraction step can be based on the Fab' and total protein contour plots only.

To observe the impact of different extraction DoE conditions on the quality of the Fab' product after extraction, non-reduced and reduced SDS-PAGE gels were conducted and can be observed in Figure 3.11 and Figure 3.12 respectively. Both Figures show 10 lanes, each with five distinct bands corresponding to five different fragments of Fab' . There are observable differences across the lanes for both gels. The top band represents Di-Fab', the second band represents Fab'-light chain and the third represents the main Fab' band. The fourth and fifth bands represent the free heavy chain and light chain respectively.

In Figure 3.11, the thickest band, which is the Fab' product at 49.5 kDa, has a relatively similar intensity across the lanes with the obvious exceptions for thicker bands in lane 5 and 9 which correspond to experiments 5 and 9. Faint bands can also be seen around 65kDa which are present in these lanes but not in others. Both experiments 5 and 9 were run at 55°C with an extraction duration of 14 hours. The contour plots in Figure 3.5 are in agreement with this observation because higher Fab' titres were observed for extractions ran at 55°C.

Although Figure 3.5 showed that Fab' titres were consistently high for all extraction durations at that temperature, which corresponds also to experiments 4 and 6, the SDS-PAGE gel shows that the respective lanes 4 and 6 do not have a thicker Fab' band. This may be because the extraction duration for these experiments is significantly shorter at 6 hours. The Fab' titre obtained in this DoE study is measured using protein G chromatography, which binds to the VH3 heavy chain of the Fab' protein and separates it from other classes of proteins in the cell suspension. Protein L chromatography on the other hand, used to purify the Fab' product before running on the SDS-PAGE gels, binds typically to the light chain of the Fab'. It may be that the quality of the Fab' product is affected by the amount of time the Fab' is exposed to the elevated temperature and the heavy and light chains denature to a different extent. SDS-PAGE gels from experiments in subsequent chapters may help to understand this phenomenon better.

Figure 3.12 shows the SDS-PAGE gels for the samples which have been reduced using NEM in order to break down the disulphide bonds in the Fab' protein, resulting in free heavy and light chains which run to the bottom of the gel. The strong band at around 27kDa actually represents two separate bands for the heavy and light chain. Similar to Figure 3.11, lanes 5 and 9 show the strongest band indicating more Fab'. The band seen at 49.5kDa represents the non-reducible Fab'. Normally NEM, an alkylating agent, reacts to the thiol groups in the disulphide bonds and breaks them down. It is clear that for a small proportion of Fab', the disulphide bond has not been broken down and suggests that either there may be insufficient NEM present in the reducing agent or more likely that the heavy and light chains in the Fab' protein are bound by stronger alternative bonds in addition to the disulphide bonds. Disulphide bonds in antibodies have been known to be susceptible to chemical modifications (Liu and May, 2012) and can form non-reducible cross linked bonds such as trisulphide or thioether bonds. Differences in the non-reducible Fab' band between different lanes suggests that different extraction conditions have an impact on the Fab' structure, stability, bond formation and denaturation process. Significantly darker bands can be observed in lanes 2 and 7 which correspond to extraction experiments running for 14 hours at 65°C. This indicates that perhaps exposing the Fab' to this more extreme condition causes irreversible changes in the disulphide bonds thus making it difficult to reduce in

further steps. It is important, particularly from an industrial perspective, that any changes to the structure of the Fab' does not impact negatively on the product safety or efficacy and that all changes in Fab' structure due to extraction conditions are understood to a greater extent.

3.4 Conclusive Remarks

The fermentation results showed reproducible growth curves and good comparison to previously published data. At the point of harvest, 40 hours post-induction, the % cell viability was above 85% in all three runs and there was approximately 24% loss of Fab' to the media at harvest. During disc stack centrifugation, some Fab' was lost in the supernatant stream. During the heat extraction and acid precipitation step, different operating conditions had an impact on the concentration of Fab', total protein and dsDNA in the extract. Considering that dsDNA is removed almost completely in the acid precipitation process, analysis of Fab' and total protein content plays a more important role in deciding the optimal operating conditions for the extraction process. Shorter extraction durations favour the highest Fab' titre however, more of the other intracellular proteins are also present in the sample, therefore a trade-off must be made. Additionally, running an extraction process for a longer duration results in a lower total protein concentration overall without impacting Fab' titre, however the quality of the Fab' may be compromised if there are changes in the disulphide bond formation. A decision must be made as to which option is more economically beneficial and to do this, cost modelling work may be needed to understand whether the costs of downstream processing will outweigh the cost of product loss. Operating at a lower specific power input was recommended overall as the contour plots for Fab' and total protein showed no significant difference between the different specific power inputs. This indicates that the level of mixing may be similar between the different impeller speeds and that there is little effect on shearing of the cells and hence Fab' release, for the range studied in this work between 0.05W L^{-1} and 0.41W L^{-1}. The information gained from this baseline experiment was designed to identify the key parameters affecting extraction outputs and to identify clear effects on these outputs. Key factors highlighted by this experiment at 2L scale will be considered in subsequent experiments and will feed into the design considerations of a scale-down model. Chapter 4

looks at the design and characterisation of a miniature stirred tank bioreactor and 24-well deep square-well plate, used as scale-down models for the 2L extraction process. The mixing performance is quantified at different scales under different operating conditions.

Exp #	Extraction Duration (hrs)	Extraction Temperature (°C)	Specific Power Input (W/L)	Impeller Speed (rpm)
1	6	65	0.41	305
2	14	65	0.41	305
3	6	65	0.05	150
4	6	55	0.05	150
5	14	55	0.05	150
6	6	55	0.41	305
7	14	65	0.05	150
8	10	60	0.23	250
9	14	55	0.41	305
10	10	60	0.23	250

Table 3.1: Operating conditions for extraction experiments in the DoE design

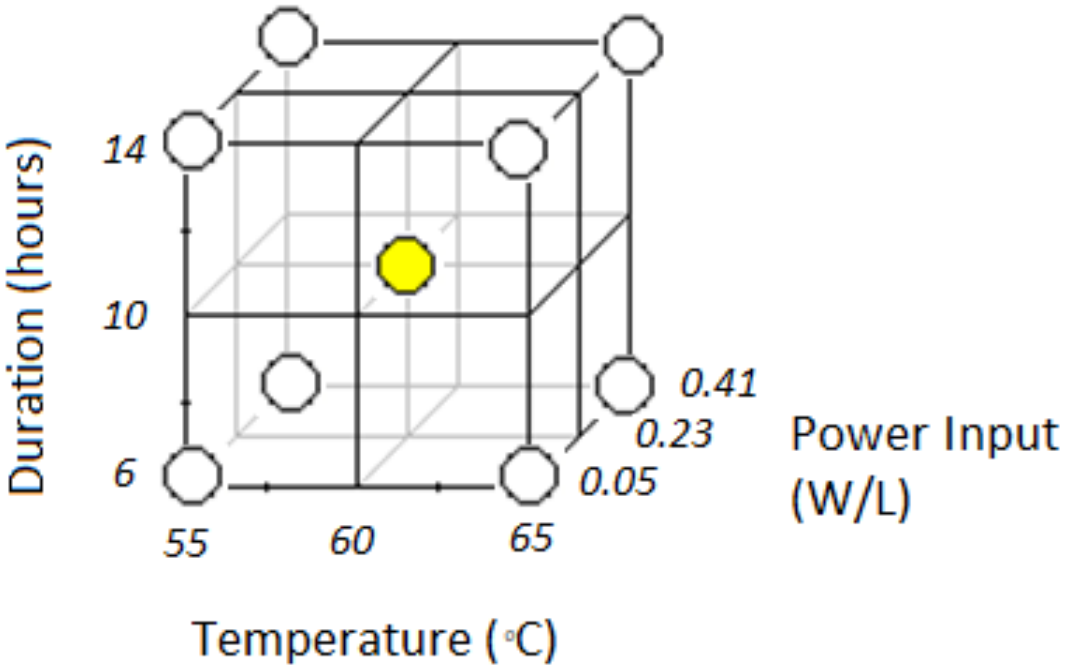

Figure 3.1: Two level full factorial screening DoE design looking at the effect of specific power input (W/L), extraction hold duration (hours) and extraction hold temperature (°C) with 2 midpoint replicates

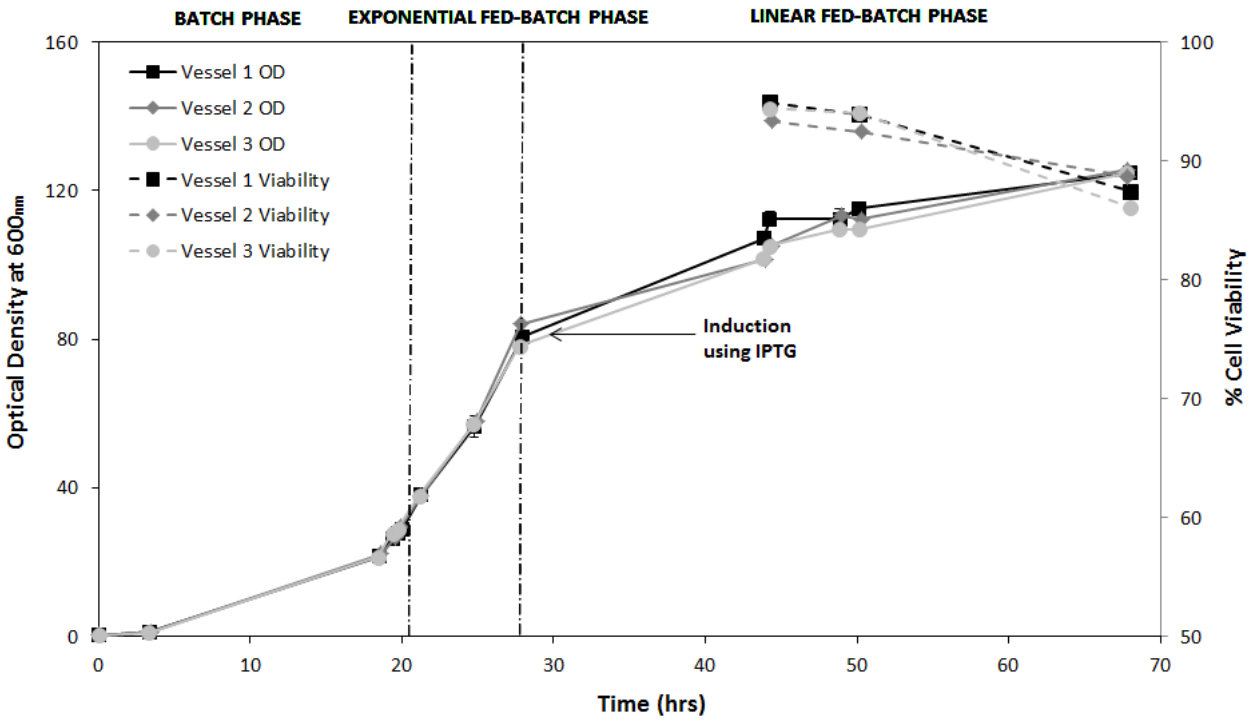

Figure 3.2: Growth curves for the *E.coli* W3110 containing plasmid A33 Fab' in three 20L vessels

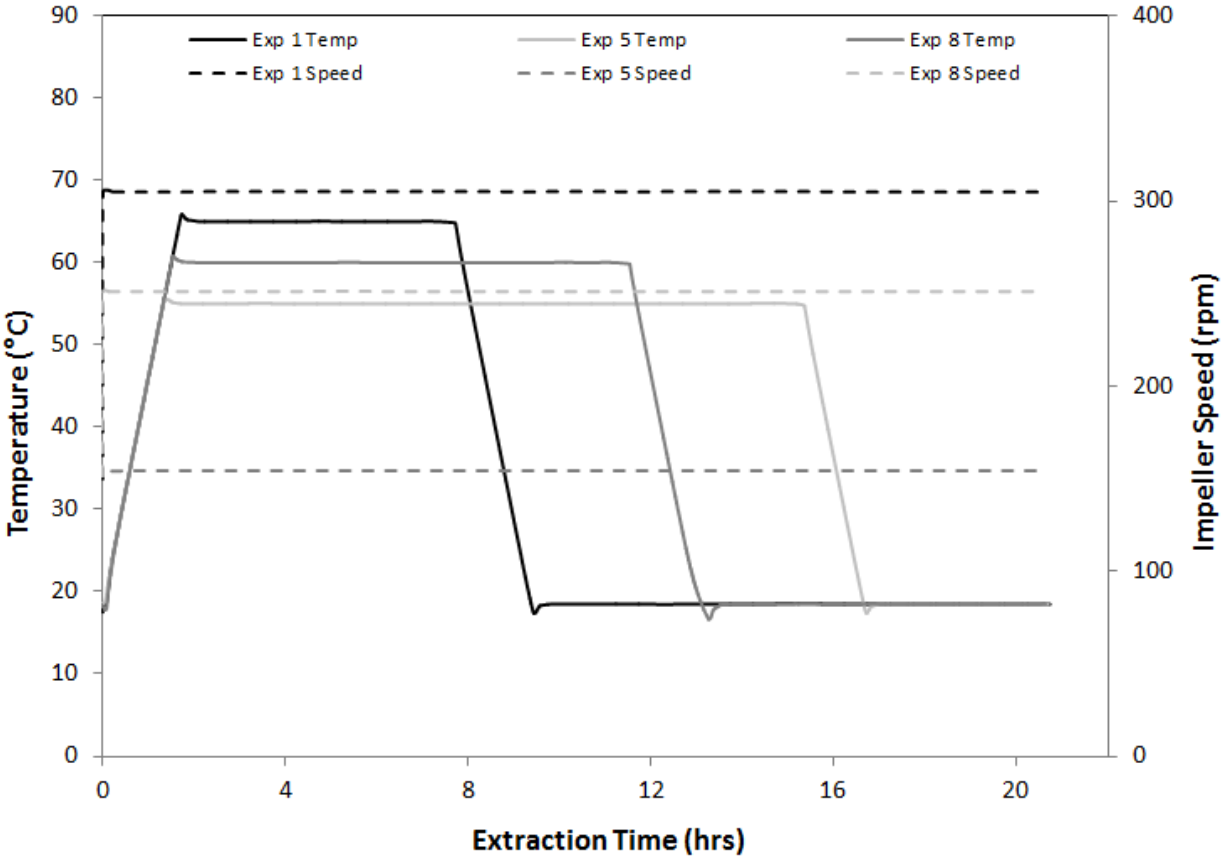

Figure 3.3: Sample heat extraction profiles and impeller speeds for Experiments 1, 5 and 8

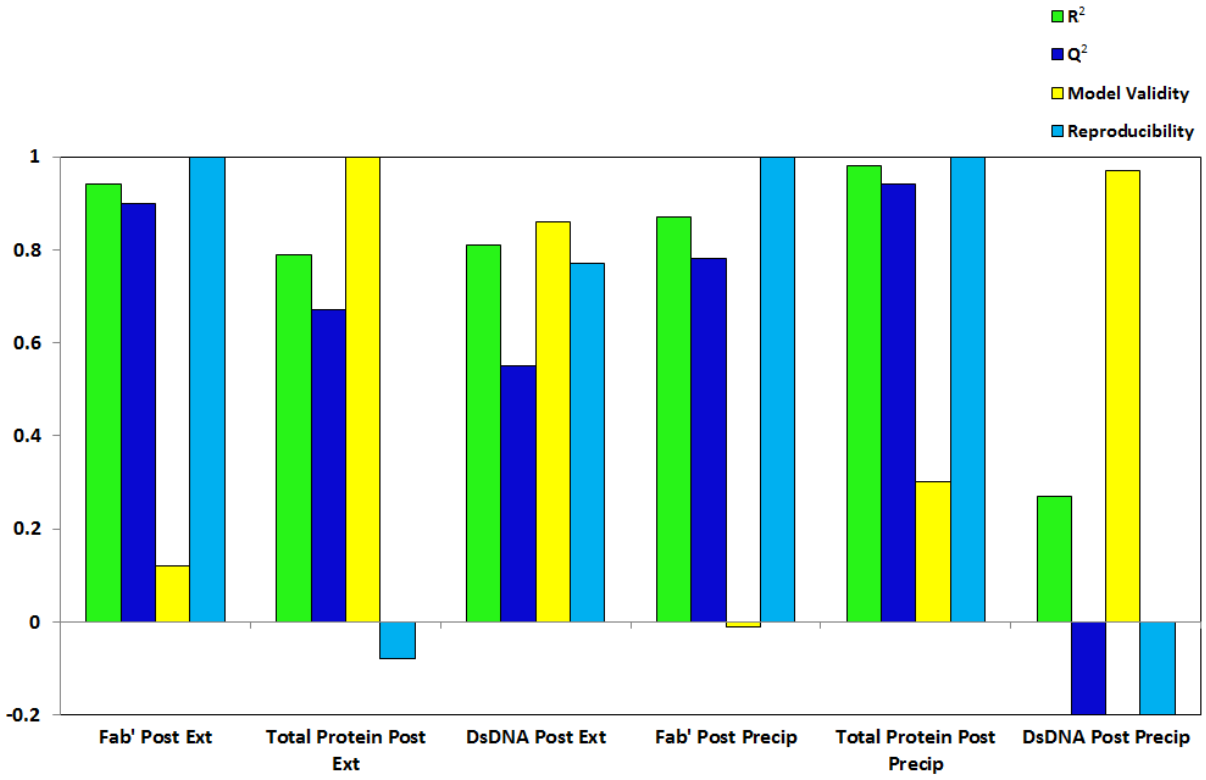

Figure 3.4: DoE summary of fit plot, using the partial least squares (PLS) model for fitting the model to the data. R^2 represents the model fit, Q^2 represents the predictability of the model, model validity is a measure of the validity of the model and reproducibility is the variation of the centre points compared to total variation

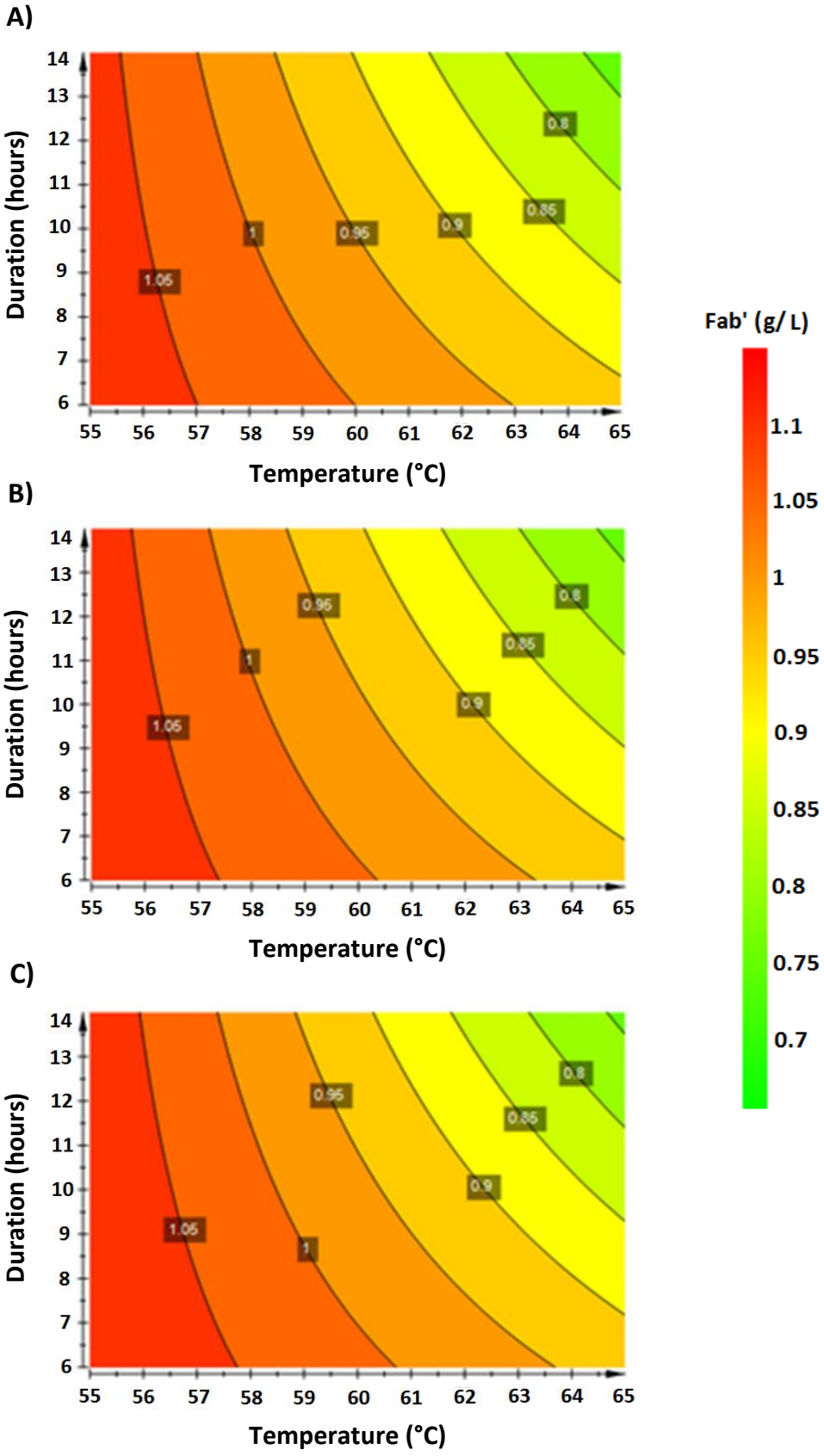

Figure 3.5: Contour plots showing the effect of extraction hold duration and temperature on Fab' titre (g L^{-1}) after heat extraction at **A)** 0.05W L^{-1}; **B)** 0.23W L^{-1}; **C)** 0.41W L^{-1}. Maximum Fab' titre in 1mL extractions was 1.229g L^{-1}. R^2 and Q^2 are 0.94 and 0.9, respectively

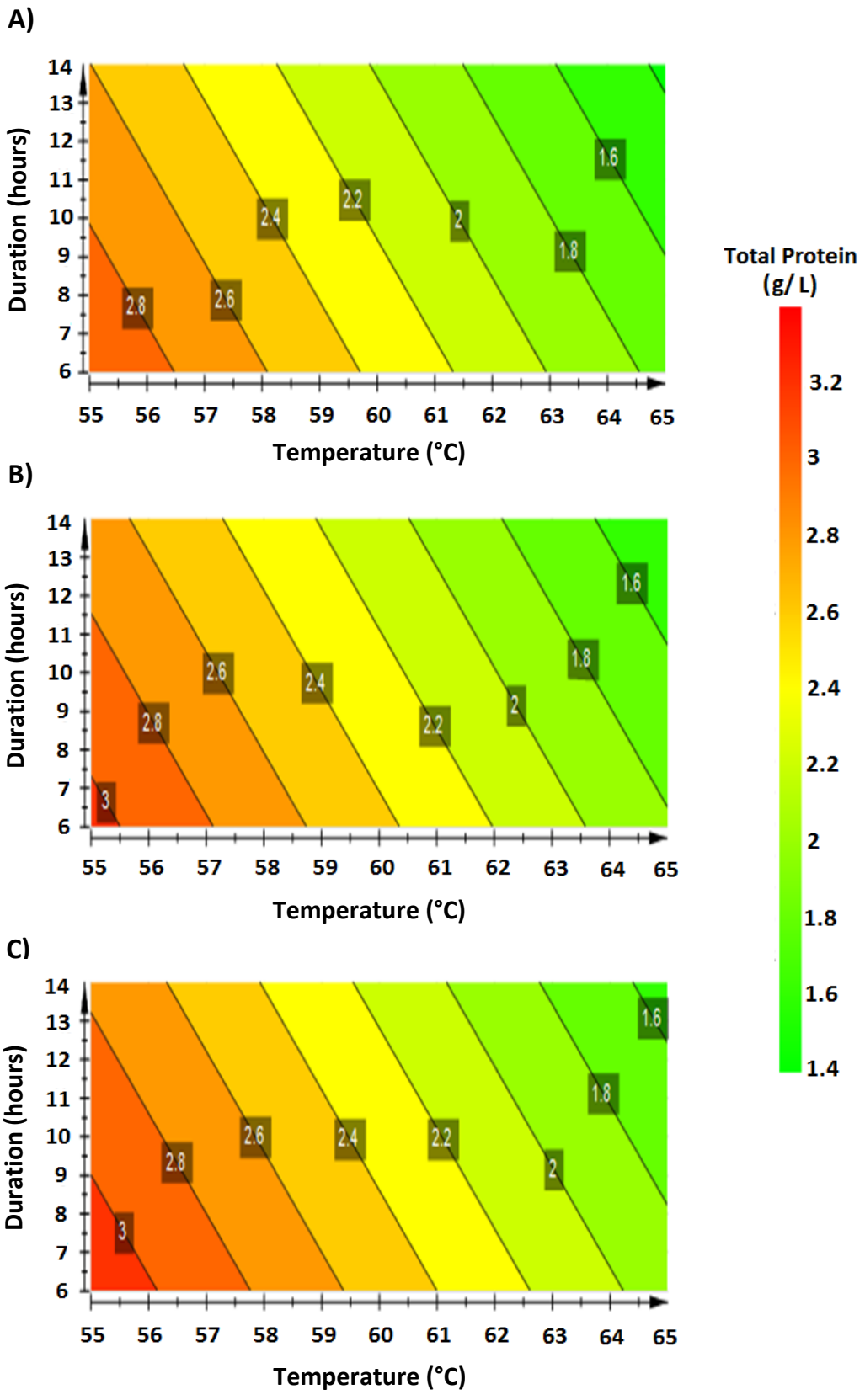

Figure 3.6: Contour plots showing the effect of extraction hold duration and temperature on total protein concentration (g L^{-1}) after heat extraction at **A)** 0.05W L^{-1}; **B)** 0.23W L^{-1}; **C)** 0.41W L^{-1}. Maximum total protein concentration is 1.229g L^{-1}. R^2 and Q^2 are 0.79 and 0.67, respectively

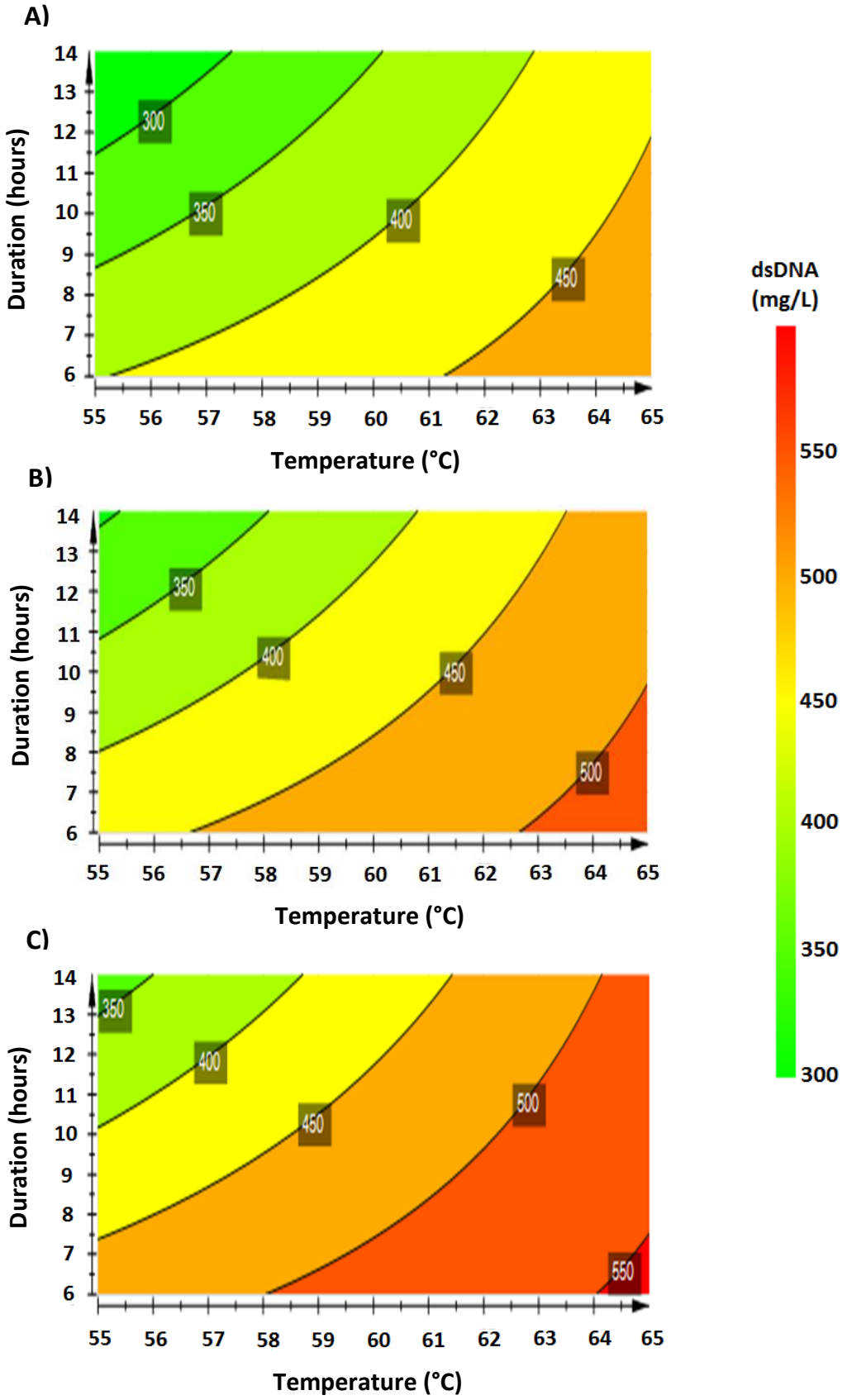

Figure 3.7: Contour plots showing the effect of extraction hold duration and temperature on dsDNA concentration (mg L^{-1}) after heat extraction at **A)** 0.05W L^{-1}; **B)** 0.23W L^{-1}; **C)** 0.41WL^{-1}. R^2 and Q^2 are 0.81 and 0.55, respectively

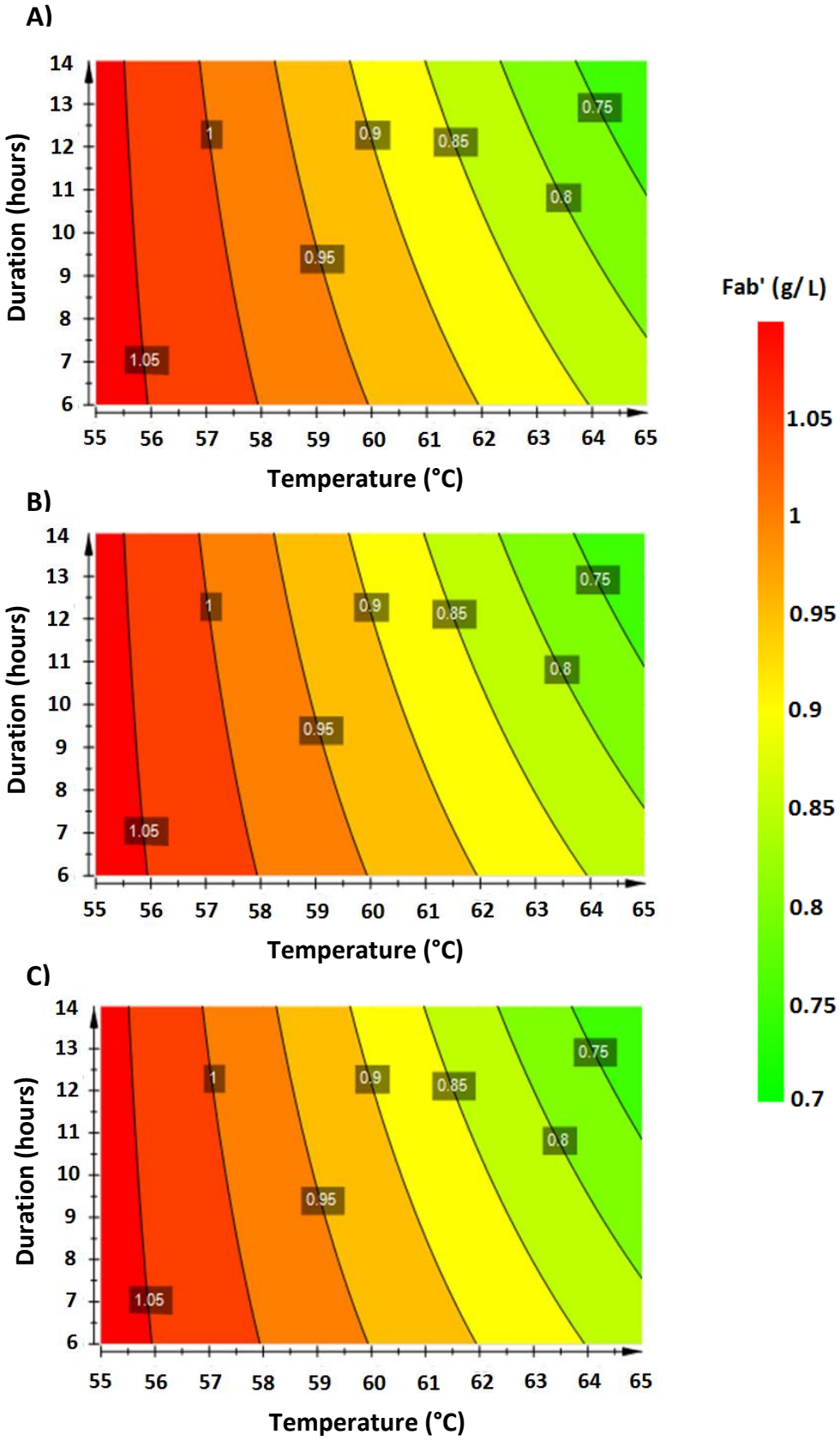

Figure 3.8: Contour plots showing the effect of extraction hold duration and temperature on Fab' titre (g L^{-1}) after acid precipitation at **A)** 0.05W L^{-1}; **B)** 0.23W L^{-1}; **C)** 0.41W L^{-1}. R^2 and Q^2 are 0.87 and 0.78, respectively

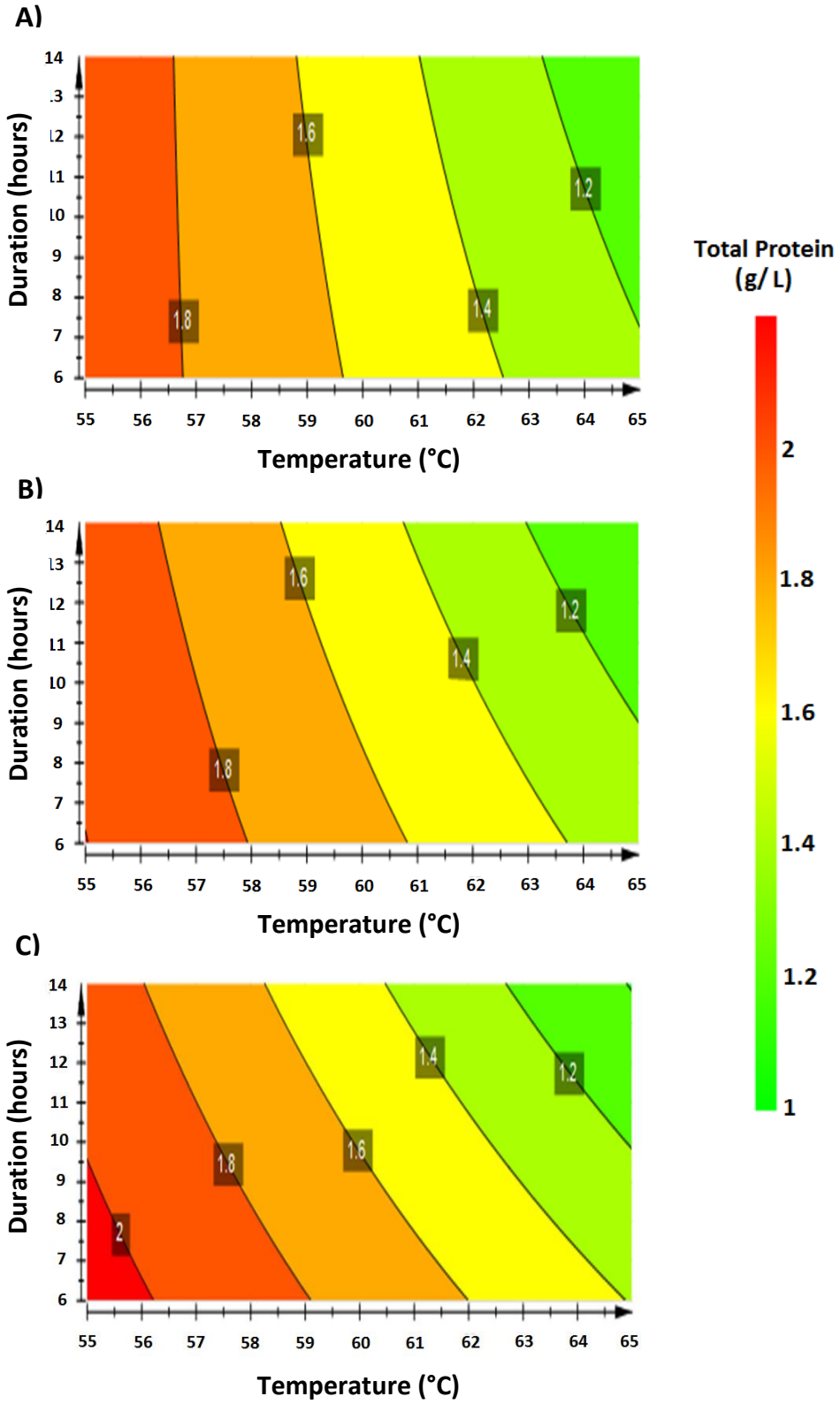

Figure 3.9: Contour plots showing the effect of extraction hold duration and temperature on total protein concentration (g L^{-1}) after acid precipitation at **A)** 0.05W L^{-1}; **B)** 0.23W L^{-1}; **C)** 0.41W L^{-1}. R^2 and Q^2 are 0.98 and 0.94, respectively

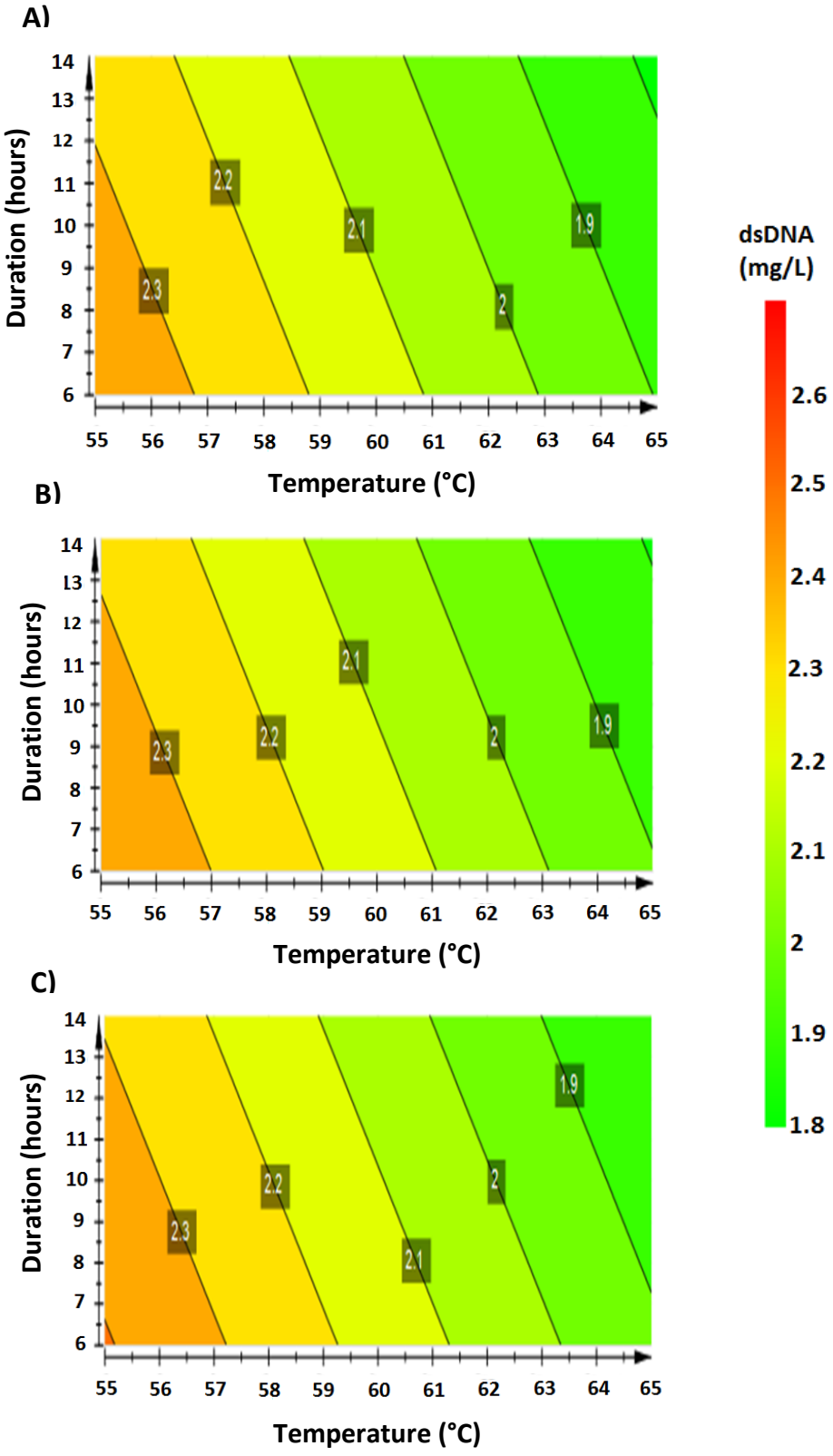

Figure 3.10: Contour plots showing the effect of extraction hold duration and temperature on dsDNA concentration (mg L^{-1}) after acid precipitation at **A)** 0.05W L^{-1}; **B)** 0.2W L^{-1}; **C)** 0.41W L^{-1}. R^2 and Q^2 are 0.27 and -0.2, respectively

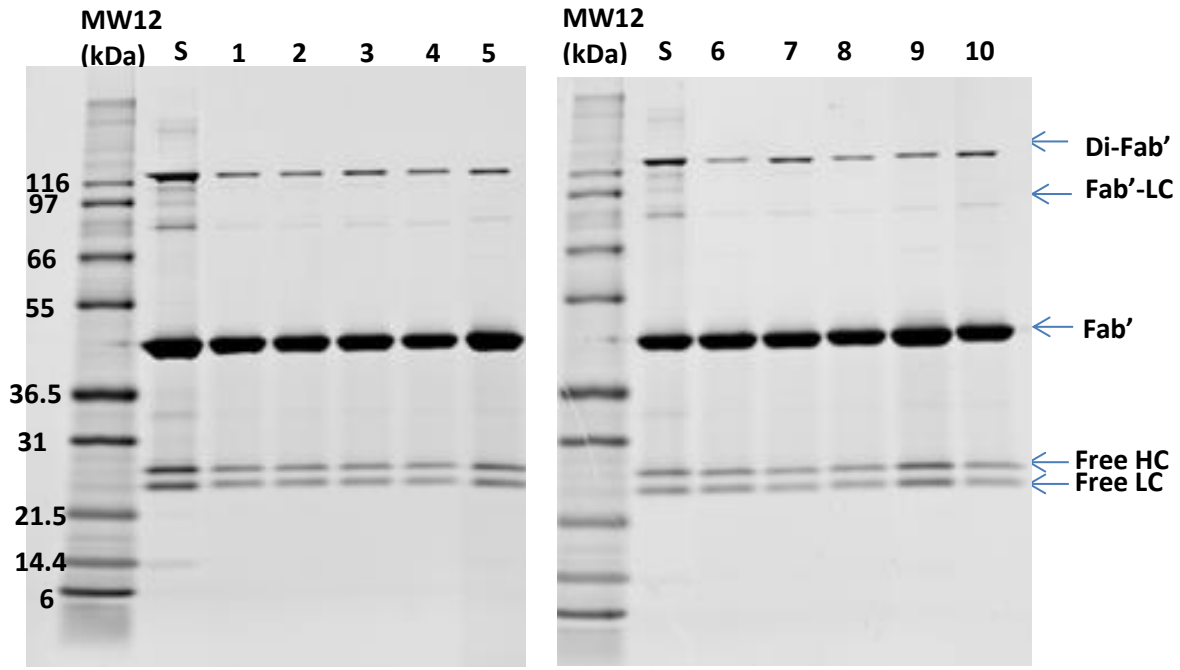

Figure 3.11: Non-reduced SDS-PAGE gels showing the purified Fab' samples taken after extraction purified using protein L chromatography. MW12 represents the molecular weight protein marker, S represents the purified Fab' standard. Lanes 1-10 represent the respective samples 1-10 as listed in Table 3.1

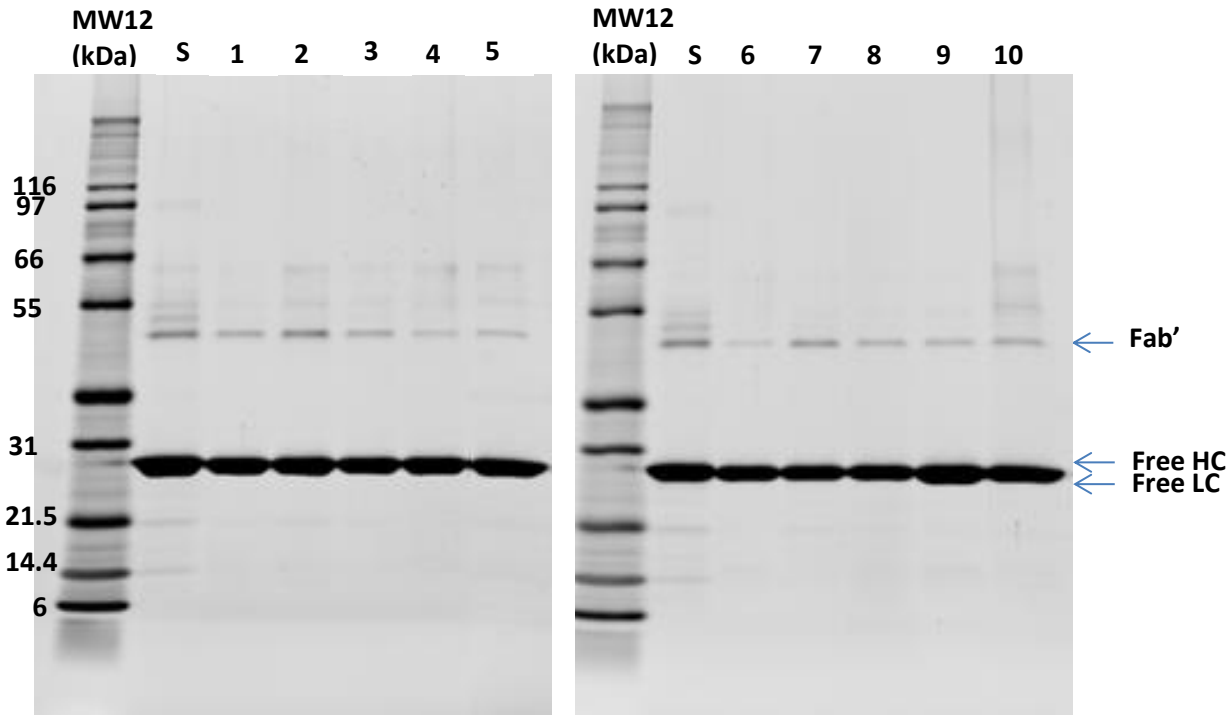

Figure 3.12: Reduced SDS-PAGE gels showing the purified Fab' samples taken after extraction purified using protein L chromatography. MW12 represents the molecular weight protein marker, S represents the purified Fab' standard. Lanes 1-10 represent the respective samples from experiment number 1-10, as listed in Table 3.1

Chapter 4

Characterisation of the Extraction Vessels at Different Scales Using Fluid Dynamic Techniques

4.1 Introduction and Aims

The need for detailed characterisation of a stirred tank vessel using fluid dynamic techniques has become an increasingly important component for better scale-up between different sized vessels (Marques *et al*., 2010). Engineering studies offer a way to gain an insight into the behaviour of a system and how different operating and geometric conditions affect hydrodynamics, which can then be replicated more accurately in another system. The information provided by these experiments can also help determine how well a process is performing and how it may be optimised. For the heat extraction process, maintaining the same heating profile in the scale-down models is crucial. The results from chapter 3 showed that the process was sensitive to heating conditions, such as extraction temperature and duration of extraction, but was not significantly impacted by specific power input (P/V). To further understand the importance of specific power input on mixing, hydrodynamic data is needed. Although there is a lot of hydrodynamic data on lab scale and large scale vessels, relatively few studies on mixing performance and flow patterns have been conducted in miniature bioreactors. In this chapter, mixing time studies were performed on a 20mL miniature stirred tank vessel to be used as a scale-down model of the 2L vessel, in order to understand how specific power input impacts mixing time (t_m) under a range of different conditions. PIV experiments on the 20mL vessel allowed flow patterns to be visualised and provided additional information on fluid velocity and vorticity.

The hydrodynamics between stirred and shaken systems are often significantly different therefore it is important to characterise the shaken system and compare it to the stirred system. There is limited data on characterisation studies of microwell plates but this is an area which is recently receiving significant attention (Barrett *et al*., 2009; Doig *et al*.,

Hermann *et al*., 2002; Isett *et al*., 2007; Nealon *et al*., 2006; Pouran *et al*., 2012; Tissot *et al*., 2010; Zhang *et al*., 2008). Each study focuses on one type of microwell plate at a time, however due to the vast number of different plates, of varying sizes and geometries, it is important to first select the appropriate plate for use as a scale-down model based on process requirements and limitations, and then extensively characterise it. Unlike between stirred systems, it is not possible to scale-down from stirred tanks to shaken plates using specific power input, tip velocity, or typical dimensionless numbers such as the Reynolds number. There have been attempts to determine specific power input in microwell plates however due to the size of the plate, it is difficult to obtain accurate measurements using standard techniques, such as torque measurements. This is due to a lack of commercially available torque meters that have the sensitivity required for such a system. For translation of the extraction process from the stirred tank vessel into microwell plates, mixing time studies will be used to provide an initial understanding of which conditions in the microwell plate allow for sufficient mixing.

The specific objectives of this chapter are:

- To investigate the effect of impeller speed (specific power input) on mixing in the 2L extraction vessel using fixed impeller positions and fill volume
- To investigate the effect of impeller speed, fill volume, impeller position and number of impellers on mixing time in the 20mL extraction vessel
- To investigate the effect of impeller speed on flow patterns, fluid velocity and vorticity in the 20mL extraction vessel using PIV experiments, both with and without the presence of baffles
- To characterise the mixing performance in a single well of a 24-well deep square-well (DSW) plate, investigating the impact of volume and shaker speed on mixing time

4.2 Experimental Approach

As part of the characterisation work, the heat extraction profiles used in the 2L vessel were established in the 20mL vessel and the 24-well DSW plate as described in section 2.4.3. An example of the heating profile established in the 20mL vessel and 24-well DSW plate are shown in Appendix 4A and 4B, respectively. The heat distribution across the plate was found to be even. Evaporation studies were conducted on the 2L vessel, 20mL vessel and 24-well DSW plate to assess whether adjustments needed to made to data obtained from analytics. This was typically found to be 2% in the 2L vessel, 10% in the 20mL vessel, and less than 1% in the 24-well DSW plate. Mixing time experiments were conducted in the 2L vessel, 20mL vessel and 24-well DSW plate as described in detail in section 2.6. PIV experiments were conducted on the 20mL vessel according to section 2.7.

4.3 Results and Discussion

4.3.1 Comparison of the Extraction Vessels

The geometry of the 20mL vessel was compared to the 2L vessel in order to assess the suitability of the small-scale vessel for use as an adequate scale-down model. Table 4.1 summarises the key geometrical ratios in the 2L and 20mL vessel. Although it would have been desirable to have a scale-down model which was geometrically the same as the large scale model, this was not possible unless a custom designed vessel was built beforehand. Typically there are many factors, both geometric and operational, that are responsible for effective scaling therefore it is impossible to maintain all geometric, power and mixing parameters between two scales. Instead, the key geometrical ratios should be maintained constant as far as reasonably possible. In this work, although the 20mL vessel used three 6-bladed paddle impellers and the 2L vessel used three 6-bladed Rushton impellers, both impellers are radial impellers and are known to behave similarly thus provide comparable mixing performance (Galaction *et al*., 2008). The power number value for the Rushton impeller varies significantly throughout literature but typically ranges between 5 (Hewitt and Nienow 2007; Magelli *et al*., 2013; Yianneskis *et al*., 1986) and 6 (Gill *et al*., 2008b).

According to Sano and Usui (1985), the power numbers in the Rushton and paddle impellers are typically 6.6 and 4.2, respectively. The power number used in this study for the Rushton impeller was taken to be 5.

The power number for the paddle impeller in the 20mL vessel was previously determined to be 1 by Ali *et al*. (2011). The power numbers for the paddle impeller are typically lower than for Rushton anyway. Shekhar and Jayanti (2002) obtained a value of 3.4 for the paddle impeller and Mununga *et al*. (2003) obtained a value of 2.3 for the paddle impeller in the turbulent regime. However, the significantly low power number for the paddle impeller in the 20mL vessel is likely due to the size and geometry of the impeller. Rutherford *et al*. (1996a) found that the power number reduced as the ratio of impeller blade thickness to impeller diameter. Additionally, Gill *et al*. (2008b) showed similar findings where the power number for a miniature Rushton impeller was found to be almost half that typically seen in literature. This was attributed to the relatively large impeller thickness to impeller diameter ratio and small size of the impeller. Table 4.1 shows that for the 20mL system, the impeller thickness to impeller diameter ratio is approximately four times large than for the 2L system which may explain the very low power number of 1 for the paddle impeller. Despite these differences in the impeller system between the two scales, adjustments were made to the power calculations in order to have the same specific power input at both scales.

Additionally, the minimum fill volume, needed in the 20mL vessel in order for the pH probe to be well submerged during the extraction process was 20mL, therefore this volume was tested for characterisation studies. This meant that the liquid height to vessel diameter ratio could not be maintained between both scales. Other important geometric ratios however, such as impeller diameter to tank diameter, impeller spacing and impeller clearance, which are all critical parameters for scale-up and scale-down, were considered to be well matched between the 2L and 20mL vessel. Additionally, both vessels had 4 baffles which were positioned in similar locations in their respective vessels. The 20mL vessel was therefore considered to be a sufficiently geometrical model to the 2L vessel.

Scale-down studies into a microwell plate facilitates parallelisation and automation with the potential to equip with micro-sensors for pH monitoring (Weiss *et al*., 2002). In order to

have sufficient volume for analytics during the heat extraction process, the minimum fill volume needed in the DSW plate was considered no less than 2mL. A microwell plate with a square wall has been known to enhance mixing and oxygen transfer (Fernandes and Cabral 2006) due to the baffling effect of the four walls. Characterisation studies found that oxygen transfer rates are typically up to 50% lower in round wells compared to squared wells (Duetz and Witholt 2004). A 24-well DSW plate was therefore considered to be the most suitable choice for scale-down from the stirred vessel into microwell plates.

4.3.2 Comparison of Mixing Time in 2L and 20mL Vessel

Mixing time studies were conducted on the 2L and 20mL vessel with a fill volume of 2L and 20mL, respectively. Figure 4.1A and B shows the mixing time curves, for the vessels as a function of Reynolds number (Re) and specific power input, respectively. Due to the difference in size of the two vessels, Figure 4.1A shows differences in the mixing time curves as a function of Re. When comparing the mixing time as a function of specific power input however, as shown in Figure 4.1B, the two mixing time curves were found to be very comparable. As expected, as the specific power input increases, mixing time (t_m) decreases. This indicates that it takes approximately the same amount of time for homogeneity to occur at both scales. The dimensionless mixing time constant (*K*), provides information about the mixing performance in a vessel and can be used to predict how quickly homogeneity is achieved irrespective of the vessel size (Ascanio 2015). This value describes the number of revolutions that the impeller takes before full mixing is achieved in a vessel (Lee and Yianneskis 1997) and is calculated from the dimensionless mixing time (Nt_m) curve when the liquid is in the turbulent regime. For the 2L and 20mL vessel, these values were calculated using equation 4.1 for each impeller speed and plotted against the Re and specific power input as shown in Figure 4.2A and B, respectively.

$$Ntm = N \times tm \qquad \text{[Equation 4.1]}$$

The *K* constant for the 2L vessel was found to be 35 whereas for the 20mL scale, it was close to 240. For a larger vessel, it typically takes a greater number of revolutions to achieve full mixing so the *K* constant is typically greater (Lee and Yianneskis 1997). This was not the case

in this study. The differences in these values are likely due to the geometry of impeller systems at the two scales. Sano and Usui (1985) found that the *K* constant was highly dependent on the impeller geometry. The relatively large blade thickness in the 20mL vessel may have hindered the rate of mixing. Although the power calculations were matched based on the power numbers provided in literature, it may be that the actual specific power input is still lower than that calculated for the 20mL vessel thus limiting mixing times. Differences in the impeller submergence may also be a factor. A larger volume of liquid above the top impeller, as indicated by larger impeller submergence in the 20mL vessel, may have increased mixing times as it takes longer for the flow patterns to be fully circulated to the top of the vessel in comparison to the 2L scale.

Normally, mixing time studies conducted in stirred tank vessels are done in vessels which are typically tenfold bigger than the size of the 20mL vessel used here. There are very few thorough studies on mixing time characterisation in miniature vessels and it is not well known if mixing performance in such a small scale vessel is similar to a large scale one however the results of the 20mL vessel are very comparable to that obtained by Vallejos *et al*. (2005). In their study, they conducted mixing time studies on a 12.5mL vessel with a single paddle impeller, 9mm in diameter, using a dye and an optical sensor to measure oscillations. The results showed that mixing time was relatively unaffected after an impeller speed reached 130rpm and a Re of 176. At this point, the maximum pumping capacity of the impeller is considered to be achieved and increasing the impeller speed further no longer impacts on mixing. These results are in good agreement with the mixing time curve observed in Figure 4.1A where good mixing is achieved at a Re close to 300. Similarly, Vellejos *et al*. (2005) compared their work to large scale vessels in other studies and also found that flow regimes in the small scale bioreactor differed considerably to large scale. They concluded that although mixing behaviour in large vessels may be replicated at miniature scale, the hydrodynamic conditions vary significantly.

Other reasons for these differences in the *K* constants between the 2L and 20mL scale may be due to the experimental technique used to obtain mixing times. For this study, the dual indicator method for mixing time (DISMT) was used to obtain measurements. Although the

method used to calculate mixing time was found to be reproducible, this technique focuses on analysing the vessel from one angle or plane. For these vessel systems, the presence of probes and baffles etc. obstructed the view of the liquid which meant that it was not possible to access the whole area of the liquid in the vessel. Instead only the liquid not obstructed were analysed. In order to evaluate the images, Matlab was used to crop regions from each image, assessing the pixels from the combined cropped areas. An example of the cropping technique from the 20mL vessel can be seen in Appendix 4C and the reproducibility of the Matlab analysis for one set of conditions can be seen in Appendix 4D. Although all efforts were made to take the largest possible area of the liquid at both scales, for the 2L vessel, there was a significant area of the liquid in the vessel which could not be accessed for analysis. An example of the 2L vessel with the DISMT reagent can be seen in Appendix 2D which shows obstructions both inside and outside the vessel. It is likely that the mixing time measurements for the 2L vessel are therefore higher in reality compared to those captured during experimentation; therefore the *K* constant may also be higher. Additionally, there are other factors that can influence mixing time which are dependent on how the tracer is added to the vessel, in this case, this is a base (NaOH). These include the position of injection of the base, the distance of the base from the liquid level, the speed of base addition (jet mixing) and the positioning of the camera in relation to the vessel. These differences therefore make it difficult to completely standardise the process and compare between studies. This however is true for all types of techniques measuring mixing time. Although it was not possible to test all these factors for these experiments, every effort was made to set up both vessels in the same way, minimising background noise, in order to improve the robustness of the method.

The *K* constant found in literature were in agreement with that obtained for the 20mL vessel. Jahoda and Machoii (1994) used the conductivity method to calculate the dimensionless mixing time constant for a triple Rushton impeller system, which was found to be around 200. For very similar systems, Vasconcelos *et al*. (2000) obtained a value of 216 and Kasat and Pandit (2004) obtained a value of approximately 220. Although the vessel and impeller system in all three studies was approximately 12 times bigger than the 20mL vessel, the *K* constant values were comparable. The impeller spacing in all three studies was three impeller diameters ($3D_i$) whereas typically, for a bioprocess, the impeller spacing is kept to

$1D_i$, as was used in the 20mL vessel. If impeller spacing is increased beyond $2D_i$ there is no overlapping of the flow streams therefore it creates dead zones between the impellers, thus causing compartmentalisation which limits mixing (Baudou *et al*., 1997, Hudcova 1989; Saravanan 2009). The fact that the *K* constant in the 20mL vessel was similar to those seen in studies with wide impeller spacing indicates that mixing is not as efficient in the 20mL vessel as it is in the 2L vessel, which is likely due to the impeller geometry in the small scale vessel.

Although there are differences in mixing efficiencies between both scales, it appears that full mixing was achieved before reaching a specific power input value around 0.05W L^{-1} for both scales. After this point, the mixing time remained relatively unchanged at around 9 seconds. This value corresponds to the findings from chapter 3, for the 2L vessel, where specific power input was found to have little impact on the extraction performance. The range tested in the DoE experiment was between 0.05 – 0.41W L^{-1}. It may be that at the lower end of this range, the cell suspension in the 2L vessel was already well mixed therefore increasing the power further did not improve mixing efficiency and hence did not impact the process performance. Chapter 5 shows process verification studies for the 2L and 20mL scale for the extraction process, at different specific power inputs, using the same impeller positions and fill volumes as those used in this particular mixing time study. The results are also compared to pilot scale extractions where available.

Further characterisation of the 20mL vessel involved looking at the impact of fill volume on mixing time. The impeller spacing was kept constant and the fill volume was varied. Figure 4.3 shows a schematic diagram of the 20mL vessel with fill volumes of 20mL, 14mL and 12mL. At 14mL, the liquid level sits in line with the top impeller. At 12mL, the liquid level sits below the top impeller so that only two impellers are submerged. Figure 4.4A and B show the mixing time curves for the different fill volumes as a function of Re and specific power input, respectively. Overall, the mixing times were higher for the 20mL fill volume but were comparable for the 14mL and 12mL volumes. This is because at 20mL there is a relatively large volume of liquid above the top impeller at 20mL which takes longer for the tracer to distribute throughout the entire volume, whereas for 12mL and 14mL the upper impeller is closer to the liquid level and faster mixing is achieved. The corresponding dimensionless

mixing time curves are shown in Figure 4.5. The *K* constants for the 14mL and 12mL fill volume are of similar values at approximately 130 and 150. The slightly lower *K* constant for the 14mL may be due to the surface of the liquid level being in line with the top impeller, which could cause the liquid to thrash, therefore creating further turbulence which encourages faster mixing. These results show that faster mixing can be achieved at an even lower specific power input value if the fill volume is relatively close to the upper impeller.

For the next set of experiments, the impeller configurations were varied in the 20mL vessel so that the impact of impeller spacing on mixing time could be observed. The original configuration had an impeller spacing of $0.95D_i$. The fill volume was kept constant at 20mL and the middle impeller was also kept in the same position. The top and bottom impellers were subsequently moved apart to achieve an impeller spacing of $1.5D_i$ and $0.6D_i$. Figure 4.6 shows the schematic diagram of the vessel with these three different configurations. Figure 4.7A and B shows the mixing time curves, for the three configurations as a function of Re and specific power input, respectively. The data from the mixing time curves indicate that moving the impellers further apart or closer together results in insignificant differences to mixing time overall. The $0.6D_i$ configuration had the worst mixing performance in the laminar regime below a Re of 200, where mixing times were almost three times greater than for the other two configurations. The flow structures for multiple impeller system is very complex and there is a body of literature describing the effect of impeller spacing on mixing and flow patterns (Baudou *et al*., 1997; Chunmei *et al*., 2008; Gogate *et al*., 2000; Hudcova and Machon 1989; Kasat and Pandit 2004; Magelli *et al*., 2003; Mahmoudi and Yianneskis 1992; Mahmoudi 1994; Mishra and Joshi 1994; Rutherford *et al*., 1996a; Wernersson and Tragardh 1999; Xinhong *et al*., 2008). The key findings from these studies have shown that different impeller spacing is responsible for different types of flow patterns. Typically, the spacing should be kept between $1\text{-}2D_i$ for efficient mixing. At this spacing, the flows produced by the individual impeller merge together (Mahmoudi 1994). Gogate *et al*. (2000) found that when the impeller spacing was less than $1D_i$, the liquid streams inclined towards each other and the efficiency of each impeller was reduced. The narrower the spacing, the more the two impellers start to behave like one thus producing one radial flow stream instead of two. In this study, although the impeller spacing was varied, the fill volume was kept constant, therefore with a $0.6D_i$ configuration; there is an even larger space between

the upper impeller and the top of the liquid level, which explains the slower mixing times at low impeller speeds. As the speed increases, however, the mixing performance for the $0.6D_i$ configuration matches that of the other two configurations. Figure 4.8 shows the dimensionless mixing time curves for three impeller configurations as a function of Re where the *K* constants for all three configurations are close to 240.

As part of the 20mL vessel characterisation, mixing time was measured for the single impeller system, in order to compare to the multiple impeller system, over a range of specific power input. The single impeller was placed in the same position as the middle impeller in the triple impeller system and then in the same position as the bottom impeller in the triple impeller system when the impeller spacing was $0.95D_i$. Figure 4.10A and B shows the mixing time curves, for the three configurations as a function of Re and specific power input, respectively. As expected, the results show that mixing times for the single impeller system at the bottom of the impeller shaft are significantly lower than when the impeller was placed in the middle of the shaft, due to the lack of flow distributed to the top of the liquid. Figure 4.11A and B show the corresponding dimensionless mixing time curves for these configurations. The *K* constants for the middle and bottom impeller are approximately 220 and 400. The value obtained for the single middle impeller is very similar to that of the triple impeller system. It is possible that for this configuration, the small screw at the bottom of the shaft acted like a mini impeller which aided mixing slightly; however the results still indicate that a single impeller is capable of good mixing provided that it is placed close to the centre of the volume in the vessel. Gogate *et al*. (2000) found that the multiple impeller system was superior to single impeller system when it came to gas phase hold up, power consumption and mass transfer, factors that must be taken into consideration when running a fermentation process, particularly using shear sensitive material. However, when it came to liquid mixing only, the single impeller system was thought to be better than the multiple impeller system at a given power input. If the choice is made to use a single impeller system instead of a multiple impeller system, increasing the impeller diameter, breadth and number of blades is suggested to improve cost efficiency (Sano and Usui 1985). Although *E.coli* cells are not considered to be shear sensitive, this may be a factor at large scale during the heat extraction process and therefore a multiple impeller system is recommended. The results from the characterisation studies therefore

indicate the importance of optimising the impeller positions and fill volumes to improve mixing, ideally with an impeller spacing of 1-2D_i, clearance of 1D_i and submergence of 1D_i.

Figure 4.12A and B shows the mixing time and dimensionless mixing time curves, respectively, for both vessels at all the impeller configurations tested. Figure 4.12A shows that the mixing time curve for the 2L is most similar to the 20mL vessel when the impeller spacing is 0.95D_i or 1.6D_i and therefore when running extraction experiments in the miniature vessel, the 0.95D_i impeller spacing configuration can be used.

4.3.3 Particle Image Velocimetry Experiments in 20mL Vessel

To understand the mixing patterns formed in the 20mL scale-down vessel with a fill volume of 20mL and an impeller spacing of 0.95D_i, PIV experiments were conducted at a range of specific power inputs with and without baffles in place. Figures 4.13–4.19 show the velocity vector and vorticity contour plots for half of the vessel at increasing impeller speed (specific power input). Vortices provide a source of turbulence (Xinhong *et al*., 2010). The vorticity bar represents vorticity measurements of red and blue which represent the core of the vortices rotating clock wise and counter clockwise, respectively. All vectors have been normalised by their respective impeller tip speed (V_{tip}) and a reference vector of 0.05V_{tip} is provided with each plot.

Figure 4.13A and B show the velocity vector plot at 50rpm and 100rpm, respectively. At 50rpm, at a Re of 66, it is clear that the vessel is not well mixed. For a radial impeller, the jet flows horizontally from the impeller and impinges on the vessel wall where it splits and circulates above and below the impeller, returning back to the impeller blade. The radial jet which is expelled from the impeller in the form of ring vortices is responsible for liquid macromixing in a stirred tank vessel (Sharp and Adrian 2001). At 50rpm, close to the impeller region, these flow patterns are present but poorly defined. The area above the top impeller in particular contains many dead zones as indicated by the uneven vorticity patterns. Vallejos *et al*. (2005), when conducting mixing time studies in their 12.5mL vessel, also observed that at low Re values, below 41, there were significant stagnant zones with many doughnut-like segregated regions. Mununga *et al*. (2003) studied the flow fields of a

paddle impeller system in an unbaffled vessel, approximately 18 times bigger than that used for this study, using CFD. They also found that at a Re of 10, during laminar flow, the circulation loop expelled from the impeller was weak and there were dead zones in the bulk fluid in the velocity vector plots. The maximum velocity value in the 20mL vessel, observed close to the impeller region, was 9 x 10^{-4}m/s. Figure 4.13B shows the velocity vector plot at 100rpm and a Re of 132, where the characteristic toroidal ring shaped vortices, above and below each impeller, become more defined, and the vorticity doubles. Mununga *et al*. (2003) also found in their work that when transitional flow was achieved, at a Re of 100, the circulation loops became stronger, bigger and more defined in general and for even higher Re, the loops reached the entire tank region. The structure of the ring vortices in this study are in good agreement with those described throughout literature for Rushton radial impellers (Chunmei *et al*., 2008; Hammad and Papadopoulos 2000, Hudcova and Machon 1989; Lamberto *et al*., 1999; Mavros 2001; Rutherford *et al*., 1996a; Yianneskis *et al*., 1986). Doubling the speed from 50rpm to 100rpm in the 20mL vessel has caused the maximum velocity values to increase 3 fold to 2.7 x 10^{-3}m/s, however there are still some stagnant areas present in the vessel, particularly near the top of the liquid level where the flow has not yet fully circulated to.

Figure 4.14A and B shows the velocity vector and vorticity contour plots at 150rpm and 200rpm, respectively. For both these vector plots, the results show that the upper and lower ring vortices for the middle impeller are similar in size. For the bottom impeller, the lower ring is slightly larger than the upper ring and the flow is inclined by about 30° to the horizontal. This level of inclination is in agreement with the study by Montante *et al*. (1999) where they observed the flow patterns of a Rushton impeller in a baffled system and found that when the impeller clearance was slightly lower than $1D_i$, the impeller stream was inclined at around 25 to 30°. For the top impeller, the upper ring is significantly larger than the lower ring and the flow extends further out to the top of the liquid level. There are still some areas towards the top left corner of the liquid which appear to be poorly mixed at 200rpm. As expected, maximum fluid velocity in the vessel at 150rpm and 200rpm increase to 4.3 x 10^{-3}m/s and 5.8 x 10^{-3}m/s, respectively. Figure 4.15A and B shows the velocity vector and vorticity contour plots at 250rpm and 300rpm, respectively. The maximum velocity in the vessel is shown to increase but the flow patterns are similar to those

observed at 200rpm. The levels of vorticity in the ring structures are relatively similar at around +80 and -80 between impeller speeds of 100rpm and 300rpm. As the speed increases however, although the ring structures for the middle and bottom impeller are relatively unchanged, the lower ring of the top impeller becomes weaker whereas the upper ring becomes stronger. This observation is in agreement with previous studies that have shown that for a multiple impeller system, the top impeller draws more power (Hudcova and Machon 1989; Kuboi and Nienow 1986) and therefore the upper ring structure is larger than the lower one. At 300rpm, it is shown that the flow circulates to the corners of the liquid and it is assumed that there is good mixing throughout the vessel.

Figures 4.16, 4.17, 4.18 and 4.19 show the velocity vector and vorticity contour plots at 400rpm and 500rpm, 600rpm and 800rpm, 1000rpm and 1500rpm, and 1750 and 2000rpm, respectively. The flow patterns are stable and similar in structure for all of these impeller speeds. Observation of vorticity values show that as the speed increases, the vorticity in the ring structures decrease. At 2000rpm, where Re is 2650, the lower ring vortices appear to diminish altogether. Molen and Maanen (1978) and Hammad and Papadopoulos (2000) found the same trend in their work as the impeller speed was increased in the turbulent regime. Initially at low speeds, there is not enough power to create ring vortices, however as the speed increases, the jet stream becomes stronger causing radial flow patterns to form, thus causing the vorticity to increase. As the flow becomes more turbulent, the ring vortices merge together until they eventually disappear. The absolute maximum velocity values increase with increasing impeller speed with the highest velocities observed in the jet stream leaving and returning to the impeller.

There is a body of literature that has focused on quantifying velocity in different parts of vessel, particularly concentrating on the velocities close to the impeller jet stream and in the bulk flow. Differences in vessel and impeller geometry and size, type and number of impellers, fill volumes, presence or absence of baffles, and impeller speeds make it difficult to compare directly between studies. The majority of work in literature has focused on stirred tanks with either a single or dual Rushton impeller system. Similar to the studies conducted for mixing time, velocity measurement studies such as PIV or LDA focus on vessels that typically are roughly tenfold bigger than the 20mL vessel used in this work.

Some of these studies have been drawn upon for comparison to the velocities obtained in the 20mL vessel. Montante *et al*. (1999), Sharp and Adrian (2001), Xinhong *et al*. (2010) and Yianneskis *et al*. (1986) studied velocities around the jet stream of a single radial Rushton impeller system. All of the studies were conducted in the turbulent regime and the maximum velocities obtained were $0.7V_{tip}$, $0.5V_{tip}$, $0.7V_{tip}$ and $0.8V_{tip}$, respectively. These correspond to velocities of 1.28m/s, 0.133m/s, 1.1m/s and 0.9m/s. Rutherford *et al*. (1996a) and Chunmei *et al*. (2008) worked with dual Rushton impeller systems in the turbulent regime and found that maximum velocities near the jet stream were $0.32V_{tip}$ and $0.5V_{tip}$, respectively. These corresponding velocities of 0.41m/s and 0.33m/s were lower than for the single impeller system. For alternative single impellers the maximum velocities were also typically lower than for the single Rushton impeller system. Odeleye *et al*. (2014) used a single marine impeller to obtain maximum velocity of $0.25V_{tip}$, corresponding to 0.64m/s. Baldi *et al*. (2002) used an axial impeller to obtain maximum velocity of $0.23V_{tip}$, corresponding to 0.87m/s. All of these velocity values obtained in literature are an order of magnitude greater than those observed in the 20mL vessel where at the highest speed of 2000rpm, the maximum velocity obtained was $0.02V_{tip}$, corresponding to 0.018m/s. The reason for this is likely due to the size of the vessel and impeller as well as the impeller geometry. Molen and Maanen (1978), Rutherford *et al*. (1996a) and Yianneskis *et al*. (1986) compared velocities in different sized vessels and found that velocities decrease as the vessel size decreases. As explained in the mixing time studies, a thicker impeller blade to impeller diameter ratio reduces the amount of power drawn by the impeller thus reducing velocities (Rutherford *et al*., 1996b). The ratio of impeller thickness to impeller diameter for the 20mL vessel is close to 0.1 which is approximately three times greater than the ratio typically observed for impellers in literature. It is likely that the low velocities obtained in this study are therefore explained by the relatively large blade thickness, as well as the impellers themselves being paddle impellers, instead of the more powerful Rushton impellers, which are typically used for bioprocesses due to their relatively large power draw and mixing capability. The lowest fluid velocities can be observed near the centre of the ring vortices where it approaches close to $0.004V_{tip}$ at the highest speed of 2000rpm.

These PIV experiments were repeated under the same impeller speeds with the baffles placed inside the vessel. Although placing baffles in the system restricts the view of the flow

patterns, they provide a better representation of the velocities and vorticities in the 20mL vessel that are expected during actual process conditions. The plots for 50rpm and 100rpm can be seen in Appendix 4E, for 300rpm and 800rpm in Appendix 4F, and for 1500rpm and 2000rpm in Appendix 4G. The vorticities and flow patterns between the baffled and unbaffled systems are comparable. Figure 4.20A and B show the impact of Re and specific power input, respectively, on the maximum velocity obtained in the 20mL vessel for the baffled and unbaffled system. It is clear that the presence of baffles has insignificant impact on the velocity values. Xinhong *et al*. (2008) conducted a similar PIV study where they pointed the laser through a baffle and between baffles to compare velocities. The results from the radial and axial velocity measurements showed insignificant difference between the two set of results which indicate that the baffles have little effect on the discharge flow field. Figure 4.20B shows that maximum velocity increases significantly at low specific power inputs but once it reaches close to 0.05W L^{-1}, corresponding to impeller speeds around 1000rpm, it is relatively unchanged. These results are in good agreement with the mixing time curves shown previously where good mixing was achieved at similar specific power inputs. Despite the relatively low velocities obtained in the 20mL vessel overall, the data from the PIV experiments demonstrate that good mixing can be achieved in this vessel. The velocity vector plots also indicate that although the liquid height to vessel diameter ratio is slightly higher in the 20mL vessel compared to the 2L vessel, the jet streams produced by the impellers are capable of reaching the top of the vessel, ensuring a homogenous environment. Therefore based on the results from these hydrodynamic studies, the 20mL vessel can be considered as a feasible scale-down option for the 2L vessel.

Despite there being an exhaustive number of studies in literature on mixing time and PIV, looking at the impact of factors such as geometry of the vessel, geometry and type of impeller, impeller positioning and fill volumes in a multiple impeller systems, a comprehensive modelling approach is required in order to attribute the impact of these different factors on the mixing performance and hence enable more effective scale-up. Additionally, most mixing time and PIV studies that are conducted in literature focus on studying stirred tank vessels without any probes, spargers and dip tubes. Although this simplifies the study significantly and makes it easier to obtain data, particularly for PIV, for a more accurate representation of mixing and flow in a vessel during a bioprocess, it is

worthwhile to leave these in and develop more advanced methods which can accommodate this. Additionally, the fluid normally tested in such mixing time and PIV studies is water, which is also the case in this study. Although the viscosity of a cell culture is likely to be slightly different to water, hence impacting mixing perfromance, it is usually accepted that *E.coli* culture exhibits low water like viscosities, thus the results from these studies can be applied to the heat extraction process. Obtaining the actual viscosity of the cell suspension during heat extraction and then mimicking the viscosity in water will make for a more accurate representation of mixing time studies. Overall there is a need for a greater level of standardisation in this field of study to make it easier to compare data between different vessels. As more and more research is focusing on understanding fluid dynamics in a system in order to inform process design, it is expected that this will soon become a reality.

4.3.4 Mixing Time Experiments in 24-Well Deep Square-Well Plate

In order to use microwell plates as another scale-down model for the large scale extraction process, mixing time studies were conducted in a 24-well DSW plate in order to see which conditions provided good mixing. The Eppendorf thermomixer, used for shaking the DSW plate, with an orbital shaking diameter of 3mm, was only able to operate at a minimum speed of 300rpm and could be increased in increments of 50rpm only. The fill volumes were tested in 0.5mL increments from 2mL to 4mL. Figure 4.21A and B show the effect of shaker speed from 300rpm to 1000rpm, and 400rpm to 1000rpm, respectively, on mixing time at varying fill volumes. As expected, Figure 4.21A shows that mixing time decreases as the shaker speed and fill volume increase. After shaker speed reaches 400rpm the mixing time remains relatively constant at less than 5 seconds, and fill volume has little impact on mixing time. A closer look at the mixing time curves, in Figure 4.21B, show that as the shaker speed increases, the mixing time decreases up to 500rpm, after which it increases slightly until it reaches 800rpm, and then decreases again above 800rpm. This trend was more obvious for the higher fill volumes of 3.5mL and 4mL. Mixing times in the 24-well DSW plate are less than 3.5 seconds above 400rpm for all fill volumes, and are comparable to values obtained by Isett *et al*. (2007) and Barrett *et al*. (2009). Isett *et al*. (2007) characterised a 24-well plate system (M24) in terms of mixing time using a colour change reaction utilising bromothymol blue. Experiments were conducted at a fill volume of 5mL using 0.1mL of acetic acid to

induce the colour change. The speeds were varied between 200rpm and 800rpm and mixing time was found to be below 5 seconds at 500rpm, and below 1 second at 800rpm. These slightly shorter mixing times in comparison to those observed in this study may be due to the higher ratio of tracer to fill volume. In this study, the ratio was 0.001, whereas Isett *et al*. (2007) used 0.02 which may have increased the reaction time. Nealon *et al*. (2006) studied the impact of jet macromixing in three different microwell plate designs. Mixing times observed in the microwell plates were all below 1 second. The speed at which the tracer was released from the pipette had an impact on mixing time. Slow release of fluid, which corresponds to low jet Reynolds number resulted in mixing times in the order of minutes rather than seconds. The jet length and volume of tracer addition also impacts mixing time. Therefore these differences in mixing time techniques may be responsible for the slightly higher mixing times in this work.

Images of the maximum liquid height in the 24-well DSW plate were taken at varying shaker speeds and fill volumes as shown in Figure 4.22. The images show, for all fill volumes, that when the speed increases from 350rpm to 500rpm, the liquid height increases during shaking. When the speed is increased to 800rpm, the liquid height is similar to the height seen at 350rpm. At 1000rpm, the liquid height increases again. The ratio of the maximum liquid height (H*) to the still liquid height (H_L) at varying speeds and fill volumes is shown in Figure 4.23. The trends in Figure 4.22 and 4.23, correspond to the trends seen in Figure 4.21B where this interesting phenomenon is seen at 800rpm. There are some studies that help explain this interesting behaviour around this shaker speed. Zhang *et al*. (2008) conducted a CFD study to obtain fluid mixing, mass transfer and energy dissipation rate in a spherical bottomed 24-well DSW plate. The orbital shaking diameter of the shaker was 3mm. The study found that power consumption initially decreased as the shaking speed was increased between 300 to 800rpm, however after 800rpm, the power consumption increased with shaking speed. This may be due to the different flow patterns that are obtained at different shaking speeds. At low speeds, the surface tension of the liquid is high and therefore an out-of-phase phenomenon is observed. Out-of-phase phenomena are observed at certain operating conditions where the liquid remains stationary and does not follow the motion of the rotating shaker, therefore the specific power consumption is effectively reduced (Büchs *et al*., 2000). The energy transferred to the liquid as the speed

initially increases, is therefore used for uniform rotational movement of the liquid and no energy is consumed for the fluid friction which is caused by mixing and fluid velocity gradients. After enough energy is effectively absorbed to overcome the liquid surface tension, in-phase phenomenon is achieved, where the liquid follows the motion of the shaker, and the energy is transferred into the bulk of the fluid thus increasing the power consumption. The speed, at which the surface tension breaks, due to the increased centrifugal force and rotation of the fluid, is called the critical shaking speed (N_{crit}). After this speed is reached, the height of the liquid in the well increases, thus increasing the surface area to volume ratio and mass transfer area, which improves mixing (Hermann *et al*., 2002). The results from thes study are in line with the characterisation studies on square-well plates, performed by Hermann *et al*., (2002), where they showed that the liquid free bottom of the well could be seen at 400rpmwith a fill volume of 2mL. Barrett *et al*. (2009) found similar trends when observing power dissipation and average shear rate in the 24-well SRW plate. They showed that increasing the shaking speed caused the power dissipation in the microwell to decrease up to a certain speed, after which it increased again. The average shear rate followed the same pattern. This was also attributed to the overcoming of the surface tension above the N_{crit} value. This phenomenon is still poorly understood but for the 24-well DSW plate in this study, it appears there may in fact be two N_{crit} values, one around 350rpm and one at 800rpm, as shown by the lowest points on the H^*/H_L graph, in Figure 4.23.

Analysis of the liquid in the 24-well DSW plate at shaker speeds between 300rpm and 400rpm for various fill volumes are shown in Figure 4.24. The images were taken at slightly different time points after addition of the tracer and are provided for illustration of the mixing patterns rather than for direct comparison at the same time point. Shaker speed at or above 400rpm caused almost immediate mixing therefore no flow patterns were observed. The flow patterns at 300rpm and 350rpm are in good agreement with those seen and described by Weheliye *et al*. (2012) when conducting PIV studies in an orbitally shaken tank. When the base was first added to the well at 300rpm, the jet stream initially went to the bottom of the well, but, as the well continued to shake, the base rose up to the top of the liquid level and formed two counter rotating vortices just under the liquid level. These vortices helped to enhance mixing in the well by passing liquid between the two rings

following a similar outline to the infinity symbol (∞). Like Tissot *et al*. (2010) observed when studying mixing in orbitally shaken vessel, the areas closest to the walls were the first to be fully mixed and the bulk fluid took significantly longer. As observed by Weheliye *et al*. (2012), there were two mixing zones established in the well; the upper zone, where the ring vortices facilitate mixing by convection, and a lower zone, where mixing was predominantly aided by diffusion. Increasing the speed of the shaker resulted in the production of larger vortices which extended to the sides and base of the well. In this study, increasing the speed to 500rpm and then above 1000rpm caused the liquid height around the edge of the well to increase, causing a greater level of turbulence in the well overall. This additional turbulence further increased the rate that these vortices were engulfed into the bulk of the liquid, causing them to disappear under two seconds. Examination of the flow patterns and turbulence levels in a shaken system helps to provide a better understanding of how the liquid mixes and is useful for scaling process that rely on sufficient mixing such as the heat extraction process. The results from the mixing time characterisation studies in the 24-well DSW plate demonstrate that in the Eppendorf Thermomixer, full mixing is achieved at shaker speeds above 400rpm but more turbulent mixing is achieved at 500rpm. Working above these shaker speeds is therefore recommended when conducting extraction experiments to ensure that the cell suspension is sufficiently mixed and heat is evenly distributed. Chapter 6 shows process verification studies for the 24-well DSW at different shaker speeds and fill volumes.

4.4 Conclusive Remarks

Hydrodynamics in a system are responsible for the mixing performance in a system and mixing time and PIV studies provide insight into how well a vessel becomes homogenous and how well the bulk fluid is evenly distributed. The information obtained can be used for more effective scaling. A comparison of the key geometrical ratios between the 2L and 20mL vessel showed that they were well matched and therefore the miniature vessel was considered for use as a viable scale-down model for the heat extraction process. The information obtained from mixing time studies showed that the mixing time curves matched between the 2L and 20mL vessels and that sufficient mixing occurred at around 0.05W L^{-1} in

both cases. Further characterisation work on the 20mL vessel showed that the impeller spacing and fill volumes both had an impact on mixing time and therefore it was recommended that where possible, the impeller clearance, impeller spacing and impeller submergence should not exceed 1 impeller diameter. The information obtained from the velocity vector plots in PIV experiments showed that at around 300rpm, the flow pattern was well formed and was able to circulate to the top of the liquid level. Increasing the impeller speed beyond this caused the vorticity to decrease. This suggests that a homogenous environment can be achieved at a specific power input of $9 \times 10^{-4} W\ L^{-1}$. However analysis of the velocity vectors showed that the maximum velocity, obtained near the impeller region, was relatively unchanged at a specific power input of around $0.05 W\ L^{-1}$, which corresponds to 1100rpm. This suggests that good mixing was achieved at this point and a further increase in speed did not impact mixing performance significantly. The mixing time results from the 24-well DSW plate showed that sufficient mixing was achieved at a shaker speed of 400rpm but analysis of the liquid height in the well indicated that turbulent mixing was achieved at 500rpm. Increasing the speed further caused the liquid height to decrease until it reached 800rpm after which it increased again. Increasing the fill volume decreased the mixing time only at speeds below 400rpm but once full mixing was achieved, the fill volume had no impact on mixing. It is therefore recommended that heat extraction experiments are conducted at a shaker speeds above 400rpm. The characterisation results from the 20mL vessel and 24-well DSW plate were useful in understanding how different parameters impact mixing performance and provide information on which parameters were important to maintain between the scale-down models and the lab or pilot scale extraction vessel in order to improve scaling of the heat extraction process. Chapter 5 and 6 focus on verification studies where the extraction process is scaled down from the lab and pilot scale stirred tank vessels into the 20mL vessel and 24-well DSW plate, respectively, for a range of different operating conditions.

Parameter	**2L**	**20mL**
Fill volume	2L	20mL
Internal vessel diameter (D_v)	130mm	24.0mm
Vessel height (H_v)	240mm	82.2mm
H_v:D_v	1.85	3.43
Liquid height (H_L)	171mm	42mm
H_L:D_V	1.32	1.75
Impellers	3 Rushton	3 Paddle
Impeller diameter (D_i)	53.0mm	8.5mm
Baffles	4	4
Baffle width (B_w)	10.0mm	0.32mm
B_w:D_v	0.08	0.13
D_i:D_v	0.408	0.354
Impeller spacing:D_i	0.95	0.95
Impeller clearance:D_i	1.0	1.0
Impeller submergence:D_i	0.5	1.3
Impeller thickness:Di	0.028	0.107

Table 4.1: Details of the 2L and 20mL vessel including key geometrical ratios

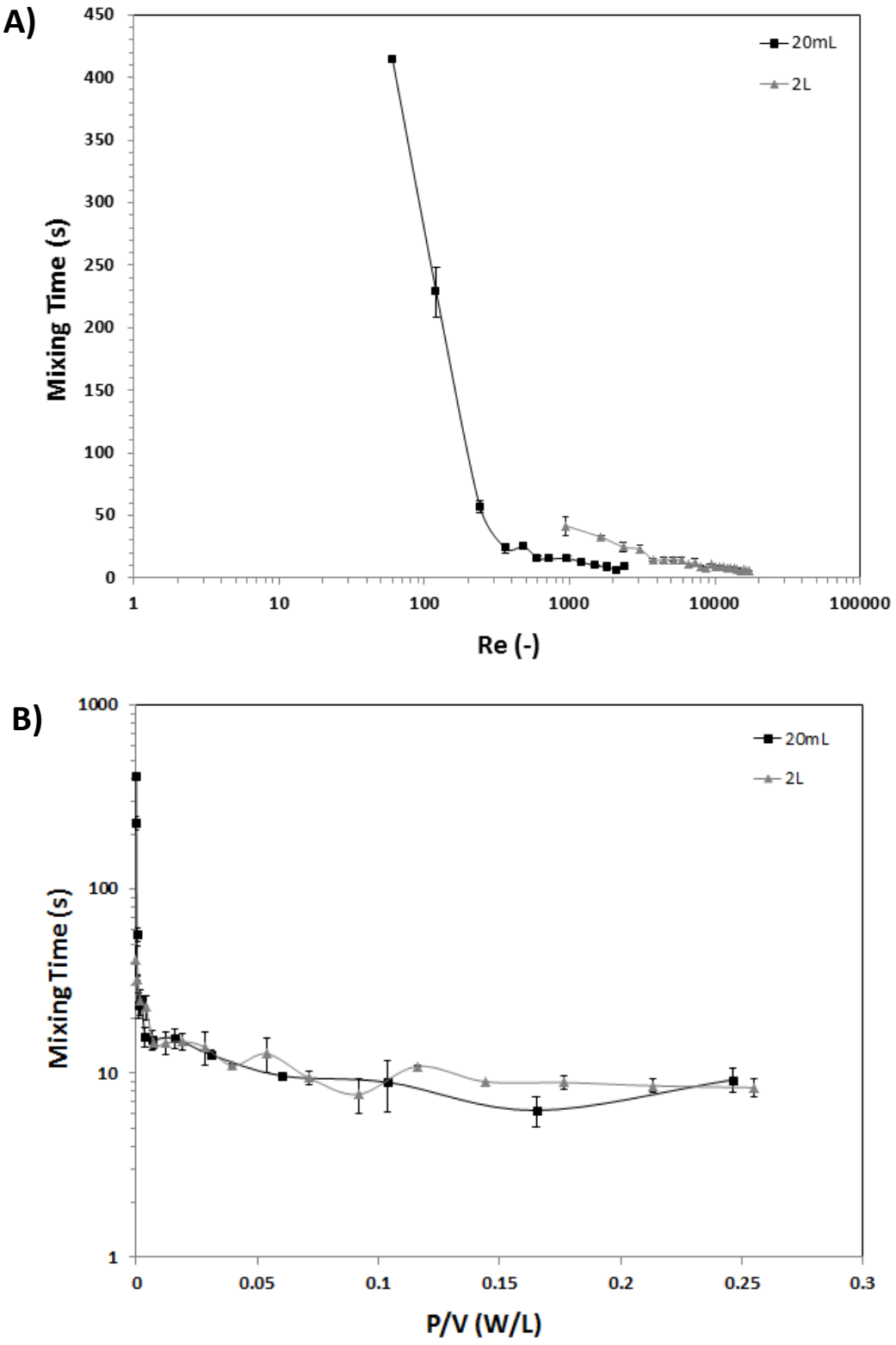

Figure 4.1: The effect of **A)** Re and **B)** P/V on mixing time in the 2L and 20mL vessel with a fill volume of 2L and 20mL respectively

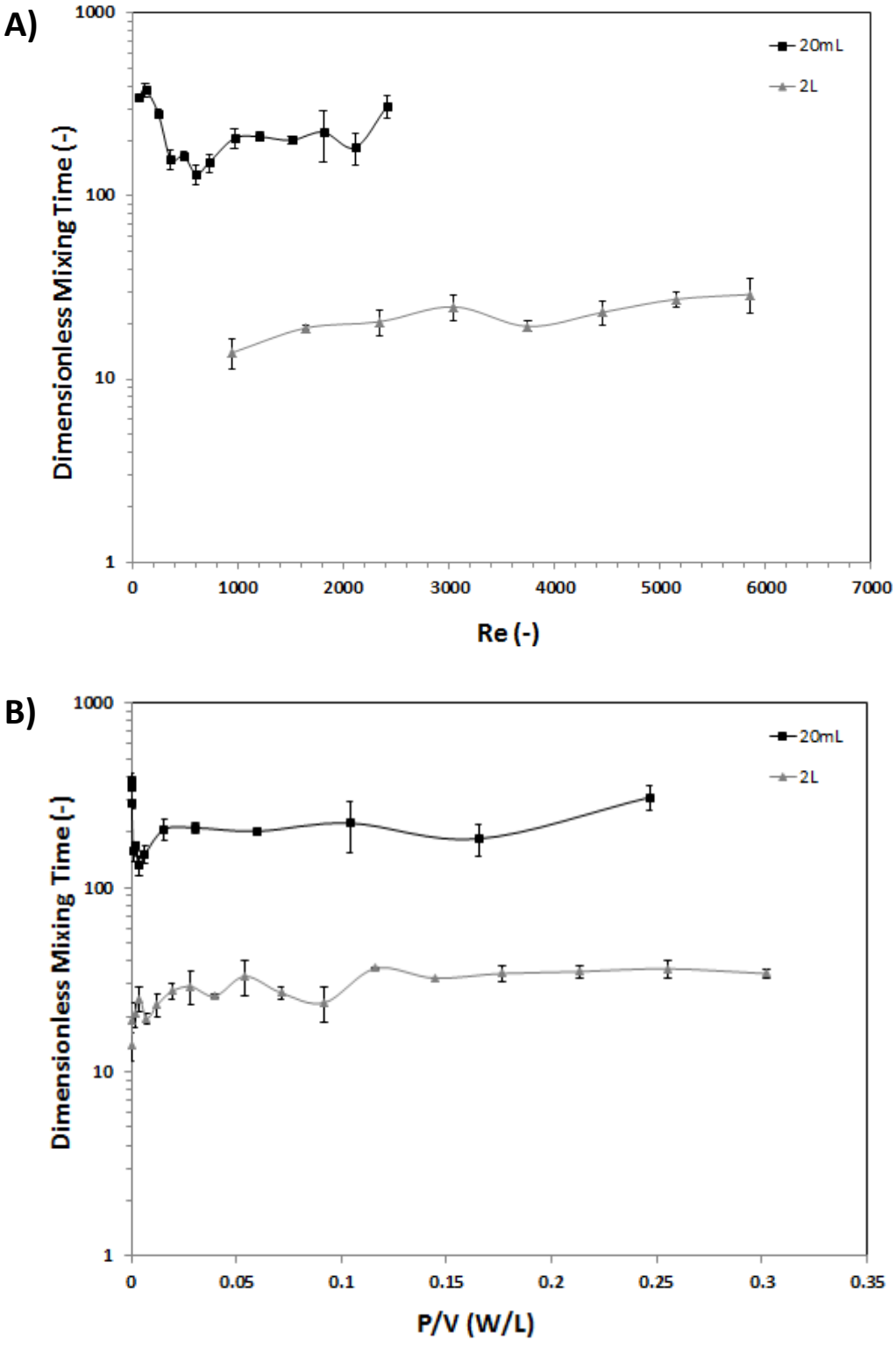

Figure 4.2: The effect of **A)** Re and **B)** P/V on dimensionless mixing in the 2L and 20mL vessel with a fill volume of 2L and 20mL respectively

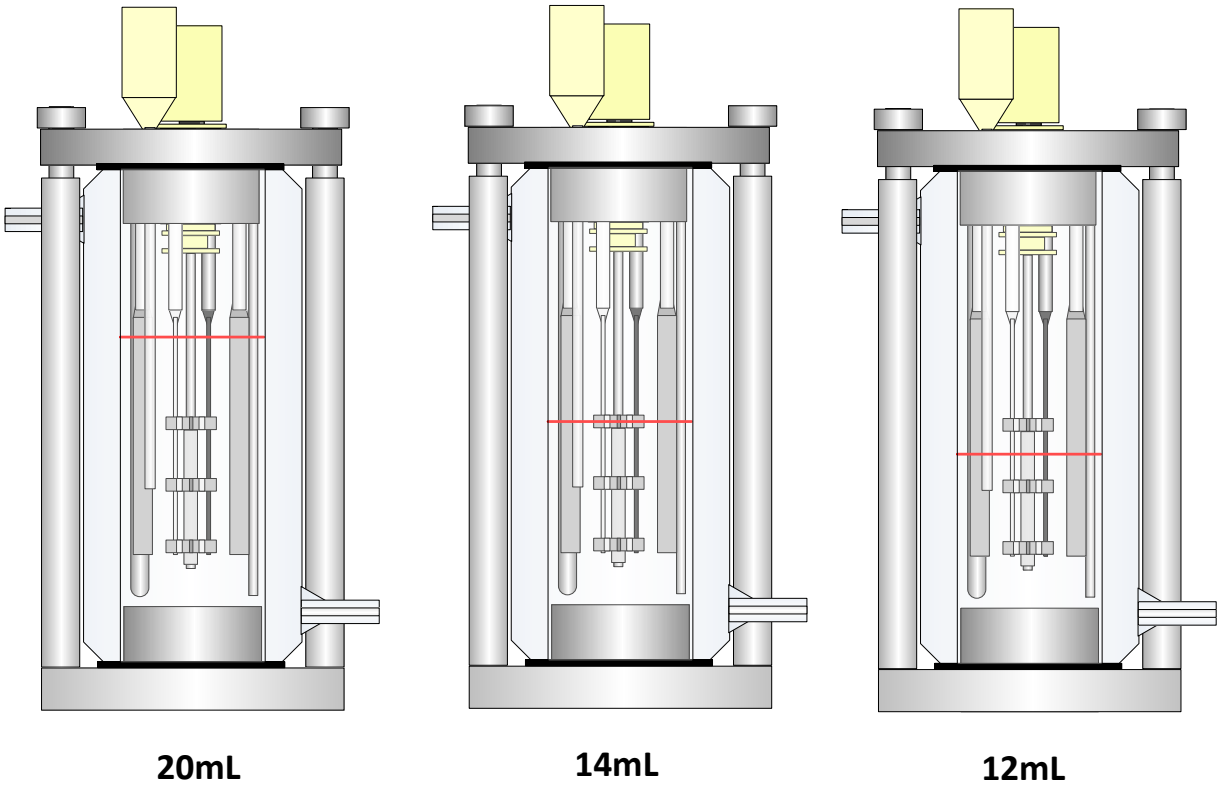

Figure 4.3: Schematic diagram of the 20mL vessel showing the position of the liquid level in relation to the impellers at a fill volume of 20mL, 14mL and 12mL

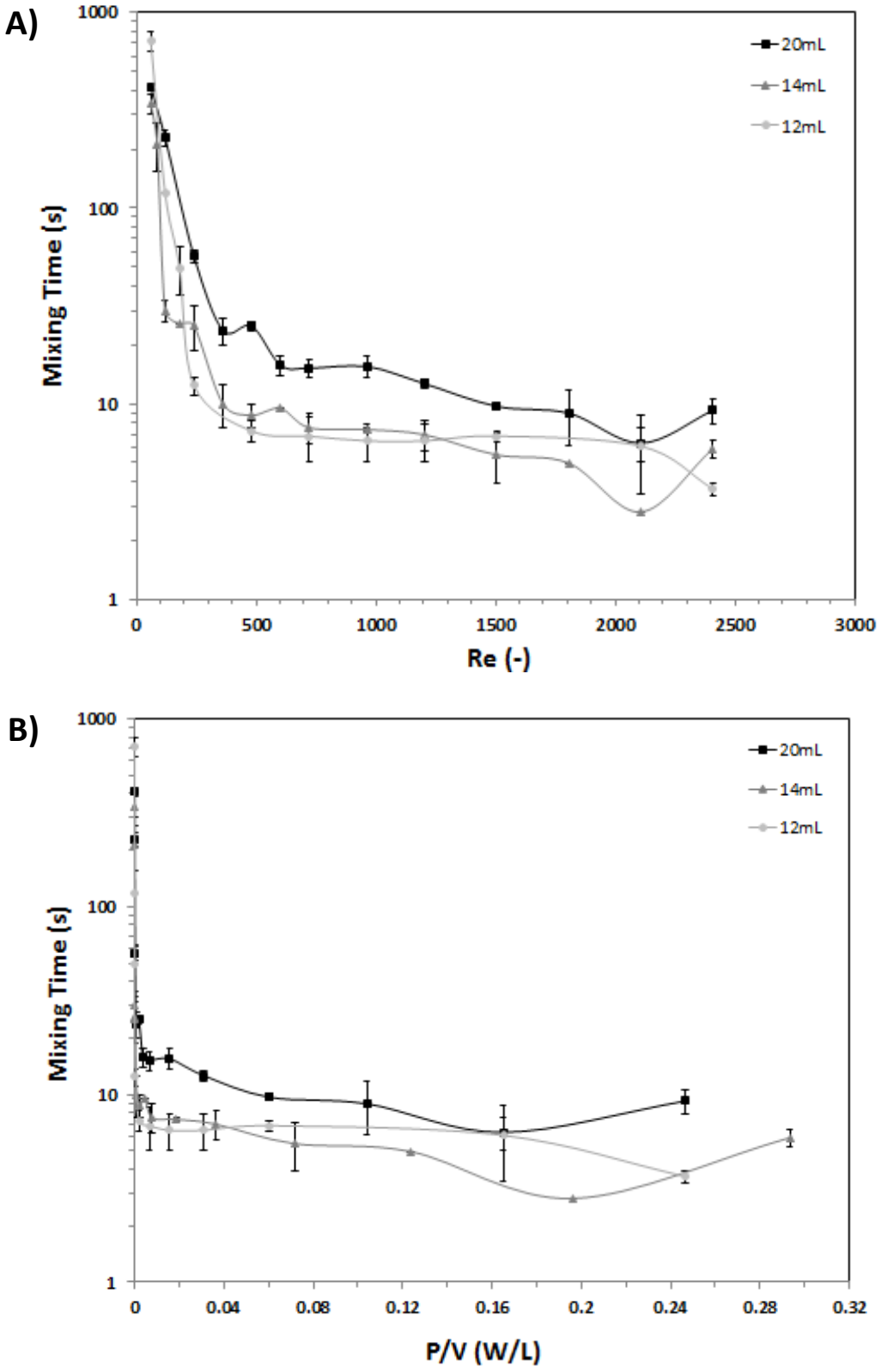

Figure 4.4: The effect of **A)** Re and **B)** P/V on mixing time in the 20mL vessel with varying fill volumes of 20mL, 14mL and 12mL

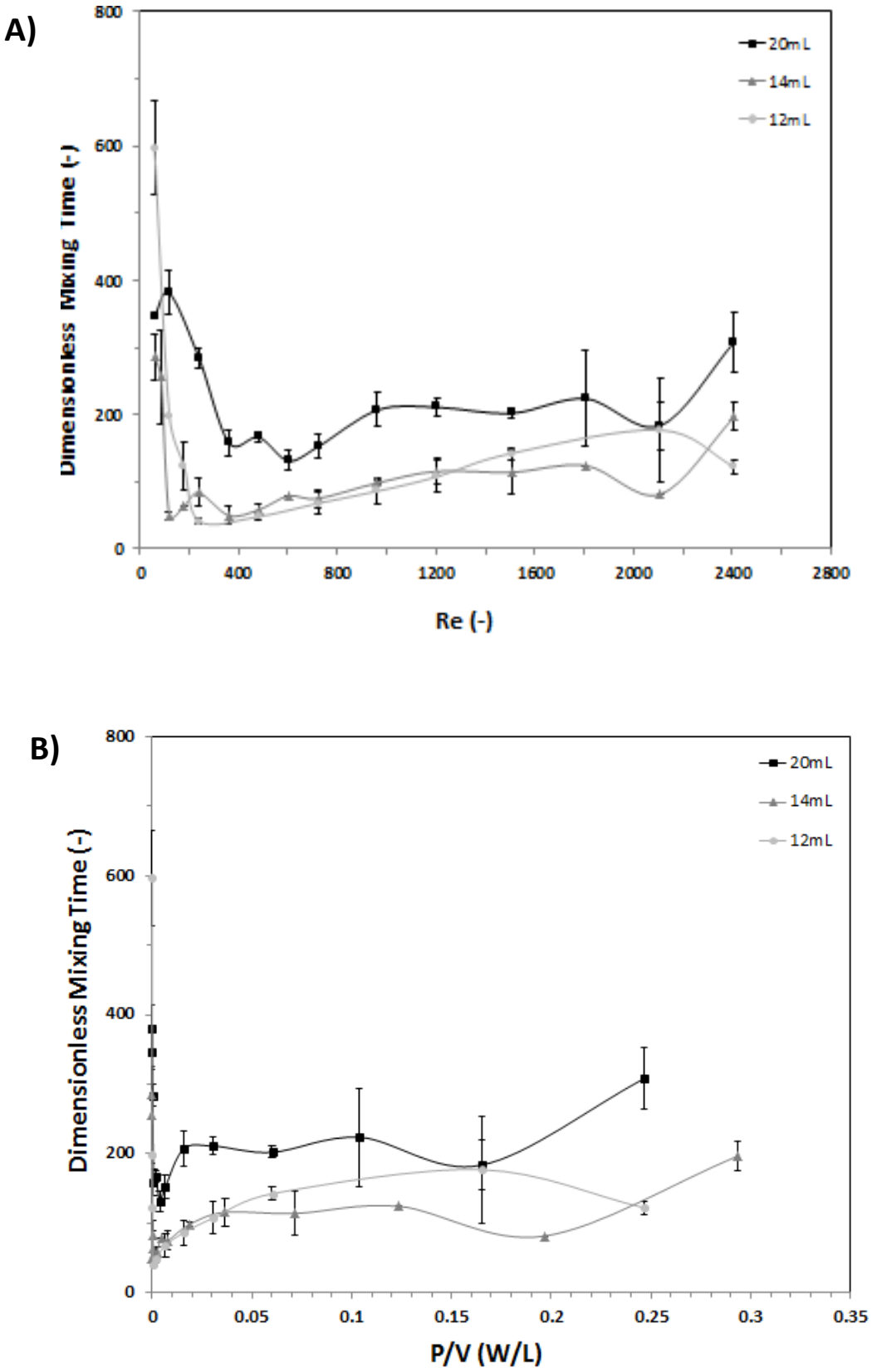

Figure 4.5: The effect of **A)** Re and **B)** P/V on dimensionless mixing in the 20mL vessel with varying fill volumes of 20mL, 14mL and 12mL

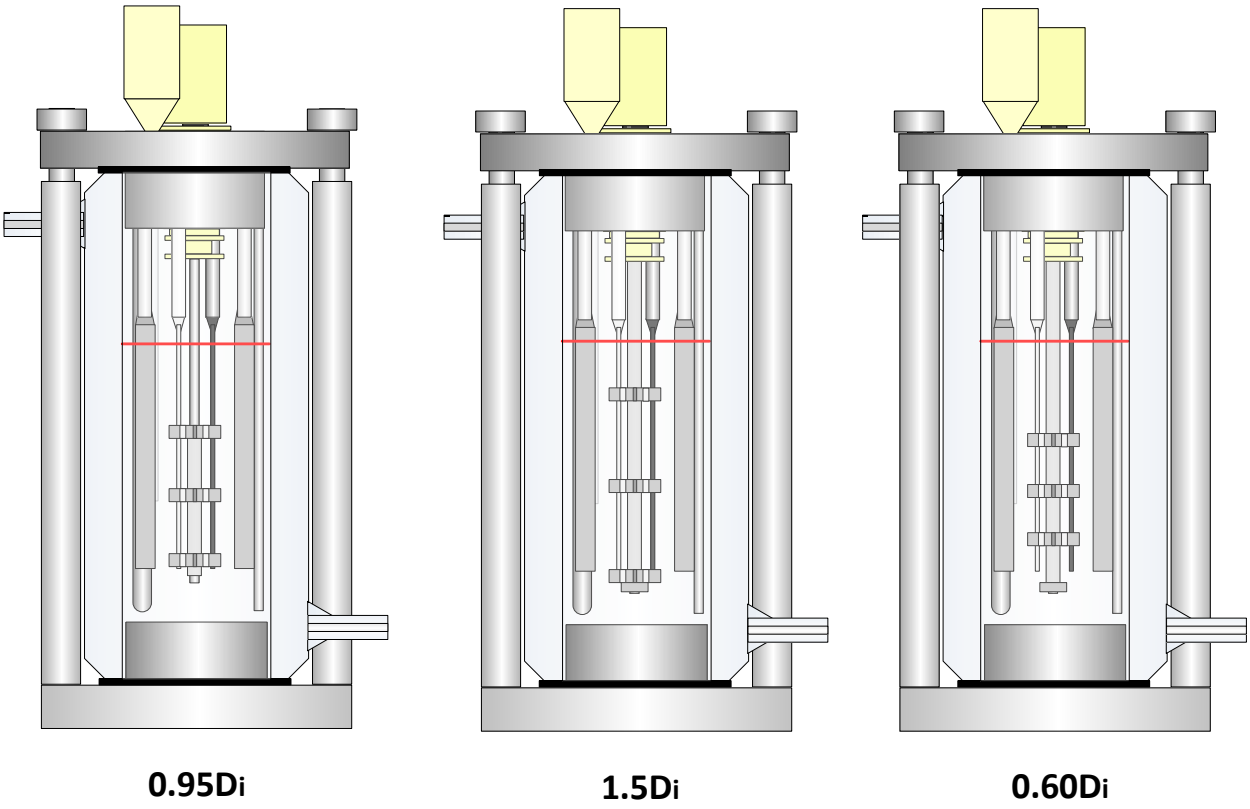

Figure 4.6: Schematic diagram of the 20mL vessel showing the position of three impellers with varying impeller spacing at a fill volume of 20mL

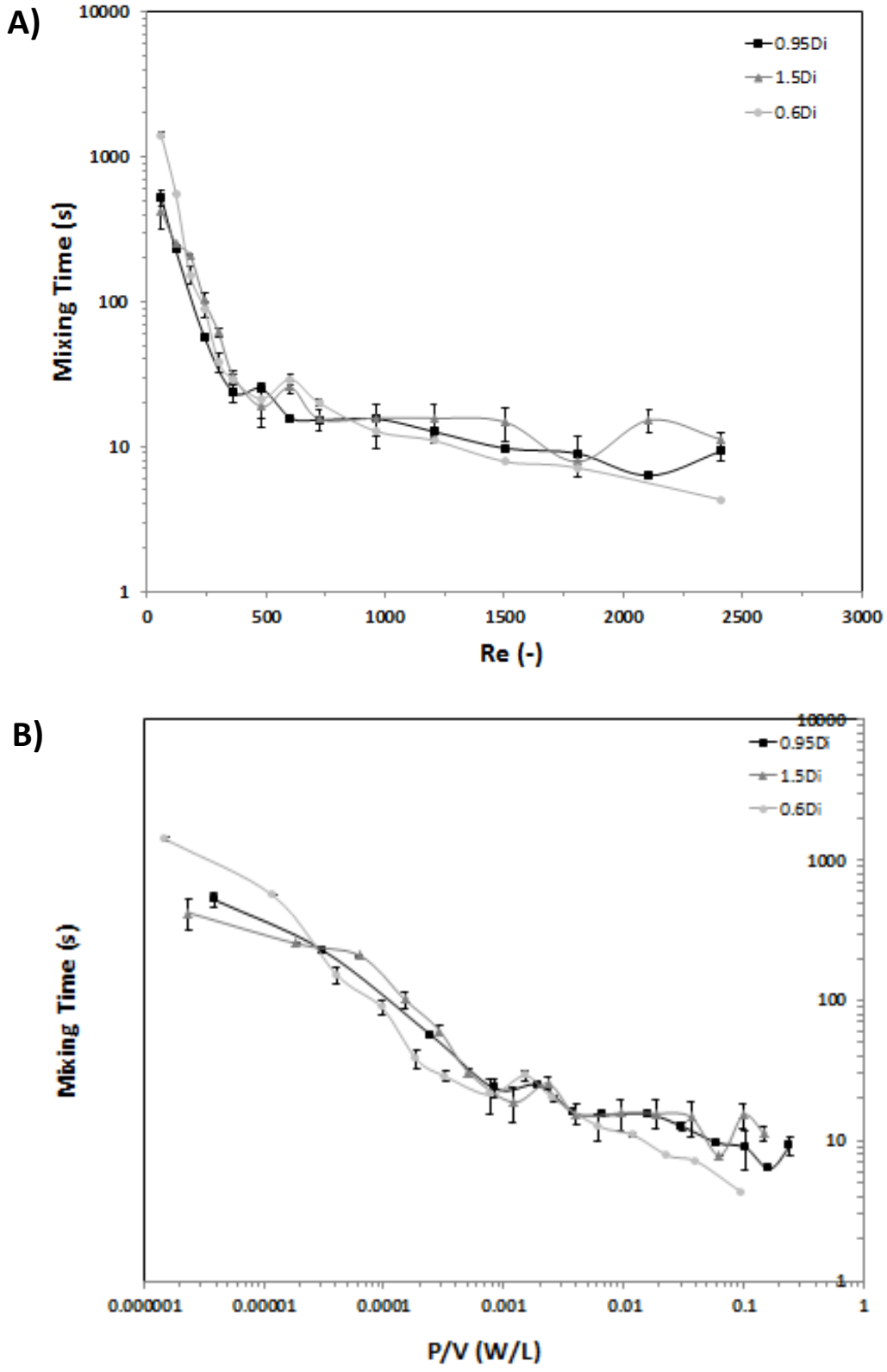

Figure 4.7: The effect of **A)** Re and **B)** P/V on mixing time in the 20mL vessel with varying impeller spacing of $0.95D_i$, $1.5D_i$ and $0.6D_i$ at a fill volume of 20mL

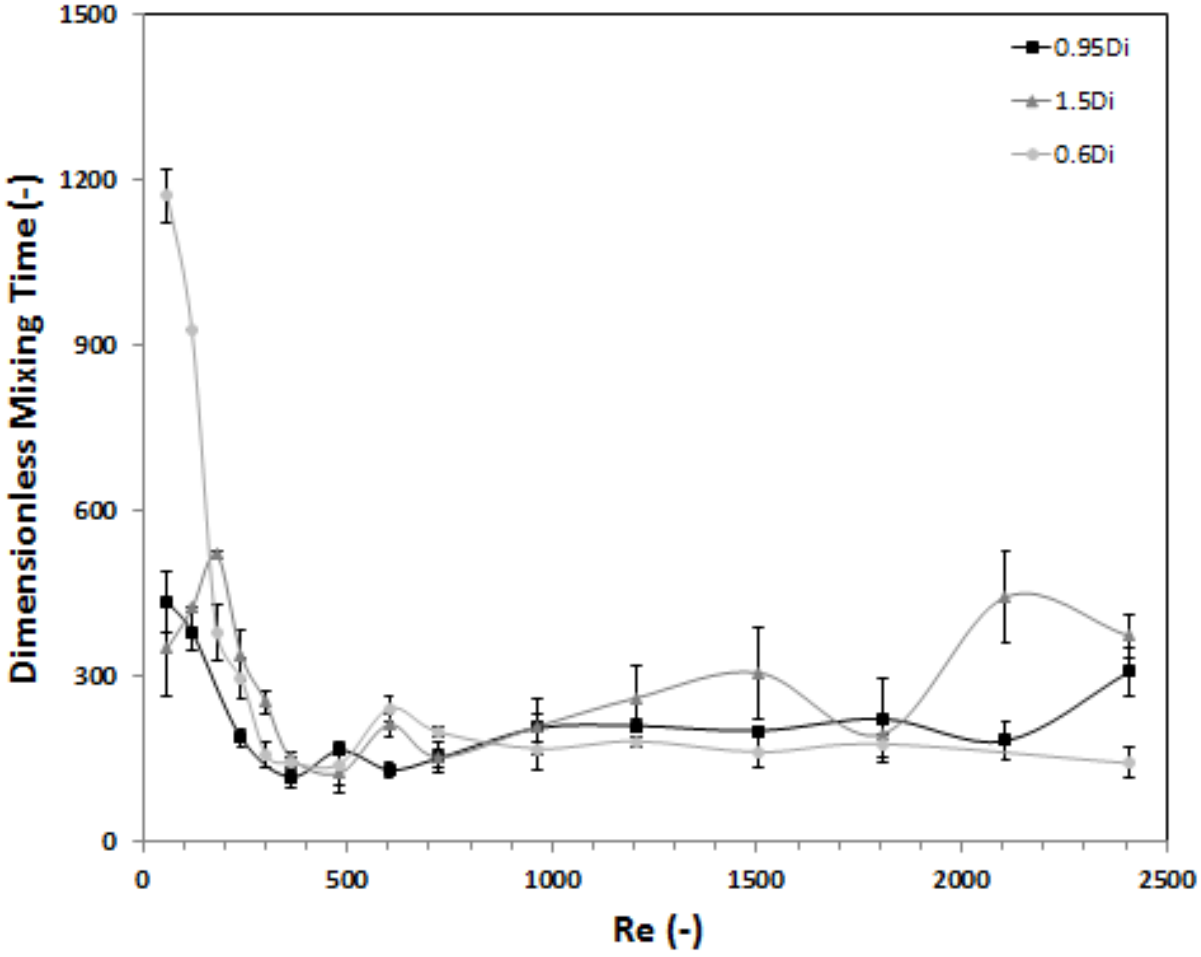

Figure 4.8: The effect of Re on dimensionless mixing in the 20mL vessel with varying impeller spacing of $0.95D_i$, $1.5D_i$ and $0.6D_i$ at a fill volume of 20mL

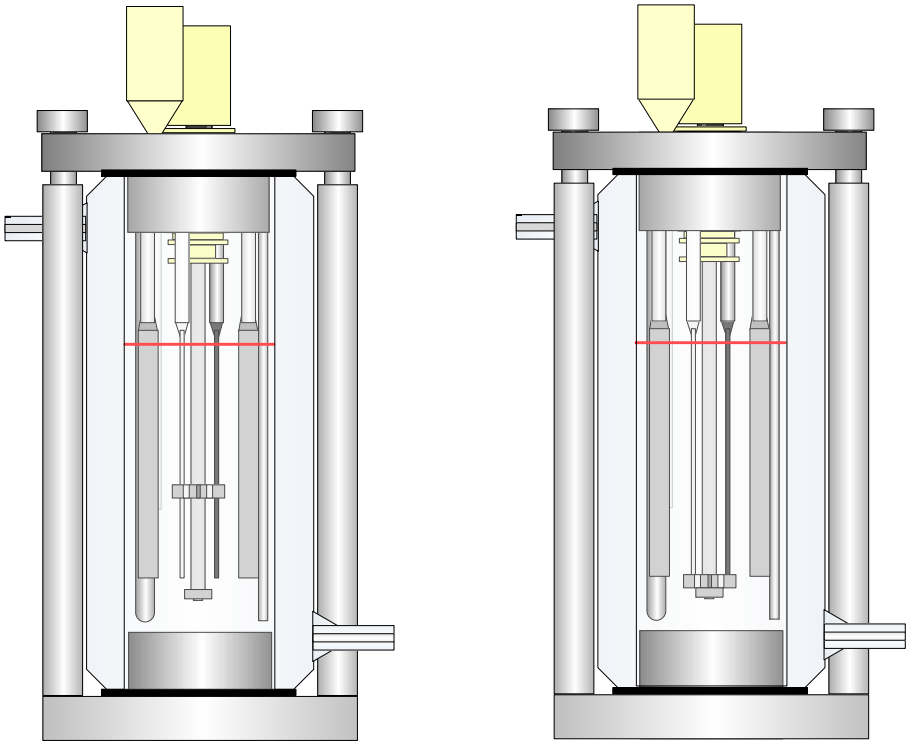

Figure 4.9: Schematic diagram of the 20mL vessel showing the position of the single impeller on the middle of the shaft and at the bottom of the shaft at a fill volume of 20mL

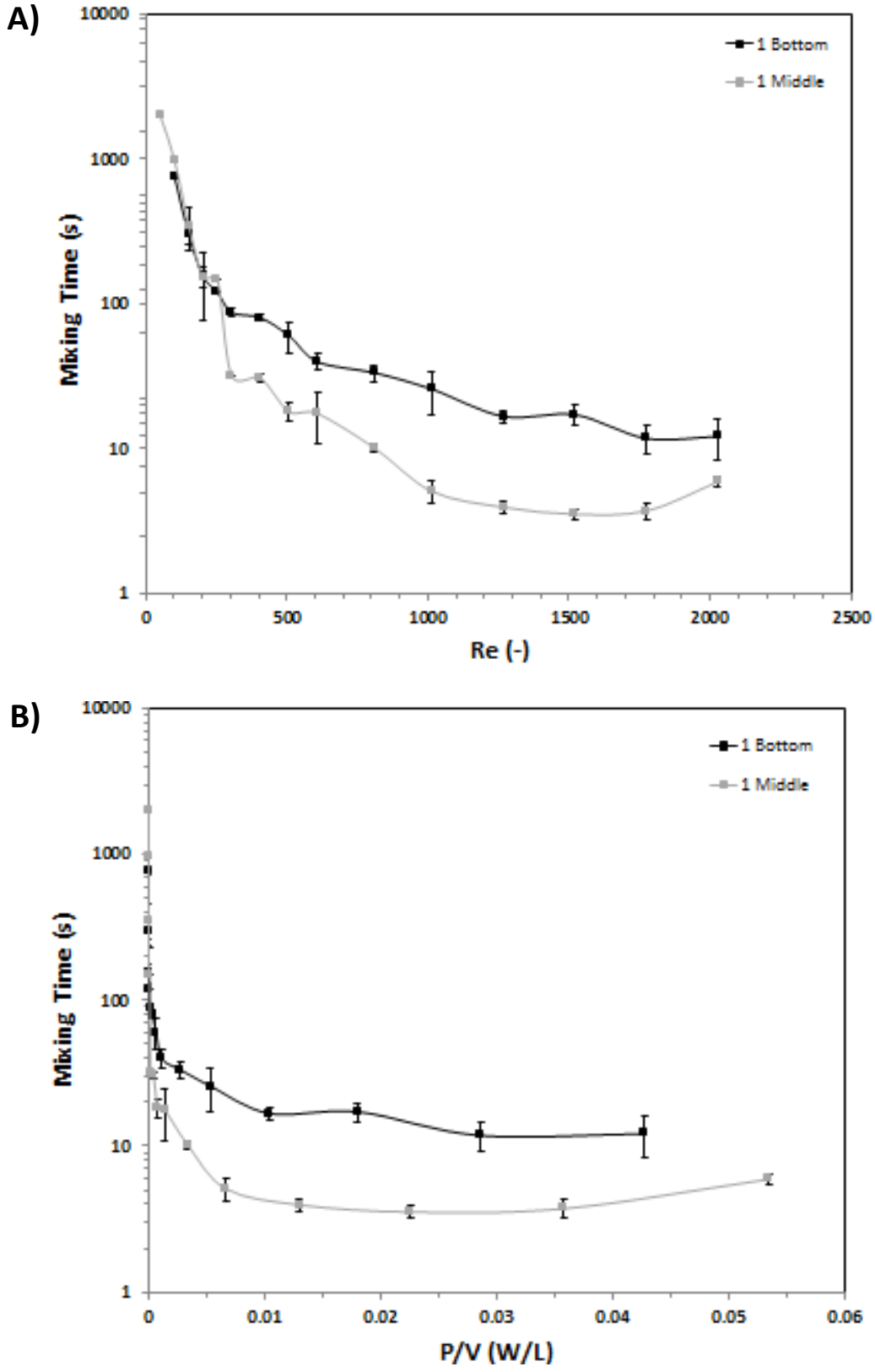

Figure 4.10: The effect of **A)** Re and **B)** P/V on mixing time in the 20mL vessel with the single impeller on the middle of the shaft compared to bottom of the shaft at a fill volume of 20mL

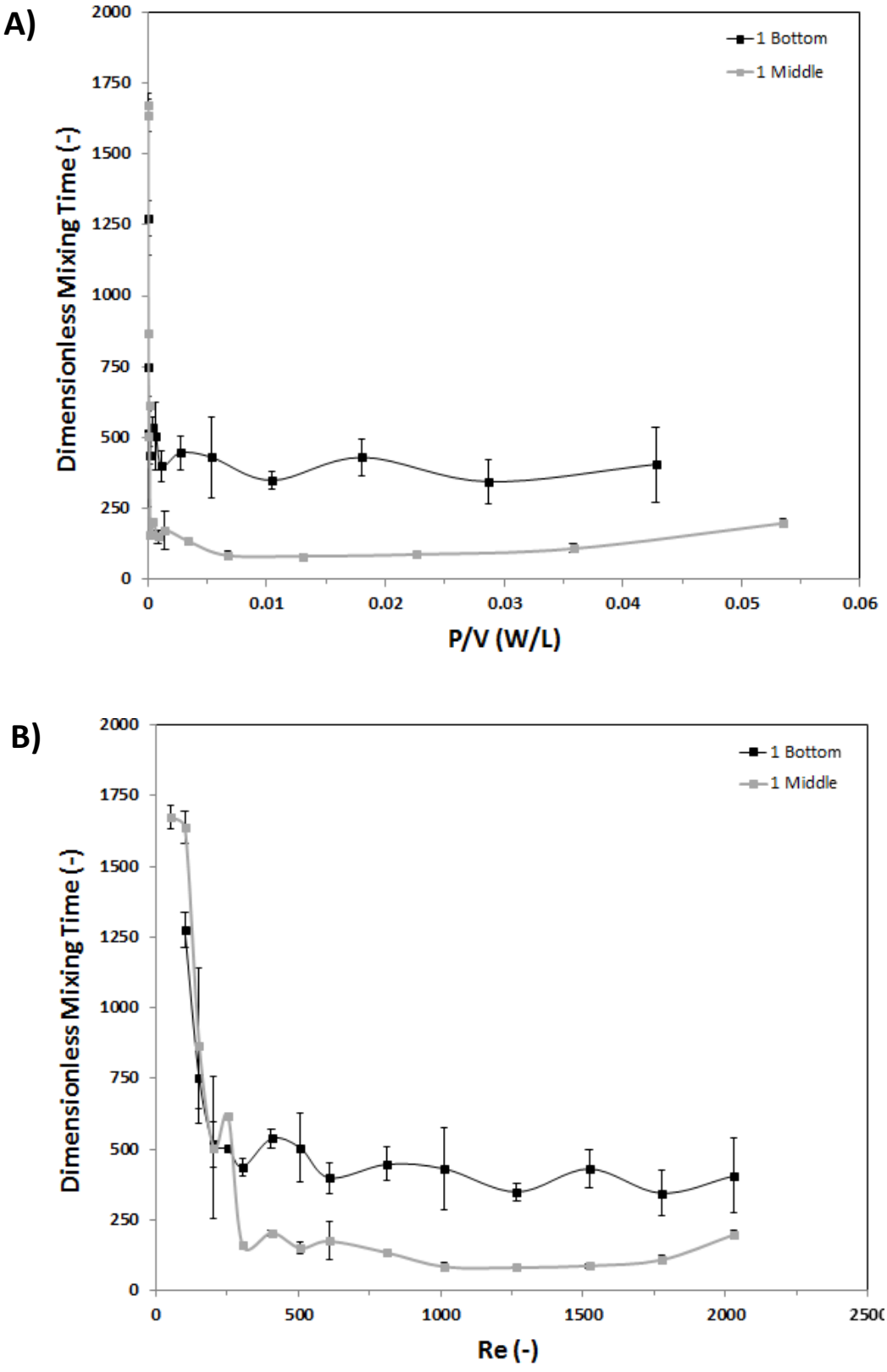

Figure 4.11: The effect of **A)** Re and **B)** P/V on dimensionless mixing in the 20mL vessel with the single impeller on the middle of the shaft compared to bottom of the shaft at a fill volume of 20mL

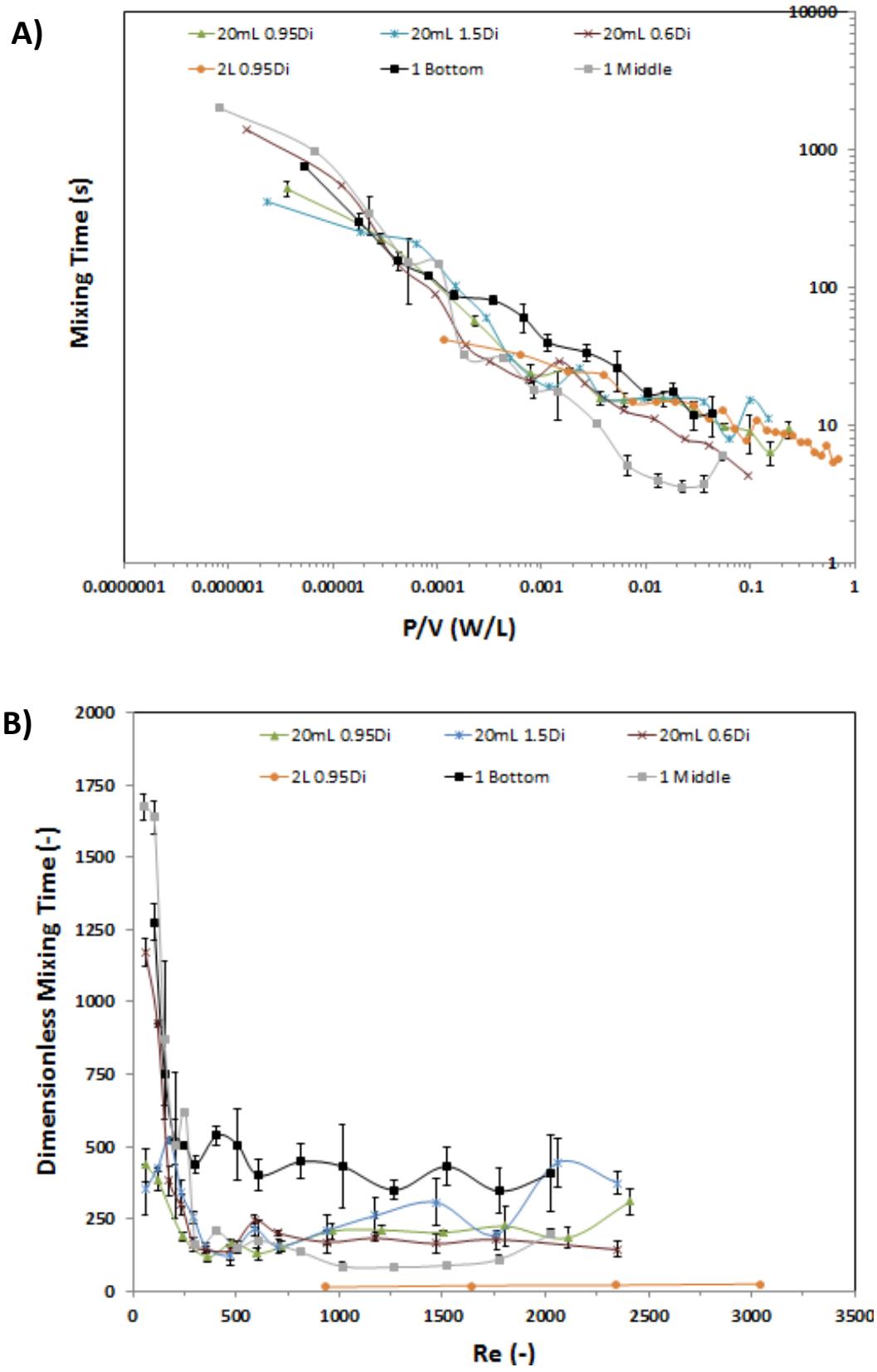

Figure 4.12: The effect of **A)** P/V on mixing time and **B)** Re on dimensionless mixing time for the 20mL vessel with varying fill volumes, varying impeller spacing, varying single impeller position in comparison to the 2L vessel

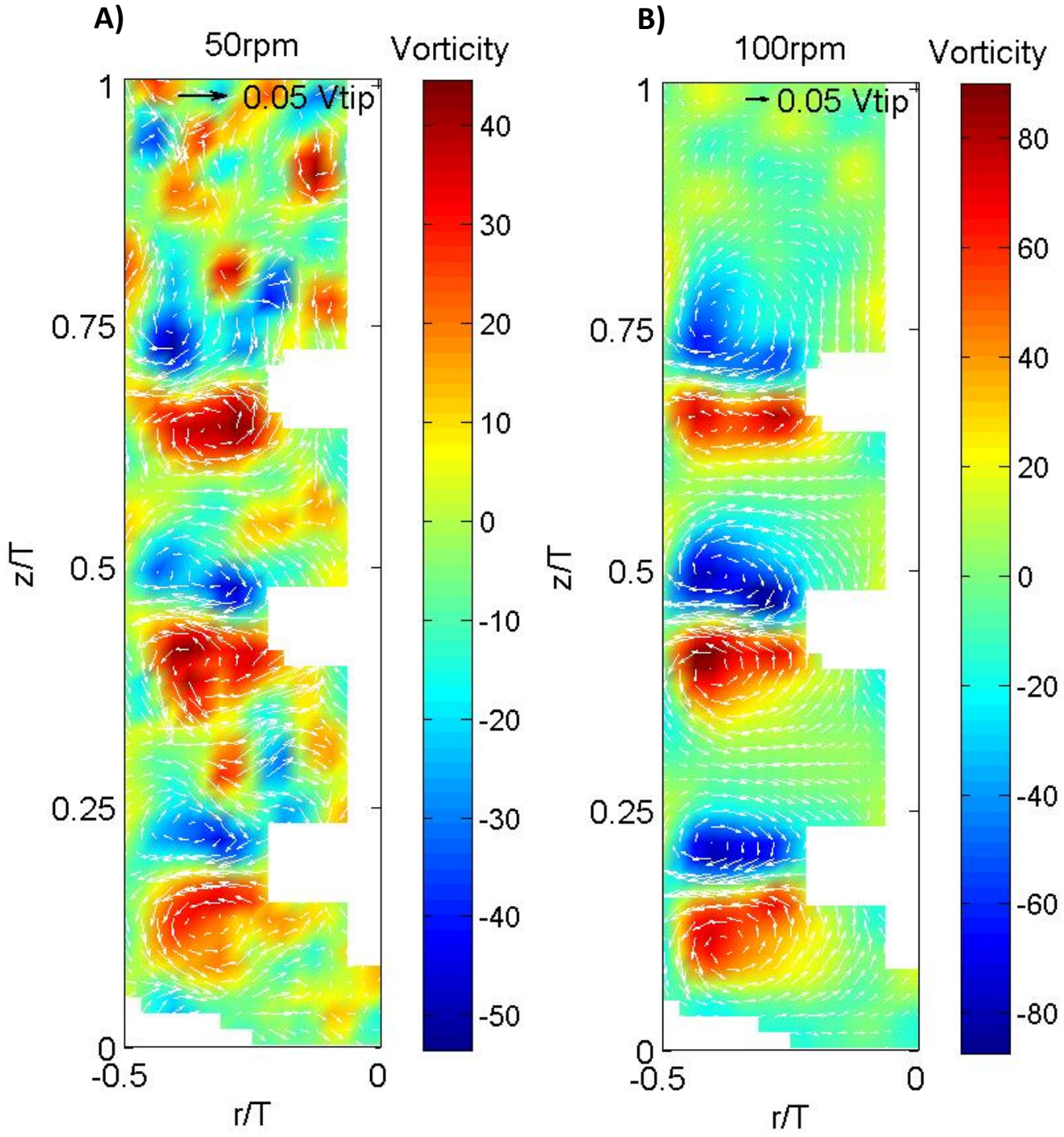

Figure 4.13: Velocity vectors and vorticity contour plots in an unbaffled 20mL vessel with a fill volume of 20mL at impeller speeds of **A)** 50rpm (P/V = 4 x 10^{-6}W L^{-1}, Tip speed = 0.022m/s, Re = 70) and **B)** 100rpm (P/V = 3.5 x 10^{-5}W L^{-1} , Tip speed = 0.045m/s, Re = 130)

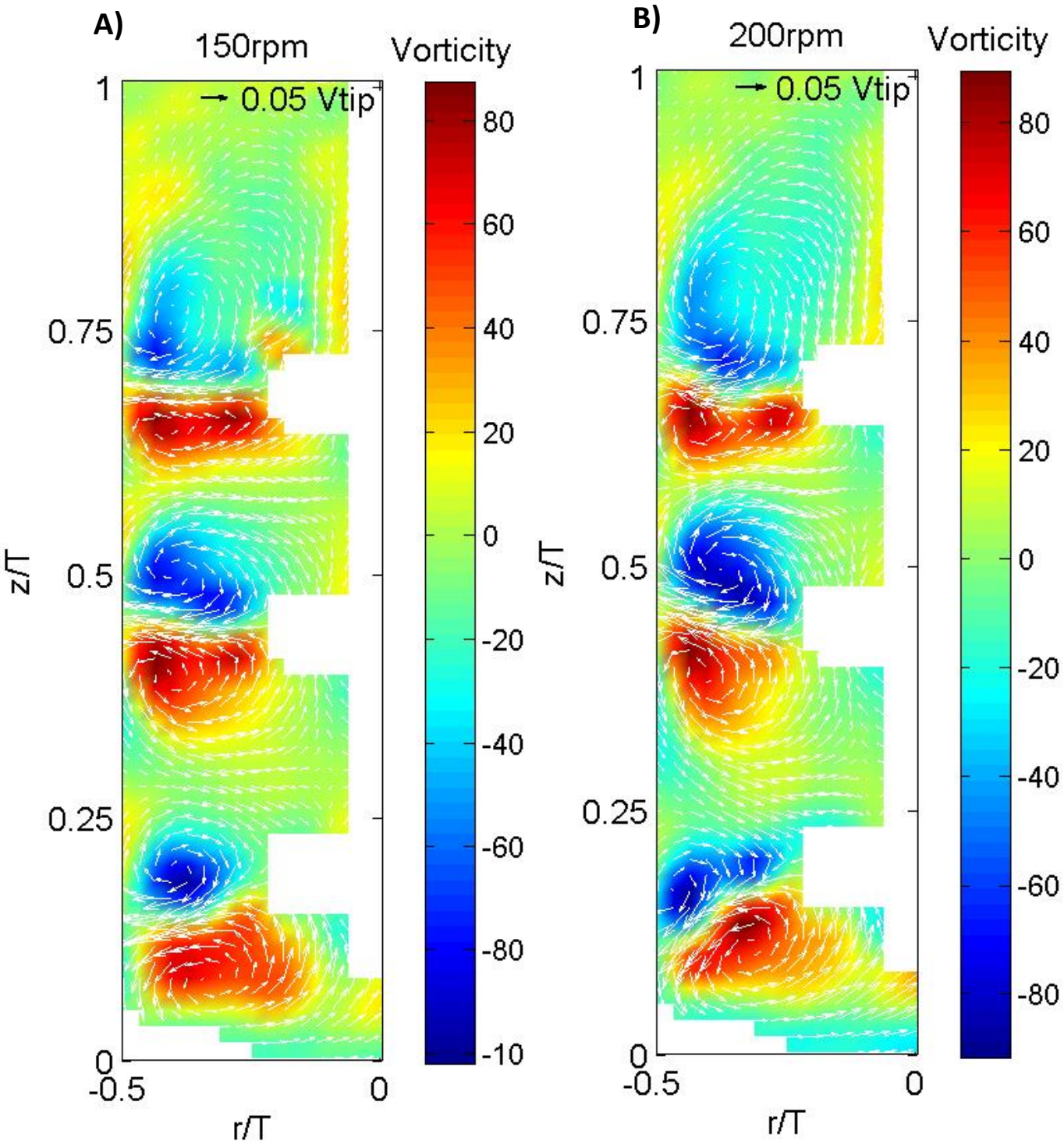

Figure 4.14: Velocity vectors and vorticity contour plots in an unbaffled 20mL vessel with a fill volume of 20mL at impeller speeds of **A)** 150rpm (P/V = 1.2 x 10^{-4}W L^{-1}, Tip speed = 0.067m/s Re = 200) and **B)** 200rpm (P/V = 2.7 x 10^{-4}W L^{-1}, Tip speed = 0.09m/s, Re = 270)

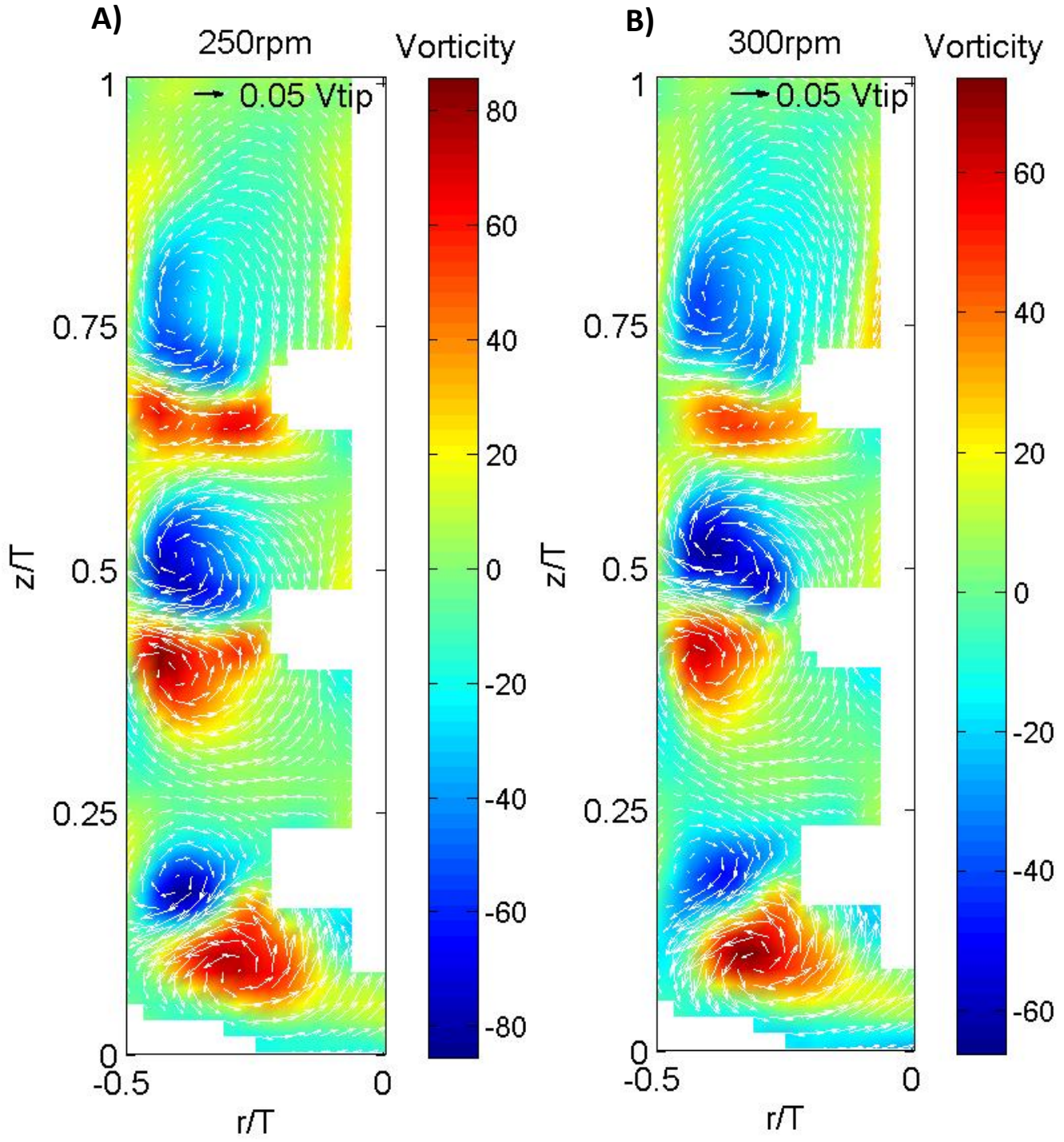

Figure 4.15: Velocity vectors and vorticity contour plots in an unbaffled 20mL vessel with a fill volume of 20mL at impeller speeds of **A)** 250rpm ($P/V = 5 \times 10^{-4} W\ L^{-1}$, Tip speed = 0.11 m/s Re = 330) and **B)** 300rpm ($P/V = 9 \times 10^{-4} W\ L^{-1}$, Tip speed = 0.13m/s, Re = 400)

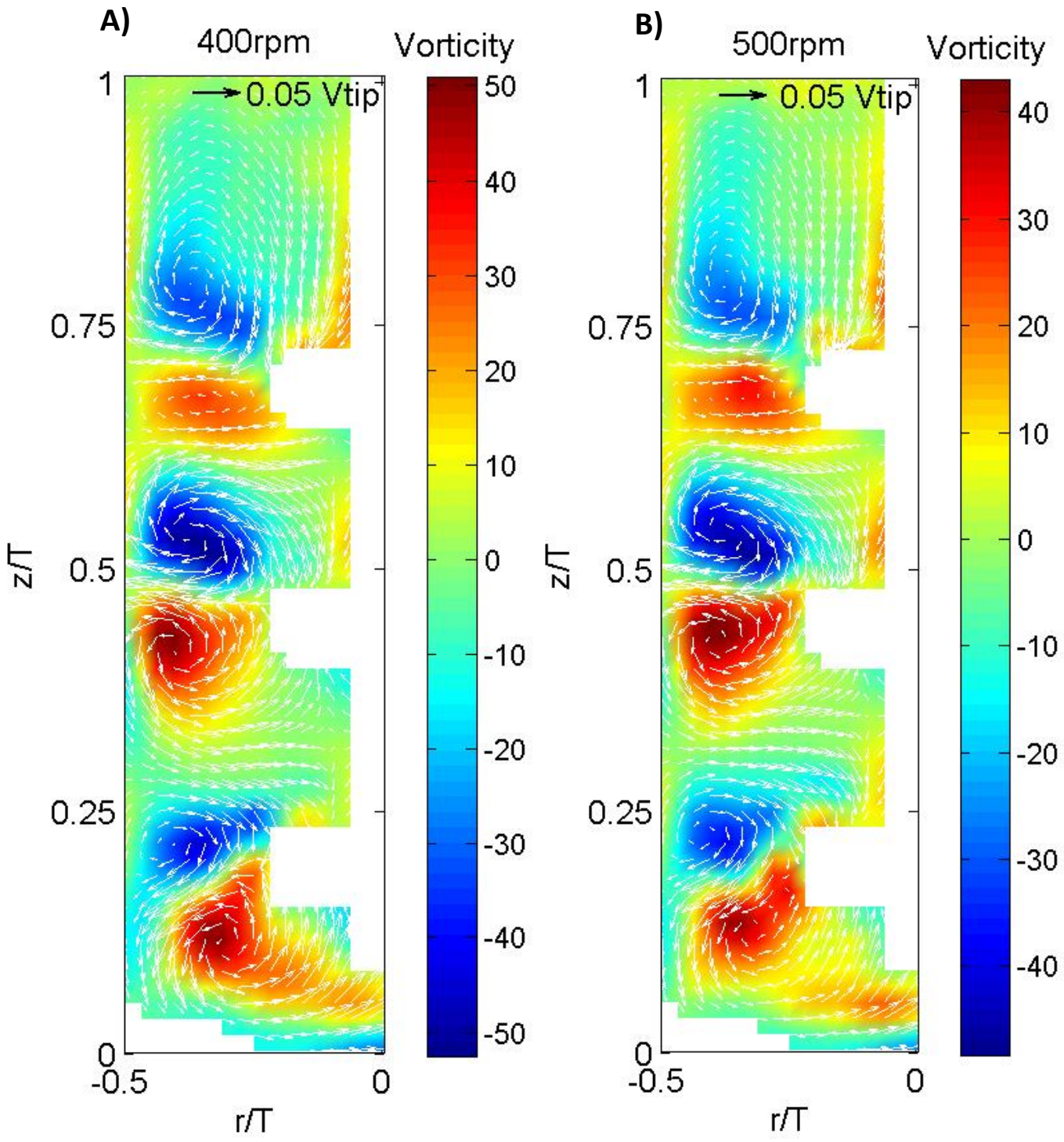

Figure 4.16: Velocity vectors and vorticity contour plots in an unbaffled 20mL vessel with a fill volume of 20mL at impeller speeds of **A)** 400rpm (P/V = 2.2 x 10^{-3}W L^{-1}, Tip speed = 0.18m/s Re = 530) and **B)** 500rpm (P/V = 4.2 x 10^{-3}W L^{-1}, Tip speed = 0.22m/s, Re = 660)

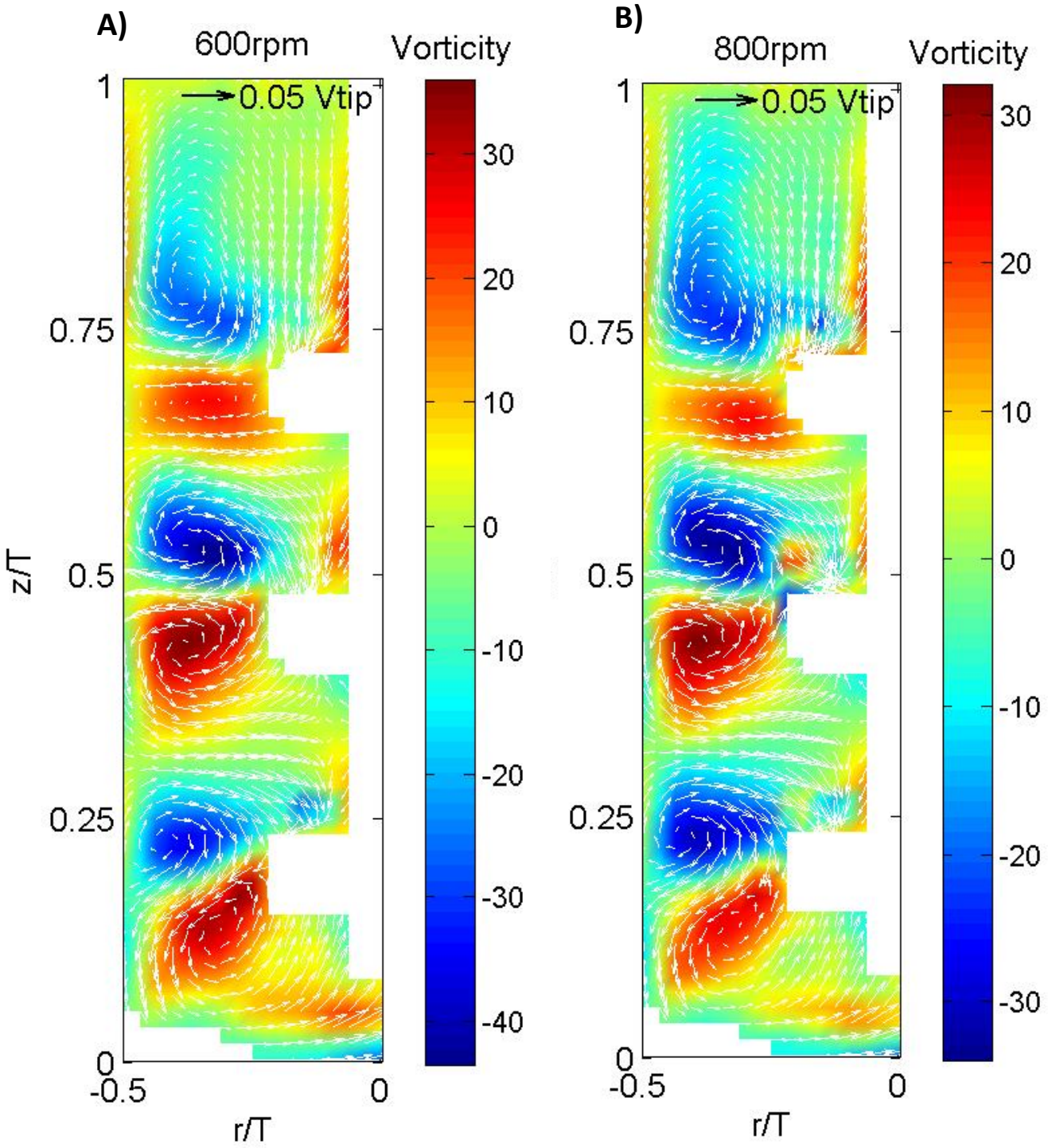

Figure 4.17: Velocity vectors and vorticity contour plots in an unbaffled 20mL vessel with a fill volume of 20mL at impeller speeds of **A)** 600rpm (P/V = 7.3 x 10^{-3}W L^{-1}, Tip speed = 0.27m/s, Re = 800) and **B)** 800rpm (P/V = 0.017W L^{-1}, Tip speed = 0.36m/s, Re = 1000)

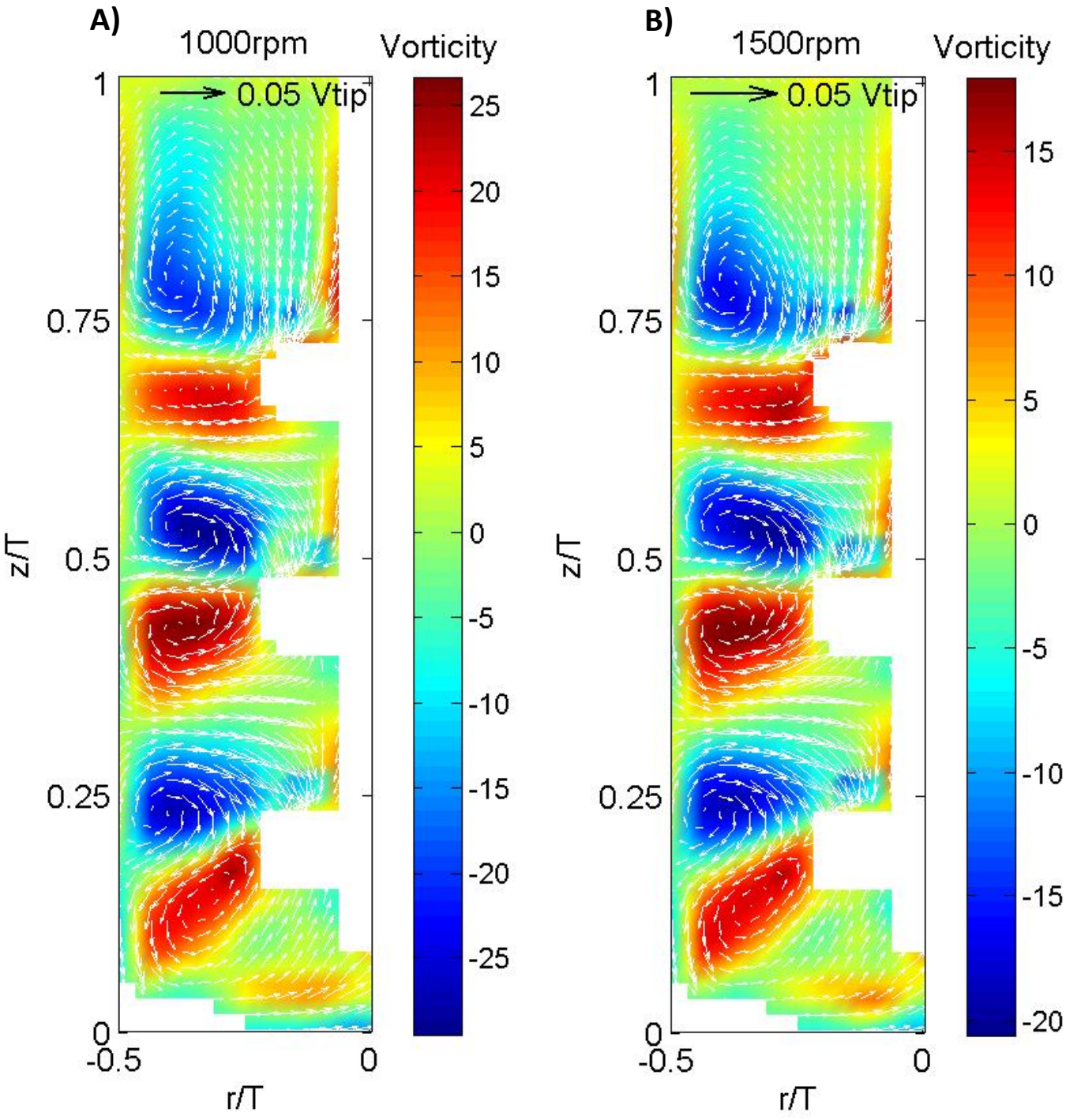

Figure 4.18 : Velocity vectors and vorticity contour plots in an unbaffled 20mL vessel with a fill volume of 20mL at impeller speeds of **A)** 1000rpm (P/V = 0.034W L^{-1}, Tip speed = 0.45m/s Re = 1300) and **B)** 1500rpm (P/V = 0.115 x 10^{-2}W L^{-1}, Tip speed = 0.67m/s, Re = 2000)

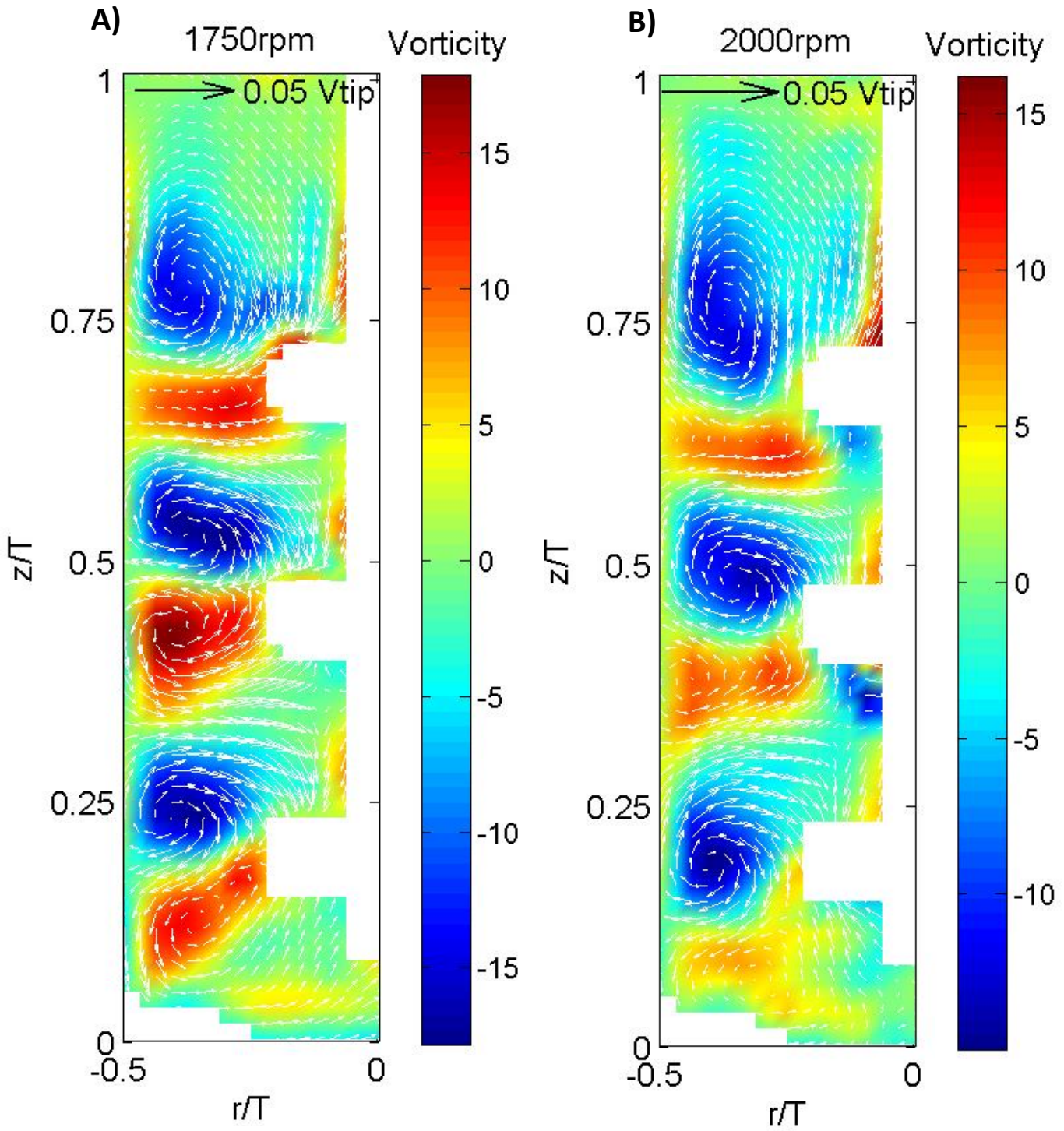

Figure 4.19: Velocity vectors and vorticity contour plots in an unbaffled 20mL vessel with a fill volume of 20mL at impeller speeds of **A)** 1750rpm (P/V = 0.18W L^{-1}, Tip speed = 0.78m/s, Re = 2300) and **B)** 2000rpm (P/V = 0.27W L^{-1}, Tip speed = 0.89m/s, Re = 2650)

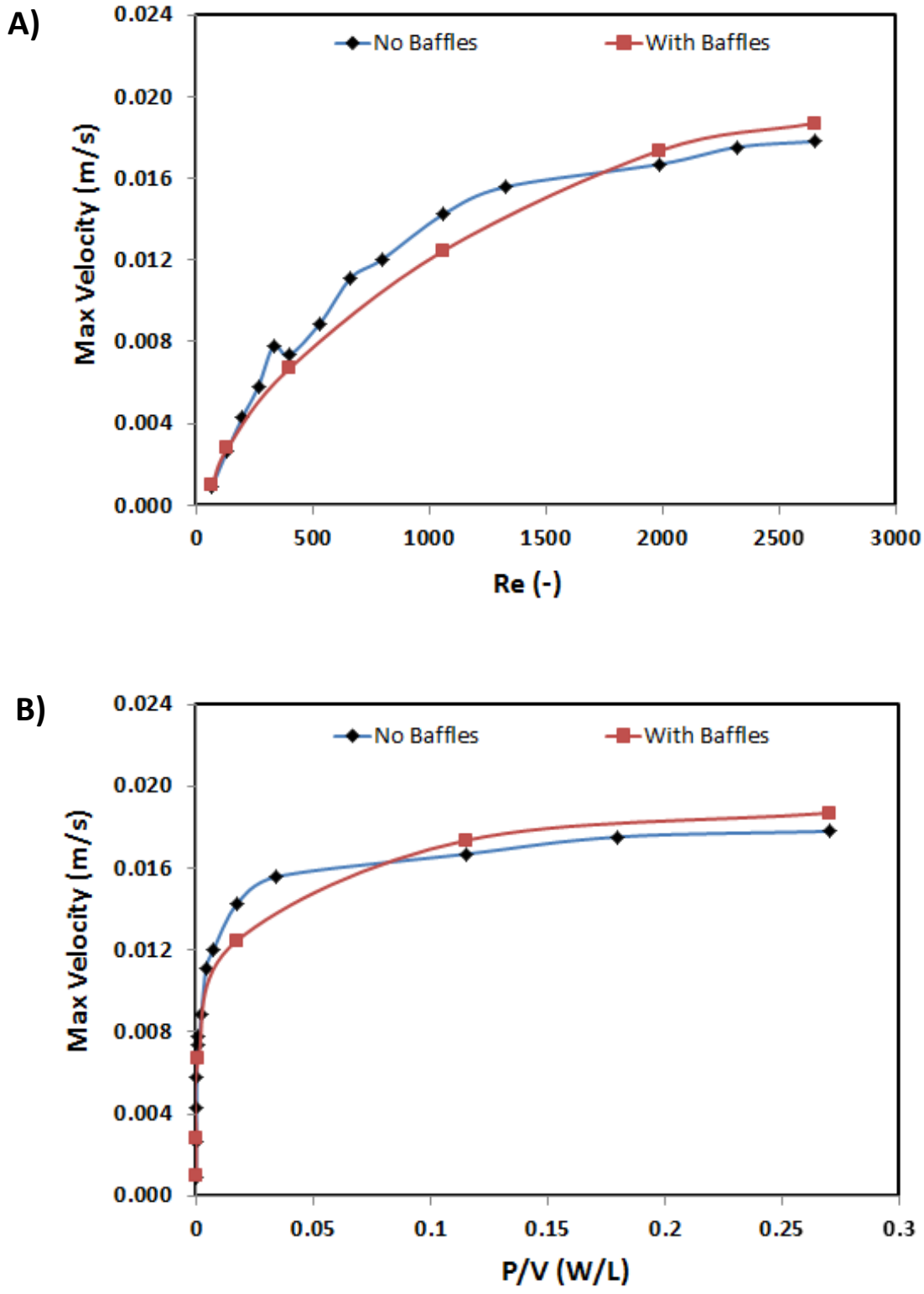

Figure 4.20: The effect of **A)** Re and **B)** P/V on maximum velocity obtained in the 20mL vessel using PIV

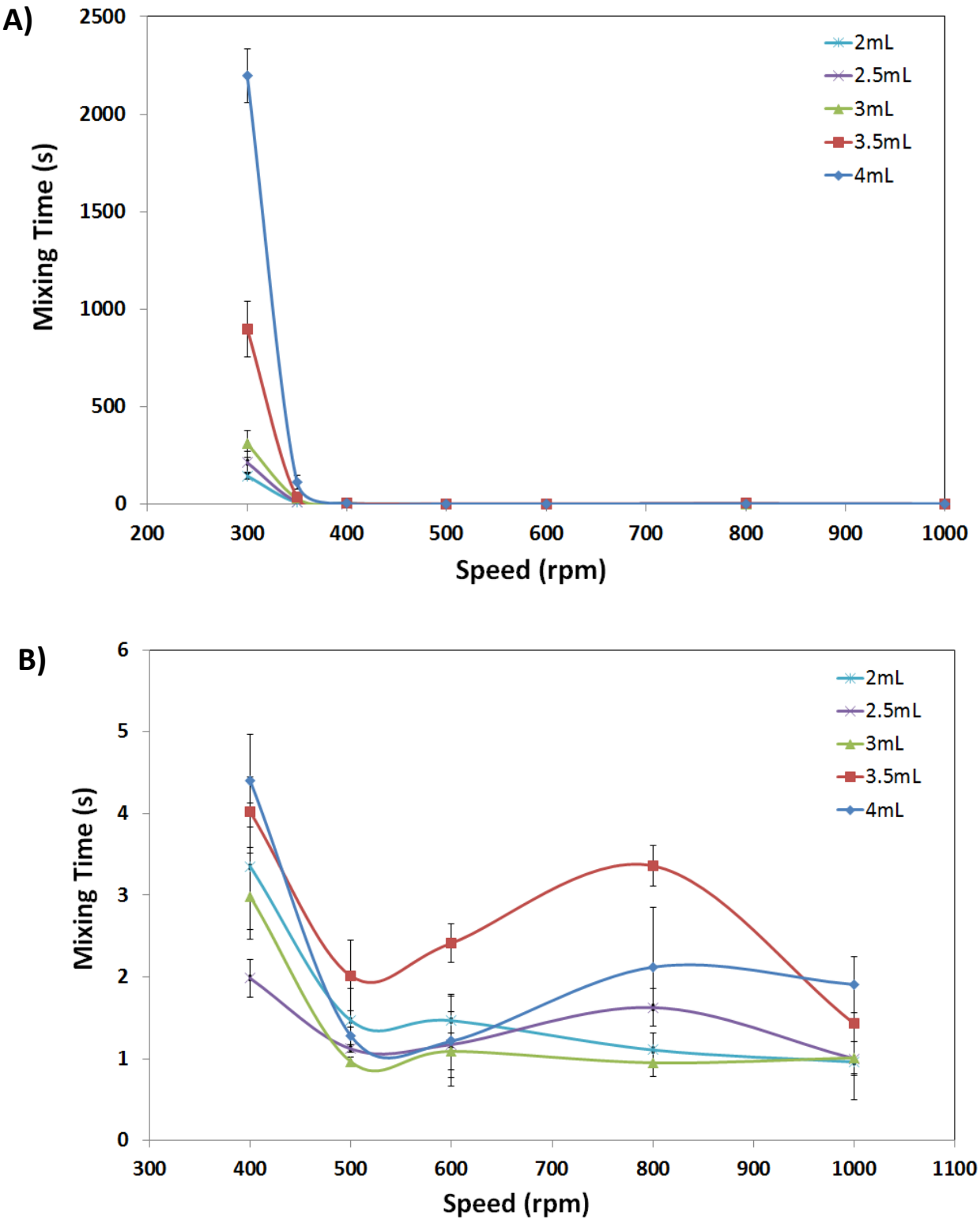

Figure 4.21: The effect of shaker speed, from **A)** 300rpm to 1000rpm and **B)** 400rpm to 1000rpm, on mixing time in a single well of a 24-well DSW plate with fill volumes of 2mL, 2.5L, 3mL, 3.5mL and 4mL

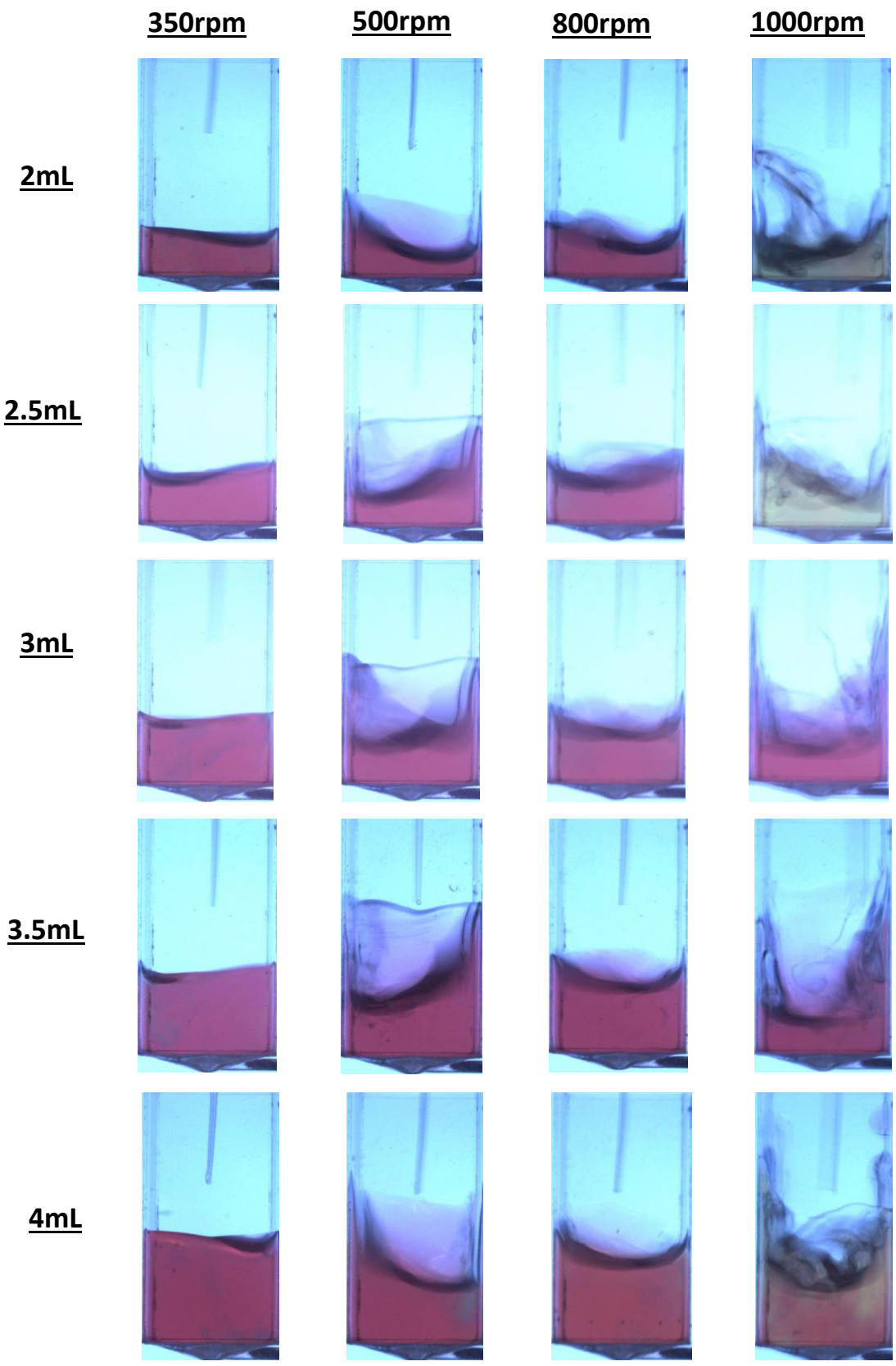

Figure 4.22: Maximum liquid height in the 24-well DSW plate at varying shaker speeds and fill volumes

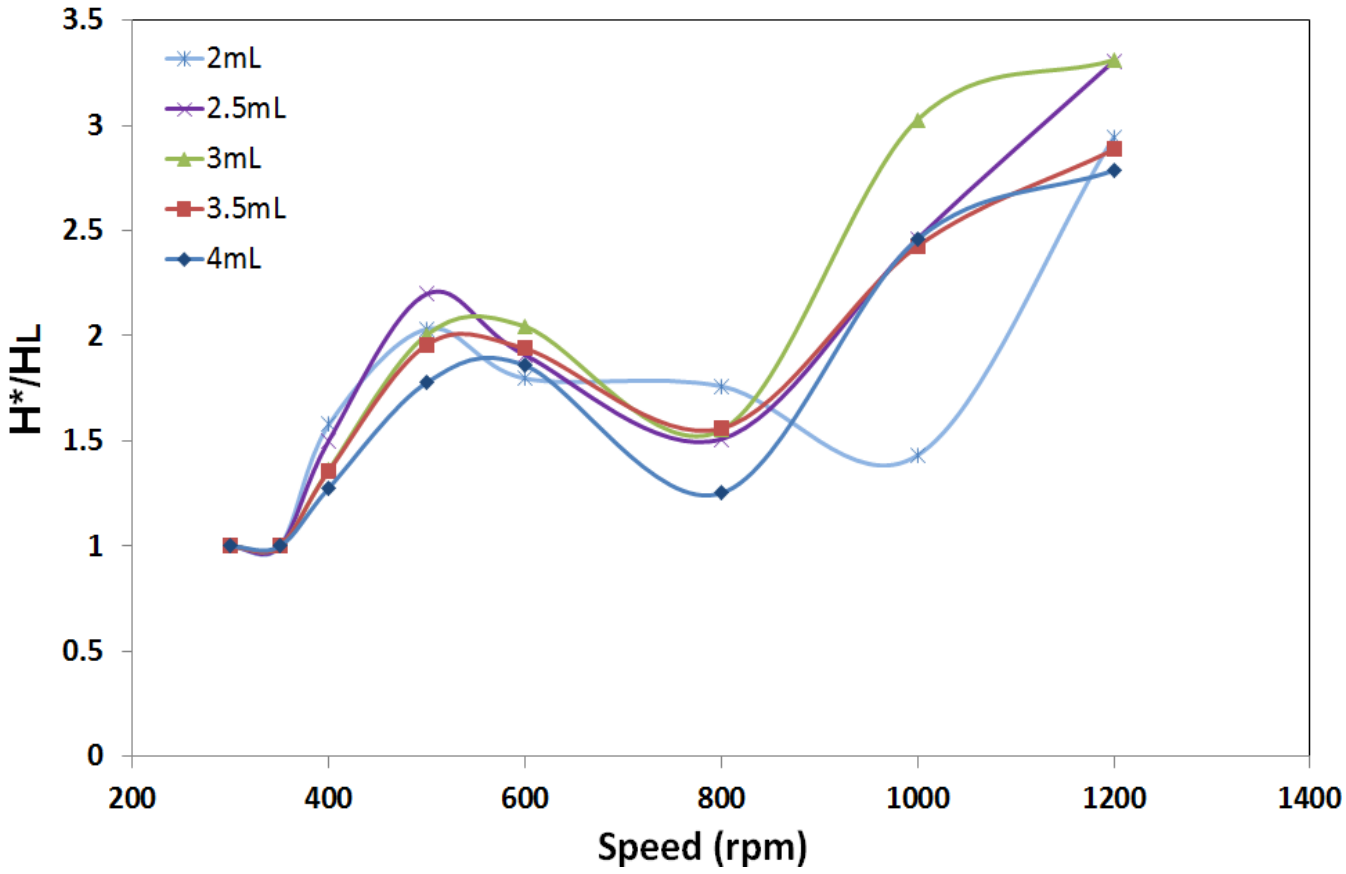

Figure 4.23: The effect of shaker speed on the maximum liquid height (H*) to still height (H_L) ratio at varying shaker speeds in a single well of a 24-well DSW plate with fill volumes of 2mL, 2.5L, 3mL, 3.5mL and 4mL

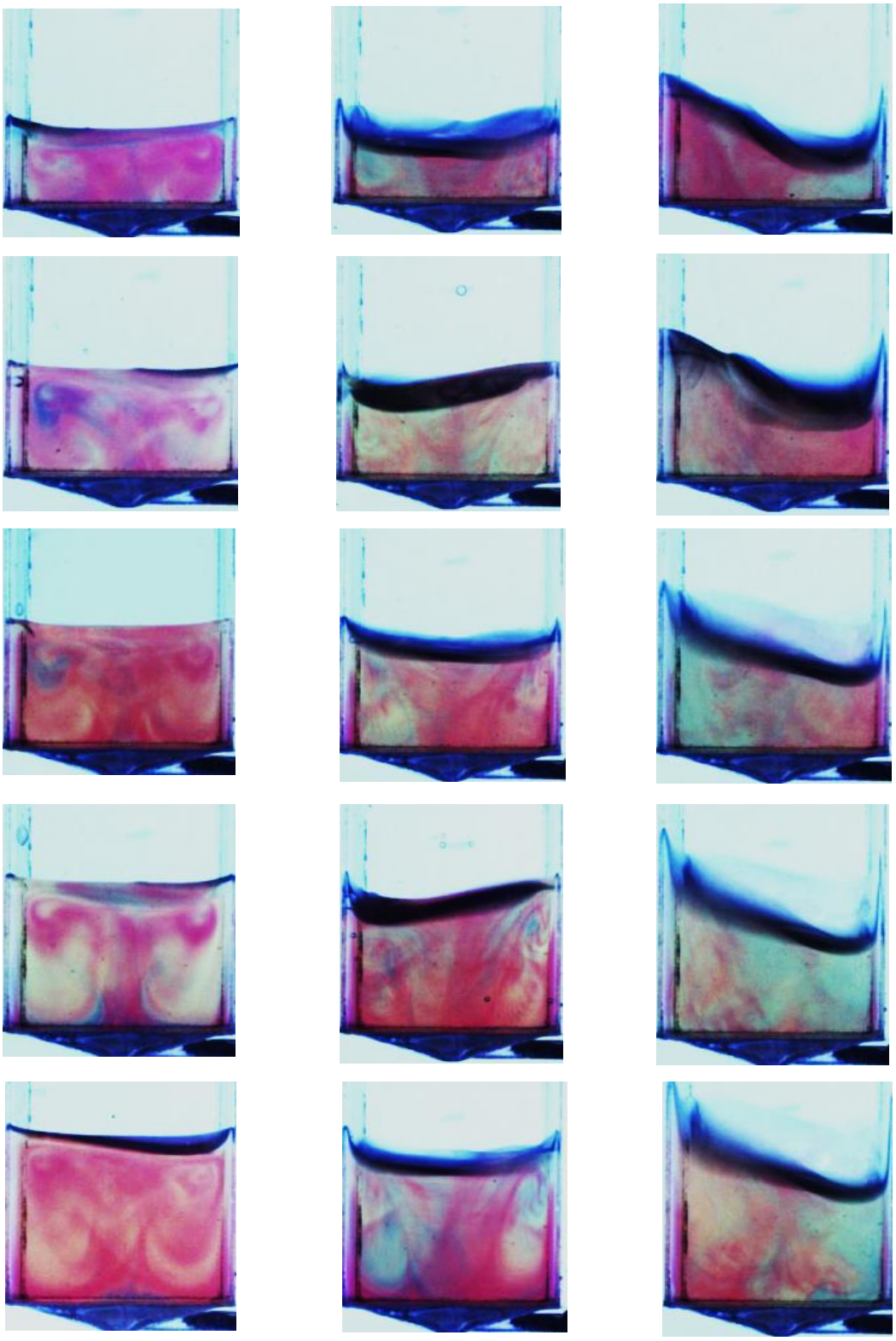

Figure 4.24: Flow patterns inside the 24-well DSW plate at varying shaker speeds and fill volumes

Chapter 5

Large-Scale Verification of the Heat Extraction Performance of the 20mL Scale-Down Vessel

5.1 Introduction and Aims

Heat extraction is one of the primary recovery processes which has been used in industry to recover Fab' from *E.coli* after the initial centrifugation step. The process uses buffers and elevated temperatures to selectively release the Fab' from the periplasmic space. This is an industrial process which is currently used by UCB for their licensed fab' product, Cimzia, that has been on the market since 2008. A review of the mechanism of action has been described in detail in Chapter 1.

The interaction of *E.coli* cells with the tris and EDTA buffers at elevated temperatures damages the cell membrane structure. It is well known that the outer membrane of the cell is disrupted by all three elements, primarily by tris and EDTA (Voss 1967; Irvin *et al*., 1981; Tsuchido *et al*., 1985; Vaara 1992) but also heat (Katsui *et al*., 1982), thus allowing the Fab' to be released from the periplasmic space. The temperatures used for cell lysis can vary but typically thermochemical disruption of the cell wall is achieved by using temperatures of 50-55°C in the presence of tris and EDTA (Tsuchido *et al*., 1985). The quality and strength of the cells prior to the heat extraction step is dependent on the upstream process and therefore may dictate the extent of damage upon exposure to the heat extraction step. Depending on the extraction conditions used to recover the Fab', different amounts of Fab' and other intracellular impurities are released into the cell suspension and the quality of the Fab' protein itself may vary. The heat extraction process relies on efficient heat and mass transfer throughout the vessel, requiring good mixing and homogeneity of the cell suspension and buffers. Chapter 3 looked at the impact of specific power input, heat extraction duration and hold temperature using a DoE approach. The heating duration and temperature at which the extraction is conducted had the most impact on the process performance whereas the specific power input had relatively low impact. The 20mL vessel

was developed to mimic the lab scale and pilot scale extraction process at UCB. Chapter 4 looked at the heating and mixing environment in the 2L and 20mL stirred tank vessels. The results from the mixing time studies indicated that the mixing times matched well between the 2L and 20mL scale and that after a specific power around 0.05W L^{-1}, mixing time was relatively unaffected. In this chapter, the heat extraction process will be conducted in the 20mL vessel and compared to the lab and pilot scale extractions over a variety of different operating conditions such as heating temperatures, heating profiles and specific power input using different strains of Fab'. The choice of operating conditions were based on the conditions typically used by UCB and those previously studied in the DoE in Chapter 3 which had the most significant impact on Fab', total protein and dsDNA. The experiments in this chapter are primarily conducted to verify the feasibility of the 20mL vessel as a suitable scale-down vessel for the lab scale and large scale extraction process. It will also further indicate which parameters the heat extraction process is most sensitive to and will help determine which parameters are important to control during scaling. Although data has been collected from different scales, the focus of this work is on the 20mL and 2L process.

The specific objectives of this chapter are:

- To conduct a number of heat extraction experiments in the 20mL vessel and compare the performance to the 2L, 20L and 200L vessels under repeated and varying operating conditions using different Fab' types
- To visualise the structure of the cell and cell membrane before and after heat extraction and acid precipitation, using scanning electron microscopy (SEM), in order to gain a better understanding of the nature of damage to the cells

5.2 Experimental Approach

Cells were harvested after fermentation using a dead end or disc stack centrifuge. The type of centrifuge used to harvest cells was dependent on the scale of the fermentation, namely disc stack centrifugation was used for 20L or 200L fermentations and dead-end centrifugation was used after 5L fermentations. The details of the fermentation and

centrifugation process conditions used for the experiments are detailed in Table 5.1 and Table 5.2, respectively. The heavy phase obtained from centrifugation was placed into the vessels of choice and heat extraction was conducted after the addition of tris and EDTA buffer under a selected heating profile. Details of the heat extraction process conditions are detailed in Table 5.3. The extraction profiles used in each experiment can be viewed in Appendix 5A. A detailed description of the heat extraction process methodology can be seen in section 2.4. The key outputs that were assessed to compare performance between different scales are the same as those in Chapter 3 which are Fab' titre, total protein concentration, dsDNA concentration and purified Fab' profiles. In addition, HCP profiles after extraction and acid precipitation were also obtained as described in section 2.5,.

In order to observe the structure of the cell and cell membrane using SEM, cell samples were taken from a 5L fermentation process after harvesting, after a 2L heat extraction process and after acid precipitation. This was from Exp #11 as seen in Table 5.3. A detailed description of the SEM methodology is described in section 2.5.9.

5.3 Results and Discussion

5.3.1 Scanning Electron Microscopy

To observe the structure of the cells using SEM at different points during the upstream and primary recovery stage, images were taken under different magnification levels of 5000, 30,000 and 40,000. As shown in Figure 5.1, it is clear that the cells are in a healthy state at the end of the fermentation stage. All cells are less than 3µm in size and display the typical rod shaped physiology, seen of an *E.coli* cell (Reshes *et al*., 2008). Although cell imaging only takes into account a sample of the cells at one time, Figure 5.2A shows that there is no observable disruption in the larger sample. At higher magnifications, as seen in Figure 5.1B, C and D, it is clear that the cells have maintained their structural integrity and the cell membrane is fully intact, as expected for healthy viable cells after fermentation. This is in

agreement with scanning electron microscopy images of *E.coli* cells from other studies (Chan 2006; Hartmann *et al*., 2010; Newton *et al*., 2016; Voulgaris *et al*., 2016).

Figure 5.2 shows the cells after a heat extraction process, once they have been exposed to the extraction buffer and a heating temperature of 59°C for 11 hours. This figure shows clear disruption to the cell sample population. A sponge-like mass on top the cells can be noted in Figures 5.2A and B. It can be postulated that this mass is formed by nucleic acids being released outside the cell wall, typically accounting for approximately 25% of the dry cell mass (Shahab *et al*., 1996). Similarly Figures 5.2C, D and F show the presence of this mass and the damaged cells. It is clear that although the cells have largely maintained their rod-like shape, there has been substantial damage to the cell membrane surface with many cells blistering and peeling off. In some cases, as shown particularly in Figure 5.2F, there is some blebbing of the cell with protrusions of the outer cell membrane. This is in agreement with the understanding of how heat, tris and EDTA affect the outer cell membrane of an *E.coli* cell. De Petris (1967) and Katsui *et al*. (1982) found that treating cells to high temperatures between 75-100°C caused thermal death and therefore blebbing of the outer membrane, creating vesicle like structures (Middleberg 1995).

The tris and EDTA compounds are believed to affect the cell surface and are responsible for causing cell death by metal starvation. The EDTA when exposed to *E.coli* cells, works by 'uncovering' the mucopolypeptide layer either by removal of interfering ions such as magnesium, manganese and calcium or by changing the surface charge or configuration of the layer thus increasing membrane permeability (Goldschmidt and Wyss 1967). When tris and EDTA are combined, they have a greater chelation ability on *E.coli* cells compared to EDTA alone (Goldschmidt and Wyss 1967). Although it is understood that the EDTA does not have an impact on the peptidoglycan layer or the inner cell membrane directly, removal of the outer membrane may cause the cell wall to weaken. The outer membrane of the *E.coli* cell is made of a lipid bilayer which contains transmembrane proteins, phospholipids and lipopolysaccharide (LPS). The LPS molecules are non-covalently bound to divalent cations such as Mg2+ and Ca2+ and also to the peptidoglycan layer within the periplasmic space. The outer membrane is therefore known to be significantly stronger than the inner

membrane, therefore if the outer membrane is disrupted, the inner cell contents are likely to be released (Middelberg 1995). It is clear that for some cells seen in Figure 5.2, there is indeed damage to both the inner and outer cell membrane with holes appearing in several places across the cell surface. Considering that samples were not taken after the centrifugation step, it is possible that the effects observed in these images are from a combination of the centrifugation and heat extraction step. Additionally it may be that the suspension of cells in the buffers over such an extended period of time has impacted on the robustness of the cells overall, making it more prone to a small level of cell damage during the mixing process.

The images shown in Figures 5.1 and 5.2 indicate that despite some limited damage to the inner cell membrane, the heat extraction process maintains the cell integrity overall with no swelling or whole cell breakage. This confirms that the extraction process is a gentler process in comparison to using alternative methods such as mechanical disruption, which significantly damages the cell structure and causes debris formation. Chan (2006) showed that when *E.coli* cells were passed through a Lab 40 high pressure homogeniser twice at 1200 bar, the cells observed under SEM were indistinguishable. In their work they could distinguish a mass of cell debris all clumped together with no sign of a cell-like structure. Although mechanical techniques such as homogenisation and sonication have been shown to cause a greater degree of Fab' release (Rayat *et al*., 2010), they also cause the release of other inner cell contents and there is a greater amount of incorrectly folded Fab' present in the suspension, making downstream processing considerably more challenging.

Cells observed under the SEM after acid precipitation, as shown in Figure 5.3, show that there is a greater presence of the inner cell contents in comparison to Figure 5.2 with the mass contributing to almost half of the sample. The image shows that the acid precipitation process causes noticeable cell to cell aggregation, and aggregation of inner cell contents. At higher magnifications of 30,000 and 40,000 (Figure 5.3B, C and D), the cells also appear to have lost their shape, with many of them twisted or collapsed. This suggests that the addition of the acid may have caused the inner cell contents, particularly dsDNA, to be extracted from within the cell therefore causing damage to its integrity. Although more

content appears to be present released from the cells, a significant proportion of this has been aggregated together which explains why the Fab', total protein and dsDNA concentration decrease after this step. A proportion of this inner cell mass could have been already present in the supernatant after the heat extraction step but was just simply not attached to the cell and therefore not captured in the SEM images. In any case, the acid precipitation step certainly helps with the aggregation of cellular components, making it easier to separate the dense cell mass from the liquid in the subsequent separation step (Roush and Lu 2008; Westoby *et al*., 2011).

5.3.2 Initial Extraction Experiments

Figure 5.4A shows a picture of all the vessels used in this chapter for the heat extraction experiments, where a 500mL red buffer bottle was used as size reference. The largest scale difference used in this work is 10,000 fold between the 20mL vessel and the 200L vessel. Figure 5.4B shows a photographic image of a typical extraction process running side by side in the 2L and 20mL vessel.

The first heat extraction study, indicated in Table 5.3 as Exp #2, was conducted at the 2L and 20mL scale using the A33 Fab'. The Fab' titre, total protein concentration and dsDNA concentration after heat extraction and acid precipitation are shown in Figure 5.5A, B and C, respectively. For this initial experiment, samples were taken from the top and bottom of the 20mL vessel after acid precipitation to check if the cell suspension was homogenous. The results, included in Appendix 5B, show that there were insignificant differences between the two measurements for all three parameters and therefore for further experiments, samples were only taken from the bottom of the vessel. The Fab' titre is shown to decrease by about 3% at the 2L scale and by 9% at the 20mL scale after acid precipitation. There is a much greater effect of the acid precipitation step on the total protein concentration which decreases by about 24% at the 2L scale and 34% at the 20mL scale. As for dsDNA, for both the 2L and 20mL process, about 98% of the dsDNA was removed by the acid precipitation step as expected. These trends are in line with results seen of the DoE experiment, presented in Chapter 3. Lyderson and Brehm-gibson (1994) showed that acetic acid was able

to aggregate DNA from Hybridoma cells, to achieve a final pH between pH 6.0 and 4.5, effectively reducing the concentration from 20µg mL^{-1} to 1µg mL^{-1}. Host cell proteins were also precipitated out leaving the antibody as the predominant high molecular weight molecule in solution. The antibody activity was found to be unaffected above pH 3.8 and the quality of the antibody, as observed using isoelectric focusing gels and hydrophobic interaction chromatography, were also not affected.

The data comparing the 2L and 20mL performance shows that the 20mL scale-down model is capable of mimicking the results obtained at the 2L scale for all three process parameters. The Fab' and total protein content, post extraction, is lower in the small scale model compared to the 2L vessel by 7% and 18%, respectively. The dsDNA concentration, however, is higher by 15%. The coefficient of variation (% CV) between the 2L and 20mL vessel for the Fab' titre after heat extraction and after acid precipitation is 5% and 10% respectively. This %CV may be considered insignificant when looking at the experiment in isolation. The %CV for total protein concentration between the two scales after heat extraction and acid precipitation is 14% and 24% respectively. This difference is significantly greater than that seen for Fab' titre for both process steps. This could be due to several reasons such as small differences in the mixing environment between the two scales which has caused these differences in the data or due to the assay used to measure total protein concentration. The error bars in Figure 5.5B correspond to ± 1 standard deviation between triplicate sample readings taken from one sample. These error bars show that there is some variability in the assay measurements. The relatively high 24% CV in the total protein concentration between both scales after the acid precipitation step is also representative of the measurement differences encountered in both the heat extraction and acid precipitation step. The acid precipitation step at both scales is effectively performed using 'different' feed material, because the quality of the cell suspension after the first heat extraction step is not perfectly matched at both scales.

The dsDNA concentration after heat extraction, as shown in Figure 5.5C, indicates that there is approximately 15% more dsDNA in the 20mL scale compared to the 2L scale, corresponding to a CV of 10%. Although this is again a small difference between the two

scales, it may indicate slight differences in the two models in terms of mixing performance. The error bars for the dsDNA graph are much smaller than for total protein which indicates that the PicoGreen assay is a fairly robust assay compared to the Bradford assay, used for total protein measurement. Further experiments will help to verify if these trends between the 2L and 20mL vessel are observed repeatedly and if the differences between the scales can be considered significant.

Figure 5.6 shows the SDS-PAGE gels run using samples after heat extraction and acid precipitation. Lanes 2-8 show the HCP profiles for all non-reduced samples. The lanes show good comparability overall between the HCP profiles for both scales. There are relatively few differences in the bands, namely slightly darker bands at 33kDa and 28kDa in the 20mL sample. However, the other bands are all present and very similar between the two scales. These results are in agreement with the Fab' titre and total protein concentration seen in Figure 5.5 where there was less Fab' and total protein in the 20mL vessel. All samples were loaded onto the gel based on normalised Fab', using the concentration obtained using protein G chromatography. Therefore the intensity of some of the bands are expected to be greater in the 20mL samples. As expected, the bands observed in Lanes 4-6, for post acid precipitation samples, are slightly lighter than those seen in Lanes 2 and 3. This is because the acid precipitation step removes some HCPs. The results show that there are no differences between the HCP profiles in Lanes 5 and 6 which corresponds to the data in Appendix 5B, confirming that the cell suspension is well mixed throughout the 20mL vessel. A comparison of the 20mL samples to the 2L sample in Lane 4 shows good comparability. There are quite a few bands, such as those near 38kDa and 31kDa which are slightly fainter in the 20mL samples. The heavy chain bands, near 28kDa however, are slightly darker. This data corresponds to the data shown in Figure 5.5B, where the total protein concentration was found to be considerably lower in the 20mL vessel compared to 2L so despite loading the gels using normalised Fab', the difference is still not accounted for in the gels.

Lanes 7 and 8 show the protein L chromatography purified samples for the post extraction samples at the 2L and 20mL scale respectively. Both profiles are well matched for these samples which indicates that the variants of the Fab' species, including the di-Fab' near

130kDa, the main Fab' at 49.5kDa, the free heavy chain near 28kDa and the free light chain near 25kDa are all present to the same degree. Lanes 9-11 show the protein L chromatography purified samples post acid precipitation on a reduced gel. Lane 9 is the Fab' standard. Lanes 10 and 11 represent the 2L and 20mL samples respectively and the profiles are again well matched for both scales. Overall, the results from the SDS-PAGE gels show that the profiles are very well matched at the two scales for both process steps with the exception of relatively small differences in a few bands. Results from Figure 5.5 and 5.6 therefore indicate that the 20mL vessel has the potential to mimic the 2L heat extraction process.

For the next experiment, Exp #3, the performance of the 20mL vessel was compared to a 2L and 20L process, this time using a different Fab' type. A schematic diagram of the 20L vessel, showing the key geometrical ratios and impeller positions are shown in Figure 5.7A. The positions of the varying fill volumes in relation to the fixed impeller position, are shown in Figure 5.7B, C, D, E and F for different experiments involving the 20L scale.

Figure 5.7B and C show the schematic diagrams for the 20L vessel used in Exp #3. For this experiment, the 20L process was run in three vessels under the same extraction conditions but different fill volumes. Two vessels had a fill volume of 17.6L (57% of the total vessel volume), corresponding to Figure 5.7B, and one vessel had a fill volume of 15.4L (50% of the total vessel volume) corresponding to Figure 5.7C. The results for the Fab' titre, total protein concentration and dsDNA concentration between the 20L, 2L and 20mL scales for Exp #3 are shown in Figure 5.8A, B and C, respectively. All concentrations have been normalised. An initial comparison of these parameters for the 20L extractions shows that when the fill volume and extraction conditions are the same, as for the 17.6L extractions, there is no noticeable difference in the Fab' titre for post extraction and post acid precipitation samples. The 15.4L Fab' titre, in comparison to the 17.6L titres, is 15% lower. This clearly indicates that despite keeping all the extraction conditions the same and using feed material from the same batch, there is a significant difference in performance due to the varying fill volume. The reason for the lower performance overall compared to 17.6L may be due to the positioning of the top impeller in relation to the liquid level. As the schematic diagrams

show in Figure 5.7B and C, although all three impellers are submerged for the 17.6L process and the 15.4L process, it is likely that the difference in performance is due to different flow patterns obtained for the two fill volumes. Visual observation during the extraction process showed that there was thrashing of the liquid where the top impeller was sitting. This may have caused significant differences in the mixing environment where it is possible that for the 15.4L extraction the liquid near the top of the suspension was not fully recirculated into the bulk of the liquid, potentially causing local gradients in the fluid, thus resulting in lower Fab' titres. It may be expected that the turbulence and thrashing seen near the top impeller and the liquid level, may have caused additional shear to the cells, potentially releasing comparatively more Fab'. This however was not the case and indicates that at a specific power input of 0.23W L^{-1} at least, *E.coli* cells are fairly resistant to shear. This is agreement with Hewitt and Nienow (2007) where it was found that unpredictable process performance during scale-up or scale-down is not due to shear damage but rather due to a dynamic environment with large spatial and temporal heterogeneities.

Another reason for this difference may be due to the fact that the experiment was run at different specific power input values. The impeller speed was kept the same for all three vessels (N = 200rpm) and therefore the specific power input may be approximately 15% lower in the 15.4L vessel compared to 17.6L. It may have been that adjusting the speed to compensate for the volume difference would have allowed for better mixing and thus a more comparable extraction performance at this scale. More likely however, adjusting the impeller positions in the 15.4L process, such that the top impeller was not sitting so close to the liquid surface, is likely to have resulted in better mixing.

The total protein and dsDNA results in Figure 5.8B and C, respectively, also confirm that concentration was lower overall in the 15.4L process, compared to the 17.6L process however, the total protein and dsDNA concentration after heat extraction for the two extractions at a fill volume of 17.6L differs by 15% and 20%, respectively, too. These differences may be caused by slight variations in the sample itself perhaps due to the nature of the cell damage, which is still not fully understood, or it may be due to the assays not being accurate enough. With the exception of the first 17.6L extraction, overall for Exp #3,

the trends seen for Fab' across the different scales are seen in total protein as well. Conversely for dsDNA, the trend is the reverse of Fab' and total protein, whereby higher Fab' titre typically corresponds to lower dsDNA concentration. The error bars obtained for the total protein and dsDNA data are similar to those observed in Figure 5.5.

Comparison of the 20mL process to the 2L process in Exp #3, shows very good comparability for Fab', total protein and dsDNA. The results for the 20mL and 2L process lie in between the data points for the 17.6L and 15.4L process. It is possible that geometrical and impeller spacing differences in the 20L vessel, compared to the 2L and 20mL model, are responsible for the differences in performance. A comparison of the schematic diagrams for the 2L and 20mL vessel, found in Chapter 2 in Figure 2.1 and Figure 2.2, respectively, shows that for both these smaller scale vessels, there is at least a space of 0.5 impeller diameter ($0.5D_i$) above the top impeller and the surface of the liquid. However for the 17.6L and 15.4L extractions, the space between the liquid level and the top impeller is less than $0.15D_i$. Another difference is that the impeller spacing in the 20L vessel is significantly different to the 2L and 20mL vessel. The impeller clearance is $1D_i$, the spacing between the bottom impeller and middle impeller is $1.3D_i$ and the impeller spacing between the middle and top impeller is $1.5D_i$. The impeller spacing for the 2L and 20mL vessels are $0.95D_i$. As discussed in Chapter 4, there have been a number of studies that have shown that the impeller spacing has a significant impact on mixing performance due to the different kinds of flow patterns that are generated in the bulk fluid. There is a difference of opinion on what the ideal impeller spacing should be but an impeller spacing of $1D_i$ where flow patterns can merge, is typically used in experiments. According to Mahmoudi and Yianneskis (1991) spacing between impellers should also be at least $1D_i$ to avoid the circulation loops clashing too much. Gogate *et al*. (2000) found that mixing efficiency increases when there are independent flow fields generated by the impellers and this is achieved when the spacing increases beyond $1D_i$. Hudcova and Machon (1989) showed that if the impeller spacing was between $0.5D_i$ and $1.5D_i$, one circulation loop per impeller is found with the discharge stream but beyond $2D_i$, the flows behave independently and mixing is compromised. According to this study, the impeller spacing in the 20L vessel may be close to optimum hence why the performance is better than for the 2L and 20mL vessel.

The SDS-PAGE gel for Exp #3 is shown in Figure 5.9. Lanes 2-10 show the HCP profiles for all non-reduced samples. The profiles observed between the 2L and 20mL samples are in agreement with the profiles seen previously at these scales in Exp #2. There is a darker band seen near 33kDa and 28kDa in the 20mL sample post heat extraction. The 2L profile, however, is very comparable to the 17.6L profile which is in agreement with Fab' and total protein concentrations observed in Figure 5.8A and B. The post extraction protein L purified samples in Lanes 8, 9 and 10 for 2L, 20mL and 17.6L samples respectively, all show very good comparability as well. This is also true for the reduced samples in Lanes 12, 13 and 14 for the 2L, 20mL and 17.6L samples respectively. The results from Exp #3 as shown in Figure 5.8 and 5.9 indicate that because the 20mL model performed in between the 17.6L process and the 15.4L process, this model has the potential to mimic 20L extraction processes in addition to the 2L process.

5.3.3 Verification of Scale-Down Tool Robustness: Extracting at Different Scales and Same Operating Conditions

The next four experiments, Exp #4-7, looked to establish whether the 20mL model was a good scale-down model for the 2L process over multiple extractions, all running under the same extraction conditions. Additional data from 20L extractions was available for comparison to the scale-down model in Exp #5 and from 200L extractions in Exp #6 and 7. A schematic diagram of the 200L vessel, showing the key geometrical ratios and impeller positions are shown in Figure 5.10A. The fill volumes in Exp #6 and Exp #7, in relation to the impellers are shown in Figure 5.10B.

Figure 5.11A, B and C shows the Fab', total protein and dsDNA concentration for the different scales in Exp #4-7. All data have been normalised. The coloured rings around the extraction scale, in each graph, indicate which data represents a particular extraction experiment. Comparison of the 20mL model to the 2L process shows that the scale-down model was able to mimic trends seen across all four extraction experiments for Fab' titre

and dsDNA concentration. For the total protein data, it seems that higher concentrations seen at the 2L scale corresponds to lower titres at the 20mL scale in general. The error bars in the data are comparable to those observed in previous experiments and, as usual, are quite large for the total protein data. A two tailed t-test was performed on the data for Fab', total protein and dsDNA between the two scales. The corresponding calculated p-values were 0.81, 0.24 and 0.79, which are all greater than the generally accepted value of 0.05 for biological experiments, indicating there is no significant difference between the data.

Comparison of the two 2L extractions in Exp #4 shows that when the feed material used for the extraction comes from the same batch and the process conditions and scale of the extraction are the same, the Fab', total protein and dsDNA concentrations are very well matched at this scale. This was observed also for Exp #5, for the 2L extractions. Comparison of all the extractions at the 2L scale indicates that, although the extraction conditions and vessel size were the same, there was considerable impact of the feed material characteristics on the extraction performance. Exp #4 and Exp #5 have higher overall Fab' titre, total protein concentration and dsDNA concentration at the 2L and 20mL scale compared to Exp #6 and Exp #7. The details of the fermentations used to generate material for all four extraction experiments are provided in Table 5.1 which show that for Exp #4 and 5, the scale of fermentation was 20L; however, for Exp #6 and 7, it was 200L. The Fab' titre, total protein concentration and dsDNA concentration leaked into the media during the 200L fermentation process appears to be significantly lower overall compared to the 20L fermentation process. Additionally, the Fab' titres obtained in the 1mL extracts were also considerably lower at the 200L scale in comparison to the 20L scale making the overall production, or total Fab', also considerably lower. A comparison of the % cell viability for all four fermentations in Exp #4-7 shows no noticeable differences between the two scales of fermentation. This indicates that the cells are lysed to a similar extent in all four experiments. The lower levels of Fab', total protein and dsDNA at the 200L scale therefore indicates that the cells are producing less of all three intracellular components to begin with, hence why the levels of these components leaked into the supernatant during the fermentation process is proportionately less. This also explains why the concentrations in Exp #6 and Exp #7, using material from 200L fermentation are lower overall. This implies

that the scale of fermentation has a direct impact on the performance of the extraction process.

The highest Fab', total protein and dsDNA concentration between all the extractions, were those in Exp #5, in particular at the 20L scale. The fill volumes for all three extractions varied at 13L, 15L and 18L (42%, 48% and 58% of the total vessel volume, respectively). Table 5.1 shows that the total amount of Fab' in the cell is significantly higher for Exp #5 compared to Exp #4, 6 and 7 which explains why the titres are the highest during the large scale extraction process. The Fab' and dsDNA trends in the 20L extraction vessels were mimicked lovely in the 20mL vessel whereas the total protein results were once more showing significant differences between scales. Comparing the Fab' titre between the 13L, 15L and 18L process, it can be observed that the highest titre is for 13L, followed by 18L and lastly by 15L. This data is in agreement with the trends observed in 20L extractions in Exp #3 as shown in Figure 5.8, where the 17.6L extractions performed better than the 15.4L extraction and were overall greater than the 2L and 20mL extractions.

The schematic diagrams for 13L, 15L and 18L fill volumes are shown in Figure 5.7D, E and F, respectively. The position of the top impeller in relation to the liquid level in the 15L extraction is similar to the 15.4L extraction, used in Exp #3, with the surface of the liquid level sitting close to the top impeller. Therefore the low performance observed for the 15L extraction is likely also due to the same reason as for 15.4L in that the mixing environment is not ideal. As the 18L extraction data shows, having even a relatively small volume of liquid above the top impeller improves the extraction performance, possibly due to better flow patterns that are established which help distribute the liquid more evenly throughout the entire vessel. The highest Fab' titre was obtained for the 13L extraction process. Although there are only two impellers submerged, there is a greater volume of liquid present above the top impeller. This allows the flow to form a more complete loop above the top impeller, thus improving the mixing performance. Figure 4.4, from Chapter 4, showed the effect of the fill volume on mixing time in a 20mL vessel. The results from the 14mL and 12mL, which roughly mimics the 18L and 13L positions in this experiment, showed comparable mixing times. It is possible that on a millilitre scale, mixing is facilitated by a greater level of

diffusion than at the larger scale, therefore differences in mixing time are small. At the larger scale, mixing may be more sensitive to impeller positioning and fill volume. Therefore conducting mixing time studies in the 20L vessel may help to explain these results and provide a better understanding of the mixing environment at large scale overall. Despite the fact that the work was conducted on a vessel with a 10,000 fold difference in scale and the difference between the two mixing time curves was very small, these results still indicate that mixing performance is superior when the impeller is well submerged under the liquid level compared to when it sits in line with the liquid level. In this experiment, the speed was adjusted in all three 20L vessels, in order to reflect the differences in volume and number of impellers submerged, helping to ensure that specific power input was maintained as close as possible to the desired value.

For Exp #6 and Exp #7, the 20mL extraction performance can also be compared to the 200L extraction. The data shows that the Fab', total protein and dsDNA concentrations for the 200L and 20mL process are very well matched despite significant differences in the geometries of the vessels, as shown in Figure 5.11B and Figure 2.2, respectively. The height of liquid to tank diameter ratio in the 20mL vessel is 1.75 whereas in the 200L vessel it is significantly higher (2.47). The impeller spacing also varies significantly between the two scales, where it is close to $1D_i$ in the 20mL vessel and more than $2D_i$ in the 200L vessel. Because of this impeller positioning, the distance between the top impeller and the surface of the liquid level differs considerably between the two scales, with the 20mL model having a submergence of $1.3D_i$ and the 200L vessel with $0.3D_i$ submergence. The effect of submergence has not been clearly documented in literature but this value is usually kept no greater than $2D_i$. Additionally, the impeller spacing and off-bottom clearance in the 200L vessel is also greater than $1D_i$ which in the body of literature is kept at $1D_i$ to promote better overlap of flow patterns which aids mixing (Bouaifi and Roustan 2001; Hartmann *et al*., 2006; Hudcova and Machon 2006; Lee and Yianneskis 1997; Montante *et al*., 1999; Rutherford *et al*., 1996; Shiue and Wong 1984; Xinhong *et al*., 2008; Xinhong *et al*., 2010; Yianneskis *et al*., 1986). A larger clearance usually results in a decrease in the pumping effectiveness of the lower impeller. There have also been numerous studies showing that having an impeller spacing greater than $2D_i$, as used in the 200L vessel, significantly reduces mixing performance because the impeller sets up its own radial discharge flow patterns that

do not interact with each other and this limits mixing efficiency (Baudou *et al*., 1997; Hudcova and Machon 1989; Kasat and Pandit 2004; Mahmoudi 1994; Saravana 2009). It may be possible that if the impellers in the 200L vessel were adjusted to achieve an impeller clearance and spacing of $1D_i$, as suggested by literature, the performance of the fermentation and heat extraction process could be improved.

The results from Exp #4-7 in Figure 5.11 have therefore provided a lot of useful information on the suitability of the 20mL vessel as a scale-down model for the 2L vessel. The small scale model was able to mimic the trends for Fab', total protein and dsDNA very well for all the extraction experiments using the same extraction conditions. The limited number of experiments conducted at the 20L and 200L scale, however, means that it is not possible to say with confidence if the small scale model can consistently mimic the pilot scale processes for future runs. The results from these experiments show that variations in feed material have a significant impact on the extraction performance as well as impeller spacing and fill volume. The variation in the feed material originates from a combination of different factors but scale of fermentation is a significant contributor. There is usually some natural variation in the growth profile of cells during fermentation. Operating a fermentation process at the 20L or 200L scale, is a complex and lengthy process and as with any fermentation process, small differences and tweaks may need to be made to the fermentation protocol in response to the requirements of the cells as they grow. The harvest centrifugation step may introduce further changes to the harvested feed material. Shear caused by disc stack centrifugation, during discharge for example, will contribute further to the quality of the cells prior to heat extraction. It is difficult to determine how or to what extent each factor, or combination of factors, during the upstream process steps, impacts on the quality of the cells going into the heat extraction process, however the parameters shown in Table 5.1 have provided a basis for understanding why the performance varies in these experiments.

Figure 5.12A shows a non-reduced SDS-PAGE gel from the 2L and 20mL scale samples in Exp #4. Lane 2 and 3 are for the two 2L post heat extraction samples. The HCP profiles between the 2L replicates are very well matched which is in agreement with the Fab' and total protein data observed in Figure 5.11A and B respectively. As observed in previous gels, the

20mL samples show some differences in the HCP profiles when compared to the 2L scale including the typical presence of an additional band at 33kDa and a significantly larger heavy chain band at 28kDa. The post acid precipitation samples are also in agreement with previous gels. The protein L purified post extraction samples Figure 5.12B show that the purified Fab' profiles match well for both scales which implies that the quality of the Fab' product obtained after the extraction process is unaffected by scale.

The SDS-PAGE gel showing the HCP profiles for the 20mL, 2L and 20L scale samples for Exp #5 are shown in Figure 5.13. Comparison of post extraction Lanes 3, 4 and 5, which represent the 13L, 15L and 18L fill volumes show significantly more intense bands for the 18L extraction process. This is in agreement with the relatively high total protein content shown in Figure 5.11B for this fill volume. Lanes 6 and 7 are the 2L replicate samples which show identical profiles as expected. The 20mL sample in Lane 2, when compared to Lanes 6 and 7 show the same particularly dark bands that are typically seen in the 20mL samples are observed again at 33kDa and 28kDa. The post acid precipitation samples in Lanes 8, 9, 10 and 11 show well matched samples at all scales with the exception of the darker band at 28kDa for the 20mL sample in Lane 8. Figure 5.14A shows the non-reduced SDS-PAGE gel which compares the HCP and Fab' profiles between the 200L, 2L and 20mL for Exp #6. The post extraction and post acid precipitation samples for all three scales are very well matched, with the exception of the darker bands at 28kDa and 33kDA observed in the 20mL scale. Similarly, Figure 5.14B shows the SDS-PAGE gel for Exp #7 where the same trends between the 200L, 20 and 20mL process can be observed. These gels are in agreement with the data presented in Figure 5.11 where the Fab' and total protein content was well matched between all three scales. The results from Exp #4, 5, 6 and 7 indicate that running SDS-PAGE gels can provide further insight about the amount of HCP present in the suspension after the extraction and precipitation step. The total protein graphs for some experiments show significantly large error bars and it is therefore difficult to assess if these trends are reliable or as a result of an assay with relatively low accuracy. Combining results from the total protein assay with the SDS-PAGE gels provides an enhanced understanding of the process.

Due to such a large difference between the 200L and 2L scale vessels, such as vessel geometry and impeller positioning for example, the results from the gels were slightly unexpected. It is possible that the mixing environment between both scales varies; therefore some differences between the profiles may have been expected. The results from the SDS-PAGE gels suggest that some types of differences in the mixing environment during heat extraction have an impact on the cells ability to release more Fab' and other intracellular impurities only, whereas other differences in the mixing environment can cause structural changes to the Fab' fragments and other HCP. This appeared to be the case for the 20mL samples where additional bands were consistently seen for each experiment. This may be due to the design of the 20mL vessel because each time the vessel was assembled, there was a small gap between the glass jacket and the base of the vessel which meant that some of the liquid would accumulate there. It was possible that the liquid in the gap did not mix fully with the bulk of the fluid. For this reason, the initial samples taken for analytics during extraction experiments were taken from the top and bottom of the vessel to see if the quality of the cell suspension taken from a close proximity to this potentially stagnant area would be the same as near the liquid surface. The results showed there were insignificant differences between the two samples, as seen in Appendix 5B and in the SDS-PAGE gels in Figure 5.6, which indicated that the liquid was homogenous in the vessel. It is possible that there is some slow exchange of liquid from the gap into the bulk fluid, however the cells may experience longer retention times in the gap where mixing is poor which, thus causing some changes to the structure of the proteins. So although the Fab', total protein and dsDNA concentrations can be mimicked with relatively good accuracy in the 20mL vessel, and the mixing performance itself is similar to the larger scale vessels, it could be that the design flaw in the vessel itself is responsible for these small differences in the gel profiles. Analysis of the profiles of the pure Fab', purified using protein L chromatography, showed insignificant differences between the 20mL vessel and the larger vessels. However, an alternative method such as high temperature reverse phase chromatography may have been more helpful in assessing Fab' quality and purity. Despite this issue, because these additional bands are consistently present in all profiles, they can be accounted for when assessing the SDS-PAGE gels. The exact impact and cause of these bands is not yet fully understood and adjustments to the design of the vessel can also be made with relative ease if needed. Overall, the results from these experiments have

demonstrated the feasibility of using this small scale model as a predictive tool for the large scale heat extraction process.

5.3.4 Verification of Scale-Down Tool Robustness: Extracting at Different Scales and Different Operating Conditions

Running multiple extraction experiments under the same extraction conditions helped establish an understanding of how well the 20mL vessel was capable of mimicking the 2L process. To further verify the suitability of the 20mL vessel as a good scale-down model, the performance of the 20mL process was compared to 2L under different extraction conditions. Exp #8, 11, 12, 13 and 14 were performed using the extraction conditions highlighted in Table 5.2. For these experiments, the heating profiles and the specific power input values were varied and the fill volume and impeller spacing were kept the same. The extractions conditions chosen for Exp #11, 12 and 13 were selected from different areas of the DoE contour plot in Figure 3.5A in Chapter 3 as these conditions were found to have a significant impact on the extraction performance. These points were from the top right hand corner of the DoE plot for Exp #11, the bottom left hand corner of the plot for Exp #12 and the centre of the plot for Exp #13. Figure 5.15A, B and C shows the Fab', total protein and dsDNA concentrations for the two scales, respectively. The results show that the 20mL process was mimicking the 2L process for all three parameters with great accuracy for all extraction conditions. A two tailed t-test was used to calculate p values of 0.26, 0.49 and 0.55 for Fab' total protein and dsDNA, respectively, indicating no significant differences between the two data sets. This shows that even if the feed material has variation and the extraction conditions are changed, the scale-down model is still able to mimic trends. This confirms that the 20mL model is capable of detecting changes in the heating and mixing conditions which can be achieved under a variety of different extraction profiles, heating temperatures and specific power input.

Because of differences in the Fab' types, the scale of fermentation, natural batch to batch variation and the extraction conditions used between all experiments, it is not possible to see the isolated impact of the extraction conditions on the performance for all five

experiments. Exp #11, 13 and 14, however, can be more easily compared because the Fab' type and scale of fermentation used in these experiments are the same. Figure 5.15A shows that titres between Exp #13 and 14 are similar but for Exp#11, the titre is significantly lower. The heat extraction profile, as shown in Table 5.3, for Exp #13 and 14 are the same but for Exp #11 the heating temperature is higher and the heating duration is also longer. This observation is in agreement with the results from Figure 3.5A from the DoE experiment in Chapter 3, where long extraction durations and high extraction temperatures resulted in lower Fab' titre and total protein concentration. The small differences between the results from Exp #13 and 14 are likely due to batch to batch variation in the feed material rather than the use of different specific power input.

For most experiments in Figure 5.15, it can be observed that the Fab', total protein and dsDNA concentrations are slightly lower than for the 2L scale process. This is in agreement with previous extraction data. The quantitative difference in performance varies across experiments but it is typically less than 10%. Although this difference is not significant, this underperformance of the 20mL vessel could be due to a number of different reasons such as geometric differences in the impeller, fill volume, differences in the perceived specific power input compared to actual power input, sampling errors and also natural batch to batch variation in the feed material. All these factors ultimately have an impact on the level of cell damage that can occur which in turns affects the quality and quantity of Fab' and host cell impurities that are released from the cell. If sufficient data can be gathered from further experiments, it may be possible to input the data into a model and more accurately attribute each factor to the performance, eventually being able to predict the performance of the 2L, 20L or 200L process using just the 20mL model with greater accuracy. The SDS-PAGE gels for Exp #8, 11 and 12 are shown in Figures 5.16, 5.17 and 5.18 respectively. The profiles of the 2L and 20mL samples taken post extraction, post acid precipitation and after protein L purification for all three experiments are comparable. The 20mL vessel has the additional bands in 28kDa and 33kDa in Figure 5.16, 5.17 and 5.18, as seen for previous experiments.

In many experiments, high Fab' titres corresponded to relatively high total protein concentrations. Although this correlation was observed in the DoE plots in Chapter 3, there were some unexpected trends between Fab', total protein and dsDNA overall. Even when running the extraction experiment in the same size vessel, using the same feed material, under the same heating and mixing conditions, there was no complete agreement between all three parameters which implies that there may not be a direct correlation between the Fab' titre, total protein concentration and dsDNA concentration. Additionally, the effect of shear and its impact on cell damage is also not well understood. The correlations between Fab', total protein and dsDNA, in both the 2L and 20mL vessel after heat extraction for Exp #2-14 are shown in Figure 5.19. Figure 5.19A indicates that there may be a weak positive correlation between Fab' and total protein, however there is no clear correlation between Fab' titre and dsDNA concentration or total protein concentration and dsDNA concentration. Although total protein and dsDNA are both indicators of cell damage (Sehdev and Spitali 2006), the data indicates that the nature of damage to the inner and outer cell membrane, responsible for different levels of Fab', total protein and dsDNA release, is complex, unpredictable and therefore difficult to control and predict. Additionally, the amount of total protein available inside a cell is significantly higher than the amount of Fab' therefore small differences in cell damage may not have a significant impact on Fab' titre but may do so on total protein content. Alternatively it may be that more accurate assays are needed, particularly for total protein which shows large error bars. A two tailed t-test was performed, to calculate the p values between the 2L and 20mL data for all thirteen experiments. These values were 0.38, 0.14 and 0.60 for Fab', total protein and dsDNA, respectively. Therefore although the total protein results may indicate differences, the statistical analysis indicates no significant difference between the performance for all three parameters.

As it is difficult to have matching results for each parameter, to measure and compare extraction performance at different scales in particular, it may be sensible to select just one or two parameters to gauge how well one scale mimics another. In this case the Fab' titre and perhaps the SDS-PAGE profiles would be the most important parameters as they show how comparable the Fab' quantity and quality is. The data obtained from the other assays can then be used for additional insights to understand the state of the process further and

significant variations between results can be investigated further. It is also important to evaluate what level of difference in performance is considered significant in the first place, particularly in an industrial setting. If these differences are considered significant, then factors which impact on this mechanism of release and therefore the quality of the feed material, in both the fermentation and centrifugation steps prior to heat extraction, need to be studied in further detail. Without sophisticated software which uses multivariate analysis (MVA) for analysing data, it may be a challenge to understand all how these different parameters are related and therefore how they may be controlled.

5.4 Conclusive Remarks

Overall, the results from this work showed that the 20mL vessel was a satisfactory model to scale-down the heat extraction process. By matching the heating and mixing environment at different scales, and conducting multiple experiments under the same and different extraction conditions, it was possible to demonstrate that the 20mL vessel was capable of detecting trends observed in the 2L vessel with good accuracy. Measuring the Fab', total protein and dsDNA concentration after heat extraction and acid precipitation provided details about the performance of the different scales. SDS-PAGE gels also provided information about the HCP and purified Fab' profiles. Although the HCP and Fab' profiles were well matched between the 20mL scale and the 2L scale, there were additional bands that were consistently seen on the 20mL HCP profiles. These differences may be due to slight differences in the 20mL vessel geometry compared to the 2L scale. Despite the presence of the same additional bands in the 20mL HCP profiles, and the slightly lower Fab' total protein and dsDNA concentrations, the results show that the 20mL vessel behaves consistently between experiments and therefore these differences can be accounted for during scale-down studies. The results showed that specific power input, within the range studied at least, did not have an impact on the extraction performance which is in agreement with the results from previous chapters. Chapter 3 showed that within the range of 0.05 - 0.41W L^{-1}, the specific power input had little impact on performance. Characterisation studies from Chapter 4 also showed that with a minimum specific power input of 0.05W L^{-1} was needed for sufficient mixing.

Initial experiments comparing the 20mL process to the 20L and 200L performance also indicated that the 20mL vessel has the potential to be used as a scale-down model for pilot scale extractions too, provided that some adjustments are made in the fill volume and impeller spacing for further experiments, as these two factors were found to have a significant impact on the extraction process. The highest Fab' titres in this work were observed in the 20L vessel, which may be due to the spacing of the impellers, which were between $1.3D_i$ – $1.5D_i$. Variation in the feed material, particularly due to the scale of fermentation, was found to have a substantial impact on the heat extraction performance. Understanding and quantifying how the feed material and other process parameters impact this process, and to what degree, would be helpful for creating a more accurate and predictable scale-down model.

Exp #	Chapter	Scale	Fab' Type	% Cell Viability	Fab' in Sup	Total Protein in Sup	dsDNA in Sup	Fab' in Ext	Total Fab'
1	3	3x 20L	A33	87.48 88.71 86.09	0.25 0.24 0.25	3.21 3.17 3.16	49.44 40.75 44.09	0.99 0.98 0.98	1.25 1.22 1.23
2	5	2x 5L	A33	91.39 91.09	0.24 0.21	3.04 2.73	18.89 16.27	0.99 0.91	1.24 1.11
3	5	4x 20L	UCB Fab' 1	83.81 82.11 76.73 86.37	0.18 0.15 0.26 0.15	3.93 3.83 4.88 3.13	42.80 33.67 146.9 56.30	0.82 0.82 0.79 0.83	1.00 0.97 1.05 0.98
4	5	4x 20L	UCB Fab' 1	89.98 88.41 92.11 90.52	0.15 0.15 0.09 0.12	2.62 2.50 2.58 2.78	24.52 22.18 22.36 23.33	0.86 0.82 0.87 0.85	1.01 0.97 0.96 0.97
5	5	4x 20L	UCB Fab' 1	85.53 82.54 82.80 85.21	0.19 0.21 0.22 0.18	3.47 3.44 3.46 2.83	39.93 42.51 46.59 23.96	0.87 0.86 0.86 0.83	1.07 1.08 1.07 1.02
6	5	1x 200L	UCB Fab' 1	90.38	0.11	1.77	12.58	0.73	0.84
7	5	1x 200L	UCB Fab' 1	89.30	0.11	1.87	20.17	0.74	0.85
8	5	4x 20L	UCB Fab' 1	88.29 85.04 85.47 83.82	0.12 0.19 0.20 0.16	3.01 3.23 3.79 3.43	26.38 35.33 38.37 38.13	0.86 0.91 0.75 0.91	0.98 1.10 0.95 1.07
9	6	4x 20L	UCB Fab' 2	Average: 91.39	0.01 0.17 0.19	1.43 2.01 1.88	7.355 95.52 106.8	N/A	N/A

					0.14	1.87	46.09		
10	6	2 x 5L	UCB Fab' 1	87.43 87.61	0.10 0.14	N/A	22.99 22.85	0.97 0.95	1.08 1.09
11	5, 6	2 x 5L	UCB Fab' 1	N/A	N/A	N/A	N/A	N/A	N/A
12	5, 6	2 x 20L	UCB Fab' 1	Average: 90.63	N/A	N/A	N/A	1.02 1.01	N/A
13	5, 6	1 x 5L	UCB Fab' 1	N/A	N/A	N/A	N/A	N/A	N/A
14	5, 6	1 x 5L	UCB Fab' 1	N/A	N/A	N/A	N/A	N/A	N/A

Table 5.1: Details of fermentation after harvest for different experiments. Fab' represents the titre in mg mL^{-1}, total protein represents the concentration in mg mL^{-1} and dsDNA represents the concentration in µg mL^{-1}. 'Sup' represents supernatant samples and 'Ext' represents 1mL extract samples conducted in the Eppendorf tubes. Titres and concentrations have been normalised for UCB Fab' 1 and UCB Fab' 2

Exp #	Chapter	Centrifuge Type	Harvest Mass Kg)	% Clarification	% Dewatering
1	3	Disc Stack	55.3	99.3	63.5
2	5	Dead End	2.70	99.5	63.5
3	5	Disc Stack	51.8	99.6	60.4
4	5	Disc Stack	69.1	99.5	64.4
5	5	Disc Stack	54.0	n/a	59.1
6	5	Disc Stack	217	99.4	67.0
7	5	Disc Stack	215	99.2	67.8
8	5	Disc Stack	77.2	99.4	57.2
11	6	Dead End	N/A	N/A	N/A
12	6	Disc Stack	N/A	N/A	N/A
13	6	Dead End	N/A	N/A	N/A
14	6	Dead End	N/A	N/A	N/A

Table 5.2: Details of centrifugation conditions for Exp #1-8 after harvest for each experiment

Exp #	Extraction Scale	Fill Volume	Heat Up Time (hr)	Hold Time (hr)	Temp (°C)	Cool Down Time (hr)	P/V (W/L)
2	20mL 2L	20mL 2L	1.5 1.5	10 10	60 60	1.5 1.5	0.23 0.23
3	20mL 2L 3x 20L	20mL 2L 17.6L 17.6L 15.4L	3.5 3.5 3.5 3.5 3.5	10 10 10 10 10	59 59 59 59 59	2 2 2 2 2	0.23 0.23 0.23 0.23 0.23
4	20mL 2x 2L	20mL 2 x 2L	4 4	11 11	59 59	4 4	0.23 0.23
5	20mL 2x 2L 3x 20L	20mL 2 x 2L 13L 15L 18L	4 4 4 4 4	11 11 11 11 11	59 59 59 59 59	4 4 4 4 4	0.23 0.23 0.23 0.23 0.23
6	20mL 2L 200L	20mL 2L 214L	4 4 4	11 11 11	59 59 59	4 4 4	0.23 0.23 0.23
7	20mL 2L 200L	20mL 2L 214.8L	4 4 4	11 11 11	59 59 59	4 4 4	0.23 0.23 0.23
8	20mL 2L	20mL 2L	5.5 5.5	10 10	60 60	5.5 5.5	0.05 0.05
11	20mL 2L	20mL 2L	1.5 1.5	14 14	64 64	1.5 1.5	0.05 0.05
12	20mL 2L	20mL 2L	1.5 1.5	6 6	55 55	1.5 1.5	0.05 0.05
13	20mL 2L	20mL 2L	1.5 1.5	10 10	60 60	1.5 1.5	0.05 0.05
14	20mL 2L	20mL 2L	1.5 1.5	10 10	60 60	1.5 1.5	0.23 0.23

Table 5.3: Details of the heat extraction conditions for each experiment

A)

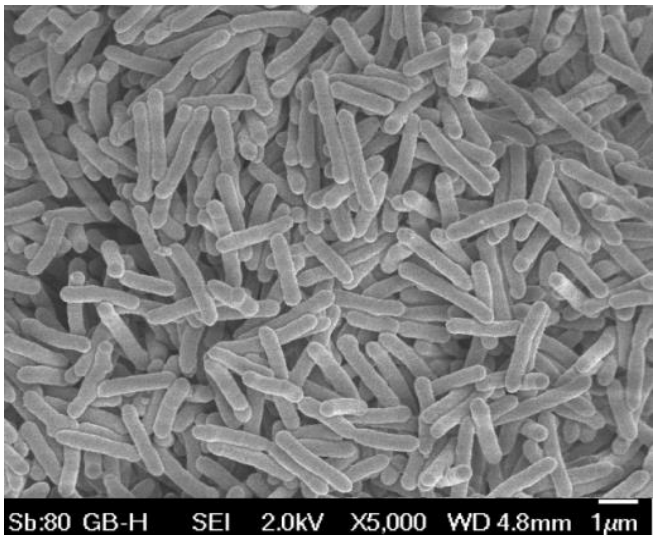

B)

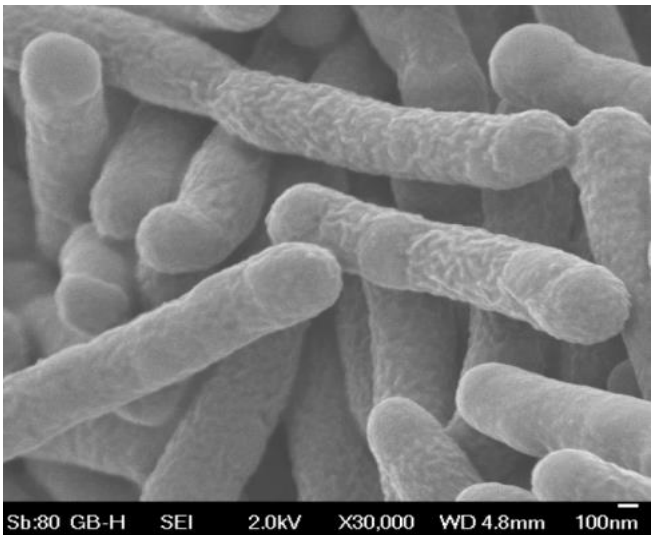

C)

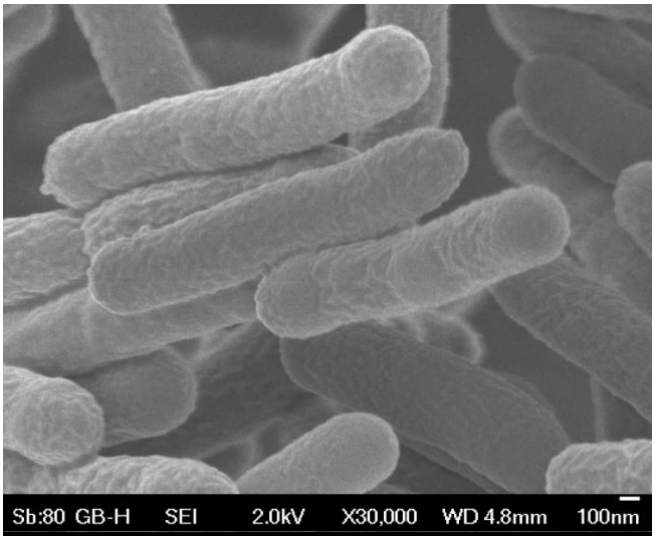

D)

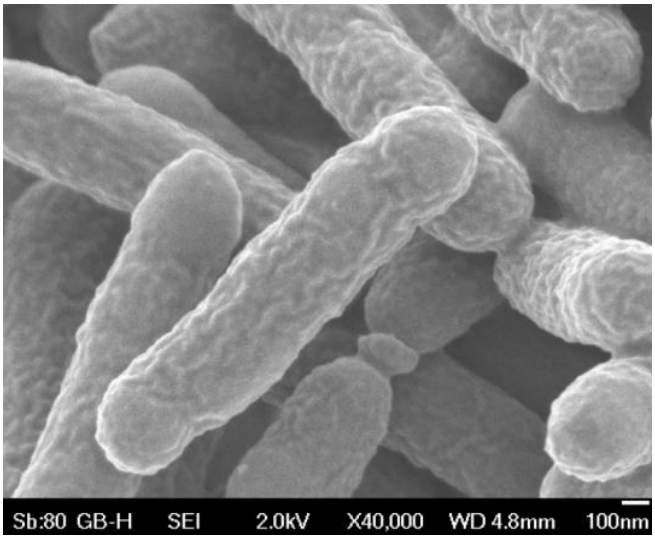

Figure 5.1: SEM image of *E.coli* cells at the end of fermentation at magnification of **A)** 5,000; **B)** 30,000; **C)** 30,000 and **D)** 40,000

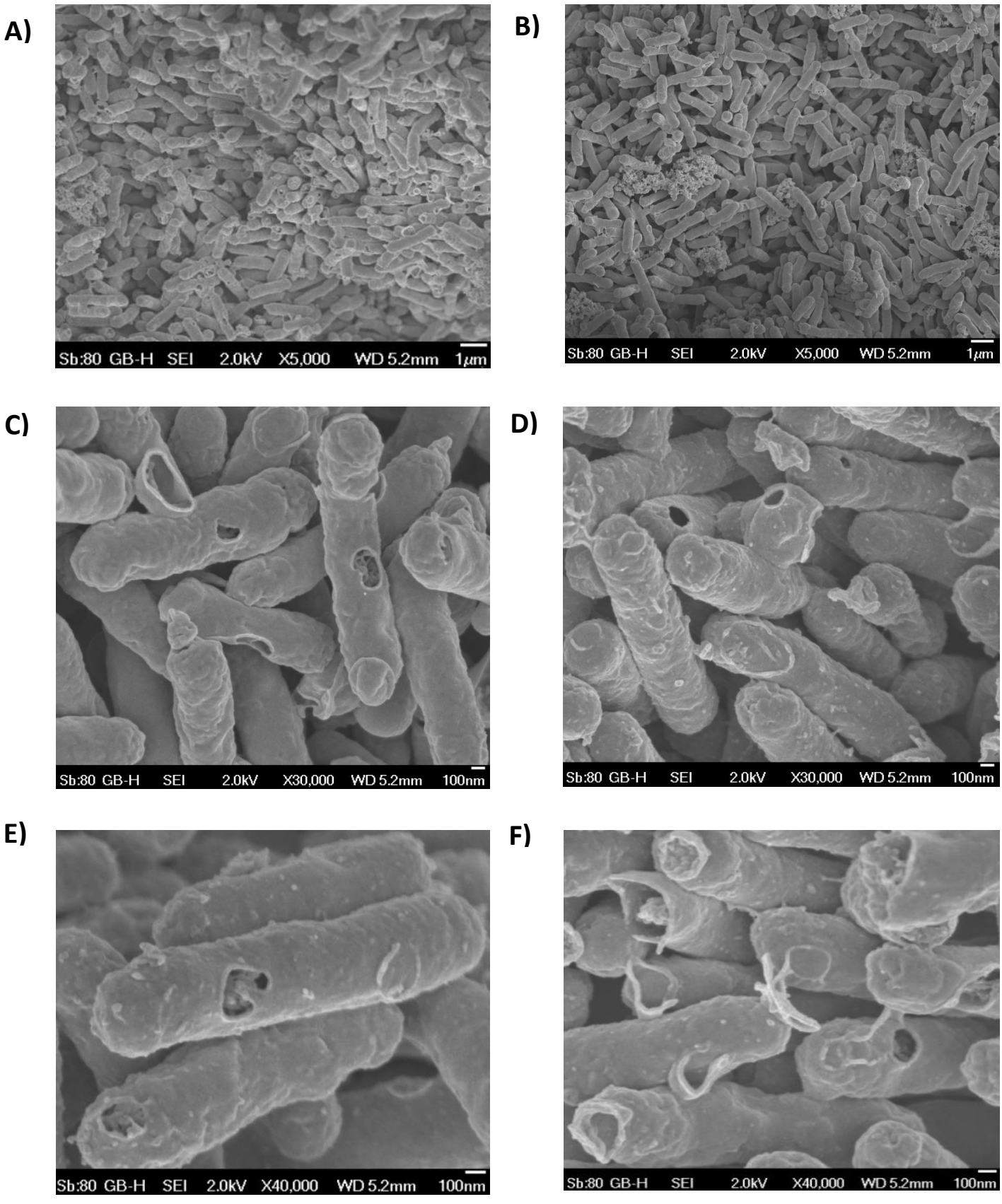

Figure 5.2: SEM image of *E.coli* cells after heat extraction at magnification of **A)** 5000; **B)** 5,000; **C)** 30,000; **D)** 30,000; **E)** 40,000; and **F)** 40,000

A)

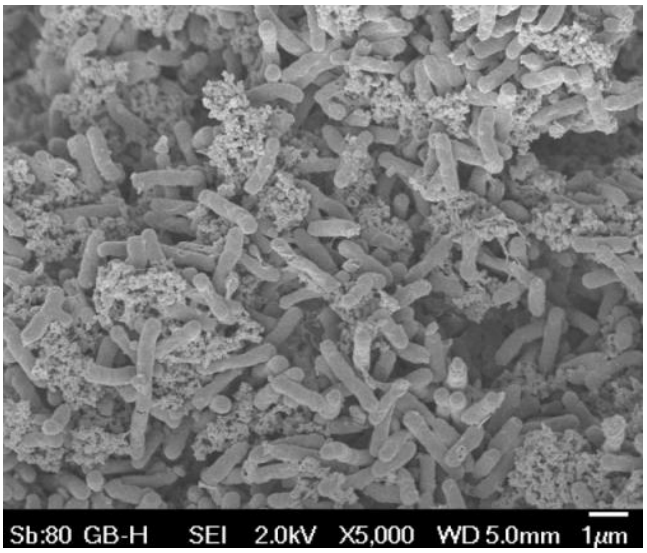

B)

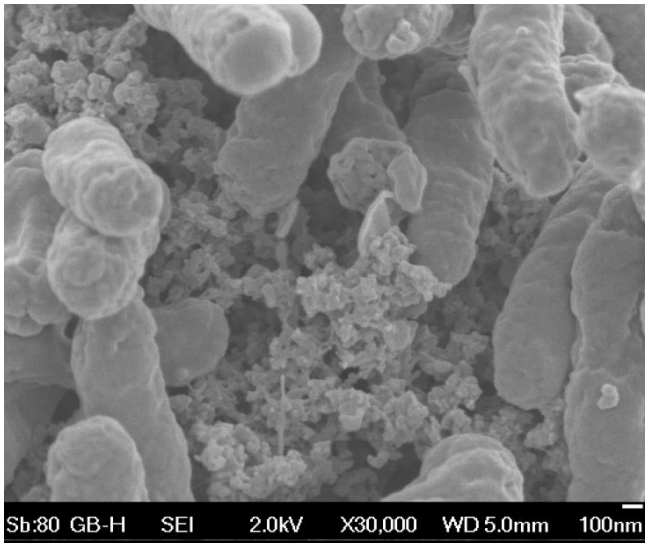

C)

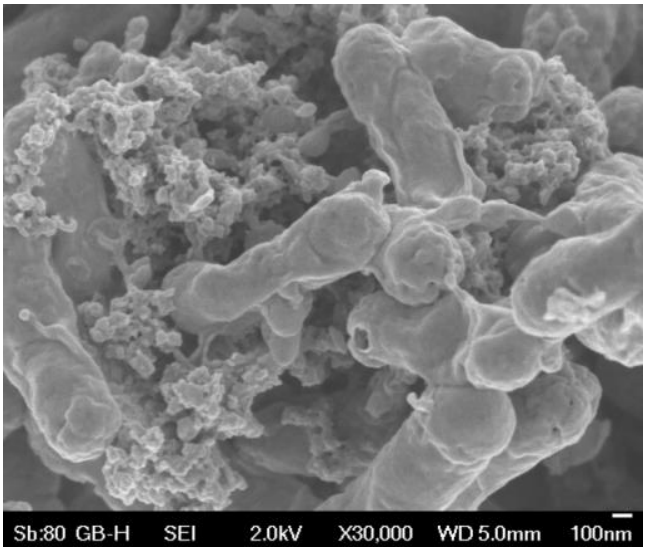

D)

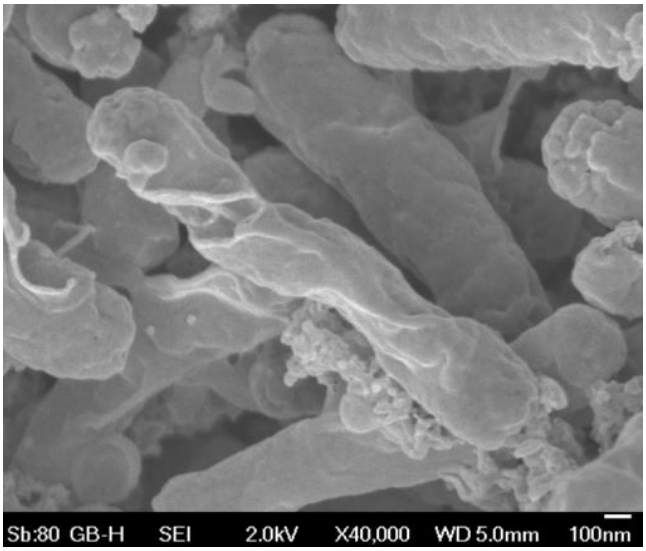

Figure 5.3: SEM image of *E.coli* cells after acid precipitation at a magnification of **A)** 5,000; **B)** 30,000; **C)** 30,000 and **D)** 40,000

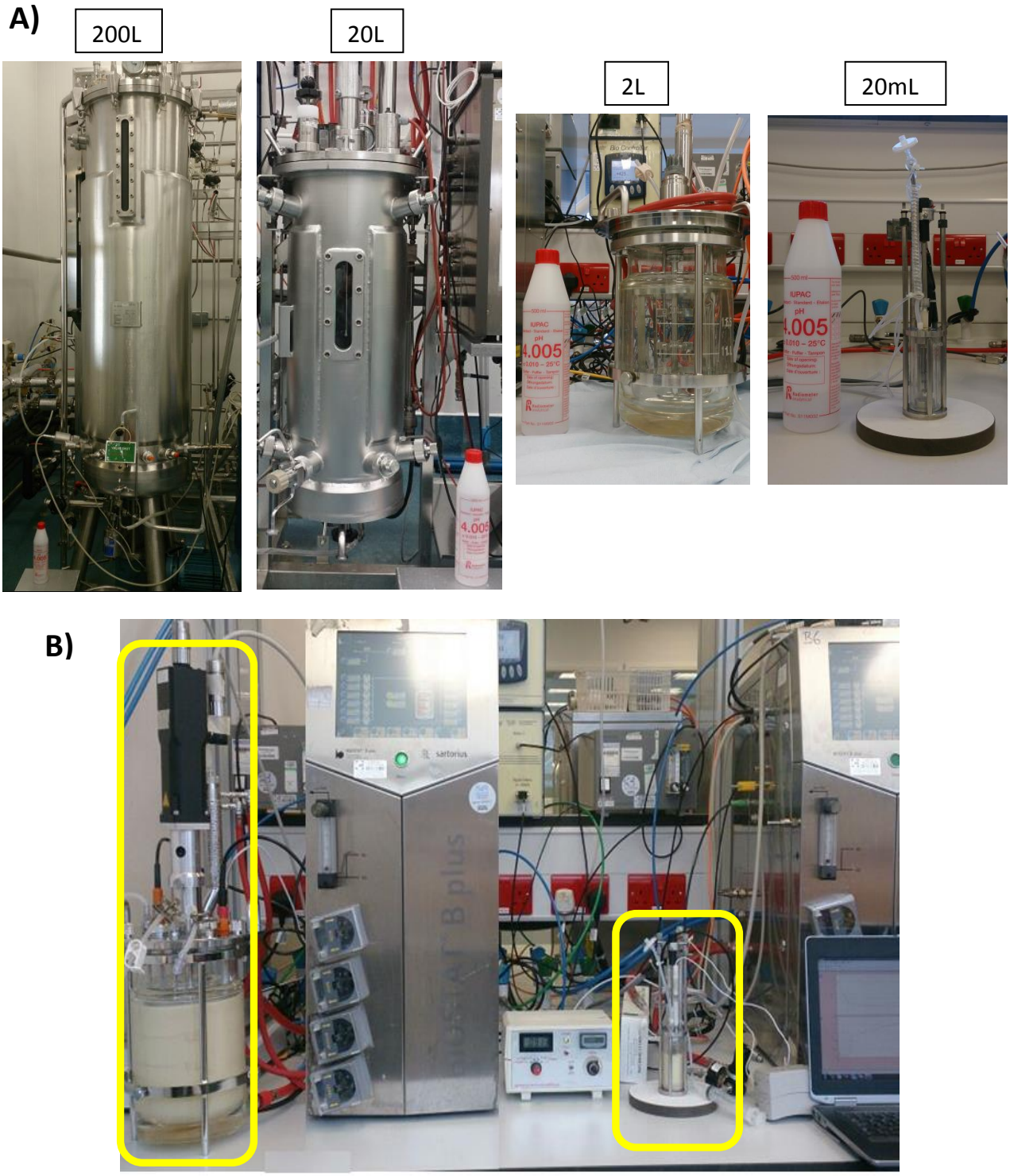

Figure 5.4: Photographic images of **A)** the 200L, 20L, 2L and 20mL vessel used for heat extraction showing using a 500mL pH 4 buffer bottle as a reference for size and **B)** a sample heat extraction and acid precipitation experiment in the 2L and 20mL vessels

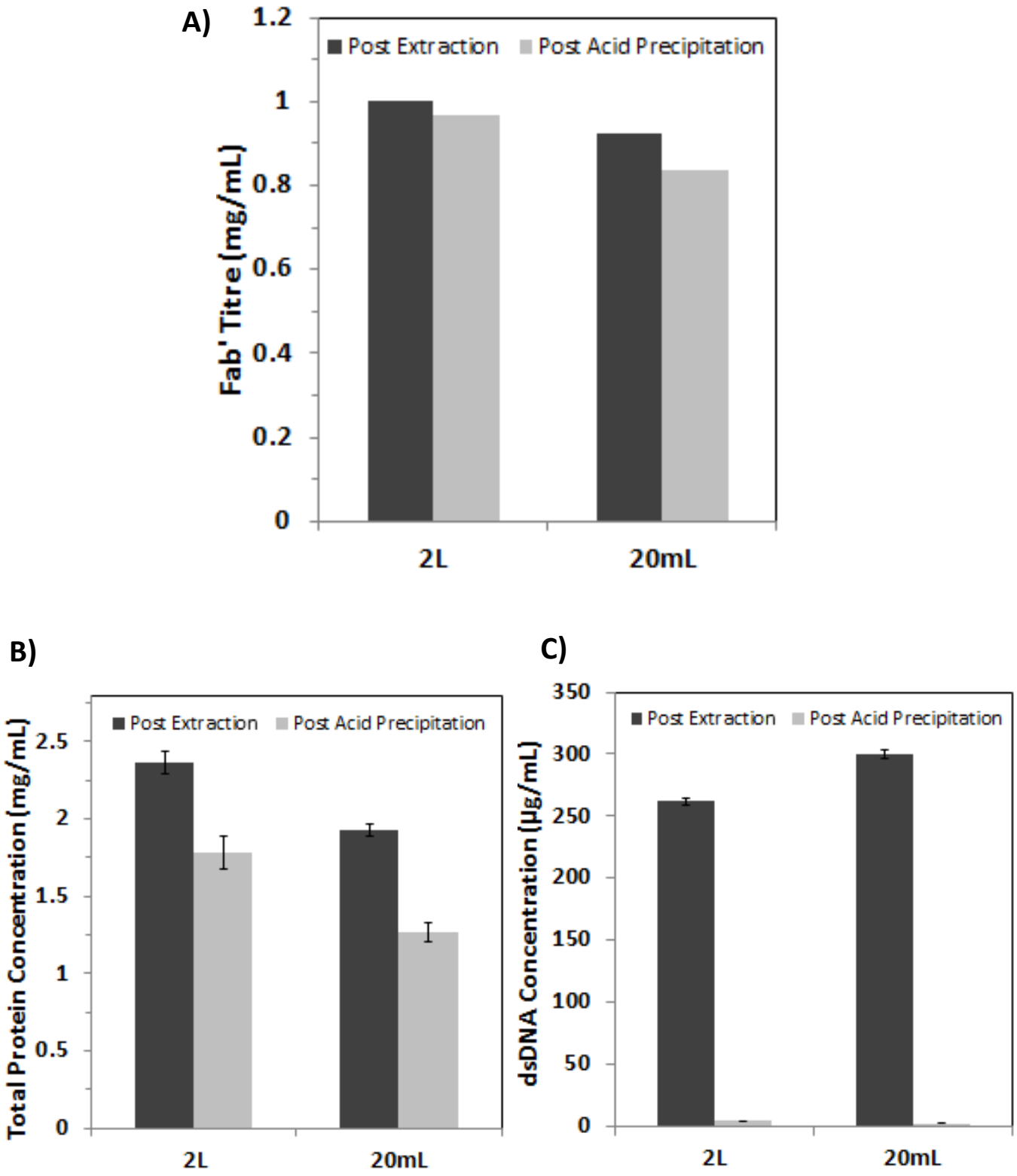

Figure 5.5: Comparison of the 2L and 20mL **A)** Fab' titre; **B)** total protein concentration; and **C)** dsDNA concentration after heat extraction and acid precipitation from Exp #2. Error bars represent ± 1 standard deviation from replicates in the assay (n=2 for **A**, n=3 for **B** and **C**)

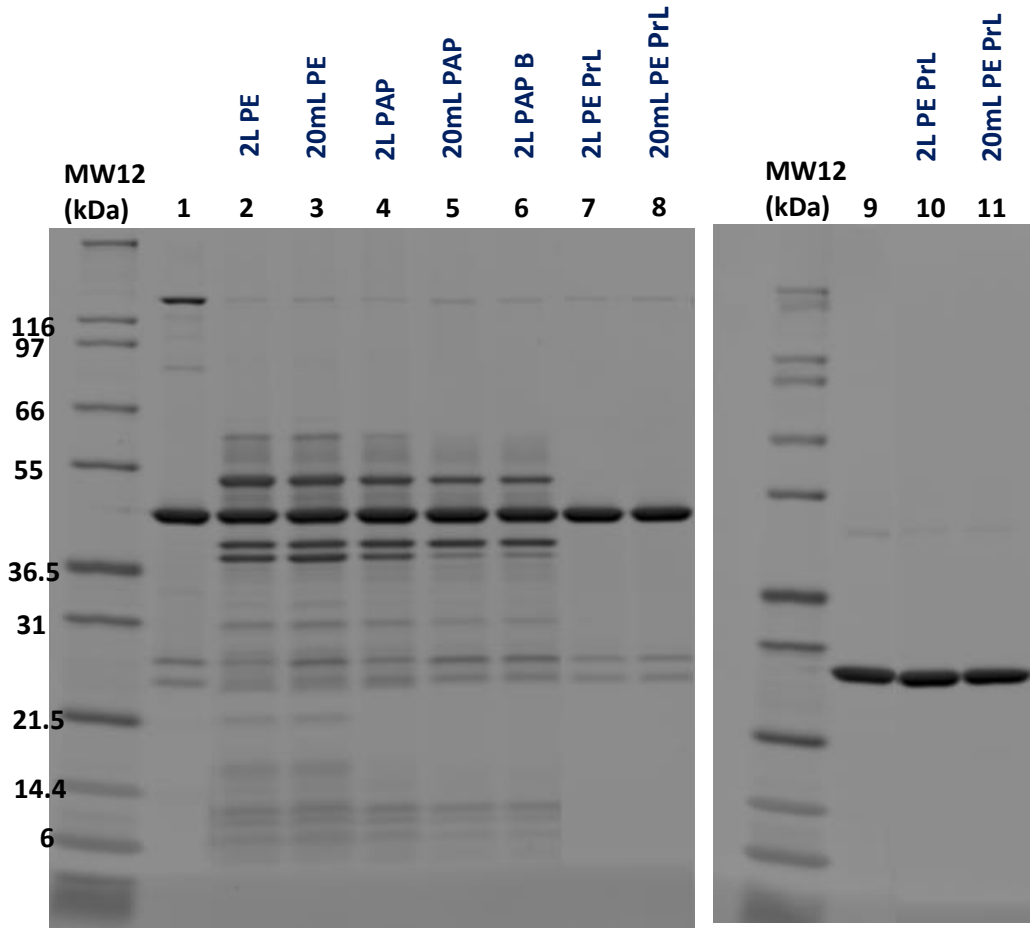

Figure 5.6: SDS-PAGE gel showing the HCP and purified Fab' profiles at the 2L and 20mL scale for Exp #2. The non-reduced gel with post extraction (PE), post acid precipitation (PAP) and post extraction (PE) protein L (PrL) purified samples (Lanes 2-8); and the reduced gel with post extraction (PE) protein L (PrL) purified samples (Lanes 10-11): Lane 1- Fab' standard; Lane 2- 2L PE; Lane 3- 20mL PE, Lane 4- 2L PAP; Lane 5- 20mL PAP top; Lane 6- 20mL PAP bottom; Lane 7- 2L PE PrL; Lane 8- 20mL PE PrL; Lane 9- Fab' standard; Lane 10- 2L PE PrL; Lane 11- 20mL PE PrL

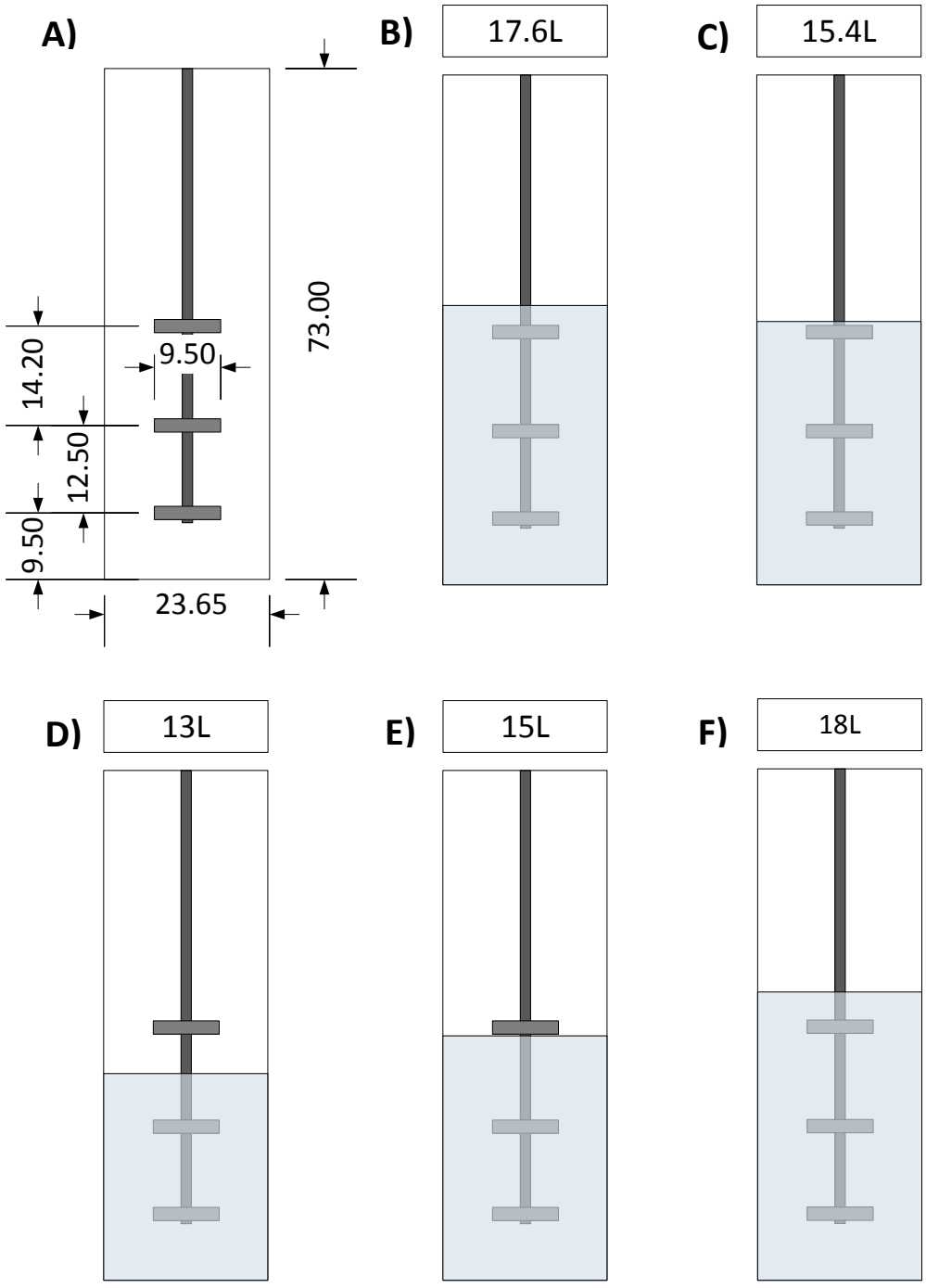

Figure 5.7: Schematic diagram of the 20L vessel showing the **A)** key dimensions and impeller spacing in cm; and with fill volumes of **B)** 17.6L as used in Exp #3; **C)** 15.4L as used in Exp #3; **D)** 13L as used in Exp #6; **E)** 15L as used in Exp #6 and **F)** 18L as used in Exp #6

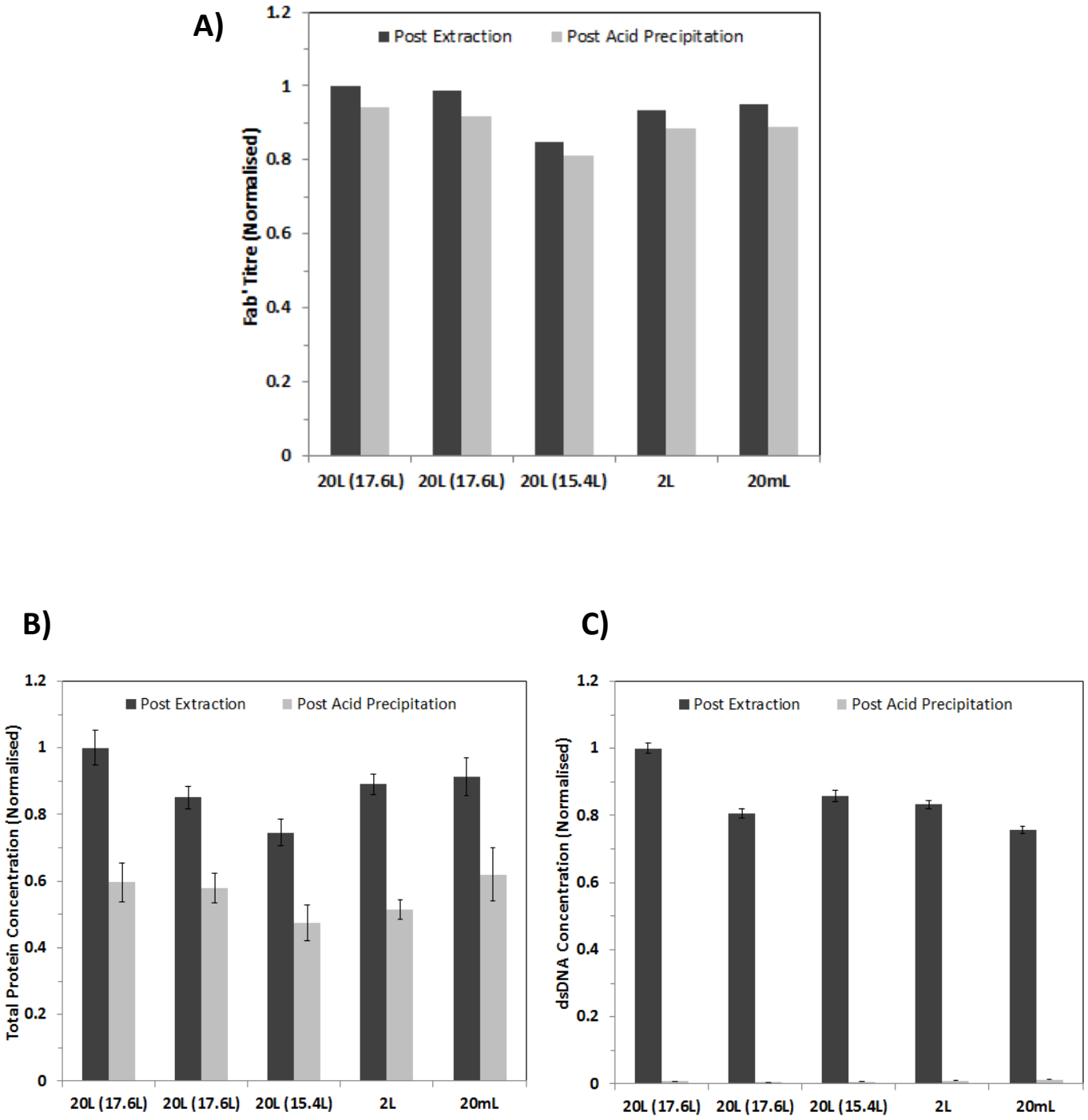

Figure 5.8: Comparison of the normalised 20L, 2L and 20mL **A)** Fab' titre; **B)** total protein concentration; and **C)** dsDNA concentration after heat extraction and acid precipitation from Exp #3. Error bars represent ± 1 standard deviation from replicates in the assay (n=3 for **B** and **C**)

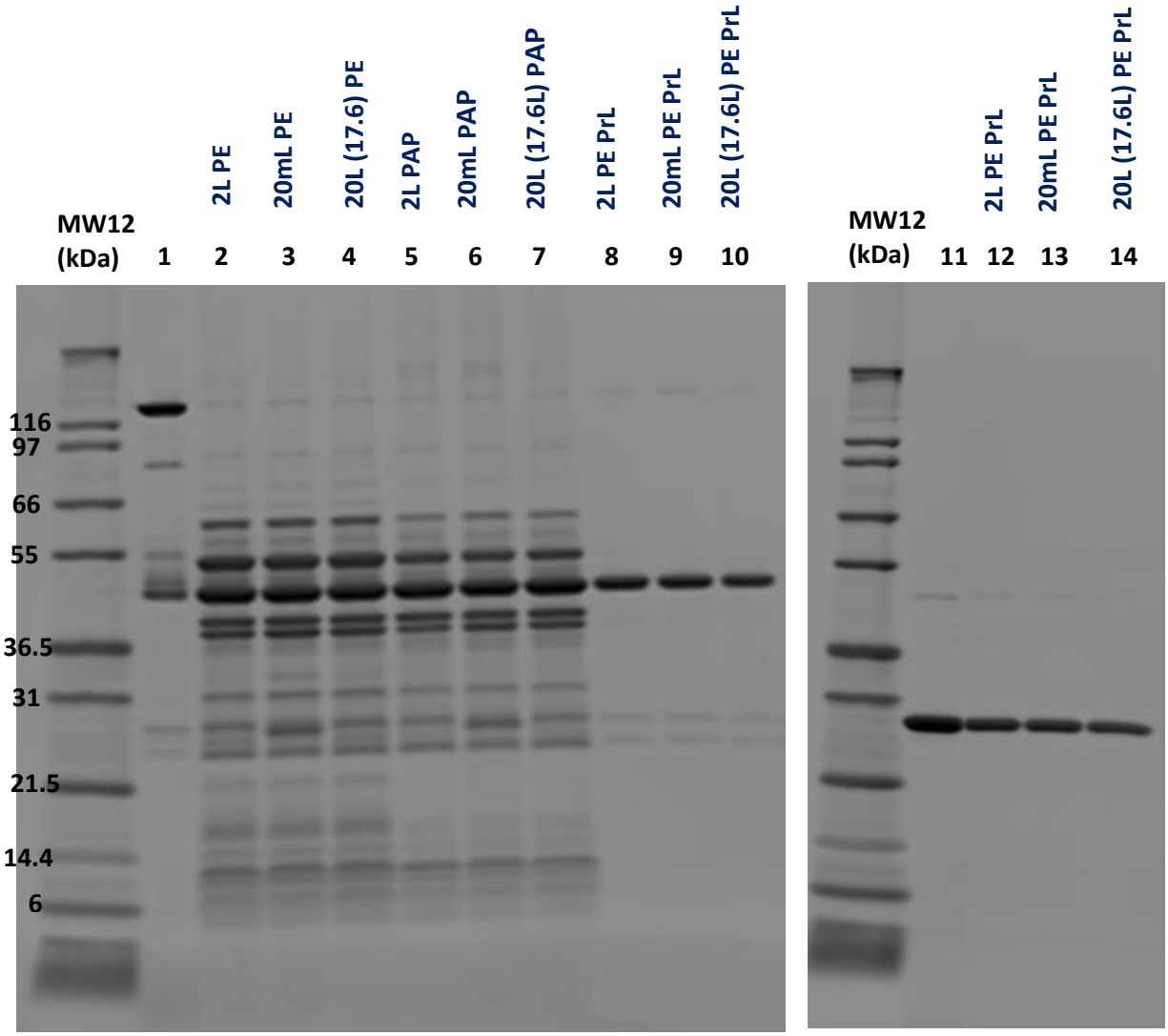

Figure 5.9: SDS-PAGE gel showing the HCP and purified Fab' profiles at the 2L, 20mL and 20L (17.6L) scale for Exp #3. The non-reduced gel with post extraction (PE), post acid precipitation (PAP) and post extraction (PE) protein L (PrL) purified samples (Lanes 2-10); and the reduced gel with post extraction (PE) protein L (PrL) purified samples at the 2L, 20mL and 20L (17.6L) scale (Lanes 12-14): Lane 1- Fab' standard; Lane 2- 2L PE; Lane 3- 20mL PE; Lane 4- 20L (17.6L) PE; Lane 5- 2L PAP; Lane 6- 20mL PAP; Lane 7- 20L (17.6L) PAP; Lane 8- 2L PE PrL; Lane 9- 20mL PE PrL; Lane 10- 20L (17.6L) PE PrL; Lane 11- Fab' standard; Lane 12- 2L PE PrL; Lane 13- 20mL PE PrL; Lane 14- 20L (17.6L) PE PrL

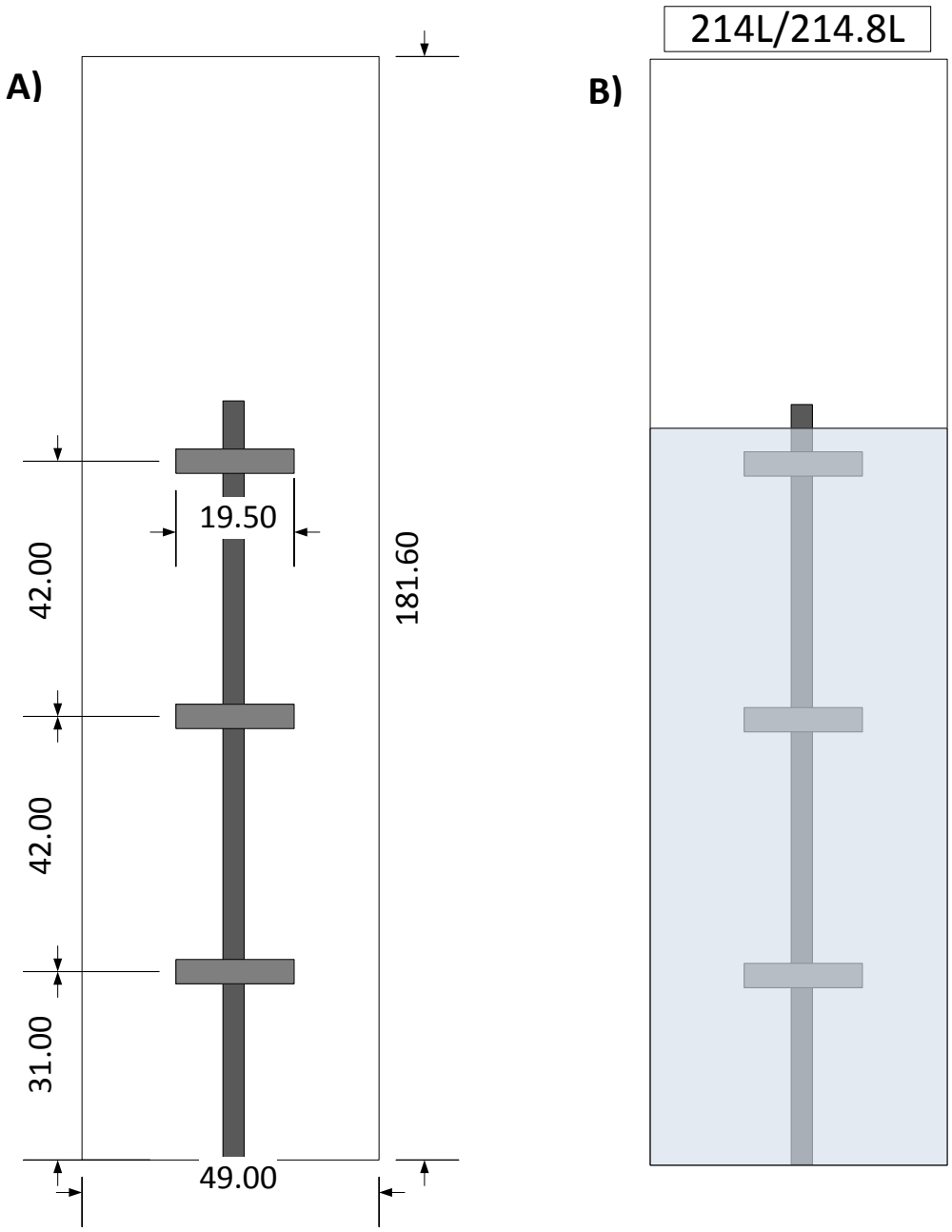

Figure 5.10: Schematic diagram of the 200L vessel showing the **A)** key dimensions and impeller spacing in cm; and **B)** with a fill volume of 214L (214.8L) as used in Exp #6 and 7

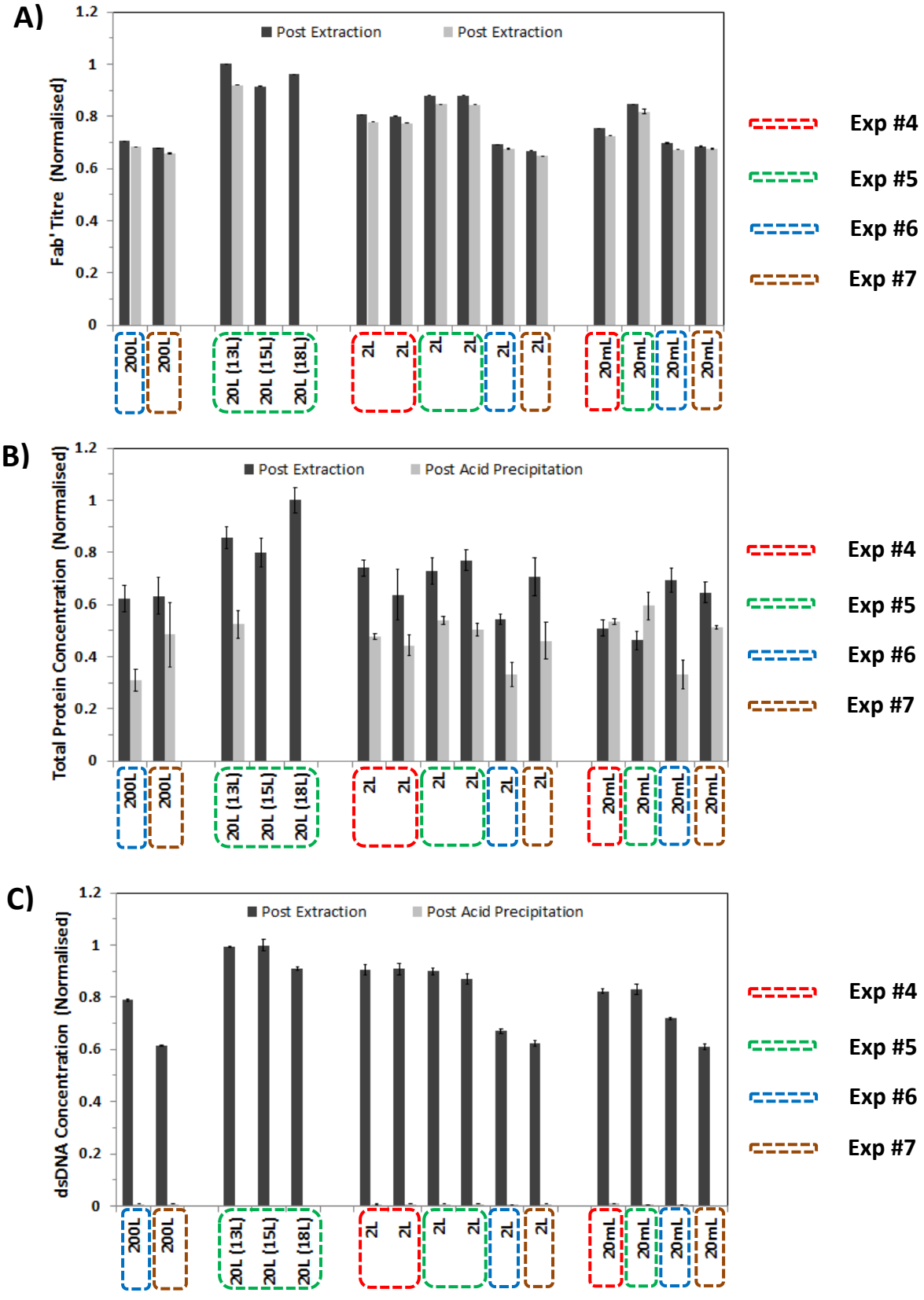

Figure 5.11: Comparison of the normalised 200L, 20L, 2L and 20mL **A)** Fab' titre; **B)** total protein concentration; and **C)** dsDNA concentration after heat extraction and acid precipitation from Exp #4-7. Error bars represent ± 1 standard deviation from replicates in the assay (n=2 for **A** and n=3 for **B** and **C**)

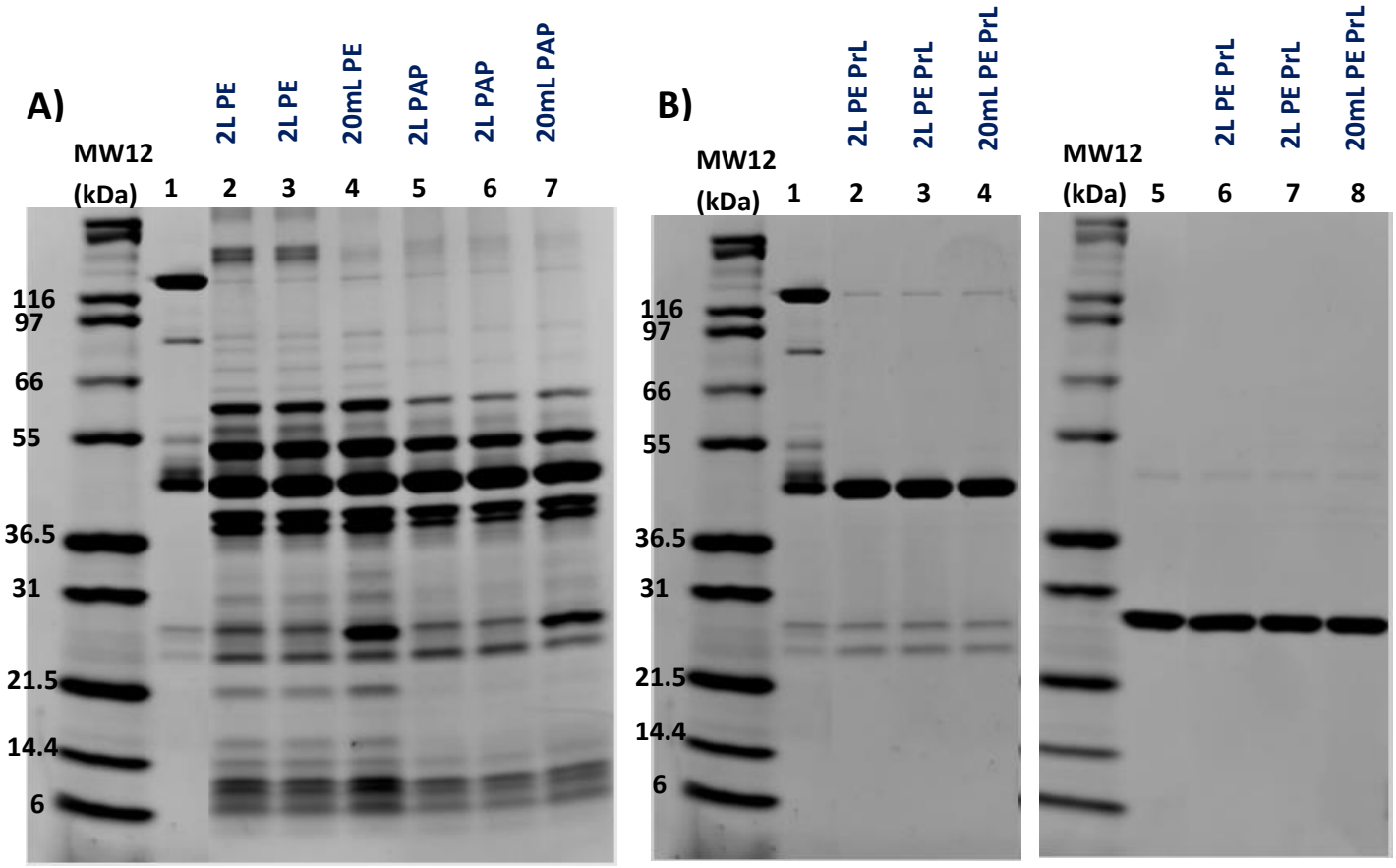

Figure 5.12: SDS-PAGE gels showing the HCP and purified Fab' profiles at the 2L and 20mL scale for Exp #4. The **A)** non-reduced gel with the post extraction (PE) and post acid precipitation (PAP) samples: Lane 1- Fab' standard; Lane 2- 2L PE; Lane 3- 2L PE; Lane 4- 20mL PE; Lane 5- 2L PAP; Lane 6- 2L PAP; Lane 7-20mL PAP. The post extraction (PE) protein L (PrL) purified samples for **B)** non-reduced samples (Lanes 2-4) and reduced samples (Lanes 6-8) conditions: Lane 1/5- Fab' standard; Lane 2/6- 2L PE; Lane 3/7- 2L PE; Lane 4/8- 20mL PE

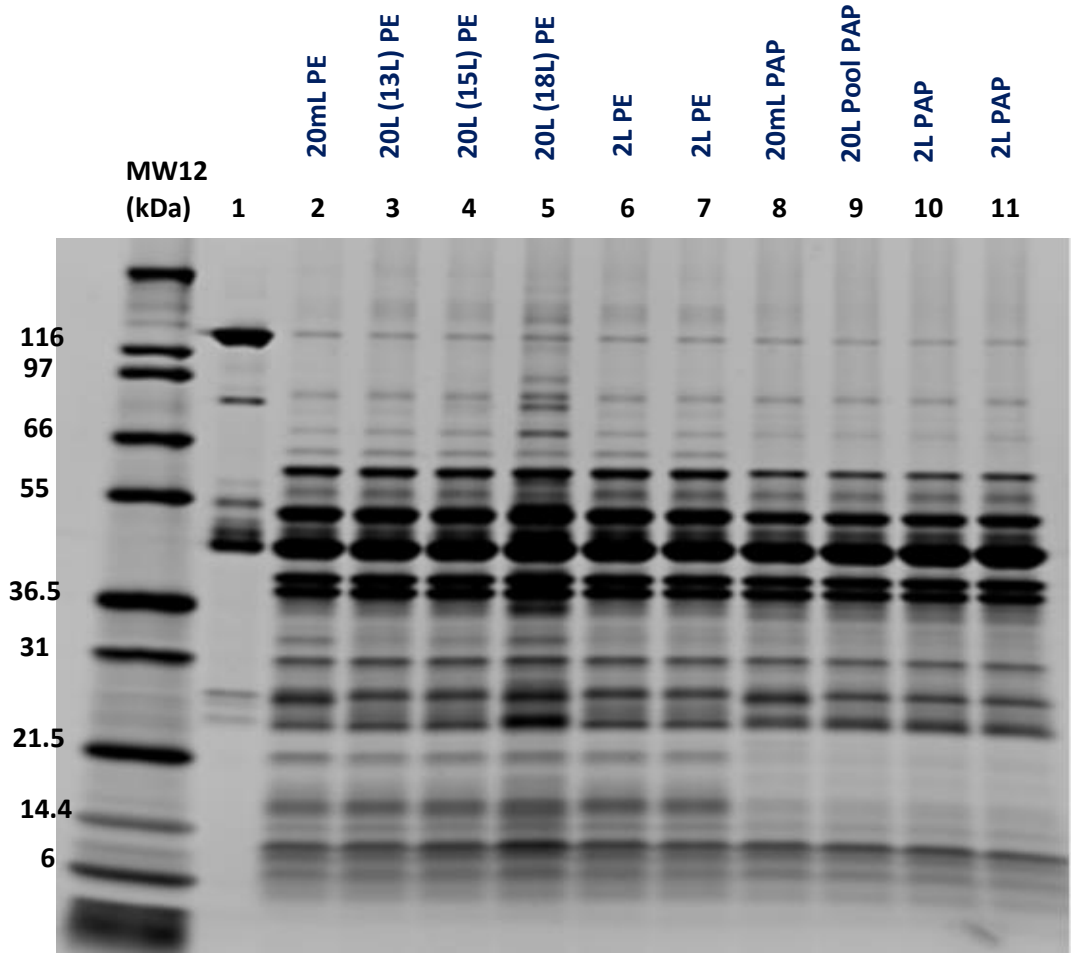

Figure 5.13: SDS-PAGE gel showing the HCP and purified Fab' profiles at the 20mL, 20L (13L), 20L (15L), 20L (18L) and 2L scale for Exp #5. The non-reduced gel with post extraction (PE) and post acid precipitation (PAP) samples: Lane 1- Fab' standard; Lane 2- 20mL PE; Lane 3- 20L (13L) PE; Lane 4- 20L (15L) PE; Lane 5- 20L (18L) PE; Lane 6- 2L PE; Lane 7- 2L PE; Lane 8- 20mL PAP; Lane 9- 20L Pooled PAP; Lane 10- 2L PAP; Lane 11- 2L PAP

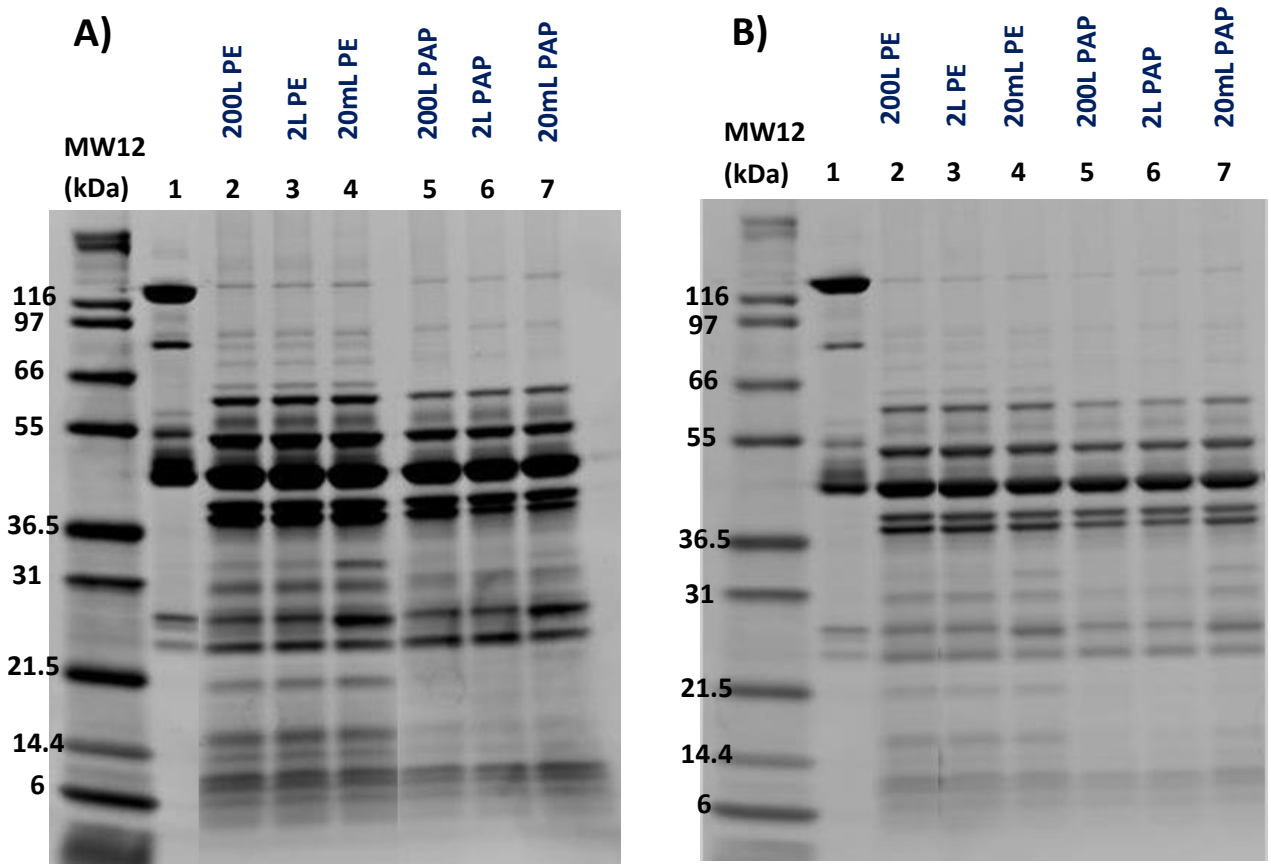

Figure 5.14: SDS-PAGE gels showing the HCP and purified Fab' profiles at the 2L and 20mL scale for **A)** Exp #6 and **B)** Exp #7. The non-reduced post extraction (PE) and post acid precipitation (PAP) samples: Lane 1- Fab' standard; Lane 2- 200L PE; Lane 3- 2L PE; Lane 4- 20mL PE; Lane 5- 200L PAP; Lane 6- 2L PAP; Lane 7- 20mL PAP

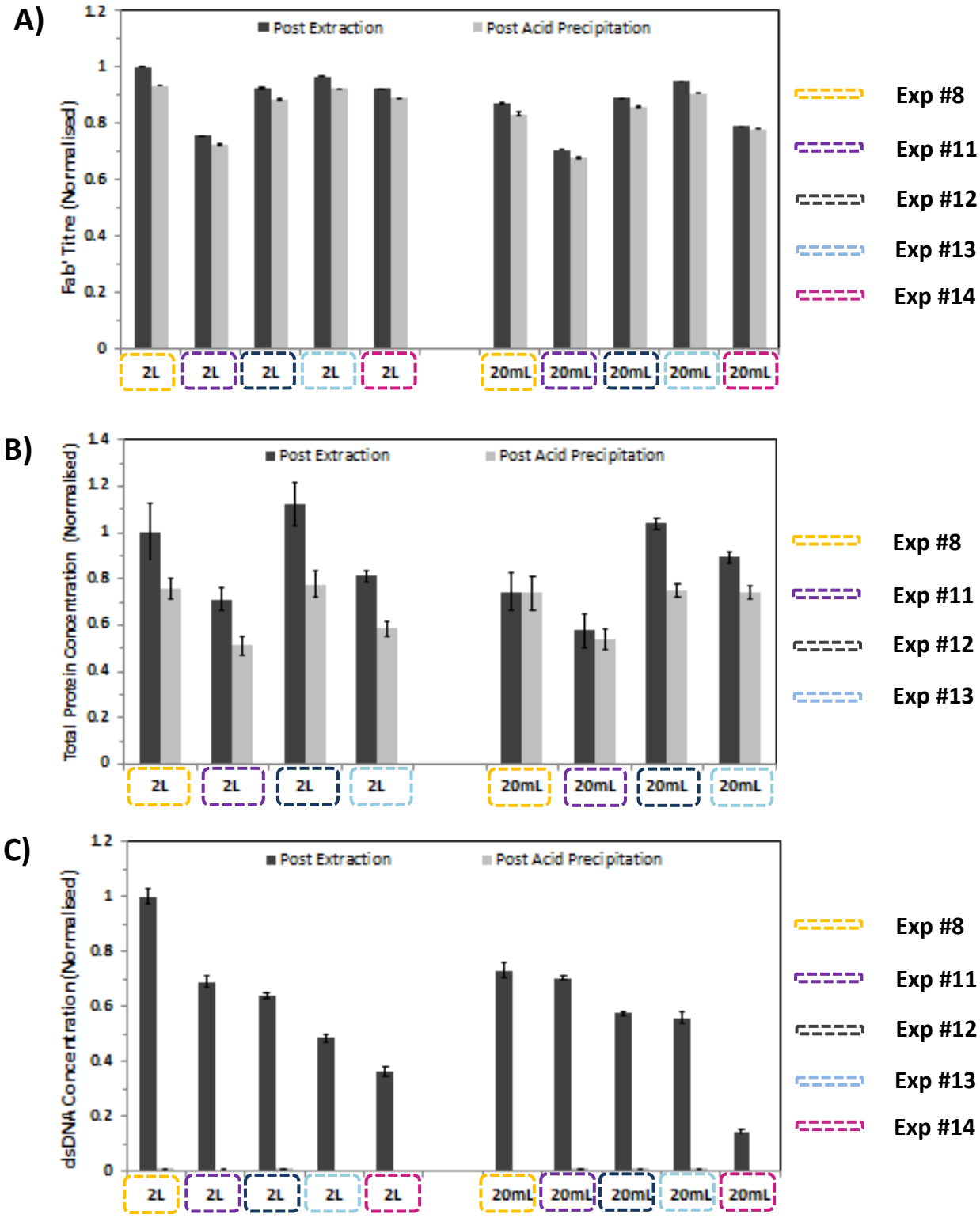

Figure 5.15: Comparison of the normalised 2L and 20mL **A)** Fab' titre; B**)** total protein concentration; and **C)** dsDNA concentration after heat extraction and acid precipitation from Exp #8, 11-14. Error bars represent ± 1 standard deviation from replicates in the assay (n=2 for **A**, n=3 for **B** and **C**)

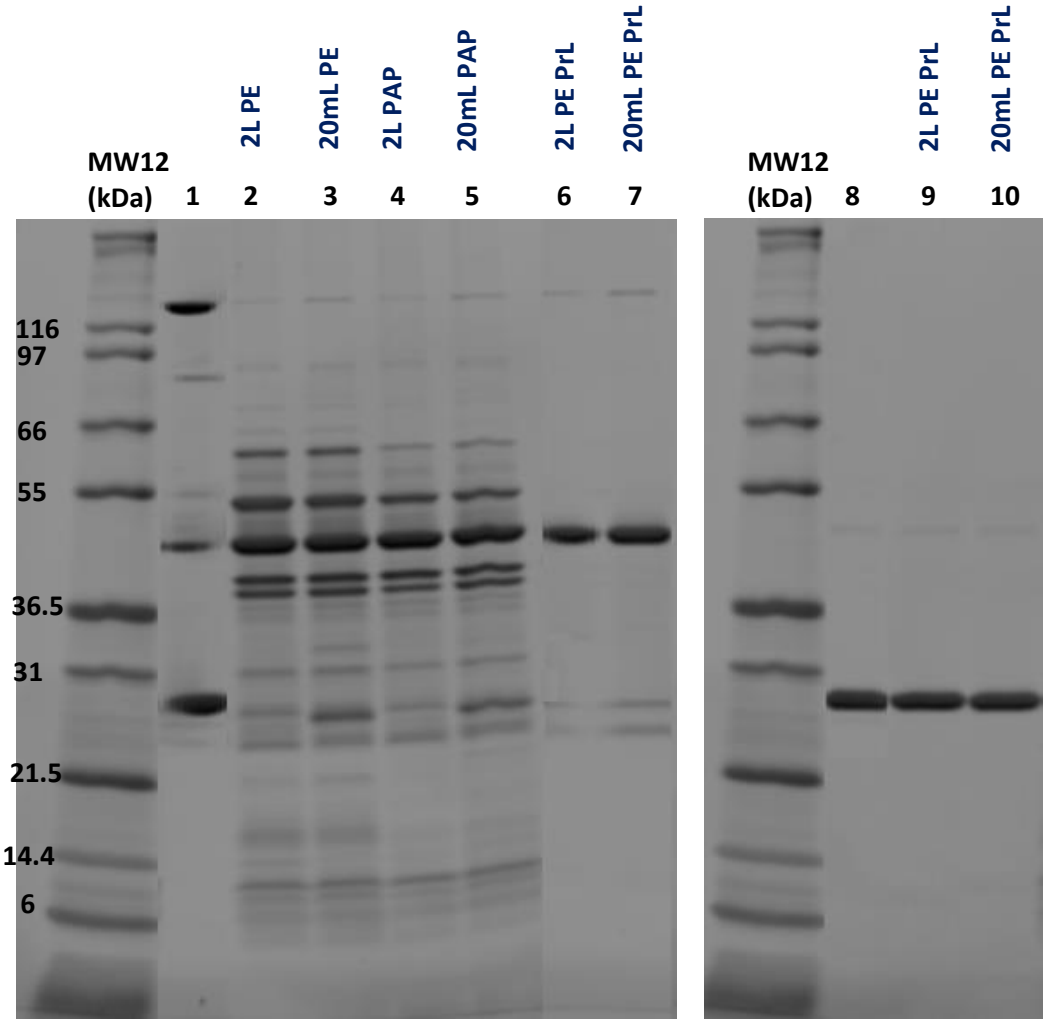

Figure 5.16: SDS-PAGE gel showing the HCP and purified Fab' profiles at the 2L and 20mL scale for Exp #8. The non-reduced post extraction (PE), post acid precipitation (PAP) and post extraction (PE) protein L (PrL) purified samples (Lanes 2-7) and reduced post extraction (PE) protein L (PrL) purified samples (Lanes 9-10): Lane 1- Fab' standard; Lane 2- 2L PE; Lane 3- 20mL PE, Lane 4- 2L PAP; Lane 5- 20mL PAP; Lane 6- 2L PE PrL; Lane 7- 20mL PE PrL; Lane 8- Fab' standard; Lane 9- 2L PE PrL; Lane 10- 20mL PE PrL

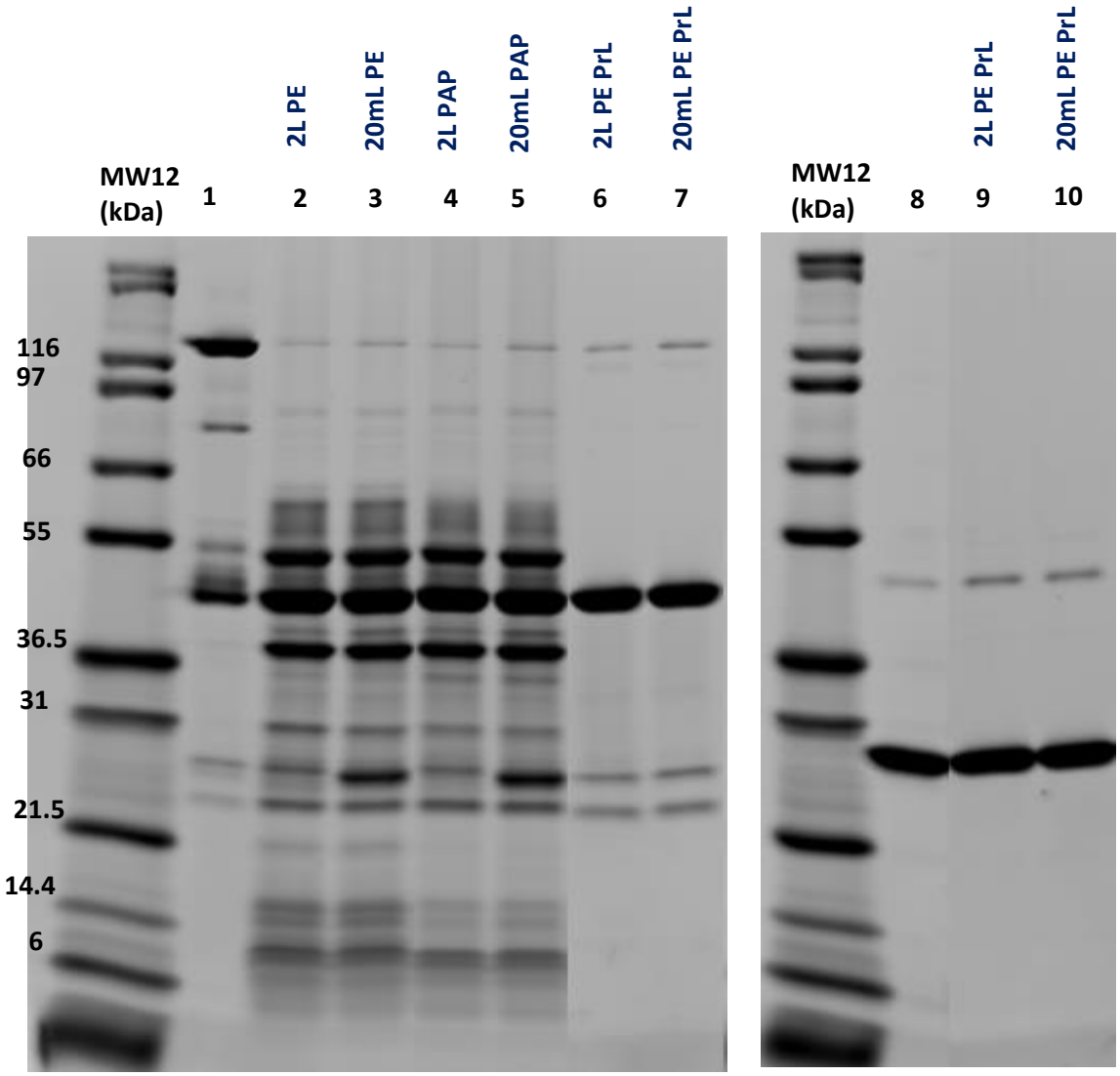

Figure 5.17: SDS-PAGE gel showing the HCP and purified Fab' profiles at the 2L and 20mL scale for Exp #11. The non-reduced post extraction (PE), post acid precipitation (PAP) and post extraction (PE) protein L (PrL) purified samples (Lanes 2-7) and reduced post extraction (PE) protein L (PrL) purified samples (Lanes 9-10): Lane 1- Fab' standard; Lane 2- 2L PE; Lane 3- 20mL PE, Lane 4- 2L PAP; Lane 5- 20mL PAP; Lane 6- 2L PE PrL; Lane 7- 20mL PE PrL; Lane 8- Fab' standard; Lane 9- 2L PE PrL; Lane 10- 20mL PE PrL

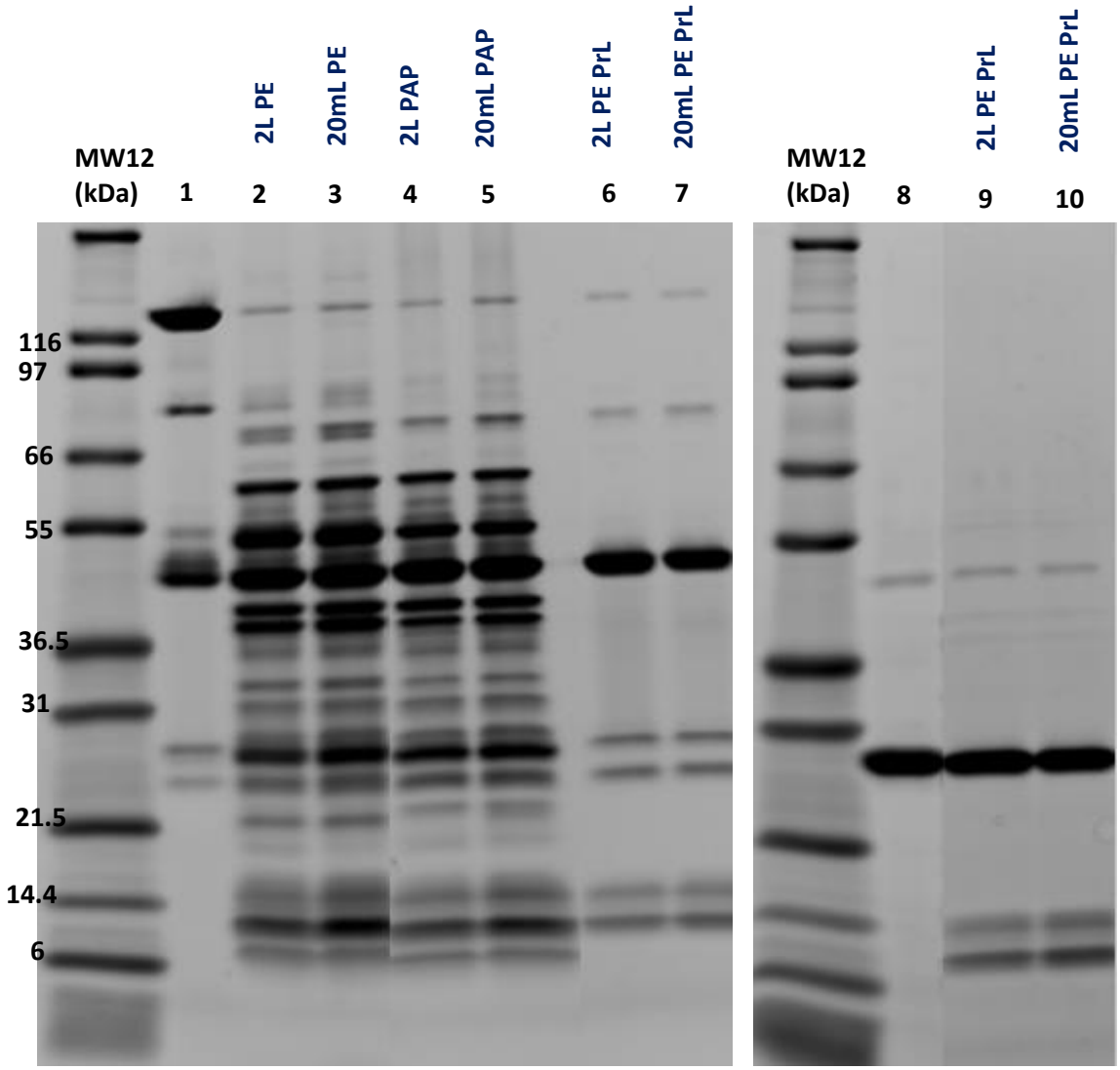

Figure 5.18: SDS-PAGE gel showing the HCP and purified Fab' profiles at the 2L and 20mL scale for Exp #12. The non-reduced post extraction (PE), post acid precipitation (PAP) and post extraction (PE) protein L (PrL) purified samples (Lanes 2-7) and reduced post extraction (PE) protein L (PrL) purified samples (Lanes 9-10): Lane 1- Fab' standard; Lane 2- 2L PE; Lane 3- 20mL PE; Lane 4- 2L PAP; Lane 5- 20mL PAP; Lane 6- 2L PE PrL; Lane 7- 20mL PE PrL; Lane 10- Fab' standard; Lane 11- 2L PE PrL; Lane 12- 20mL PE PrL; Lane 13- 2L PE PrL

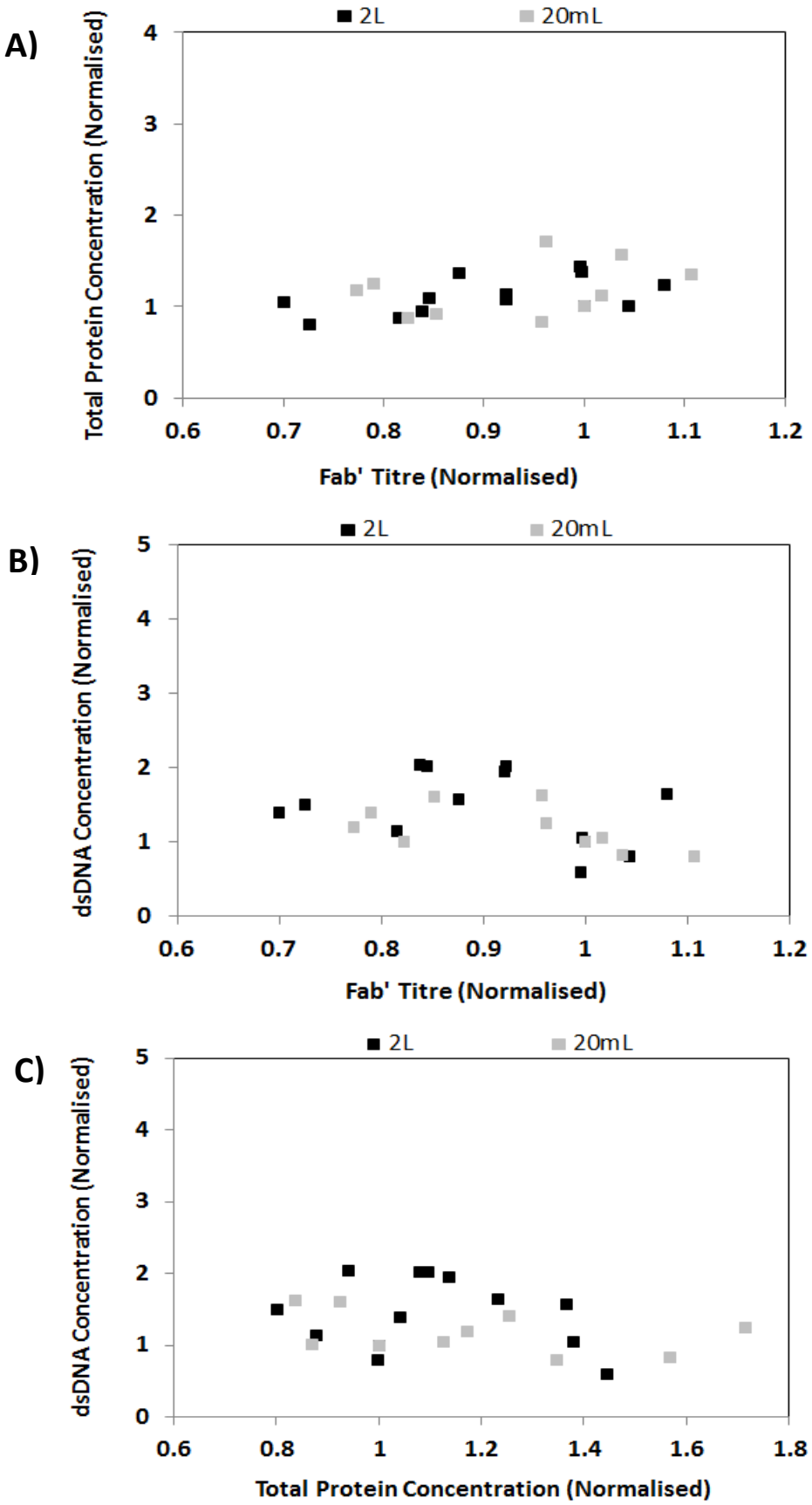

Figure 5.19: Correlation between the **A)** Fab' titre and total protein concentration; **B)** Fab' titre and dsDNA concentration and **C)** total protein concentration and dsDNA concentration in the 2L and 20mL vessel for Exp #2- 14

Chapter 6

Development and Verification of a Microwell System for Heat Extraction

6.1 Introduction and Aims

The summary of the literature review in Chapter 1 has shown that process development work in increasingly being shifted shaken or stirred millilitre scale options. Microwell plate format in particular are suitable for developing automated protocols and have shown successful application for bioprocesses such as fermentation and biotransformation (Fernandes and Cabral 2009). These systems have a number of advantages, such as high throughput, opportunity for automation and reduced process development costs, but they are not useful unless processes developed in these microwell plates can be scaled accurately to lab or pilot scale. Scaling between different size stirred tank vessels alone can be difficult; however scaling between bioreactors with such different type of motion can be even more challenging. Microwell technology can help to rapidly improve and optimise a bioprocess provided that it can mimic a large scale process in terms of geometry, hydrodynamics and power consumption characteristics.

There have been a number of studies conducted for scale-down of cell cultivations from stirred tank reactors into microwell plates (Barrett *et al*., 2009; Chen *et al*., 2009; Doig *et al*., 2005; Isett *et al*., 2007; Zhang *et al*., 2008). Only very few studies focused on downstream processing unit operations and scaling down an industrial heat extraction into microwell format. Previous data from Chapters 4 and 5 has shown that the extraction process can be mimicked between stirred tank vessels of different sizes provided that the heating profile was kept the same and there was a sufficient level of mixing. The system was considered to be sufficiently mixed once the mixing time was no longer dependent on speed, or specific power input. Once this was achieved, the extraction performance was found to be not affected by an increase in specific power input. Characterisation of mixing time in the 24-

well deep square-well (DSW) plate showed that sufficient mixing was achieved at a shaken speed at or above 400rpm. The experiments in this chapter build on the findings of Chapter 4 and are primarily focused on verifying if extraction performance can be successfully mimicked in microwell plates provided that the cell suspension is fully homogenous and the heating profiles are matched.

The specific objective of this chapter is:

- To conduct a number of heat extraction experiments in the 24-well DSW plate, under different operating conditions, and to compare the performance to the 2L and 20L stirred tank vessels.

6.2 Experimental Approach

Cells were harvested after fermentation using a dead end or disc stack centrifuge, depending on the scale of fermentation, and then extracted using tris/EDTA buffers under heated conditions in the stirred tank vessel, as described in section 2.4. The details of the fermentation and centrifugation process are shown in Chapter 5 in Table 5.1 and 5.2, respectively. The details of the process conditions used for the experiments in this chapter are detailed in Table 6.1. The extraction profiles used in each experiment can be viewed in Appendix 6A. The key outputs that were assessed to compare performance between different scales are the same as those in Chapters 3 and 5 which are Fab' titre, total protein concentration, dsDNA concentration and HCP and Fab' profiles, which were obtained as described in section 2.5. All Fab', total protein and dsDNA concentrations have been normalised to the post extraction Fab', total protein and dsDNA concentrations, respectively, in the stirred tank vessel for each individual experiment.

6.3 Results and Discussion

6.3.1 24-Well DSW Extraction in Comparison to 20L Extraction

Figure 6.1A shows a picture of all the vessels used in this chapter for the heat extraction experiments where a 500mL red buffer bottle was used as size reference. The largest scale difference in these experiments is 10,000 fold between the 24-well DSW (2mL) and the 20L vessel. Figure 6.1B shows a picture of the acid precipitation step set up in the 24-well DSW plate after the end of the heat extraction step.

Initial extraction studies were conducted using the UCB Fab' 2, to compare extraction in the 24-well DSW plate to four extractions conducted at the 20L scale (Exp #9). The fill volume in the 20L vessel was 18.2L and the specific power input was maintained at 0.23W L^{-1}. For the 24-well DSW plate, the fill volume was kept at 2mL and the shaker speed was kept constant at 1200rpm. The cells were extracted at 60°C for 10 hours. Previous data from Chapters 3 and 5 have shown that the extraction performance is sensitive to temperature and therefore it is crucial that the heating profile was well matched at all scales therefore efforts were made to mimic the temperature profile very closely to the set point. This was achieved nicely on the Eppendorf Thermomixer. The heating profile measured across the plate during heat extraction can be observed in Appendix 6B. Figure 6.2A, B and C shows the Fab', total protein and dsDNA concentration, respectively, for the 18.2L extractions and the 24-well DSW plate. The results from this first experiment show that the extraction performance can be mimicked very well in the DSW plate for Fab' titre and total protein concentration with only a 2% and 5% difference, respectively. The dsDNA concentration in the DSW plate is 13% lower than that observed at 18.2L, however these differences are not considered to be significant. The error bars in the DSW plate, which represent ± 1 standard deviation between replicates, are relatively small considering the fill volume being tested is only 2mL.

Figure 6.3 shows the SDS-PAGE gels obtained from samples from the DSW plate and from one 18.2L extraction in Exp #9. Figure 6.3A shows the post extraction samples on a non-reduced gel. Lanes 2-7 represent the DSW samples, taken from different wells across the plate, and Lane 9 represents one 18.2L sample. The HCP profiles in the DSW show good

comparability overall and also matches reasonably well with the 18.2L sample. Small differences can be observed between the profiles in the DSW, particularly for the heavy chain band at 28kDa. Figure 6.3B shows the post acid precipitation samples on a reduced gel. Lanes 2-6 represent DSW samples and Lane 9 represents the 18.2L sample. The HCP profiles show relatively good comparability within the wells in the DSW plate as well as to the 18.2L sample. There are some noticeable differences in the intensity of some bands across the DSW plate, particularly for the heavy chain. These small differences in the samples across the plate may be due to the amount of cells that were initially added to each well. Cell solutions were added manually; therefore it is possible that the overall ratio of heavy phase to buffer varied slightly during the experiment. For the post acid precipitation samples in Figure 6.12B, acetic acid was added to each well one by one and a micro-pH probe was used to measure initial and final pH, as shown in Figure 6.1B. Appendix 6B shows a table with the starting pH, the final pH and the amount of acid added to wells A2, D2, C3, B4 and D5. Although the final pH value was very similar across the wells, the starting pH for wells D2 and D5 were lower than for the other wells, therefore a slightly lower volume of acetic acid was added in those wells. Wells D2 and D5 represent Lanes 3 and 6, respectively, which corresponds to the more intense heavy chain bands seen in the HCP profiles. Measurements to obtain % evaporation values in the DSW plate showed that evaporation was less than 1% across the plate over the duration of the extraction process, which for Exp #9 was 13 hours. Therefore the differences in starting pH in wells D2 and D5, are likely due to error introduced by manual addition of heavy phase and extraction buffer. When adding these components, a balance was used to measure the weight in each well. Although the balance was calibrated and tared, and every effort was made to ensure the required weights were added to each well, it may be that a more sensitive balance and the use of a multi-channel pipette was required for more accurate measurements of additions. The use of an automated platform would also help reduce these differences.

Figure 6.3C shows the non-reduced gel with post extraction samples, purified using protein L chromatography. Lanes 2-6 represent samples from the DSW plate and Lane 8 represents the 18.2L sample. The Fab' profiles between the wells are well matched however the Fab' profile in the 18.2L sample shows additional bands at 33kDa, 14kDa and 6kDa. The two

bands close to the bottom of the gel represent Fab' fragments. These bands appear to be very faintly present in the DSW samples too but the gel resolution is not clear enough to be certain of their relative intensity. Purified post extraction samples were run on a reduced gel, as shown in Figure 6.3D. The profiles between the well samples and the 18.2L sample are well matched. The SDS-PAGE gels for Exp #9 therefore show reasonably good reproducibility between shaken samples in the wells and between these and the 18.2L stirred tank vessel. The gel images were manipulated in order to overexpose the gels and intensify the band intensity. The level of overexposure was done based on judgement of what was considered reasonable for capturing the bands and therefore small variations in overexposure may exist between different gels, making it difficult to quantitatively compare different gels. Densitometry analysis is a useful tool which may be used in the future to quantify bands, thus allowing for a more direct comparison of samples across different plates.

6.3.2 24-Well DSW Extractions in Comparison to 2L Extractions

Exp #10-14 were conducted using UCB Fab' 1, in order to compare extraction performance between the DSW plate and the 2L stirred tank vessel. The extraction conditions, such as extraction hold time and specific power input or shaker speed were changed across these different experiments, as presented in Table 6.1, to see if the DSW plate was comparable to the 2L vessel under various conditions. The % evaporation across the plates was less than 1% for all experiments therefore this factor was not considered to be responsible for any difference observed between the two scales. Exp #10 was conducted using the same extraction conditions as Exp #9. Figures 6.4A, B and C show the Fab', total protein and dsDNA concentrations between the 2L vessel and the DSW plate. The Fab' titre in the DSW plate was shown to be 7% higher than the 2L scale, however this difference is not considered to be significant. The total protein concentration was 15% lower and the dsDNA concentration was 50% lower in the DSW plate. Data from the harvest sample of the fermentation, as shown in Table 5.1 in Chapter 5, indicates no significant deviations in the % cell viability or dsDNA concentration for this experiment which may have explained these differences in the extraction data. These differences may therefore be due to differences in

the mixing environment between the two scales. As discussed in Chapter 5, the correlation between the Fab' titre, total protein concentration and dsDNA concentration is not fully understood but dsDNA release is typically related to shear and cell damage. It is possible that shear in the DSW plate is slightly lower than in the stirred tank vessel.

Figure 6.5A, B, C and D shows the SDS-PAGE profiles for non-reduced post extraction samples, non-reduced post acid precipitation samples, non-reduced post extraction purified samples and reduced post extraction purified samples, respectively. Lanes 2-7 in all gels represent samples from the DSW plate and Lane 9 represents the 2L sample. Despite small differences in the bands between the wells, the profiles are very similar overall and show that each individual well is capable of being used as a mini extraction vessel. Figure 6.5A shows that the 33kDa band, which is present in the DSW samples, is missing in the 2L sample. Again, this may be due to differences in exposure of gels leading to relative differences in band intensity. The gels in Figure 6.5B, C and D also show good comparability of the DSW and the 2L samples and therefore indicate that the DSW plate is capable of mimicking the 2L process very well. Fab', total protein and dsDNA concentrations have been normalised for experiments using UCB Fab' 1 and 2 (Exp #10 and 9). Results showed an excellent comparison between the extraction performance in the DSW plate and the stirred tank vessels. Comparison of the significantly different SDS-PAGE profiles between Exp #10 and 9 further demonstrates that the DSW plate is capable of differentiating the performance of very different strains.

In Exp #11 the heating profile was varied so that the cells were extracted at 64°C for 14 hours. The shaker speed and fill volume in the DSW plates were also varied as shown in Table 6.1. Figure 6.6A, B and C shows the Fab', total protein and dsDNA concentration, respectively, between the 2L vessel and the DSW plate. Figure 6.6A shows that the Fab' titres in the DSW plate for all volumes tested were on average 18% greater than for 2L vessel. The shaker speed and the fill volume appear to have no effect on the extraction performance. Similarly, it can be observed from Figure 6.6B and Figure 6.6C that total protein and dsDNA concentrations are both on average 17% greater in the DSW plate compared to 2L. It is possible that differences in the extraction profile, between Exp #9-10

and Exp #11 as seen in Appendix 6A, are responsible for these higher concentrations in the DSW plate. In Exp #11, the cells were exposed to higher temperatures and longer extraction durations compared to any other experiment. Under these more extreme conditions, it is possible that cells are damaged to a greater extent thus causing more proteins and dsDNA to be released, therefore causing the viscosity to increase (Sehdev and Spitali 2008). If this is the case, it may be that differences in shear and overall mixing environment between the 2L vessel and DSW plate become more important when the viscosity is changed and therefore has a greater impact on extraction performance. The data for DSW samples in Figure 6.6 are in agreement with the mixing time data observed in the DSW plate, presented in Chapter 4, where it was found that increasing the shaker speed above 400rpm and increasing the fill volume above 400rpm did not impact mixing time. It is possible once a minimum threshold of power is achieved, increasing the speed further does not impact performance in the system. Similar observations were found in the stirred tank vessel. The mixing time and process verification results from Chapter 4 and Chapter 5, respectively, showed that once a minimum specific power input of around 0.5W L^{-1} was achieved, extraction performance was not affected by further increases in impeller speed.

Figures 6.7A, B, C and D shows the SDS-PAGE profiles for non-reduced post extraction samples, non-reduced post acid precipitation samples, non-reduced post extraction purified samples and reduced post extraction purified samples, respectively. Lanes 2-5 in all gels represent samples from the DSW plate at a speed of 1200rpm with increasing fill volume. Similarly, Lanes 7-10 represent DSW samples at a speed of 500rpm with increasing fill volume. Lane 12 represents the 2L sample. The results from all four gels show that the fill volume in the DSW plate does not have an impact on the HCP and Fab' profiles. Additionally, disregarding small differences possibly due to gel exposure, the shaker speed also does not have a significant impact on the HCP and Fab' profiles. These results are in agreement with the data from Figure 6.6. The SDS-PAGE profiles in the DSW samples are also very similar to the 2L sample. In Exp #12, the heating profile was varied again so that the cells were extracted at 55°C for 6 hours. The fill volumes and shaker speeds in the two DSW plates were kept the same as for Exp #11. Figures 6.8A, B and C shows the Fab', total protein and dsDNA concentration, respectively, for the 2L vessel and the DSW plate. These

results show that fill volume and shaker speed have no effect on extraction performance, as previously observed. Figure 6.8A and 6.8B show that Fab' and total protein concentrations are on average 4% and 11% higher, respectively, in the DSW plate in comparison to the 2L vessel. The dsDNA concentration, in Figure 6.8C, however is 25% lower in the DSW plate in Exp #12 compared to in Figure 6.6C. These differences may again be caused by the smaller extraction profile, as seen in Appendix 6A, which is potentially responsible for making it less viscous. This may affect the mixing performance between the two scales and therefore impact overall extraction performance.

Figure 6.9A, B, C and D shows the SDS-PAGE profiles for non-reduced post extraction samples, non-reduced post acid precipitation samples, non-reduced post extraction purified samples and reduced post extraction purified samples, respectively. Lanes 2-10 in Figure 6.9A and B represent samples from the DSW plate and Lane 12 represents the 2L sample. Lanes 2-5 and 7-10 in Figure 6.9A and B represent samples from the DSW plate and Lane 12 represents the 2L sample. Lanes 2-3 and 5-6 in Figure 6.9C and D represent samples from the DSW plate and Lane 8 represents the 2L sample. As observed in previous gels, the HCP and Fab' profiles are well matched between samples in the DSW as well as between the DSW samples and the 2L sample. A quick comparison of the Fab' profiles in Figure 6.9C and D to Figure 6.7C and D show the significant presence of Fab' fragments near the bottom of the gel at 14kDa and 6kDa. These fragments may be caused by the small heating profile for Exp #12 as seen in Appendix 6A. It may be that these fragments are initially present in the cell suspension during extraction but exposure of the Fab' to higher temperatures for a prolonged period of time results in higher clarification, which is possibly why they were not seen for Exp #9, 10 or 11.

The next experiment, Exp #13, looked at another scale-down study between the 2L and DSW plate. The cells were extracted at 60°C for 10 hours. Figure 6.10A, B and C shows Fab', total protein and dsDNA concentration, respectively, between the 2L and DSW plate. The results are in agreement with data from most of the previous extractions, where typically the Fab', total protein and dsDNA content were found to be slightly higher in the DSW compared to the 2L vessel. The data from Exp #9-13 indicates that a shaker speed higher

than 500rpm results in a good mixing environment which is sufficient for scaling between a stirred tank vessel and a shaken microwell plate. At this speed, mixing time in the shaker, as presented in Figure 4.21B in Chapter 4, was found to be less than 3 seconds for all fill volumes. Figure 4.22 showed that the flow became quite turbulent at 500rpm and the liquid height was also relatively high at this speed, as shown in Figure 4.23, thus promoting faster mixing. These figures also showed that at speeds of 1000rpm and above, the liquid height was significantly higher and there was thrashing of liquid on the sides of the wall which further promotes mixing.

The final experiment, Exp #14, compared the performance of the DSW plate to the 2L vessel for a range of shaker speeds including speeds below 500rpm. The cells were extracted at 60°C for 10 hours. Three plates were tested at speeds of 1200rpm, 400rpm and 350rpm with varying fill volumes in each plate. The Fab', total protein and dsDNA concentration in the 2L vessel and DSW plate are shown in Figures 6.11A, B and C, respectively. A comparison of the wells at different fill volumes shows that, regardless of shaker speed, fill volume has no significant impact on extraction performance. The Fab' and total protein concentrations are not affected by the varying shaker speeds. For dsDNA, however, the results indicate that as the speed decreases, the dsDNA concentration also decreases. It is possible that at these low speeds, the cells are exposed to a relatively low shear environment. Figure 4.24 from Chapter 4, showed that at 350rpm, the flow was distributed around the well in ring vortices via convection and there was no thrashing of the liquid along the edges of the well. This gentle mixing may have caused the removal of the outer membrane of the cells during the extraction process, whist limiting damage to the inner membrane, thus releasing most of the Fab' from the periplasm but preventing the release of dsDNA from inside the cell. The mixing time curves from Figure 4.21B in Chapter 4, showed that mixing was relatively fast at less than 5 seconds for 400rpm and were similar to 500rpm and 1200rpm. However, analysis of the mixing patterns, presented in Figure 4.24, and the relative liquid height, presented in Figure 4.23, shows that mixing is not as turbulent as it is for speeds of 500rpm or greater. This indicates that although mixing may be considered to be sufficiently fast in the DSW plate it is also important to have a relatively high level of turbulence in the wells and therefore possibly work with conditions where the maximum height of the liquid to still

height (H*/HL) is greater than 2, in order to more accurately mimic mixing conditions in the stirred tank vessel.

Figure 6.12A and B shows the HCP profiles from the post extraction and post acid precipitation samples, respectively, on non-reduced SDS-PAGE gels. Lanes 2-5, 6-10 and 12-15 represent the DSW plates at 1200rpm, 400rpm and 350rpm, respectively, at the four different fill volumes. The profiles are comparable between wells from the same plate and appear to be comparable also between the three plates, when taking into consideration the relative band intensities in each profile. The higher band intensities in Lanes 6-15, are likely due to increased overexposure only. The DSW plate samples in all three plates are also comparable to the 2L sample. Figure 6.13A and B shows the Fab' profiles from post extraction samples on a reduced and non-reduced SDS-PAGE gel, respectively. Lanes 2-4, 6-8 and 10-12 represent the DSW plates at 1200rpm, 400rpm and 350rpm, respectively. Samples from wells with fill volumes of 2.5mL, 3mL and 3.5mL were run on the gels. The profiles show that between wells of the same plate, the profiles are well matched. A comparison of profiles between the three plates shows that Fab' fragments are present at 14kDa and 6kDa for the DSW plate at 400rpm and 350rpm. These bands are not present in the plate at 1200rpm or the 2L vessel. Taking into account exposure differences for the three plates, the Fab' fragment bands appear to be slightly more intense for the 350rpm lanes compared to 400rpm which again indicates that mixing conditions at 350rpm are not sufficient for this mimicking the extraction process. The trends seen for these Fab' fragments and for dsDNA concentration in Figure 6.11C, for Exp #14, demonstrate that extractions in the DSW plate should be conducted at 500rpm or above to best mimic mixing in stirred tank vessels.

The results from Exp #14 are therefore very interesting because they highlight the importance of having sufficient mixing conditions for optimum extraction performance. Figure 6.11 alone would imply that the optimum conditions, where Fab' titre is highest and dsDNA concentration is lowest, is at 350rpm. However, SDS-PAGE analysis showed that there is fragmentation of the Fab' protein at this speed resulting in small fragments in the mixture which are likely to make Fab' purification in DSP more challenging. The data from

Exp #14 therefore shows that it is important to check the quantity and the quality of the Fab' protein, and also other cell related impurities when scaling down the extraction process, thus selecting process conditions where all these parameters are well matched. The trends seen in the extraction performance in the DSW plates have been explained by the characterisation studies in Chapter 4. The results from Figure 4.1 and 4.20 indicated that mixing times were matched between the stirred tank vessels around 0.05W L^{-1} and the DSW plate at a shaker speed of 350rpm and a fill volume of 2mL. It may therefore be expected that at these conditions, the extraction performance between the stirred and shaken system would also be well matched, if based only on mixing time. As indicated previously, at 400rpm, for all fill volumes, the mixing time curves showed that sufficient mixing was achieved because mixing time was relatively unchanged at this speed and above. The results from these experiments, however, showed that this was not the case and that sufficient mixing was actually not achieved until 500rpm. The small differences in viscosity between water, used in mixing time studies, and *E.coli* cells, used in extraction, may have impacted on the mixing performance. It is possible that the slightly higher viscosity of *E.coli* cells, compared to water, has marginally reduced mixing efficiency. Evaluating the flow patterns, height of liquid and levels of turbulence, in the well, are therefore crucial for effective scaling as they provide a more thorough understanding of the mixing environment in a system than just mixing time.

The extraction data from this chapter confirms the findings from Chapters 4 and 5 showing that to mimic the heat extraction process at different scales or different systems, sufficient turbulent mixing, achieved above a minimum specific power input or shaker speed where mixing is no longer affected, is required. Data combined from mixing time and PIV studies helped to provide this information. The PIV experiments were able to provide quantitative information on fluid velocity in the 20mL system and showed that the maximum velocity levels in the vessel were not affected significantly above a specific power input of 0.05W L^{-1} and that mixing could be considered sufficient. Similarly, analysis of both the mixing time curves and the mixing patterns in the 24-well DSW plate showed that sufficient mixing was achieved at shaker speeds above 500rpm. Process verification studies were in agreement with the fluid dynamic studies. Determining this threshold value and the conditions where

this threshold value is met in each individual system, regardless of system size or geometry, may therefore serve as an excellent parameter for scaling the heat extraction process.

6.4 Conclusive Remarks

Overall the 24-well DSW plate was able to mimic the 2L and 20L extraction process across a range of different operating conditions with good accuracy. The performance was found to be better in the DSW plates compared to the 2L process. Evaporation during all extractions in the DSW was less than 1% and so this was not the reason for the higher concentrations. Although there is only one set of data available for comparison of the DSW plate to the 20L scale, the results showed that performance was better matched than for the 2L scale. These results correspond to the results from Chapter 5 where it was found that generally, performance in the 20L vessel, at relatively high fill volumes, was better than in the 2L vessel. It may be that mixing in the 20L vessel is close to optimum for a stirred tank vessel and this is mimicked in the DSW plate at a shaken speed of 500rpm or above. Due to the nature of the experiment, number of varibles and the differences in the number of replicates between the 2L and DSW plate, calculating significant differences between the two scales was complicated. However, an attempt was made to compare the 2L vessel and DSW plate at a fill volume of 2mL and a speed of 500rpm using a two tailed t-test, as these conditions in the DSW plate were considered sufficient for mimicking the 2L scale. this applies to Exp #11, 12 and 13. The calculated p values for Fab', total protein and dsDNA were 0.10, 0.01 and 0.56, respectively. This indicates that there is no significant difference between the performance in the two scales for Fab' and dsDNA as they are both above the 0.05 threshold, however, there is some statistical difference between the total protein data. Considering that there were no noticeable differences between extraction performance in the DSW plate at 500rpm and 1200rpm, it is consequently recommended that any further extractions conducted in 24-well DSW plates are done with a minimum shaker speed of 500rpm. The results from this chapter have therefore demonstrated that a 24-well DSW plate may be used to scale-down the heat extraction. Further optimisation and automation of the liquid handling part of the process such as addition of cells, buffers and acetic acid, which may be achieved using a robotic system such as TECAN, is expected to improve accuracy and reduce differences between wells, as well as improving scalability.

Exp #	Extraction Scale	Fill Volume	Heat Up Time (hr)	Hold Time (hr)	Temp (°C)	Cool Down Time (hr)	Shaker Speed (rpm) or P/V (W/L)
9	24-well DSW 4 x 20L	2mL 4 x 18.2L	1.5	10	60	1.5	1200rpm 0.23
10	24-well DSW 2L	2mL 2L	1.5	10	60	1.5	1200rpm 0.23
11	24-well DSW 24-well DSW 2L	2mL, 2.5mL, 3mL, 3.5mL 2mL, 2.5mL 3mL, 3.5mL 2L	1.5	14	64	1.5	1200rpm 500rpm 0.05
12	24-well DSW 24-well DSW 2L	2mL, 2.5mL, 3mL, 3.5mL 2mL, 2.5mL, 3mL, 3.5mL 2L	1.5	6	55	1.5	1200rpm 500rpm 0.05
13	24-well DSW 2L	2mL, 2.5mL, 3mL, 3.5mL 2L	1.5	10	60	1.5	500rpm 0.05
14	24-well DSW 24-well DSW 24-well DSW 2L	2mL, 2.5mL, 3mL, 3.5mL 2mL, 2.5mL, 3mL, 3.5mL 2mL, 2.5mL, 3mL, 3.5mL 2L	1.5	10	60	1.5	1200rpm 400rpm 350rpm 0.23

Table 6.1: Details of the heat extraction conditions for each experiment in Chapter 6. Heat up time (hr), hold time (hr), temperature (°C) and cool down time (hr) are the same for each scale within an experiment

A)

20L

2L

20mL

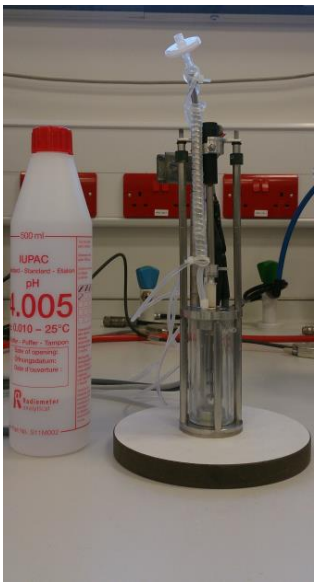

2 - 3.5mL

B)

Figure 6.1: Photographic images of **A)** the 20L, 2L, 20mL vessel and 24-well DSW plate and thermoshaker system and **B)** a sample acid precipitation experiment in the 24-well DSW plate after heat extraction, in a thermoshaker system

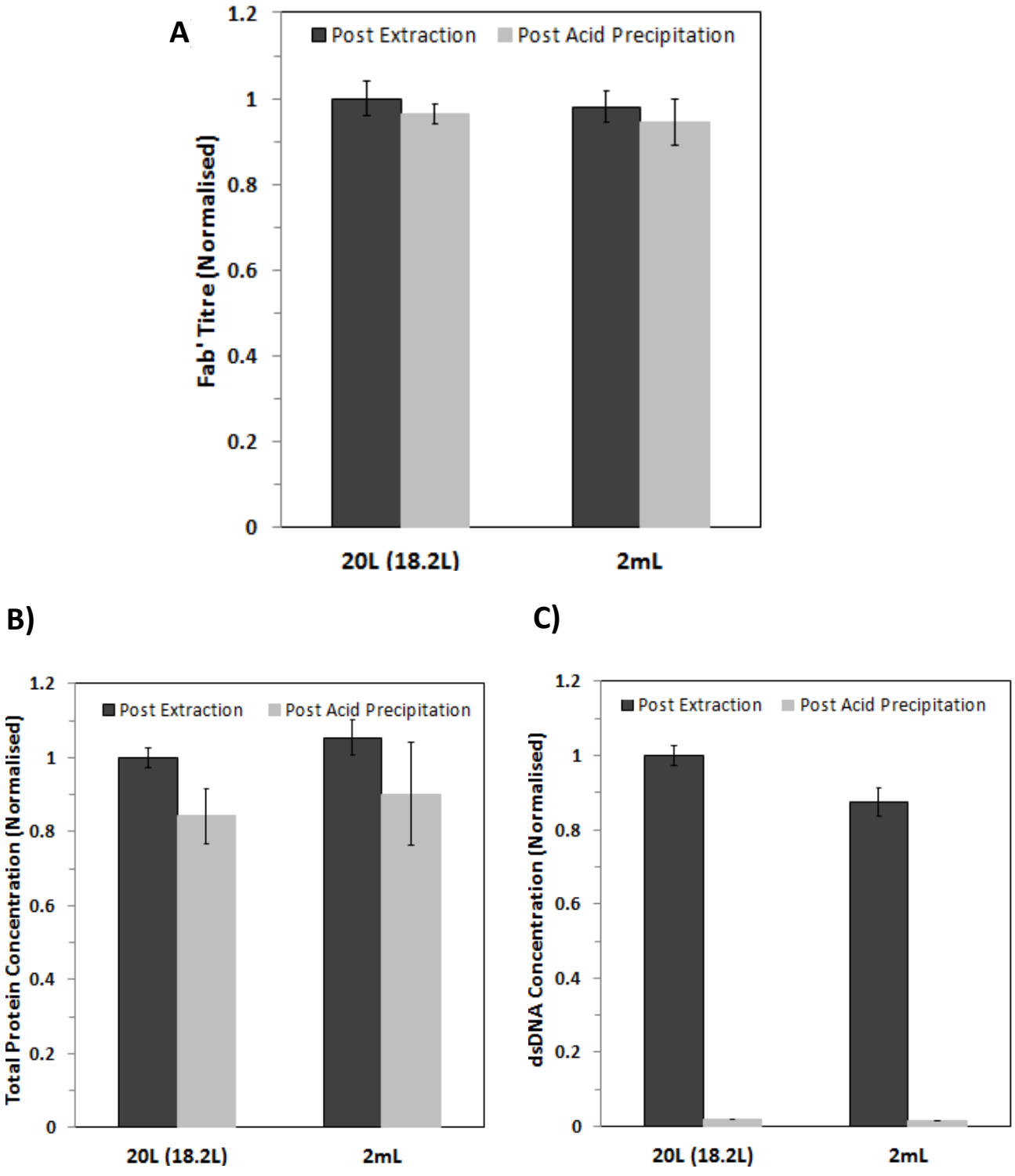

Figure 6.2: Comparison of the normalised **A)** Fab' titre; **B)** total protein concentration; and **C)** dsDNA concentration after heat extraction and acid precipitation in the 20L and 24-well DSW plate from Exp #9. Error bars represent ± 1 standard deviation from replicate samples (n=4 for 20L, n=8 for 2mL)

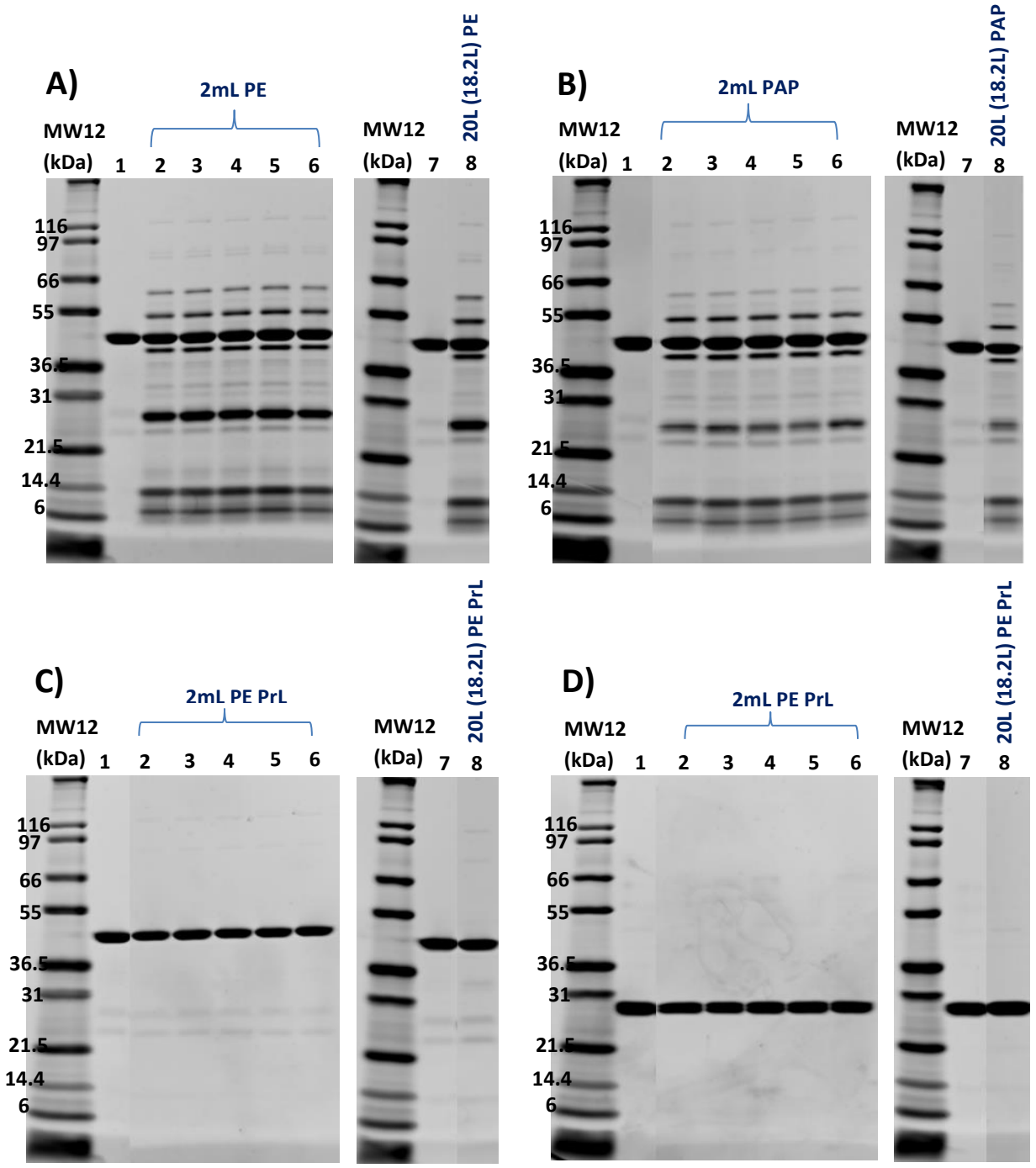

Figure 6.3: SDS-PAGE gels showing HCP and purified Fab' profiles at the 20L (18.2L) and 24-well DSW plate (2mL) scale for Exp #9. The non-reduced gel **A)** shows post extraction (PE) samples; Lane 1- Fab' standard; Lanes 2-6 DSW (2mL) from wells A1, D1, B3, C4 and A6 respectively; Lane 7- Fab' standard; Lane 8- 20L (18.2L). The non-reduced gel **B)** shows post acid precipitation (PAP) samples; Lane 1- Fab' standard; Lanes 2-6 DSW (2mL) from wells A2, D2, C3, B4, and D5 respectively; Lane 7- Fab' standard; Lane 8- 20L (18.2L). Post extraction (PE) protein L (PrL) purified samples were run on non-reduced gel **C)** and reduced gel **D)** for samples; Lane 1- Fab' standard; Lanes 2-6 DSW (2mL) from wells A1, D1, B3, C4, and A6 respectively; Lane 7- Fab' standard; Lane 8- 20L (18.2L)

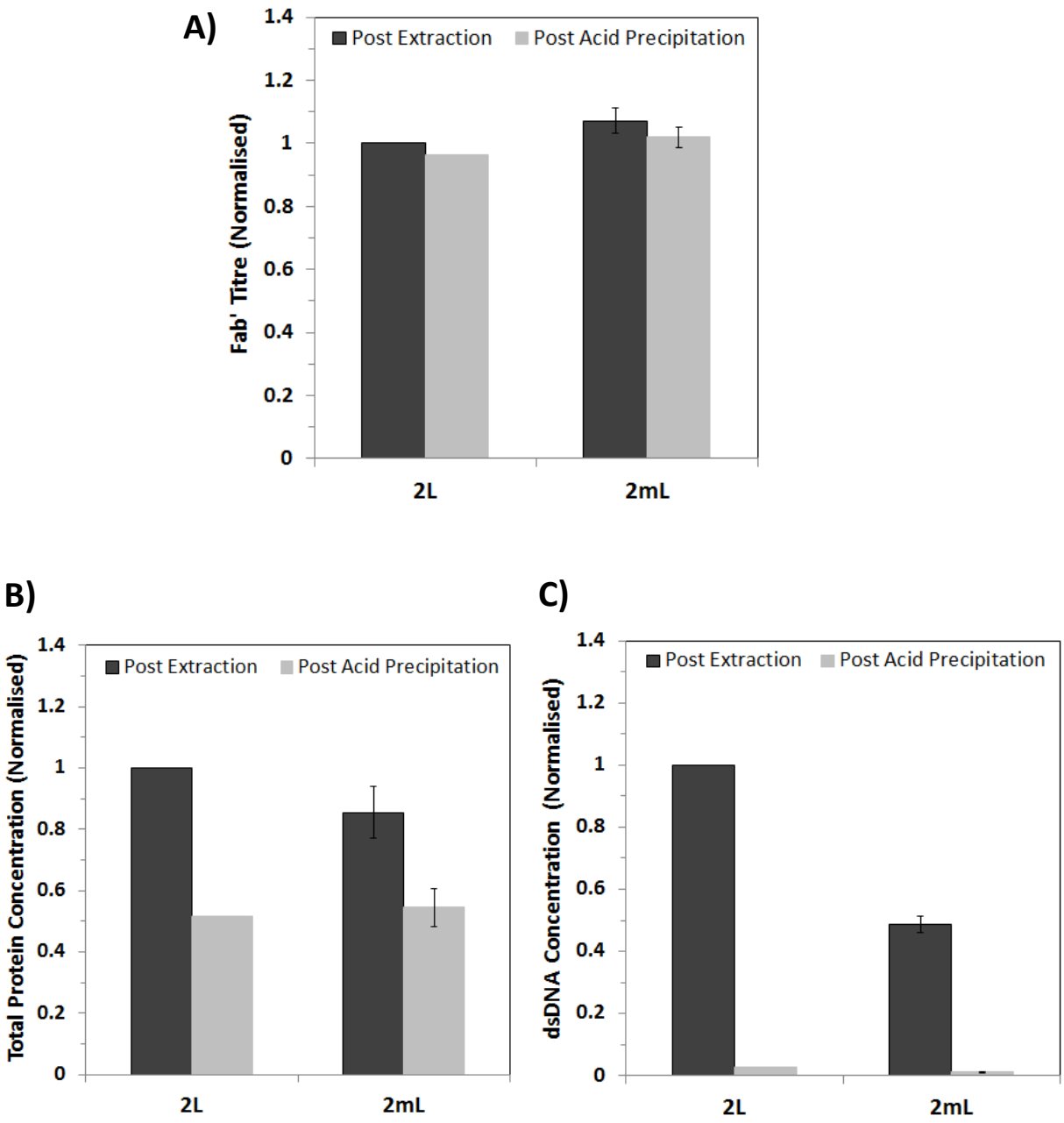

Figure 6.4: Comparison of the normalised **A)** Fab' titre; **B)** total protein concentration; and **C)** dsDNA concentration after heat extraction and acid precipitation in the 2L and 24-well DSW plate from Exp #10. Error bars represent ± 1 standard deviation from replicate samples (n=12 for 2mL)

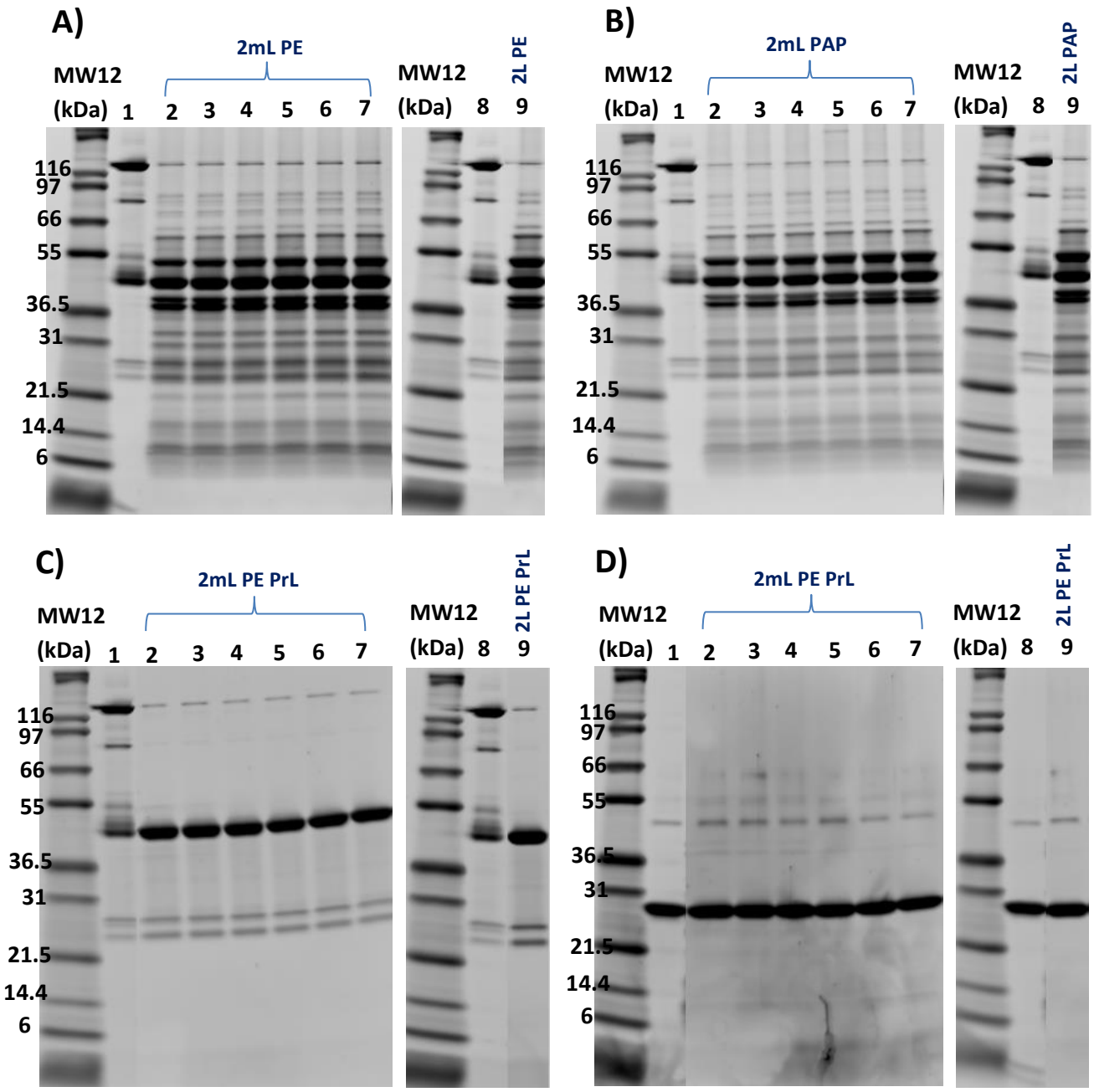

Figure 6.5: SDS-PAGE gels showing HCP and purified Fab' profiles at the 2L and 24-well DSW plate (2mL) scale for Exp #10. The non-reduced gel **A)** shows post extraction (PE) samples; Lane 1- Fab' standard; Lanes 2-7 DSW (2mL) from wells A1, D1, B3, C4, A6 and D6 respectively; Lane 8- Fab' standard; Lane 9- 2L. The non-reduced gel **B)** shows post acid precipitation (PAP) samples; Lane 1- Fab' standard; Lanes 2-7 DSW (2mL) from wells A2, D2, C3, B4, A5 and D5 respectively; Lane 8- Fab' standard; Lane 9- 2L. Post extraction (PE) protein L (PrL) purified samples were run on non-reduced gel **C)** and reduced gel **D)** for samples; Lane 1- Fab' standard; Lanes 2-7 DSW (2mL) from wells A1, D1, B3, C4, A6 and D6 respectively; Lane 8- Fab' standard; Lane 9- 2L

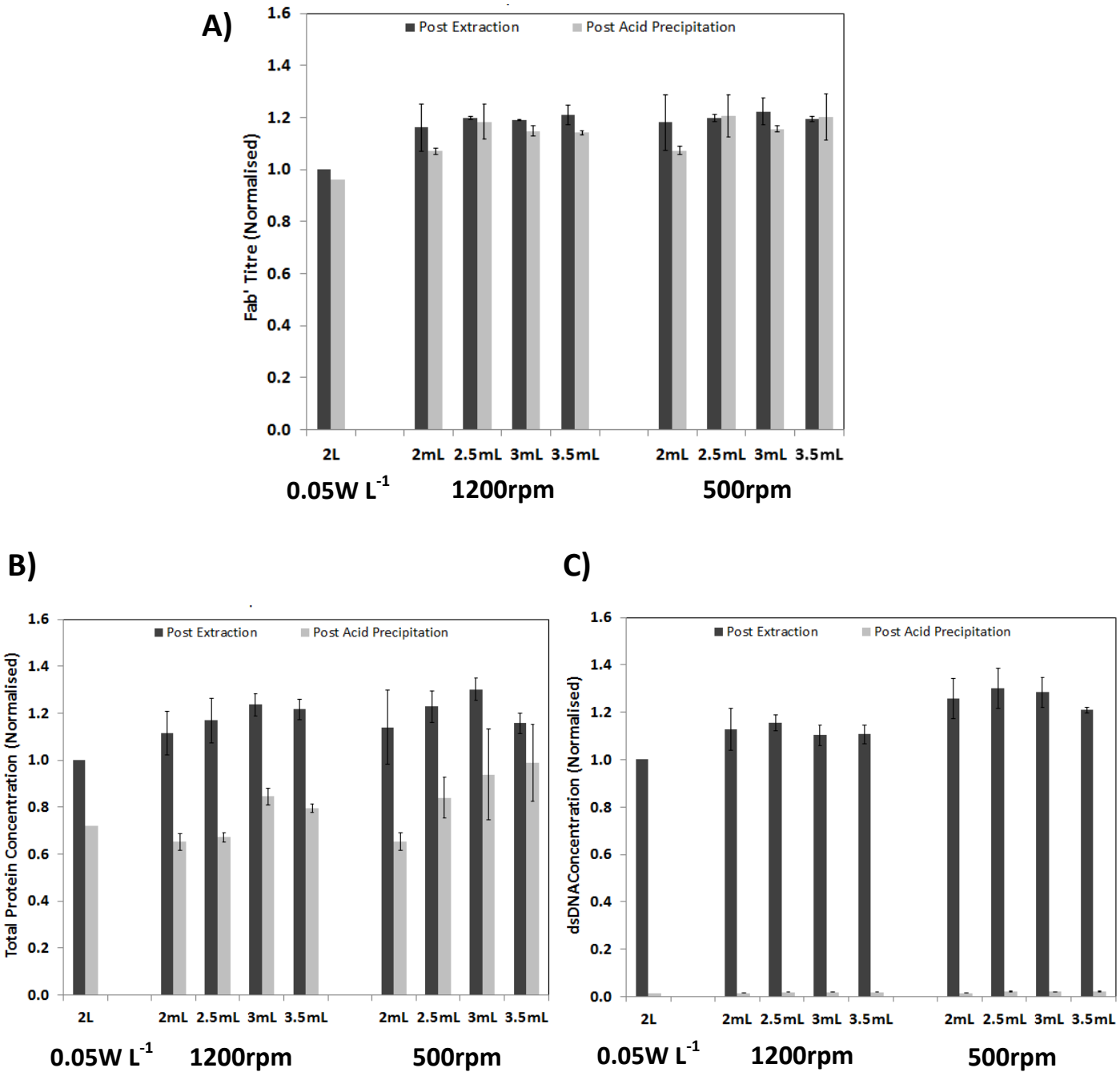

Figure 6.6: Comparison of the **A)** Fab' titre; **B)** total protein concentration; and **C)** dsDNA concentration after heat extraction and acid precipitation in the 2L and 24-well DSW plate from Exp #11. Error bars represent ± 1 standard deviation from replicate samples (n=3 for 2mL)

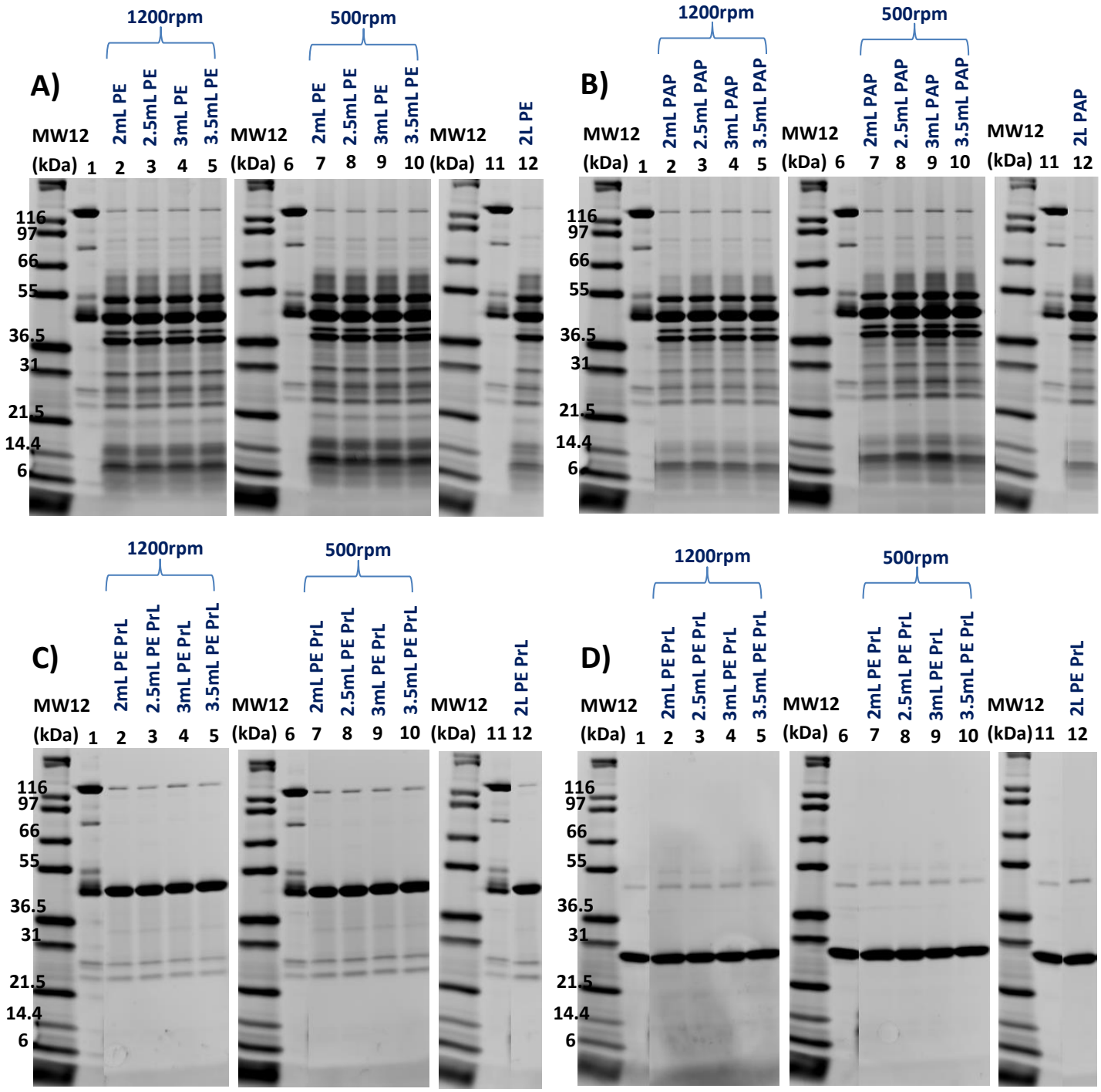

Figure 6.7: SDS-PAGE gels showing HCP and purified Fab' profiles at the 2L and 24-well DSW plate scale for Exp #11. The **A)** non-reduced gel with post extraction (PE) samples; **B)** non-reduced gel with post acid precipitation (PAP) samples; **C)** non-reduced gel with post extraction (PE) protein L (PrL) purified samples and **D)** reduced gel with post extraction (PE) protein L (PrL) purified samples. Lane 1- Fab' standard; Lane 2- 2mL, 1200rpm; Lane 3- 2.5mL, 1200rpm; Lane 4- 3mL, 1200rpm; Lane 5- 3.5mL, 1200rpm; Lane 6- Fab' standard; Lane 7- 2mL, 500rpm; Lane 8- 2.5mL, 500rpm; Lane 9- 3mL , 500rpm; Lane 10- 3.5mL, 500rpm; Lane 11- Fab' standard; Lane 12- 2L

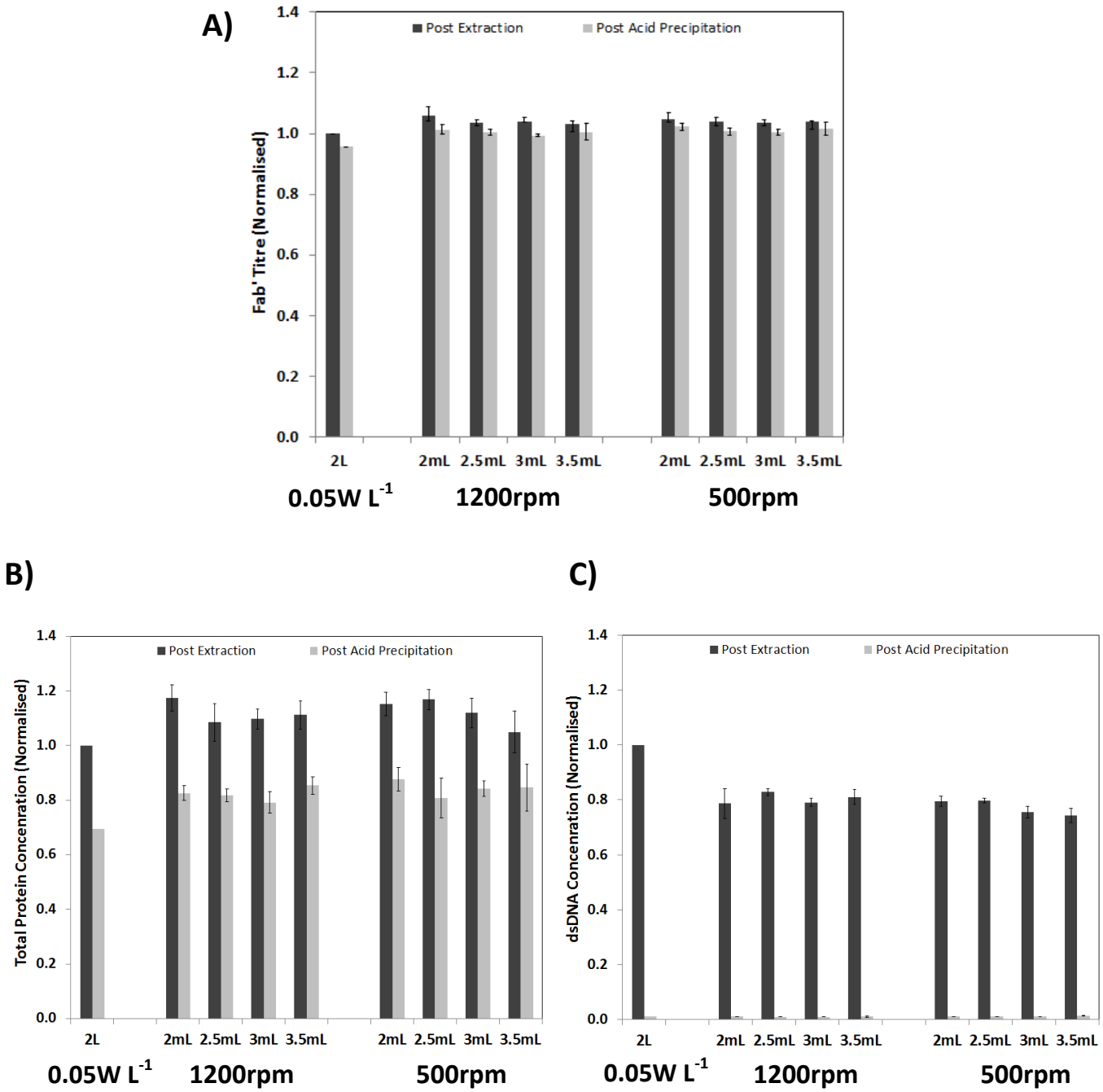

Figure 6.8: Comparison of the **A)** Fab' titre; **B)** total protein concentration; and **C)** dsDNA concentration after heat extraction and acid precipitation in the 2L and 24-well DSW plate from Exp #12. Error bars represent ± 1 standard deviation from replicate samples (n=3 for 2mL)

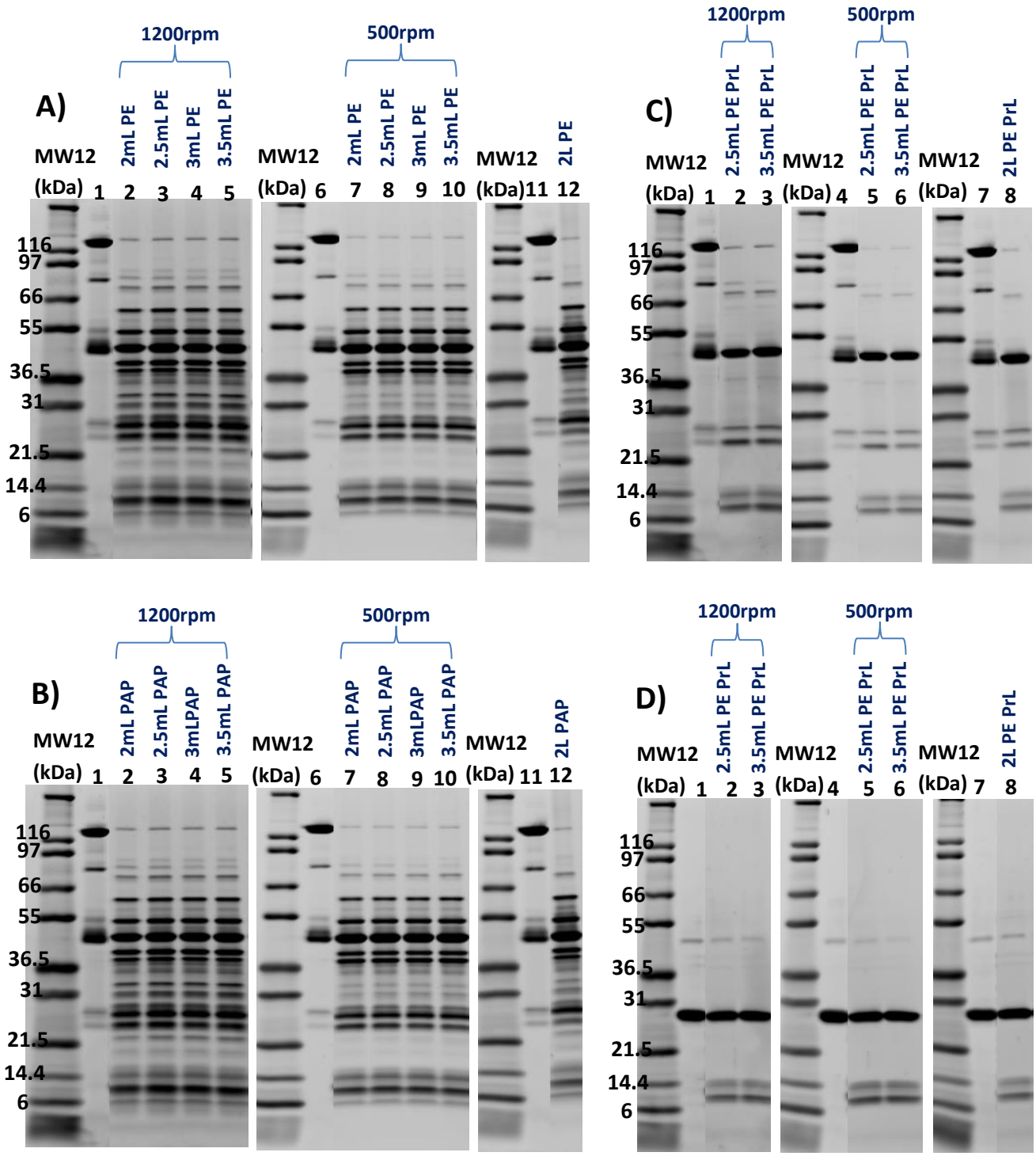

Figure 6.9: SDS-PAGE gels showing HCP and purified Fab' profiles at the 2L and 24-well DSW plate scale for Exp #12. The **A)** non-reduced gel with post extraction (PE) samples; **B)** non-reduced gel with post acid precipitation (PAP) samples: Lane 1- Fab' standard; Lane 2- 2mL, 1200rpm; Lane 3- 2.5mL, 1200rpm; Lane 4- 3mL, 1200rpm; Lane 5- 3.5mL, 1200rpm; Lane 6- Fab' standard; Lane 7- 2mL, 500rpm; Lane 8- 2.5mL, 500rpm; Lane 9- 3mL, 500rpm; Lane 10- 3.5mL, 500rpm; Lane 11- Fab' standard; Lane 12- 2L. The post extraction (PE) protein L (PrL) purified samples on a **C)** non-reduced gel and **D)** reduced gel: Lane 1- Fab' standard; Lane 2- 2.5mL, 1200rpm; Lane 3- 3.5mL, 1200rpm; Lane 4- Fab' standard; Lane 5- 2.5mL, 500rpm; Lane 6- 3.5mL, 500rpm; Lane 7- Fab' standard ; Lane 8- 2L

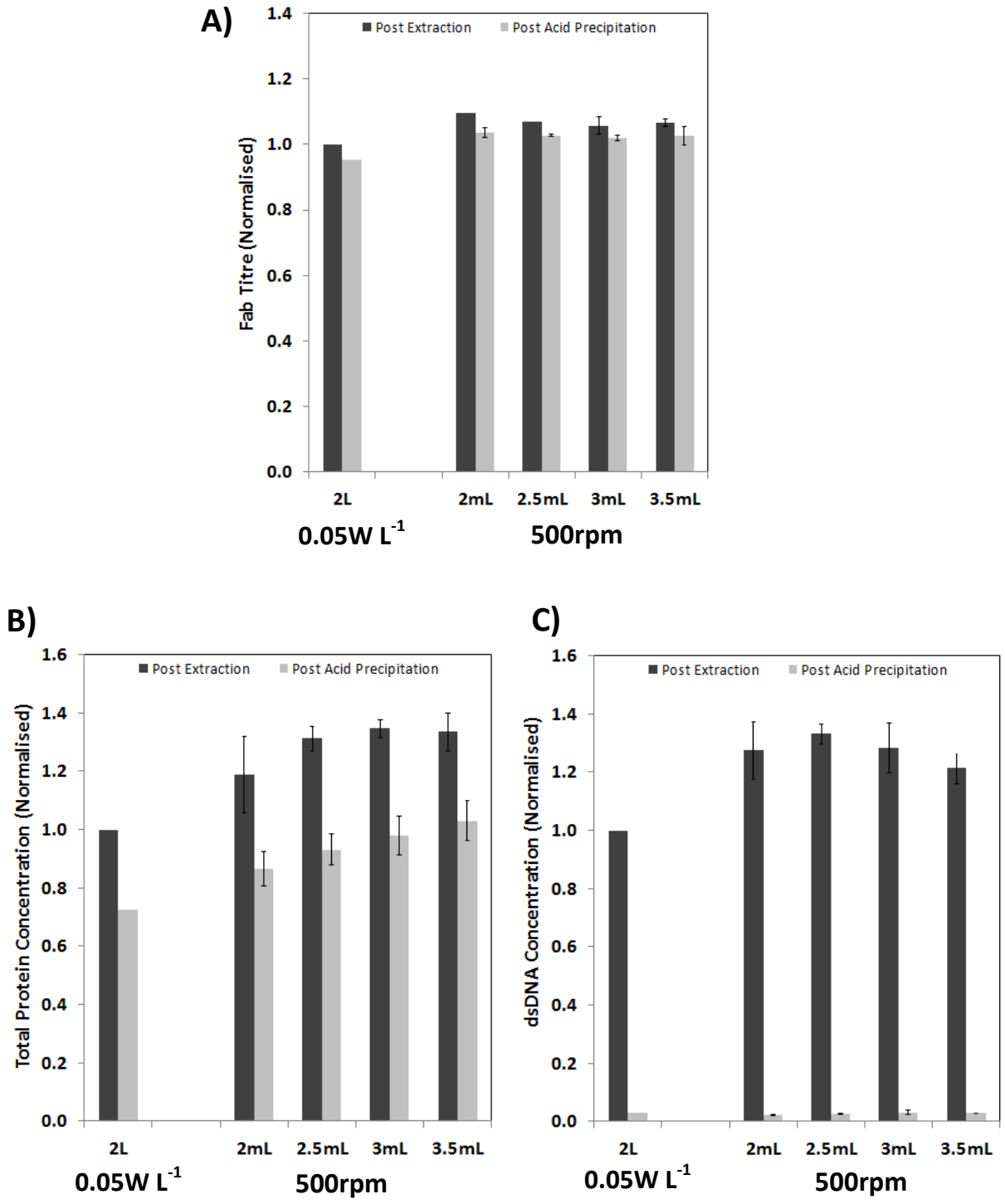

Figure 6.10: Comparison of the **A)** Fab' titre; **B)** total protein concentration; and **C)** dsDNA concentration after heat extraction and acid precipitation in the 2L and 24-well DSW plate from Exp #13. Error bars represent ± 1 standard deviation from replicate samples (n=3 for 2mL)

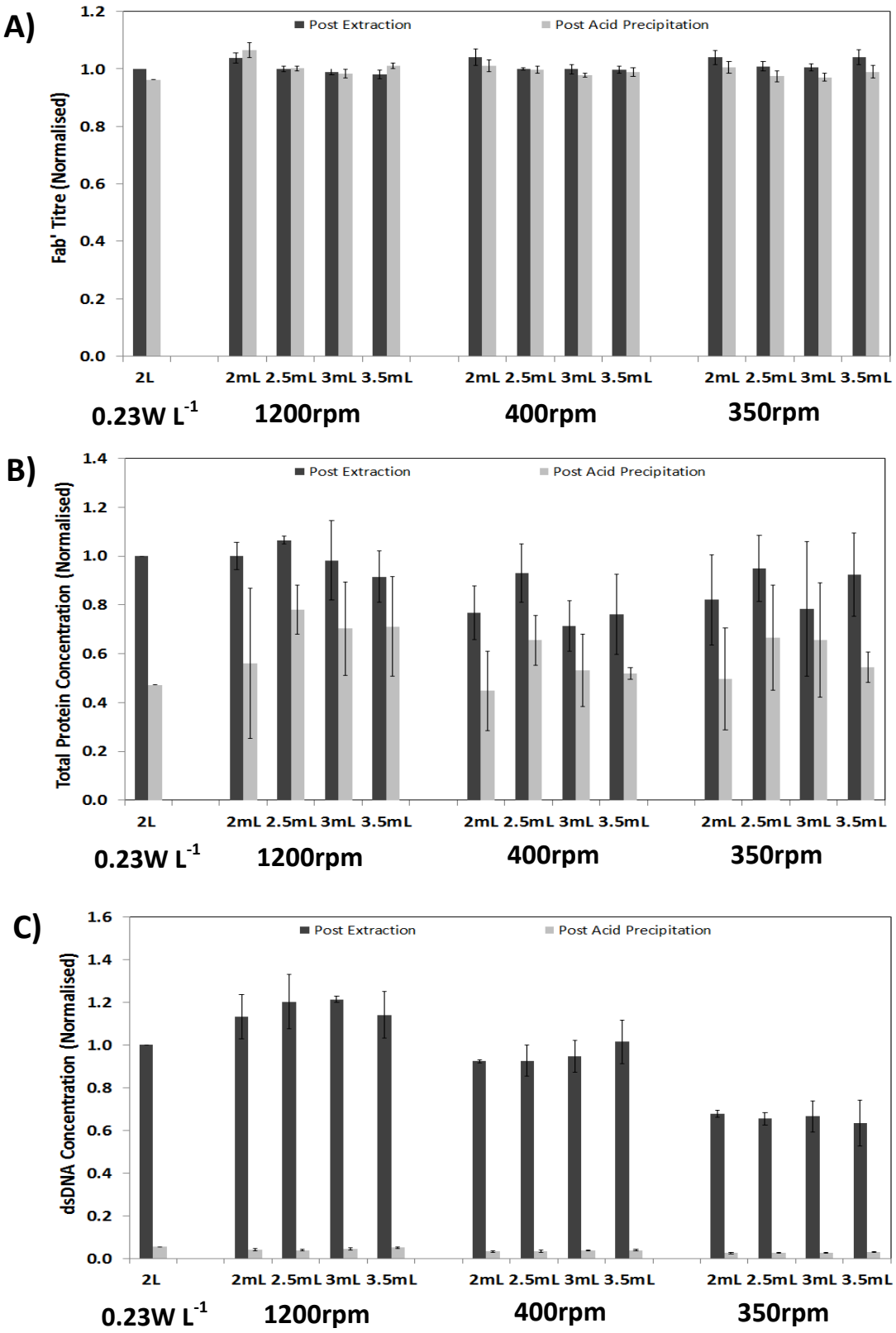

Figure 6.11: Comparison of the **A)** Fab' titre; **B)** total protein concentration; and **C)** dsDNA concentration after heat extraction and acid precipitation in the 2L and 24-well DSW plate from Exp #14. Error bars represent ± 1 standard deviation from replicate samples (n=3 for 2mL)

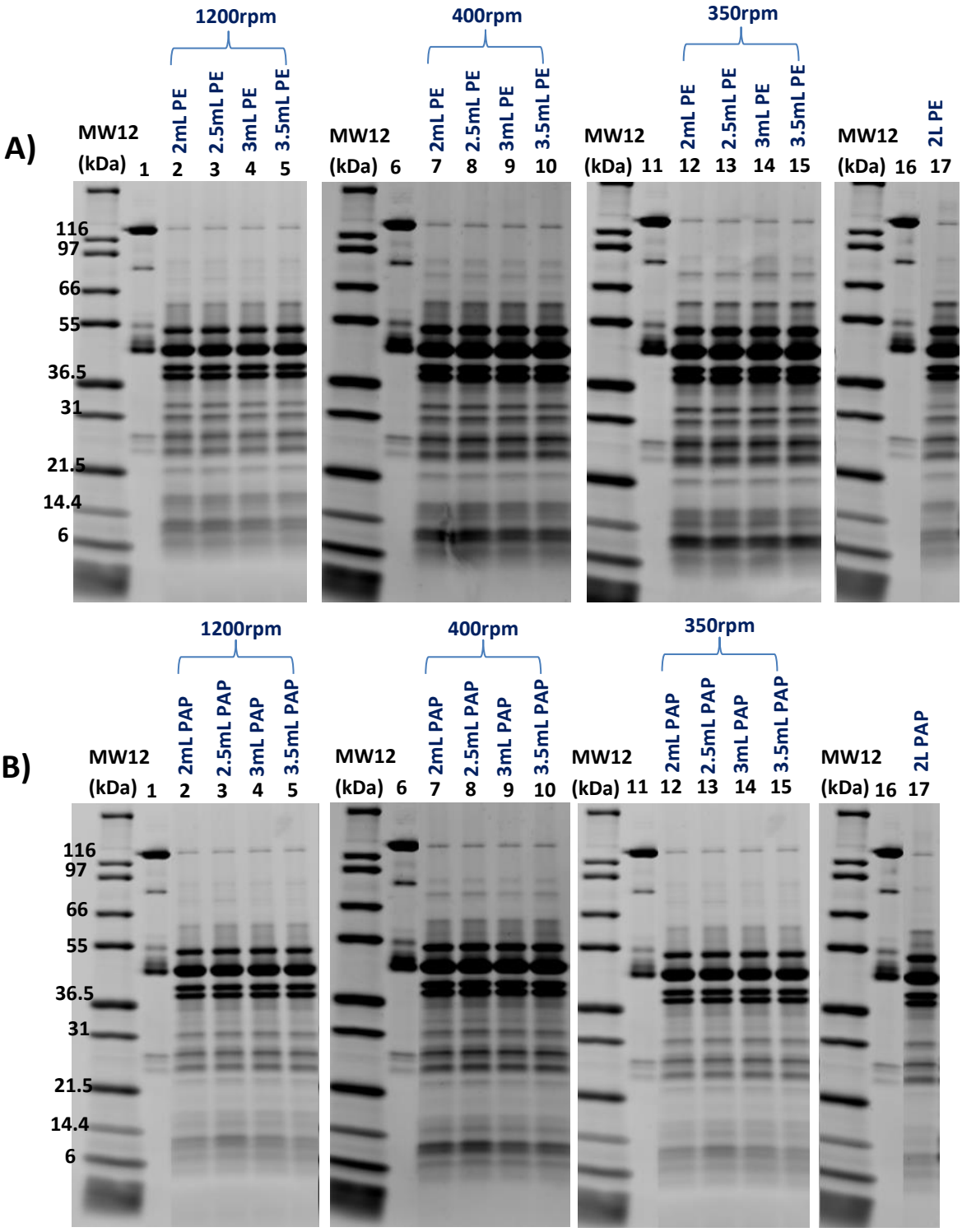

Figure 6.12: SDS-PAGE gels showing HCP profiles at the 2L and 24-well DSW plate scale for Exp #14. The **A)** non-reduced gel with post extraction (PE) samples; **B)** non-reduced gel with post acid precipitation (PAP) samples: Lane 1- Fab' standard; Lane 2- 2mL, 1200rpm; Lane 3- 2.5mL, 1200rpm; Lane 4- 3mL, 1200rpm; Lane 5- 3.5mL, 1200rpm; Lane 6- Fab' standard; Lane 7- 2mL, 400rpm; Lane 8- 2.5mL, 400rpm; Lane 9- 3mL, 400rpm; Lane 10- 3.5mL, 400rpm; Lane 11- Fab' standard; Lane 12- 2mL, 350rpm; Lane 13- 2.5mL, 350rpm; Lane 14- 3mL, 350rpm; Lane 15- 3.5mL, 350rpm; Lane 16- Fab' standard; Lane 17- 2L

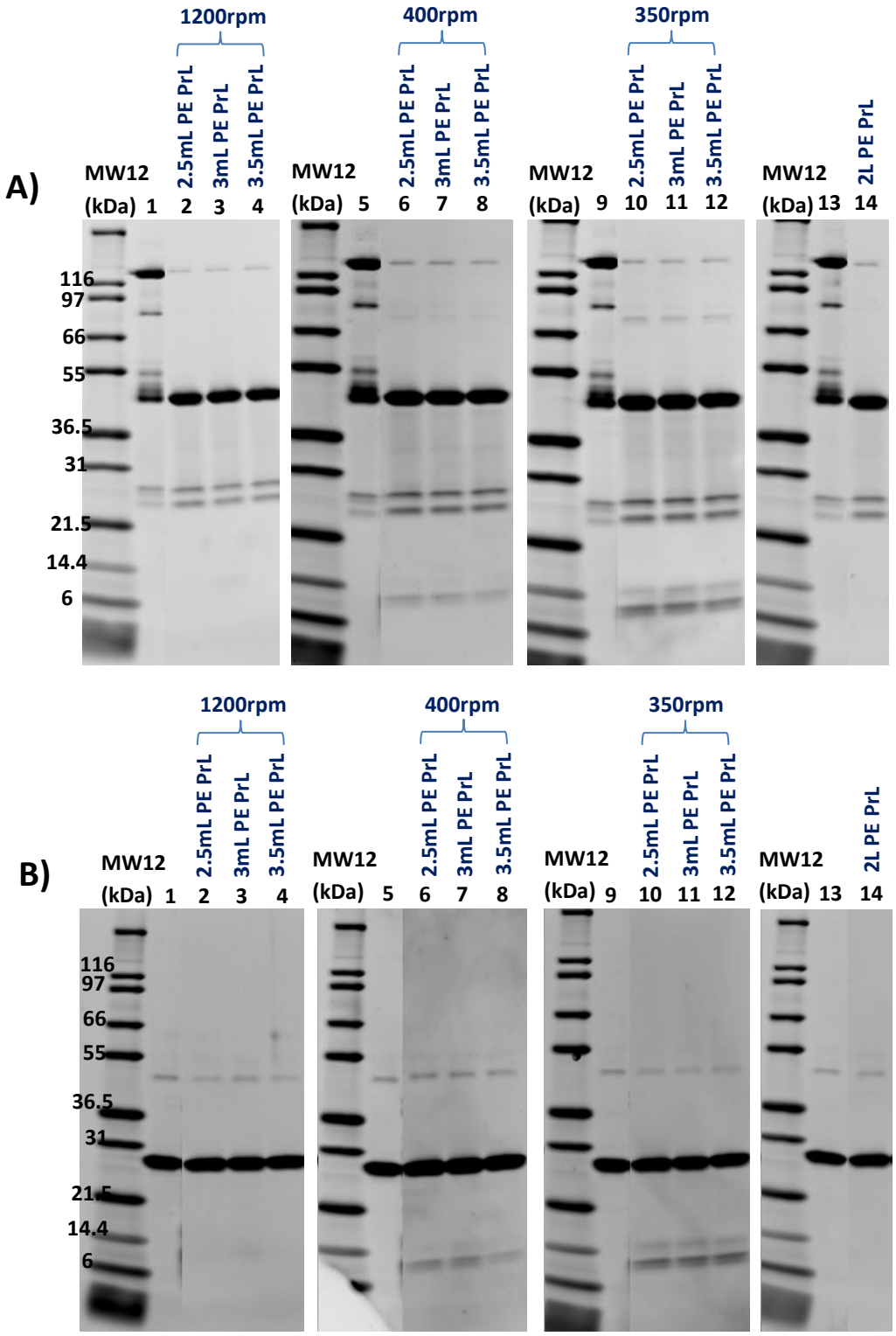

Figure 6.13: SDS-PAGE gels showing purified Fab' profiles at the 2L and 24-well DSW plate scale for Exp #14. The **A)** non-reduced gel with post extraction (PE) protein L (PrL) purified samples; **B)** reduced gel with post extraction (PE) protein L (PrL) purified samples: Lane 1- Fab' standard; Lane 2- 2.5mL, 1200rpm; Lane 3- 3mL, 1200rpm; Lane 4- 3.5mL, 1200rpm; Lane 5- Fab' standard; Lane 6- 2.5mL, 400rpm; Lane 7- 3mL, 400rpm; Lane 8- 3.5mL, 400rpm; Lane 9- Fab' standard; Lane 10- 2.5mL, 350rpm; Lane 11- 3mL, 350rpm; Lane 12- 3.5mL, 350rpm; Lane 13- Fab' standard; Lane 14- 2L

Chapter 7

Conclusion and General Discussion

7.1 Key Findings from Present Work

The main objective of this work was to create a scale-down model capable of mimicking the large scale heat extraction process, at UCB, for the recovery of periplasmic Fab' from *E.coli* cells. A miniature 20mL vessel and a 24-well deep square-well plate were analysed for their suitability and geometric similarities to the large scale vessel, after which they were characterised and used to scale-down the extraction process from 2L, 20L and 200L scale for a variety of different conditions. An initial DoE study was conducted in the 2L scale vessel to understand the impact of extraction duration, extraction temperature and specific power input (P/V). The DoE experiment showed that extraction temperature and duration had the biggest impact on the process, where increasing the temperature and extraction duration caused the Fab' titre and total protein concentration to slowly decrease. There was no significant difference in extraction performance at the different specific power input values, which were tested in the range of 0.05W L^{-1} and 0.41W L^{-1}. This indicated that specific power input may not be sufficient to scale this process alone and that further information was needed on the hydrodynamics in the 2L vessel.

Fluid dynamic studies were therefore conducted on the 2L lab scale vessel, and the 20mL vessel and 24-well DSW plate scale-down models. Mixing time studies, conducted using the global DISMT colorimetric technique showed that mixing times between the 2L and 20mL vessels were comparable over the same range of P/V values. The mixing time curves for both scales showed that mixing time was relatively constant, at 9 seconds, above specific power input of 0.05W L^{-1}. The results from the 2L mixing time curves were in agreement with the data obtained from the DoE study. They suggest that for scaling purposes, the extraction process may require sufficient mixing only, with enough power to keep the cell suspension homogenous and to evenly distribute heat throughout the vessel. This threshold for the required level of mixing may be determined for different scales by carrying out

mixing time studies and then scaling the extraction process based on the corresponding minimum specific power input value where mixing time no longer changes. Increasing the power above this value does not appear to enhance or impair the process performance and therefore if the current process is operating at values above the required amount, it may not be economically desirable.

The initial data from the 20mL mixing time studies showed that the vessel may be suitable for use as a scale-down model of the 2L vessel. As part of vessel characterisation, additional mixing time studies were conducted to see if changing the fill volume and impeller positioning impacted the mixing performance. The results showed that mixing time was faster when the fill volume was decreased and impeller submergence was less than 1 impeller diameter. The mixing time curve for the 2L vessel matched most closely to the 20mL vessel when impeller spacing was kept at 0.95 impeller diameter for both vessels. In order to verify that there were no dead zones in the 20mL vessel when using a fill volume of 20mL and an impeller spacing of 0.95 impeller diameter, PIV studies were conducted at varying speeds. The results showed that stable flow patterns, which extended to all of the liquid in the vessel, were formed around 300rpm (9×10^{-4}W L^{-1}) after which the levels of vorticity decreased. Analysis of the maximum velocity values, seen close to the impeller region, showed that the velocity plateaus around 1100rpm (0.05W L^{-1}) which corresponds to the value obtained in the mixing time curve where mixing was no longer affected by specific power input. The characterisation data therefore shows that sufficient mixing in the 20mL vessel can be achieved at this impeller spacing and fill volume above 0.05W L^{-1} and therefore the vessel may be used for conducting extraction experiments.

The 20mL vessel was used to run a series of extraction experiments and compared to the performance of the 2L, 20L and 200L extractions. Samples were taken after heat extraction and after acid precipitation and measured for Fab' titre, total protein concentration, dsDNA concentration, HCP profiles and Fab' profiles in order to show comparability between different scales. Samples taken post harvest, post extraction and post acid precipitation were observed under the microscope, using SEM. The images showed that the extraction process caused a significant amount of damage to the outer cell membrane but the cell

structure was still kept relatively intact. Post acid precipitation, the cells had lost more of their structural integrity and there was significant aggregation of dsDNA and other intracellular impurities. These results are in agreement with current understanding of how the heat extraction step permeabilises the outer cell membrane during heat extraction, and how the acid precipitation step aggregates cells and nucleic acids in order to make subsequent DSP operations easier. The 2L and 20mL vessels were used to conduct heat extraction experiments under the same operating conditions and under different operating conditions, where the heating profiles and specific power input values were varied. The data was able to verify that the 20mL vessel could detect trends in the 2L vessel for a variety of different conditions and therefore was a viable scale-down model for the 2L extraction process.

There were some differences in the quality of the feed material, which are likely to be caused by the scale at which fermentations were operated in, that affected the extraction performance, however, the small scale vessel was able to detect the trends seen in the 2L vessel. The 20mL vessel was also able to differentiate between different strains expressing different types of Fab' in the experiments. The results showed that Fab' titres were typically greater in the 2L and 20mL vessel when the material came from 20L fermentations instead of 200L fermentations. A comparison of the 20L and the 20mL extractions showed that Fab' titres were typically 15% higher in the 20L vessels when the fill volume was sufficient enough for the top impeller to be well submerged. The impeller spacing in the 20L vessel was between 1.3 – 1.5 impeller diameter which may also have been responsible for better flow patterns in the vessel resulting in the slightly higher titres. When the fill volume was in line with the top impeller, the performance was decreased which may be due to poor circulation of the liquid, caused by entrainment and thrashing of the liquid near the top of the vessel which limit mixing and heat distribution. Without characterising mixing and flow patterns in the 20L vessel, it is difficult to know for certain if this is the reason for the decreased performance. The 20mL vessel was also capable of scaling down 10,000 fold to mimic the performance of the 200L vessel. A brief analysis of the impeller spacing in the 200L vessel suggests that mixing and extraction performance could be improved at this scale if the spacing was reduced to 1 impeller diameter.

To further scale-down the extraction process from stirred tank vessels into shaken, single-use micro-well plates, the 24-well DSW plate was characterised for its mixing performance and used to verify its suitability as a scale-down model. Mixing time studies in the DSW plate, at different fill volumes and shaker speeds, showed that mixing time was relatively unchanged above 400rpm but that more turbulent mixing was achieved at 500rpm and then above 1000rpm. A series of heat extraction experiments were conducted in the DSW plate at different fill volumes, between 2mL – 3.5mL, and at different shaker speeds 350rpm, 400rpm, 500rpm and 1200rpm. The data was compared to the 2L and 20L extraction process, and showed that the DSW plate was capable of mimicking the extraction performance in both stirred tank vessels at 500rpm and 1200rpm and was also able to differentiate between different Fab' types used. These results were in agreement with the data observed in the mixing time studies. At 350rpm and 400rpm, Fab' titres were comparable to the 1200rpm results, however, analysis of the dsDNA concentration and Fab' profiles in the SDS-PAGE gels indicated that operating at these lower speeds may have allowed the cell suspension to stay homogenous but the low turbulence in the wells could have been responsible for limited damage to the inner cell membrane. The results from this research project have demonstrated that with the help of fluid dynamic techniques, the heat extraction process can be scaled down from a lab and pilot scale vessel into a miniature stirred tank vessel and a shaken 24-well DSW plate.

7.2 General Discussion and Future Work

The issue of scale-up and scale-down has always been a complicated one as it requires an understanding of the impact of a large number of parameters on a process performance. Processes such as heat extraction and acid precipitation are highly dependent on efficient mixing and therefore an appropriate mixing related scaling parameter must be chosen. Mixing time, dimensionless mixing time, heat transfer, mass transfer, turbulence, shear, velocity and flow patterns are all characteristics that can be assessed between scales to help determine how efficient the mixing is in a vessel. Evaluating each characteristic at each scale is not possible firstly due to time and cost restraints but also because the techniques used to measure them are not suitable for use with each scale or type of vessel. For example DISMT

and PIV are not compatible with stainless steel vessels, which are used at large scale. Therefore one way to characterise these parameters is to use fluid dynamic tools on a representative scale-down model from which valuable information can be obtained regarding mixing performance at different conditions and then the information may be used to optimise performance at the small scale and the large scale. Computational fluid dynamics (CFD) is a powerful tool that can be used to obtain qualitative and quantitative information on fluid flow in a system and therefore may be considered for use in the future to provide insight on mixing performance at different scales to better scale-up the heat extraction process.

One aspect to consider for scaling of any mixing related process, when working with biological material, is the issue of shear. A number of studies have demonstrated that viable *E.coli* cells are robust and therefore not sensitive to shear. Often studies use the term shear to explain poor process performance during scale-up, for example when running fermentations, however, if studies at the small scale demonstrate that at relatively high power inputs, the cells are not damaged and performance is not affected, then at large scale, shear should also not be an issue. The differences in performance are thus likely to be due to spatial and temporal heterogeneities which impact cell damage or cell lysis (Hewitt and Nienow 2007). Once *E.coli* cells are subjected to high temperatures in tris/EDTA, it is possible however that shear does impact on the cells, because the outer cell membrane is weakened. The level of shear susceptibility may also vary depending on the particular cell lines being used; however this is still an area that is not fully understood. The DoE study showed that between 0.05W L^{-1} and 0.41W L^{-1}, the heat extraction performance was not affected. The levels of shear exerted on the cells are likely to differ significantly between this range studied however as the performance was not affected, it indicates that shear was not impacting the process. Considering that the extraction process was not conducted in any scale below 0.05W L^{-1} or above 0.41W L^{-1}, it is not known how performance would be affected, however mixing time and PIV data suggests that mixing performance would decrease and therefore extraction performance is likely to be compromised. The experiments conducted in the pilot scale vessels in this work, where heterogeneities may be expected to occur, did not go above 0.23W L^{-1}, therefore again, the differences in

performance between experiments are unlikely to be related to shear and most likely due to the impeller spacing and the positon of the impellers, in relation to the fill volume, which results in differences in mixing. Other parameters that may provide additional useful information about the quality of the cells post fermentation, post centrifugation, post extraction and post acid precipitation, and which may explain impact of shear on extraction performance, are PSD and viscosity.

The nature of cell damage and the amount of release of intracellular components such as Fab', total protein and dsDNA therefore requires further understanding. As the data from multiple experiments indicated, the Fab' titre, total protein concentration and dsDNA concentration do not always correlate with each other, therefore understanding how much cell damage has occurred, is not always straightforward. Additionally, it is important to note that the quantity of Fab', total protein and dsDNA measured in the cell suspension after completion of the extraction process may not necessarily be an indicator of cell damage, and hence of the extraction performance, alone. The data from Chapter 5 showed that the feed material had a significant impact on these measured values and therefore obtaining higher Fab' titres after extraction, for example, may also be due to higher productivity or higher viability during the fermentation process, and not just because the extraction conditions were better. With the current large scale extraction process, the ratio of buffer and heavy phase is adjusted between experiments to account for differences in cell concentration after centrifugation. These adjustments are based on the dewatering level achieved in the disc stack centrifugation process. For example, at a higher dewatering percentage, the cell concentration is greater, and therefore the ratio of buffer to heavy phase is increased in order to achieve a final cell concentration of the harvested material after fermentation. An alternative technique that may be used to account for this feed material variability is to adjust the ratio of heavy phase to buffer based on periplasmic Fab' titre instead of cell concentration. This method would take into account the total amount of Fab' that is available in the cells for extraction, after the centrifugation stage. This is particularly useful when using different types of centrifuges to harvest the material because the disc stack centrifuge exerts more shear on cells than the dead-end centrifuge and therefore causes more cell damage, which means a greater percentage of Fab' may be lost in the light phase. The method used to measure Fab' productivity, however, must be

accurate, and the measurement must be obtained quickly, so that a decision can be made on what the ratio of buffer and heavy should be. This can be quite challenging due to the time taken to experimentally obtain this value which is why batch to batch variability is currently accounted for by making adjustments to cell concentration values that are easier and faster to obtain.

Therefore to study the impact of shear, mixing and feed material on cell damage, and hence extraction performance, further experiments can be conducted in the future. This may be achieved by running the extraction process in multiple small scale vessels of the same size, using material from the same feed material, under the same heating conditions, and then varying conditions which can impact mixing and shear such as specific power input, impeller spacing, impeller geometry, number of impellers and fill volume. A wider range of specific power input values can also be tested this time. A DoE approach can be used to run a study of this size and depth to test for optimum conditions and these experiments may be repeated using material from different fermentation batches or using different Fab' types. A study of this size is likely to generate a significant amount of data and therefore advanced statistical tools, such as MVA, would be useful in helping to process the information in a meaningful way. The results from such a study may help to better attribute the impact of the feed material, scale and mixing, on the extraction process.

The data from the 20mL vessel characterisation studies and the extraction verification studies have already demonstrated that impeller positioning and impeller submergence has a significant impact on the mixing efficiency and extraction process. In the 20mL vessel, the relatively high impeller thickness and impeller submergence may have limited mixing efficiency, and in the 200L vessel, it is possible that the relatively high impeller spacing did so as well. The extraction data from the 20mL vessel and 200L vessel however showed excellent comparability thus indicating that the mixing performance is similar, despite differences in the impeller positioning and fill volume ratios between the two scales. Therefore if the impeller thickness was reduced and the fill volume was reduced, so that impeller submergence was close to 1 impeller diameter in the 20mL vessel, the mixing efficiency may improve. Similarly if the impeller spacing in the 200L vessel was reduced to

more closely mimic the 20L vessel, and another impeller was added to accommodate for large fill volumes, the mixing efficiency and extraction performance may also improve. Due to the challenge associated with manually changing the positions of the impellers in large scale vessels, only the fill volume and specific power input values are typically changed during current experiments. However if optimisation of a large scale process is required, this is an aspect which should definitely be taken into consideration. Having information on the hydrodynamics in the pilot scale vessels, such as mixing time, would be helpful to verify some of these changes too and to see if the minimum specific power input, where mixing time is no longer affected by an increase in speed, is also 0.05W L^{-1} as was determined for the 2L and 20mL vessel. Transducer techniques, using conductivity or pH probes, may be used to measure variation in these respective properties. Although this method does not have the advantages of the global DISMT technique, it will still provide valuable information which can be used for better scaling.

The results from the 24-well DSW plate system also show a lot of promise for as a scale-down model, however there is room to improve the accuracy of the current method by using an automated robotic system to conduct the liquid handling steps such as the addition of the heavy phase, the extraction buffer and acetic acid. Automating this process is likely to reduce the error between the wells significantly. Furthermore, to establish the thermoshaker for scaling the extraction process into the DSW plate, it is important that other heating profiles with alternative heat up and cool down rates are also mimicked accurately. This is likely to be quite challenging and may require the setup of several programmes, which must be changed manually, however this is certainly possible to achieve and if established will allow extractions to be run for a range of different conditions.

Other suggestions for future work include taking additional samples for SEM imaging which will help build a better picture of how each stage of the upstream and primary recovery process impacts cell damage. For example, samples can be taken after centrifugation; both disc stack centrifugation and dead-end centrifugation, to study the extent of cell damage just before the extraction process. Also, samples may be taken at different parts of the extraction process to see when most of the damage occurs. Observing a sample taken

shortly after the heavy phase and buffer is initially mixed, and then comparing it to the sample once its reached maximum temperature, may indicate whether tris/EDTA and heat both affect cell membrane removal. Additionally, quantifying the band intensity of the original SDS-PAGE gels using densitometry will to better compare the HCP and Fab' profiles between different scales.

7.3 Validation Considerations

UCB have licensed their Fab' product, called certolizumab pegol (Cimzia), and it is currently being used to treat patients suffering from rheumatoid arthritis. As part of process development work, efforts are continuously being made to improve the performance of the manufacturing process which includes increasing productivity and reducing impurities, in order to improve DSP steps, whilst keeping costs low. Any changes made to the manufacturing process must be validated to ensure that the quality of the product is not disadvantaged and that it still meets current good manufacturing practice (cGMP) regulations and standards. The validation issues discussed here will focus on fermentation, centrifugation and heat extraction (primary recovery).

As discussed in this work, one of the factors that the performance of the heat extraction process is dependent on is the quality of the feed material. In order to study the impact of different parameters during the heat extraction process, and confidently attribute the performance to the extraction step in the scale-down model, rather than due to feed material variation, it is important to understand first how the fermentation and centrifugation steps impact on the quality of the feed material. Culturing cells in bioreactors, in general, is a lengthy and complex process, and one which is prone to some degree of variation due to the nature of working with biological material. Although the *E.coli* fermentation process is a relatively robust process, the quality of the final harvested material can vary slightly, which can then impact the subsequent steps.

In order to further improve the quality of the process and product, and increase process control during the upstream process, a QbD approach must be taken where the impact of

critical process parameters (CPP) on the critical quality attributes (CQA) can be assessed. For scaling purposes, it is important to consider not only process related parameters but also scale related parameters such as geometry of the equipment, positions of impellers, power input, shear and mixing. All of these different parameters ultimately affect the quality of the cells in the harvest material, which is then introduced to the centrifuge, and then finally into the heat extraction step. The % cell viability and Fab', total protein and dsDNA concentration in the supernatant are some factors assessed for the harvest material when running extraction experiments. Other factors which may be helpful in providing additional understanding of the quality of the feed material are PSD and viscosity. These parameters can potentially provide a further understanding of the nature of cell damage to the cells and how the cells behave upon exposure to environments with different levels of shear. The disc stack centrifugation step, for example, is known to exert a significant level of shear to the cells (Chan *et al*., 2006; Rayat *et al*., 2016). When working at industrial scale, in particular, it may also be useful to measure these parameters after the centrifugation step, any hold steps, or after the cell suspension passes through ancillary operations such as pumping and pipe flow. If the levels of shear are not monitored or controlled, some amount of cell lysis may occur which will increase the level of impurities in the broth and impact subsequent steps. Long holding times after the cells are transferred from the fermenter to the centrifuge or from centrifuge to the extraction vessel may also cause the cells to aggregate or lyse, or cause the Fab' product to fragment or form adducts, hence impacting the quantity and quality of the product. Essentially, measuring the quality of the feed material during these different steps, but most importantly just before it enters the heat extraction vessel, is important to do in order to increase understanding of the heat extraction process and to help to improve process design.

For the extractions in the scale-down models, used in this work, the fermentation process was conducted at the 5L, 20L or the 200L scale. The cells were then harvested using either the disc stack centrifuge or the dead-end centrifuge before running the extractions. As mentioned earlier the future work section, it is important that the fermentation and centrifugation process prior to the extraction step is operated in the same way so that the feed material going into the scale-down model is more consistent between experiments. If there are certain limitations during experimentation that prevent the ability to run

fermentation or centrifugation the same way each time, as was the case for this work, other techniques may be needed in order mimic the quality of the feed material between runs. For example, if it is not possible to run the disc stack centrifugation process to harvest the cells for each scale-down extraction process, and the dead-end centrifuge is the only option available, then the centrifuged material may be processed using a lab scale shear device to mimic the shear exerted during the disc stack centrifugation process (Chan 2006).

Once these key parameters in the upstream process have been eliminated, controlled or accounted for, the results from the heat extraction process can then be attributed to the extraction process itself and the equipment used for extraction can be validated. Running the same extraction conditions in multiple lab scale vessels (for example three 2L vessels) and multiple small scale vessels (for example three 24-well DSW plates), using the same feed material for all six extractions, means the effect of feed material can be eliminated and the true reproducibility of both the lab scale model and the scale-down model can be assessed. To validate the extraction process itself, conducted at any scale, the identified CPPs for the extraction process must be controlled. There are a number of parameters which have been mentioned throughout this work but the most important ones, that must be maintained, relate to heating and mixing conditions in the vessel. The temperature profile and impeller speed is routinely controlled in the lab scale and pilot scale extraction vessels using the Sartorius MFCS software. The temperature and pH probes have been chosen for their robustness and their ability to withstand the high temperatures needed for the extraction process. These probes are tested and calibrated for use before each experiment to ensure that all readings are accurate. It is crucial that there is confidence that the values obtained for pH and temperature are representative of the whole fill volume during the process. This is particularly important to test for the pilot scale or industrial scale process where it is possible that mixing is not sufficient and there may be temperature or chemical gradients present in the liquid during the process. In order to obtain accurate and reliable information about the state of extraction and acid precipitation process, samples are taken for analytics. It is therefore important that samples taken from within the vessel for analytics are also representative of the whole fill volume. This can be done by putting the pH and temperature probe, and sampling port, in different parts of the liquid including

in any areas where it is suspected that dead zones may exist and take measurements from there. Unless the fill volume can be visualised and studied for mixing using global mixing time techniques, this is remains a challenge for any industrial scale process.

Another factor that may be important to control is the hold time for the cell suspension before it is added to the extraction vessel. After the centrifugation process, the heavy phase is usually collected into a hold tank where it is first weighed before it is added to the extraction vessel. If the cells sit for a significant period of time before addition to the vessel, there may be some cell settling. Therefore if hold times are expected to be relatively long, and the cells are to be distributed into more than one vessel, it may be important that during the hold process, the cells are being continuously well mixed as to avoid density gradients. If mixing the cells during the hold stage is not feasible, then an accepted range for hold times must be determined where it is shown that cell settling is not significant. The rate at which additions are made to the vessel may also need to be controlled. This includes addition of the heavy phase and buffers for the extraction process and the rate and position of acetic acid for the acid precipitation process. As with any process, it is absolutely critical that assays used to measure the CQAs are validated. This essentially requires comprehensive experiments to be conducted to ensure that the quantitative measurements obtained from the assay are true and that the assay is reproducible. The time difference between when the samples are taken and when they are analysed must also be controlled. Where possible, automation of assays is highly recommended in order to reduce operator error. As with any manufacturing process, if there are any changes that are made to the operating conditions, process control or any other in-process characteristic, the process needs to be re-validated. For example, it was demonstrated in this work that the position of impellers and the fill volume, during the extraction process, had a significant impact on the process performance. Therefore if changes were to be made to the manufacturing scale vessel such as re-positioning of the impellers, to improve mixing and homogeneity, it is important to validate the process again with a minimum of three consecutive runs to ensure that the change has not adversely affected the quality of the Fab' product.

The scale-down models provided strong evidence of comparability to the large scale vessels and therefore if the decision was made to adopt the scale-down models for routinely scaling down the extraction process, further work can be done to optimise and validate the vessels. For the 20mL vessel, the temperature profile was tightly controlled by the MFCS software, however the speed was controlled using a separate overhead stirrer. Although it is assumed that the stirrer speed is unchanged for the duration of the process, however to improve confidence in the system, it may be useful to source an overhead stirrer system that can facilitate programmable mixing and can log the speed. Additionally, it is important to address the issue of the small gap between the glass jacket and the base of the vessel and to try and eliminate it before further use. This gap may be removed by designing a better fitted glass jacket or alternatively, a custom made o-ring may be used to fill in the gap. In doing so, this may improve the performance of the vessel. Additionally, for monitoring pH during the extraction and acid precipitation step, a more robust miniature pH probe is needed. Currently, commercially available micro pH probes, that are small enough to be used in miniature vessels, are not robust enough for use in extraction, where the process is lengthy and the temperatures are typically around 60°C. Monitoring of pH in the 20mL vessel was therefore done only for the acid precipitation process. This was also the case for the 24-well DSW plate.

In the shaken DSW plate system, the heating and mixing conditions were provided by a thermoshaker. The heating profiles that were set up on the shaker, to mimic the heating profiles of the large scale extraction process, had to be split into two programmes due to limitations on the number of settings that could be achieved in one programme. Therefore to complete the whole profile, the shaker was switched to the second programme, manually, after a known period of time. Maintaining the heating profile is crucial for the extraction process, and as this switch relies on an operator to be present, particular care must be taken to ensure this is done in a timely manner. As with the 20mL vessel, although temperature in the DSW plate could be logged, the shaker speed could not. It is expected that an off the shelf thermoshaker of this nature, which is used routinely in labs, has been qualified by the manufacturer and therefore runs continuously at the set speed for the duration of the process. With regards to cleaning of the extraction vessels, it is important

that product and process related substances are thoroughly removed. For the 20mL vessel, once the process is complete and all relevant samples have been taken, any remaining cell solution can be poured into a container and killed using Verkon. The vessel can then be disassembled and cleaned using 70% ethanol and ethanol wipes, and flushed using plenty of sterile water. As the 24-well DSW plate is single-use, it can be disposed of in the biohazardous bins. When working with single-use plastic based materials, such as the polypropylene DSW plates, the issue of leachables and extractables may be an issue, particularly at high temperatures; therefore studies may be needed to demonstrate that toxic components from the plate are not leached into the product or that the product is not absorbing any product. This is known to be an issue with micro-titre plates made from polypropylene plastic which can happen at high temperatures. It was has been shown that using boiling NaOH and hot HCl before use, helped reduce this problem (Becker *et al*., 1996). This issue can be evaluated by looking at the extractables profiles using chromatography or mass spectrometry to see if any cause of action needs to be taken.

Finally, if either the 20mL vessel or the 24-well DSW plate is to be used to run heat extractions, it is important that the process is set-up and operated in the same way for each experiment. In order to do this, a standard operating procedure (SOP) and batch record file can be written up to ensure that all operators are trained, according to good lab practice (GLP) to assemble, operate, dissemble (and clean where appropriate) the small scale vessels.

7.4 Industrial Applications and Economic Impact of Present Work

There is continuous pressure on biopharmaceutical companies to reduce their research and development times and to improve process knowledge, whilst reducing costs, in order to decrease the time it takes for a product to reach the market. Therefore there is a drive in industry to invest in technology that can help to improve robustness of the process, increase throughput, and enhance process understanding. This research project utilised some of the most advanced tools in bioprocessing, focusing on three key approaches to help achieve this for the heat extraction process. These approaches can be applied to other bioprocesses.

This includes firstly developing representative scale-down models which, once they have been shown to be capable of mimicking the large scale process for a variety of different conditions, can be used to quantify and model key process parameters. Not only do small scale models consume considerably less raw material and resources but if the model can be run in parallel and can be automated, such as the 24-well DSW plate, this becomes an even more attractive option for the company to invest in and develop. The second approach is to use DoE, a tool typically used in QbD, to further speed up process development times. This is particularly important for inherently complex bioprocesses where a significant number of parameters need to be investigated but the time taken to conduct experiments one at a time is not feasible. The third approach is to use fluid dynamic techniques to characterise the scale-down model in order to gain a deeper understanding of the hydrodynamics in the system which allows for more effective scaling. The approach taken and the data collected in this work can be extended to other industrial processes, particularly ones that are heavily dependent on mixing, for more effective scaling.

The approach taken in this work was to scale-down the extraction process in a step-wise manner. First scaling from a lab scale stirred system into a miniature scale stirred system and then going into a shaken system. The data from characterisation studies was useful in providing insight into the large scale process. Although geometry and power input between the stirred and shaken system may not match, the mixing intensity or mixing performance can be well matched. Two key variables to consider, when identifying problems in mixing, include mixing time (time scale) and the required homogeneity. The choice of scaling parameter depends on the limiting factor during the process because it is this factor which controls the chemical reaction and therefore should be identified first before attempting to scale. This can be done by employing tools such as DoE. Therefore if a fast reaction is required at all scales, the preferred choice for scaling may be specific power input, because this relates to the local turbulent energy dissipation in the vessel which depends on Kolmogorov length and time scales (Wernersson and Tragardh 1999). However, if fast dilution reaction is needed, the circulation time or mixing time may need to be kept constant instead. For other processes, such as the heat extraction process, achieving good homogeneity throughout the system is key for effective scaling.

The depth of data obtained for the 20mL vessel in this work during the characterisation studies is novel for a vessel of this size. Typically, characterisation studies are conducted on vessels that are a magnitude greater and they are done without the presence of probes, dip tubes or spargers, all of which would be present during an actual bioprocess and would impact mixing performance. A lot of mixing time studies are still conducted using intrusive methods that require the use of probes to be present in the liquid which further causes deviation from the real mixing performance that occurs during a bioprocess. In this study it was possible to obtain representative mixing time measurements, with the presence of these probes etc., because the global mixing time technique, DISMT, was used with a high speed camera to remove objectivity. There have been a number of studies that have demonstrated the suitability of miniature bioreactors to scale-down a bioprocess (Ali *et al*., 2011; Betts *et al.,* 2006; Gill *et al*., 2008a; Gill *et al*., 2008b; Lamping *et al*., 2003; Kusterer *et al*., 2008) and some effort has been made to characterise some aspects of power and mixing, however no work has been done to characterise a miniature stirred tank vessel with a multiple impeller system in terms of mixing time and PIV combined. Collecting information on fluid velocity and flow patterns under varying impeller speeds with different impeller spacing and fill volumes, shows which parameters most impact mixing and therefore process conditions may be optimised.

The results from the characterisation and process verification studies in this work showed that mixing performance was impacted more by impeller spacing and fill volume than on specific power input. A lot of companies still use specific power input as a basis of scaling for processes that rely primarily on good mixing and therefore may be using more power in their processes than is necessary. Power inputs in stirred tanks are high, typically 1–5kW m^3 (Gogate *et al*., 2000) and therefore if energy can be saved by reducing the power input and making adjustments to impeller spacing and fill volumes instead, whilst still maintaining good mixing performance, then this is highly desirable. This is especially true for processes which last for several days, rather than hours. For instance, a typical vessel of 10,000L, with a residence time of 6 days will consume 3000kWh power per batch according to Einsele (1978) and Rowland (1992).

The data from the 24-well DSW plate studies demonstrated that this type of micro-well plate, in conjunction with an Eppendorf thermomixer, is capable of mimicking heating and turbulent mixing conditions that are seen in a large scale stirred tank vessel for the extraction process. With further development, a significant part of the process in the DSW plate may be automated using a liquid handling robotic system such as TECAN, to improve robustness. The major additional cost, to the company, associated with running the extraction process in the thermoshaker system is related to the purchasing of thermocouple data loggers (~£500 for a 12-channel data logger) and heating block for the thermoshaker (~£500 for one block). Once these items are purchased however, the equipment is expected to last for many years and the cost of consumables for one extraction experiment, including the cost of DSW plate, thermocouple and aluminium seal is relatively inexpensive, at just under £10 per extraction. This small initial investment in the shaken plate system means that the quantity of raw materials can be reduced 1000 fold, when comparing to the 2L vessel, and therefore is an attractive option for use as a scale-down model.

Appendices

Appendix 2A: Calibration curve for protein G HPLC

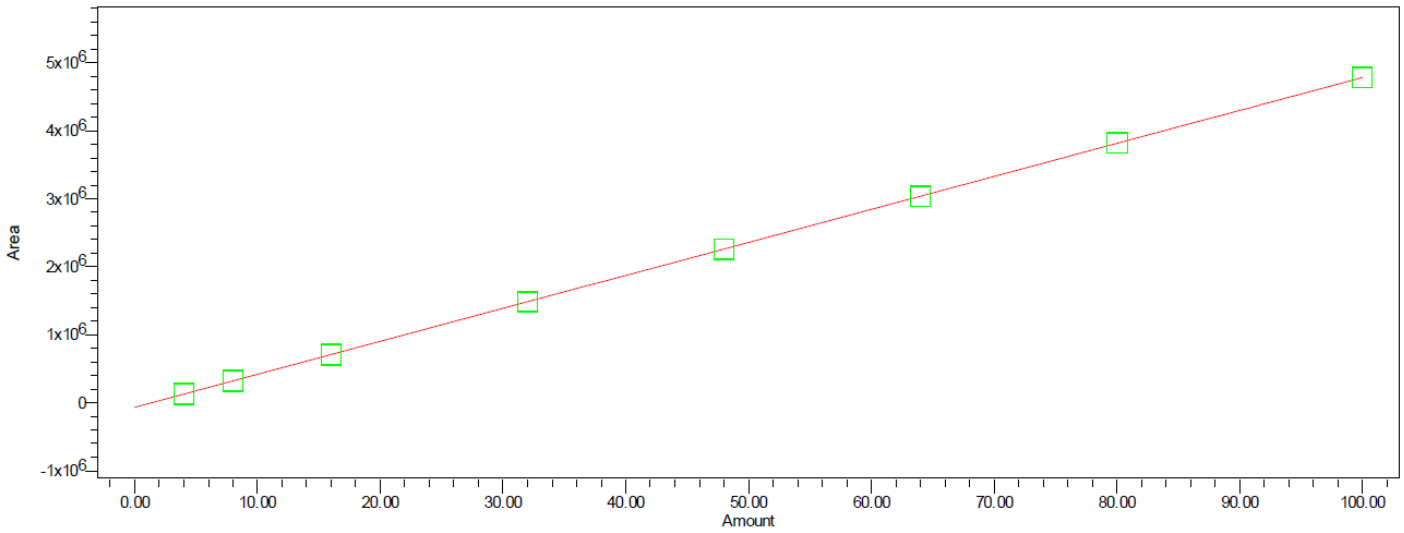

A typical calibration curve of the Fab' standard obtained using the Empower 2 software used to determine Fab' titre

Appendix 2B: Calibration Curve for Bradford Assay

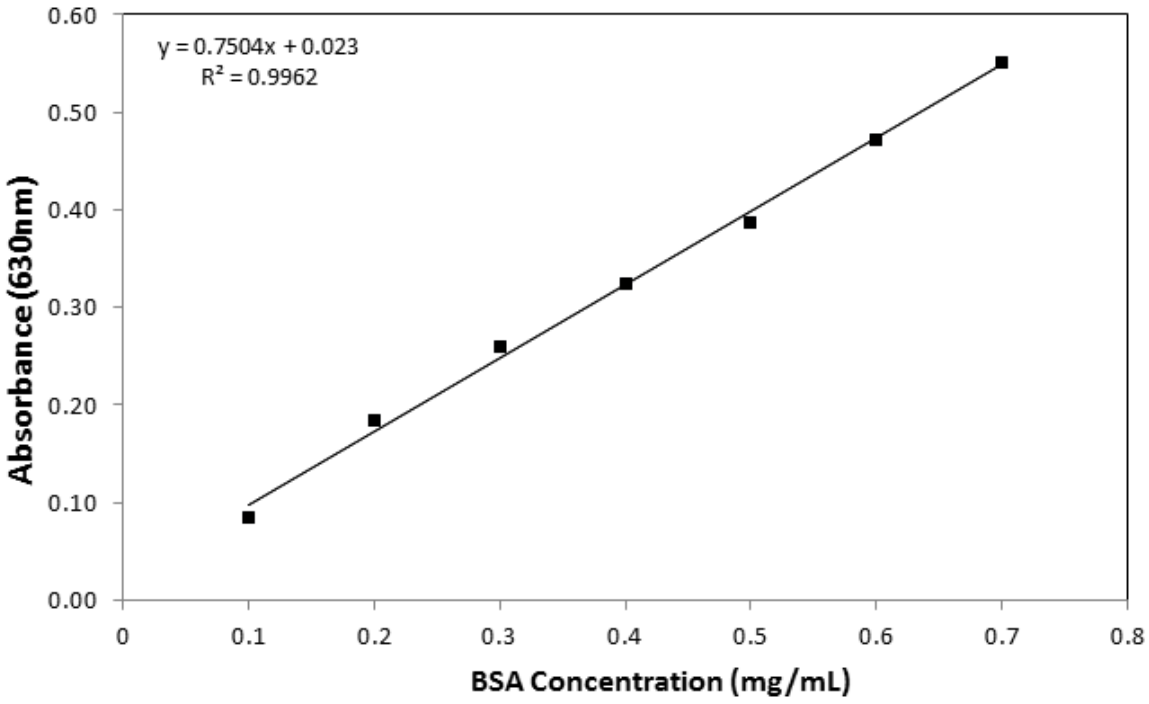

A typical calibration curve for the total protein Bradford Assay used to determine total protein concentration

Appendix 2C: Calibration Curve for PicoGreen Assay

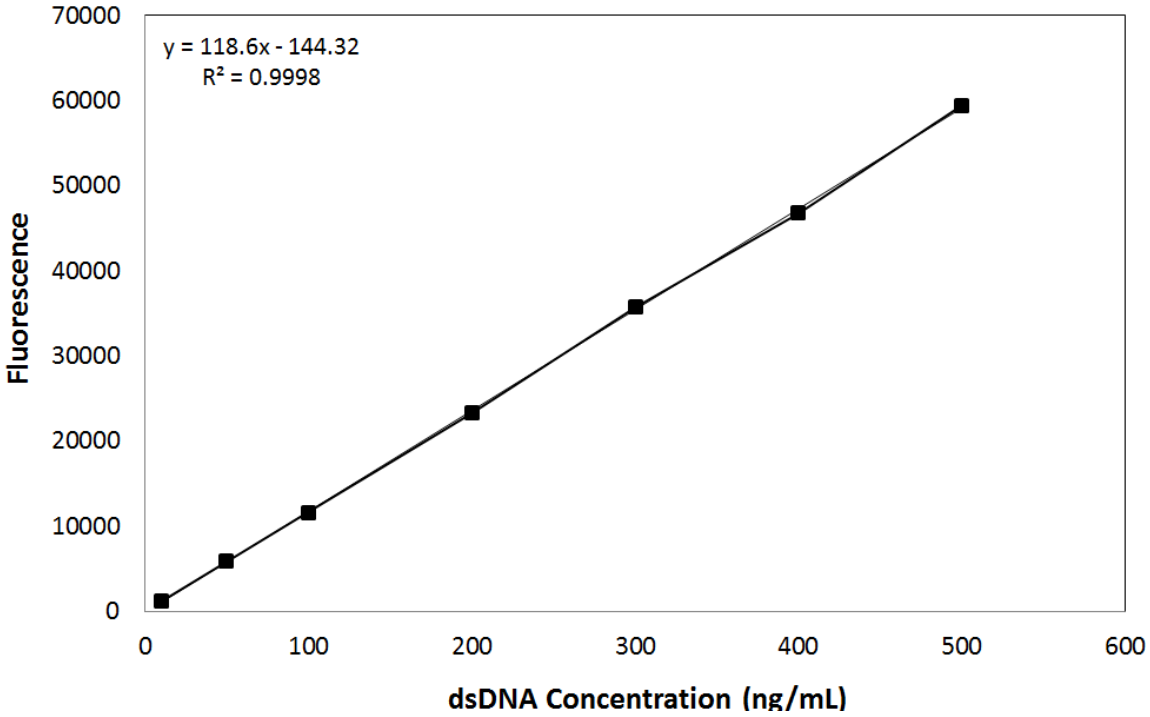

A typical calibration curve for the dsDNA PicoGreen Assay used to determine dsDNA concentration

Appendix 2D: DISMT Reagent Images

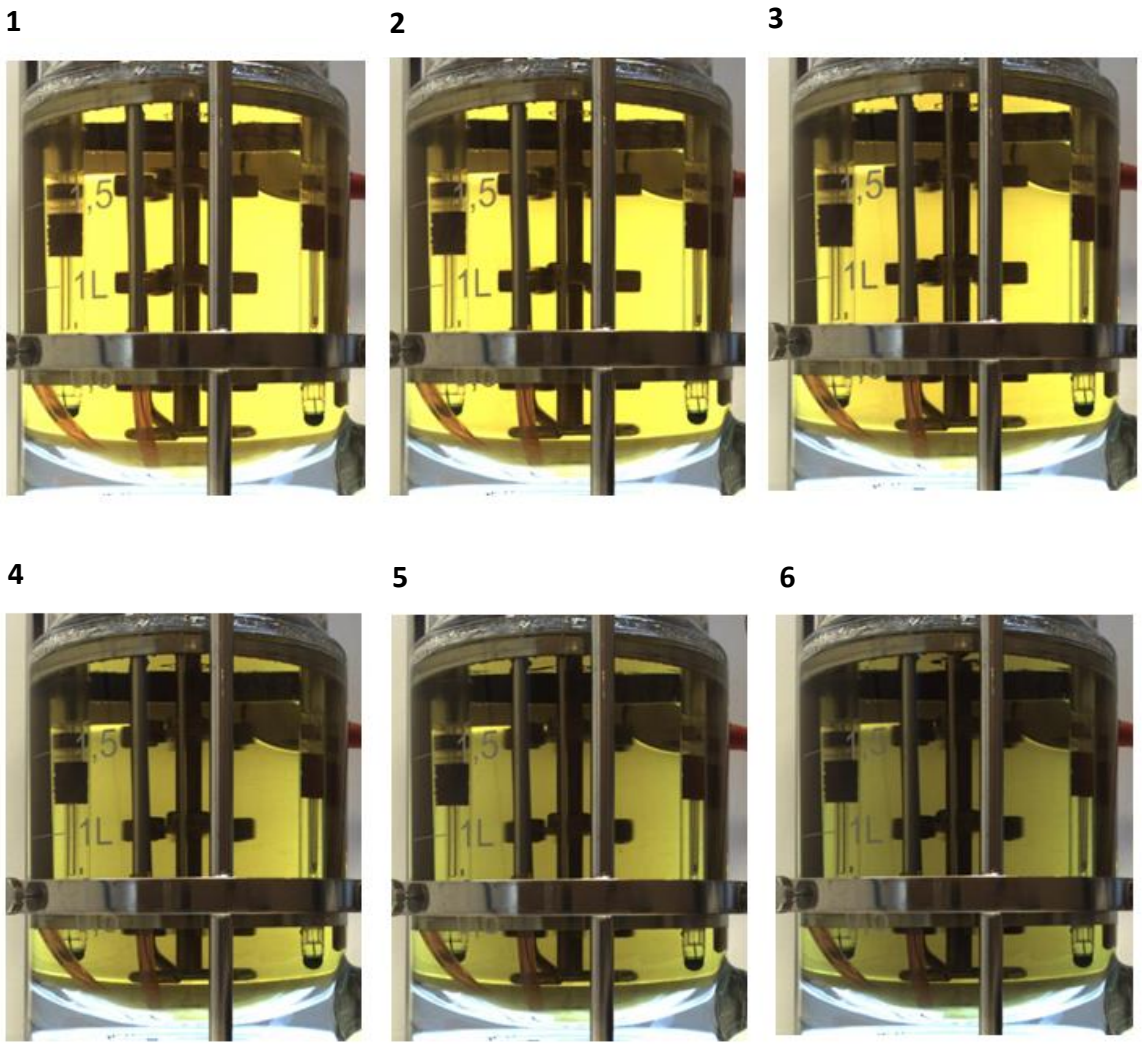

Images showing the colour of the final DISMT reagent in the 2L vessel after re-using the reagent multiple times. The numbers 1-6 represent the number of times the test was repeated

Appendix 4A: Heat profiles during heat characterisation in 20mL vessel

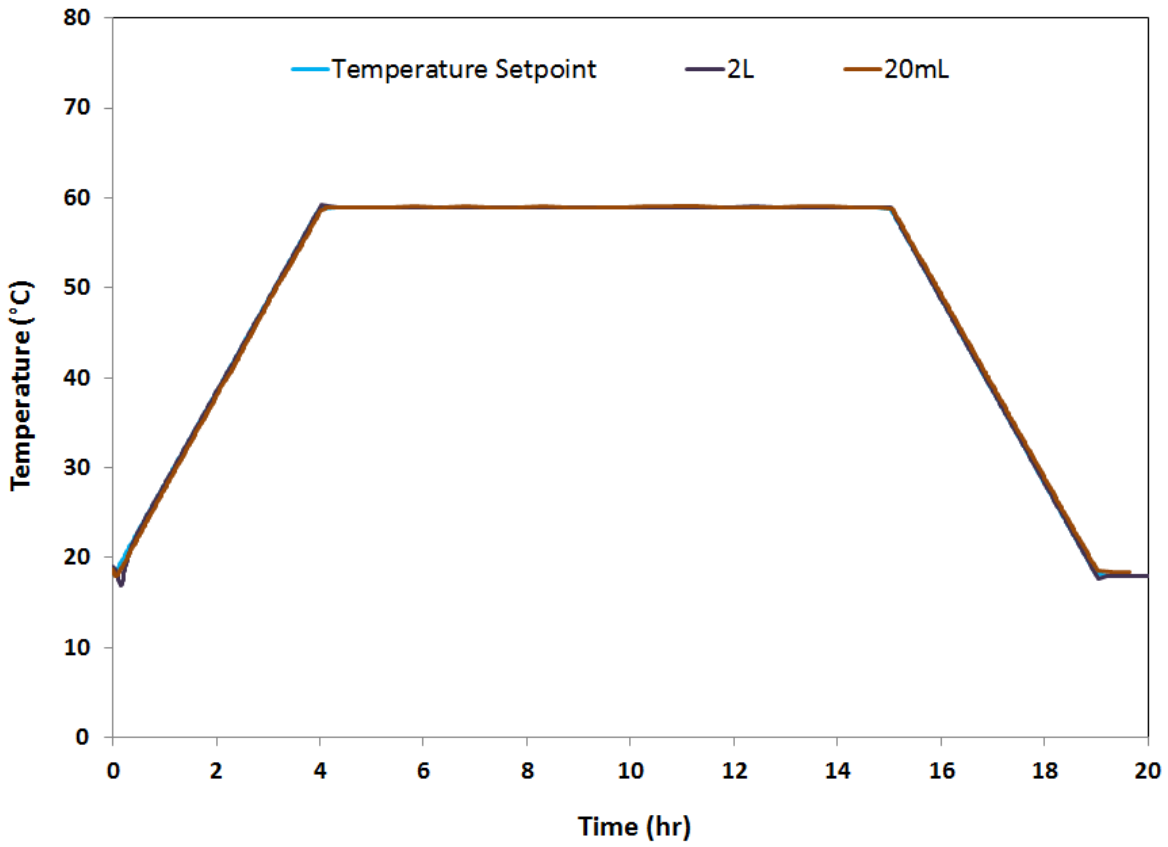

Example of the temperature profile in the 2L and 20mL vessel, using DI water, with a fill volume of 2L and 20mL respectively at a specific power input of 0.23 W/L

Appendix 4B: Heat profiles during heat characterisation in 24-well deep square-well plate

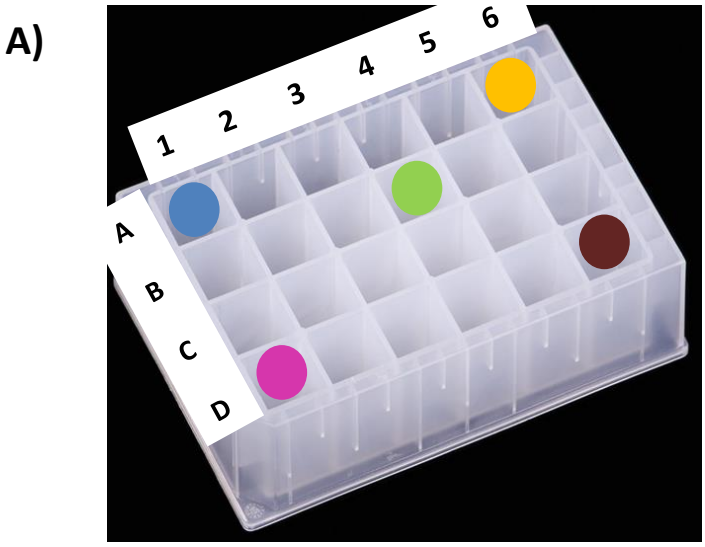

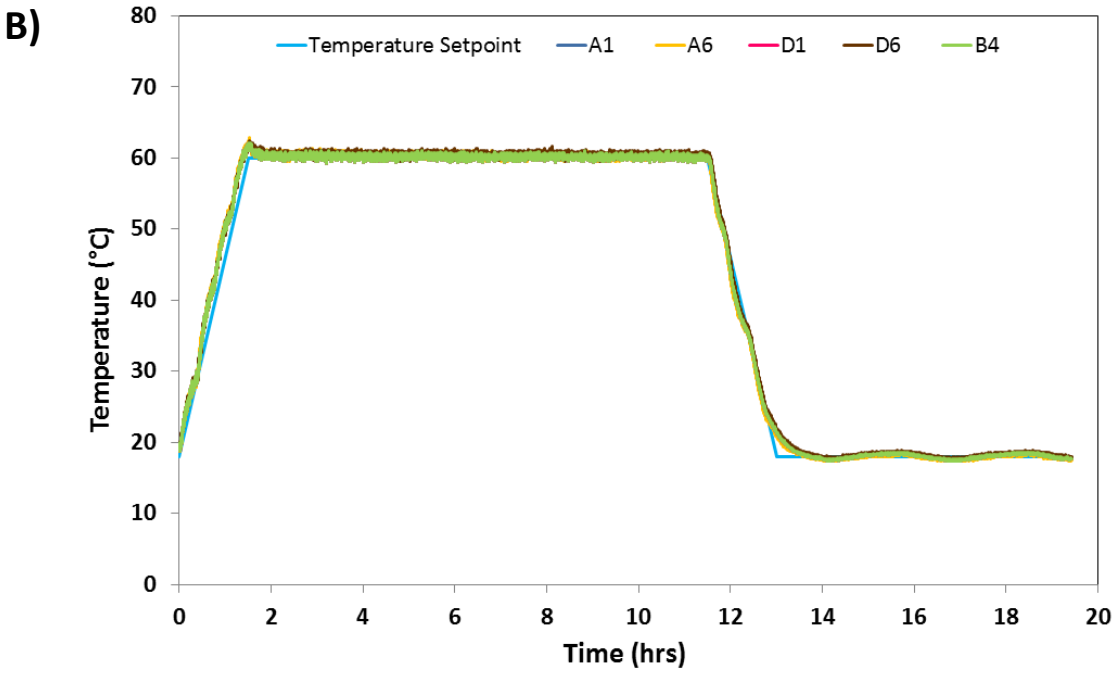

Positions chosen in a 24-well DSW plate **A)** to measure heating profile using DI water, with a fill volume of 3.5mL at a shaken speed of 1200rpm; and traces of the temperature profile **B)** in the different well positions

Appendix 4C: Example of Matlab image processing for mixing time experiments using the 20mL vessel

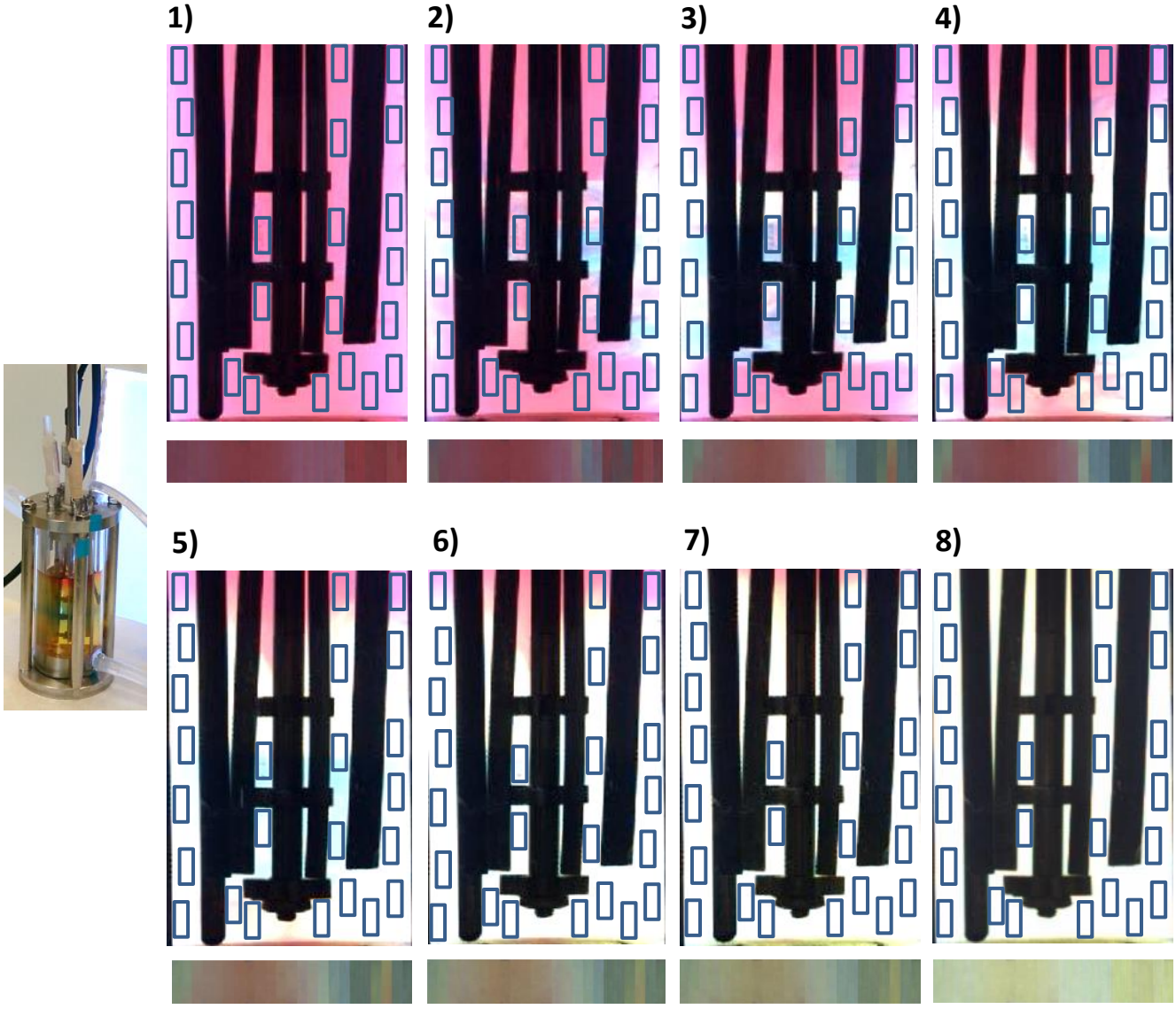

Specific areas of the image were cropped in order to analyse pixels in the liquid. The cropped regions were joined together in a concatenated image using Matlab, as shown below each vessel image, 1-8, and the standard deviation between the pixels were used to measure mixing time as the experiment progressed

Appendix 4D: Example of the standard deviation curves obtained using Matlab

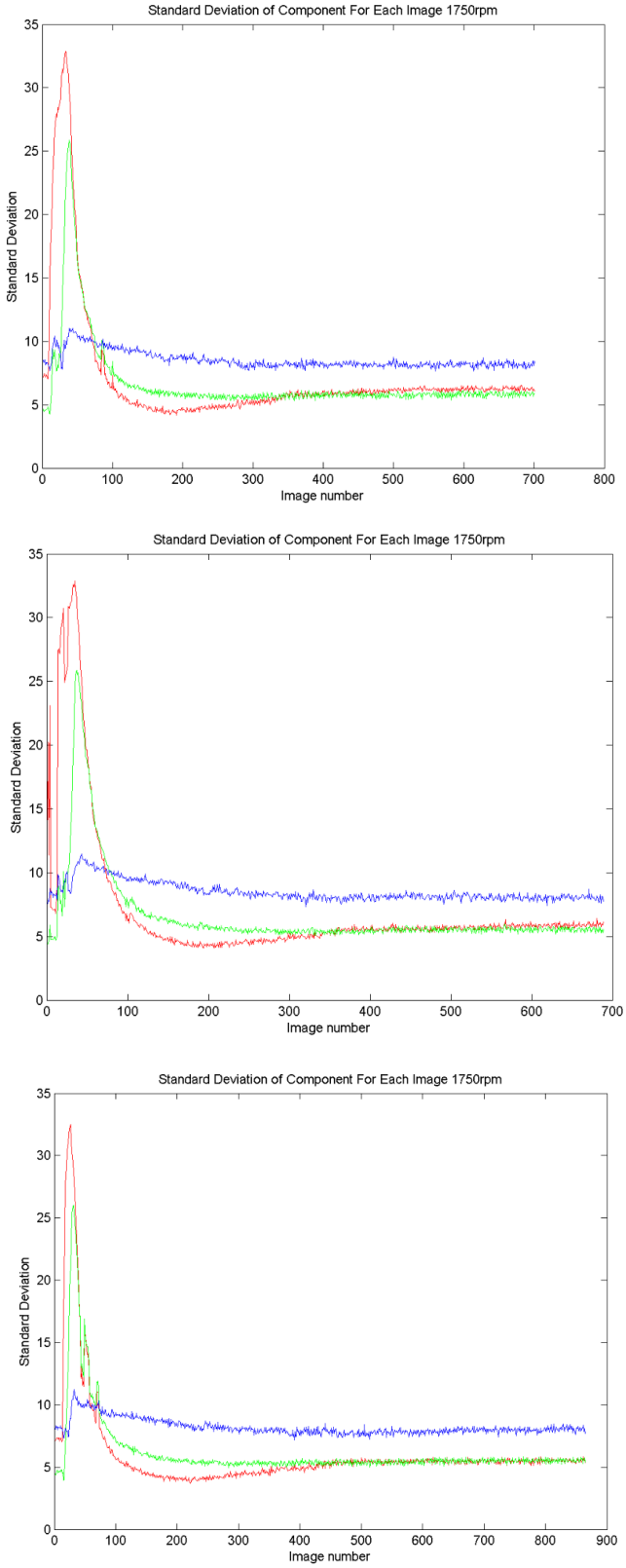

The standard deviation curves for the red, green and blue pixel components in the 20mL vessel, at a speed of 1750rpm (0.18W L^{-1}) to obtain mixing time measurements (n=3)

Appendix 4E: Velocity vectors plots for baffled 20mL vessel at 50rpm and 100rpm

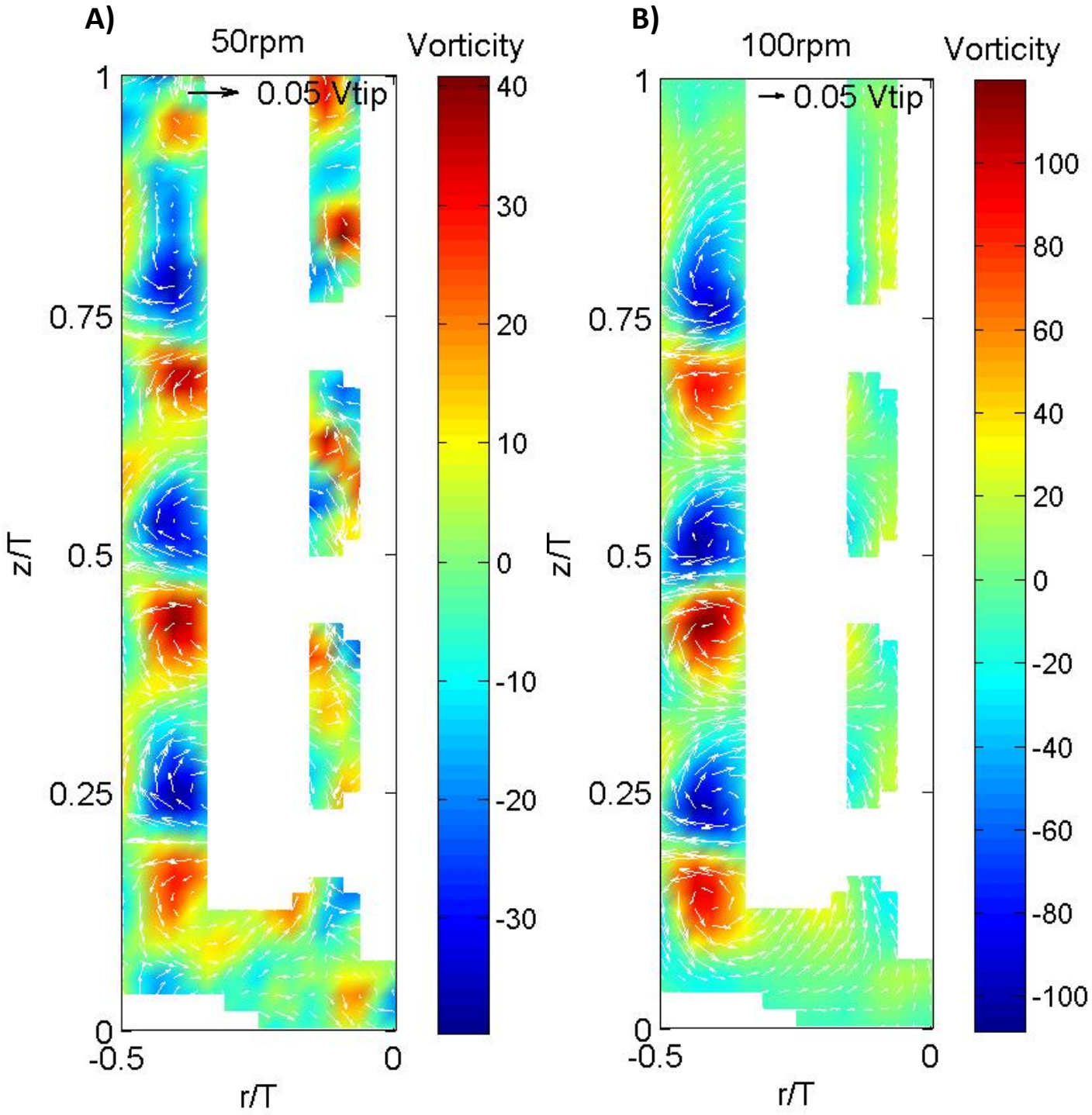

Velocity vectors and vorticity contour plots in an baffled 20mL vessel with a fill volume of 20mL at impeller speeds of **A)** 50rpm (P/V = 4 x 10^{-6}W L^{-1}, Tip speed = 0.022m/s, Re = 70) and **B)** 100rpm (P/V = 3.5 x 10^{-5}W L^{-1} , Tip speed = 0.045m/s, Re = 130)

Appendix 4F: Velocity vectors plots for baffled 20mL vessel at 300rpm and 800rpm

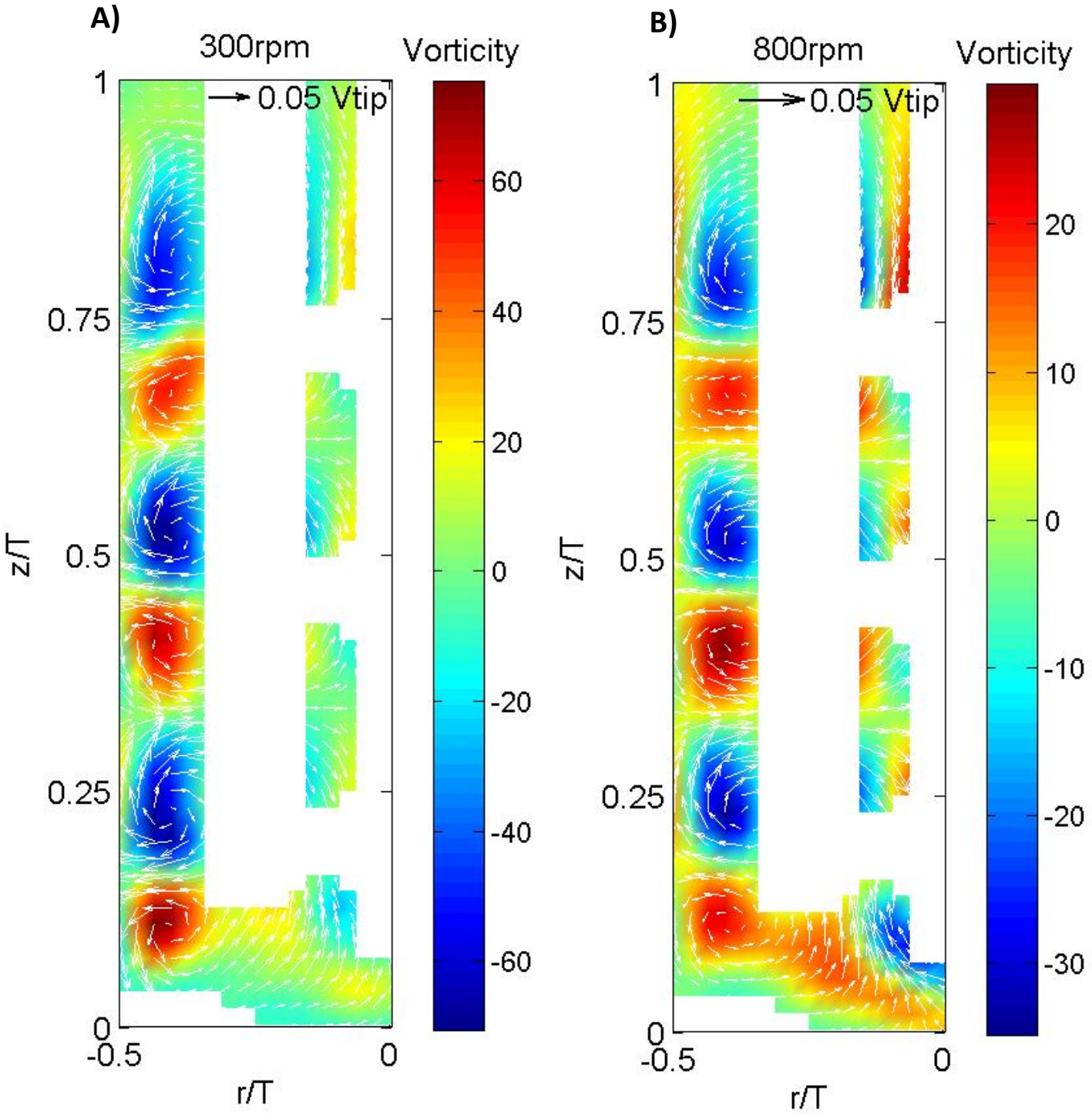

Velocity vectors and vorticity contour plots in an baffled 20mL vessel with a fill volume of 20mL at impeller speeds of **A)** 300rpm (P/V = 9 x 10^{-4}W L^{-1}, Tip Speed = 0.134m/s, Re = 330) and **B)** 800rpm (P/V = 1.74 x 10^{-2}W L^{-1}, Tip Speed = 0.36m/s, Re = 1000)

Appendix 4G: Velocity vectors plots for baffled 20mL vessel at 1500rpm and 2000rpm

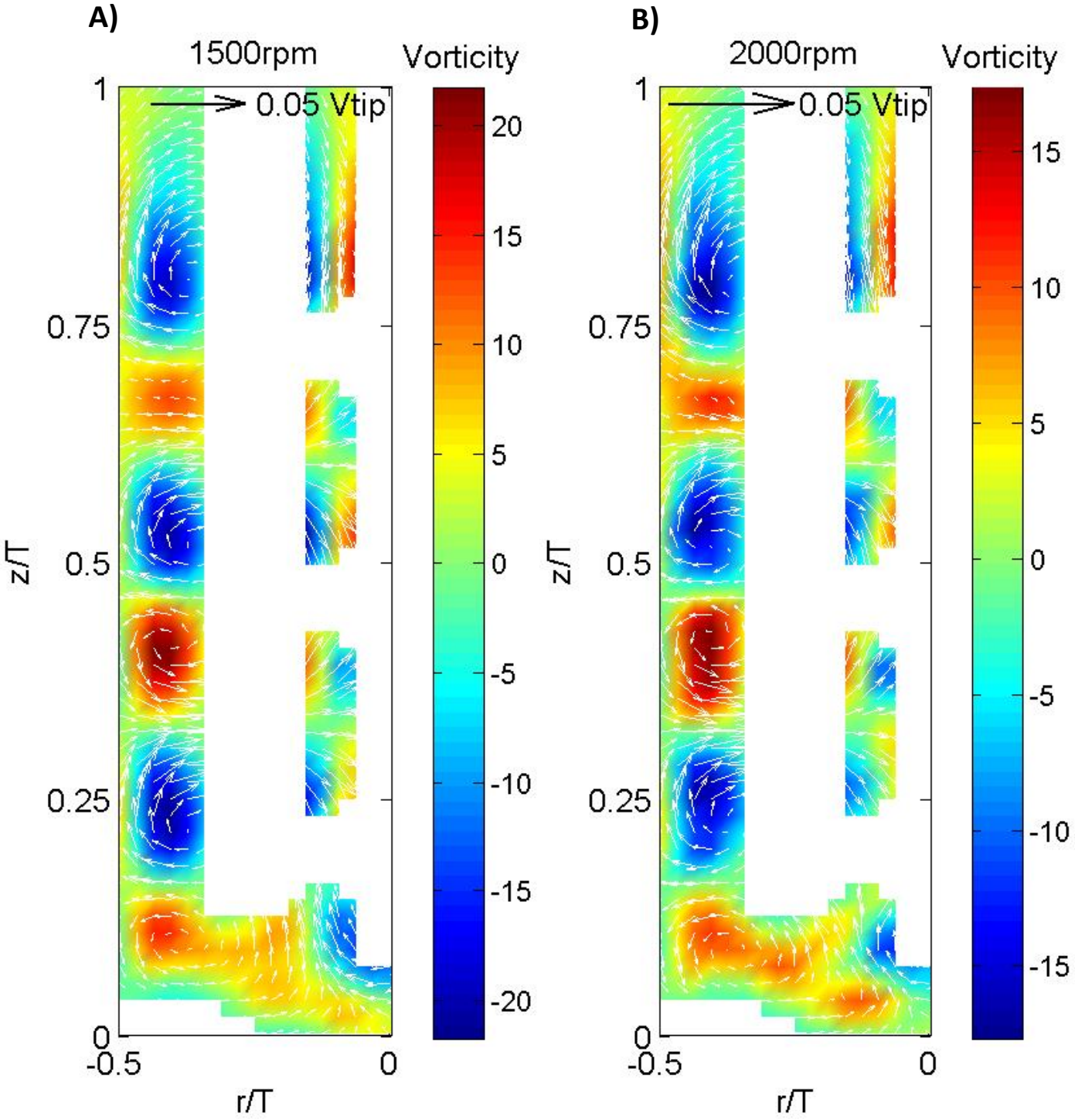

Velocity vectors and vorticity contour plots in an baffled 20mL vessel with a fill volume of 20mL at impeller speeds of **A)** 1500rpm (P/V = 0.115W L^{-1}, Tip Speed = 0.67m/s, Re = 2000) and **B)** 2000rpm (P/V = 0.27W L^{-1}, Tip Speed = 0.89m/s, Re = 2650)

Appendix 5A: Temperature and specific power input profiles for Exp #2-14

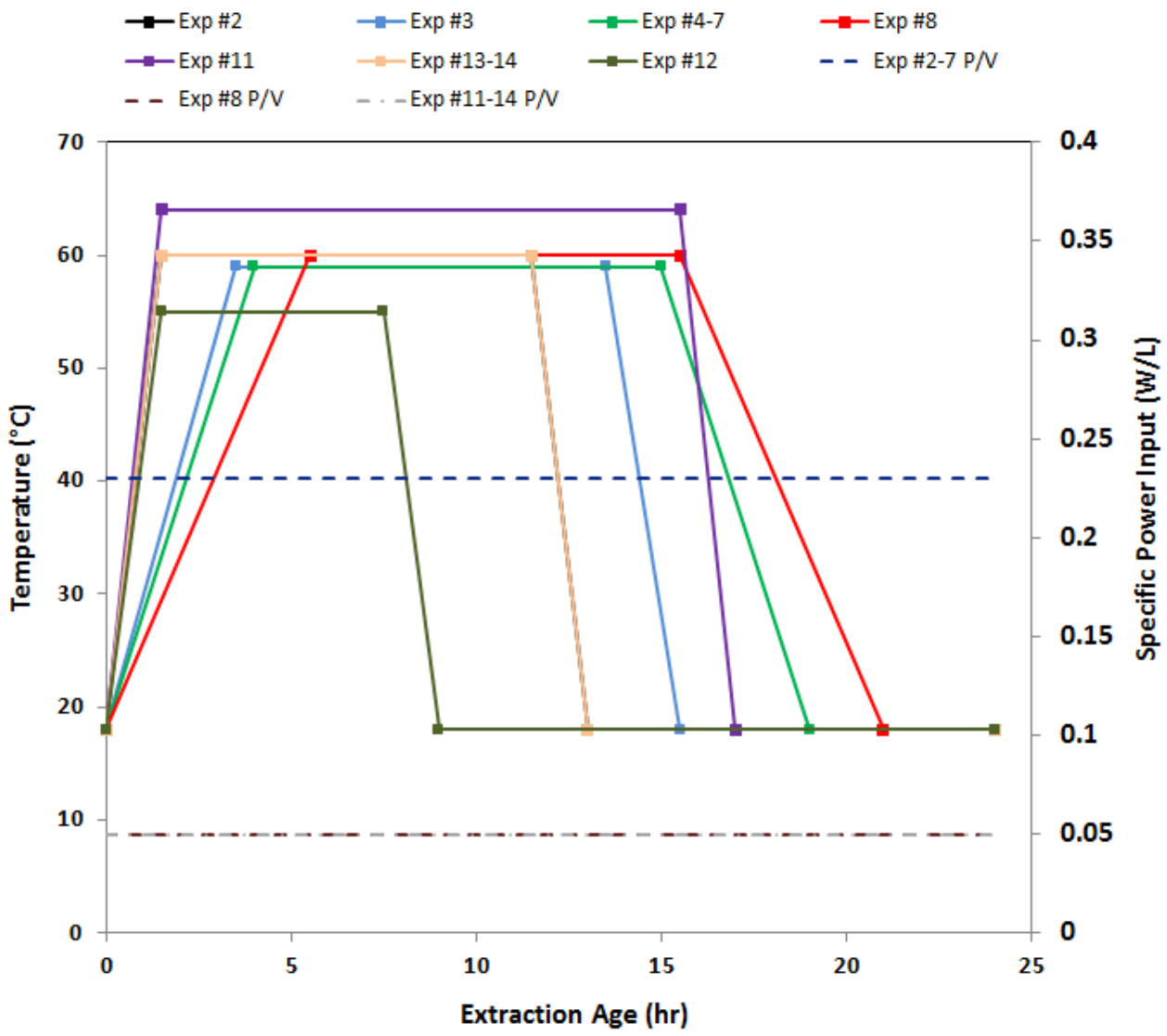

Temperature profiles are shown in solid lines and the specific power input profiles are shown in dashed lines

Appendix 5B: Fab', total protein and dsDNA concentration after acid precipitation Exp #2

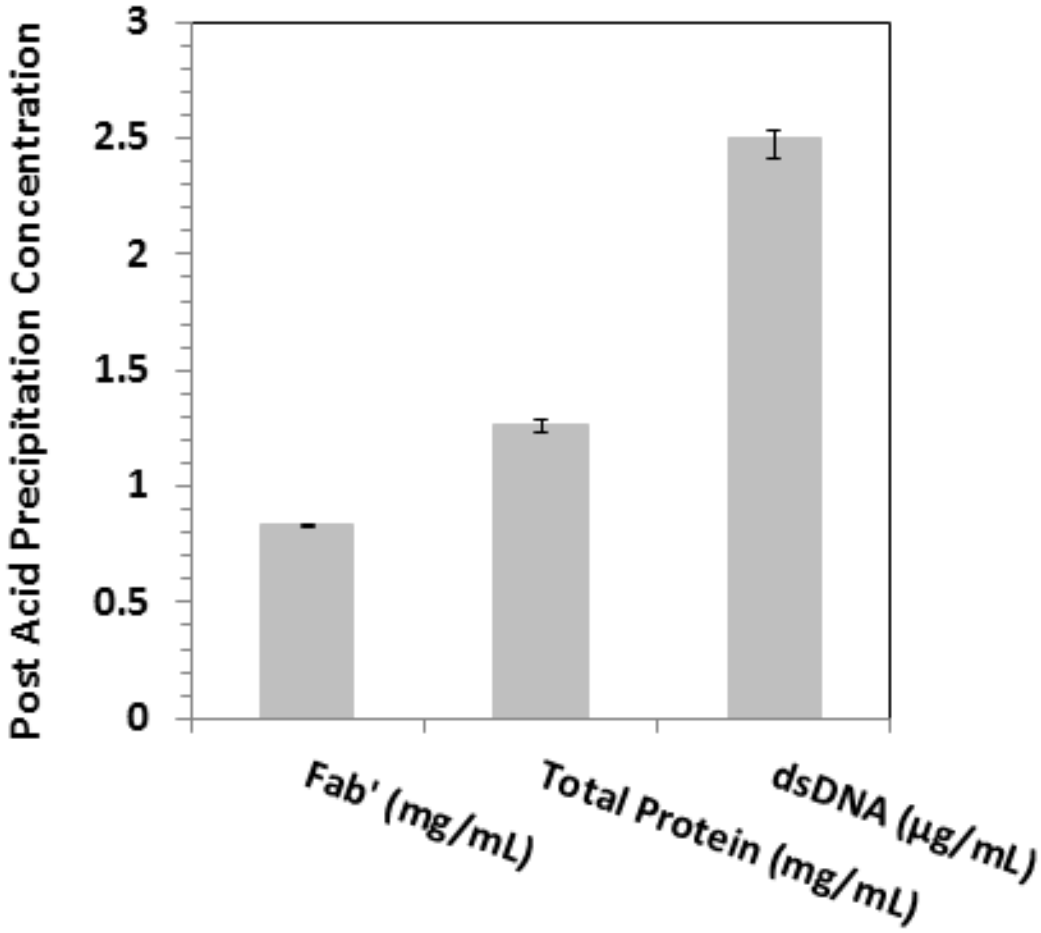

Fab', total protein and dsDNA concentration was measured from samples taken from the top and bottom of the 20mL vessel after acid precipitation. The error bars represent the difference between the average measurements (n=2)

Appendix 6A: Temperature and specific power input profiles for Exp #9-14

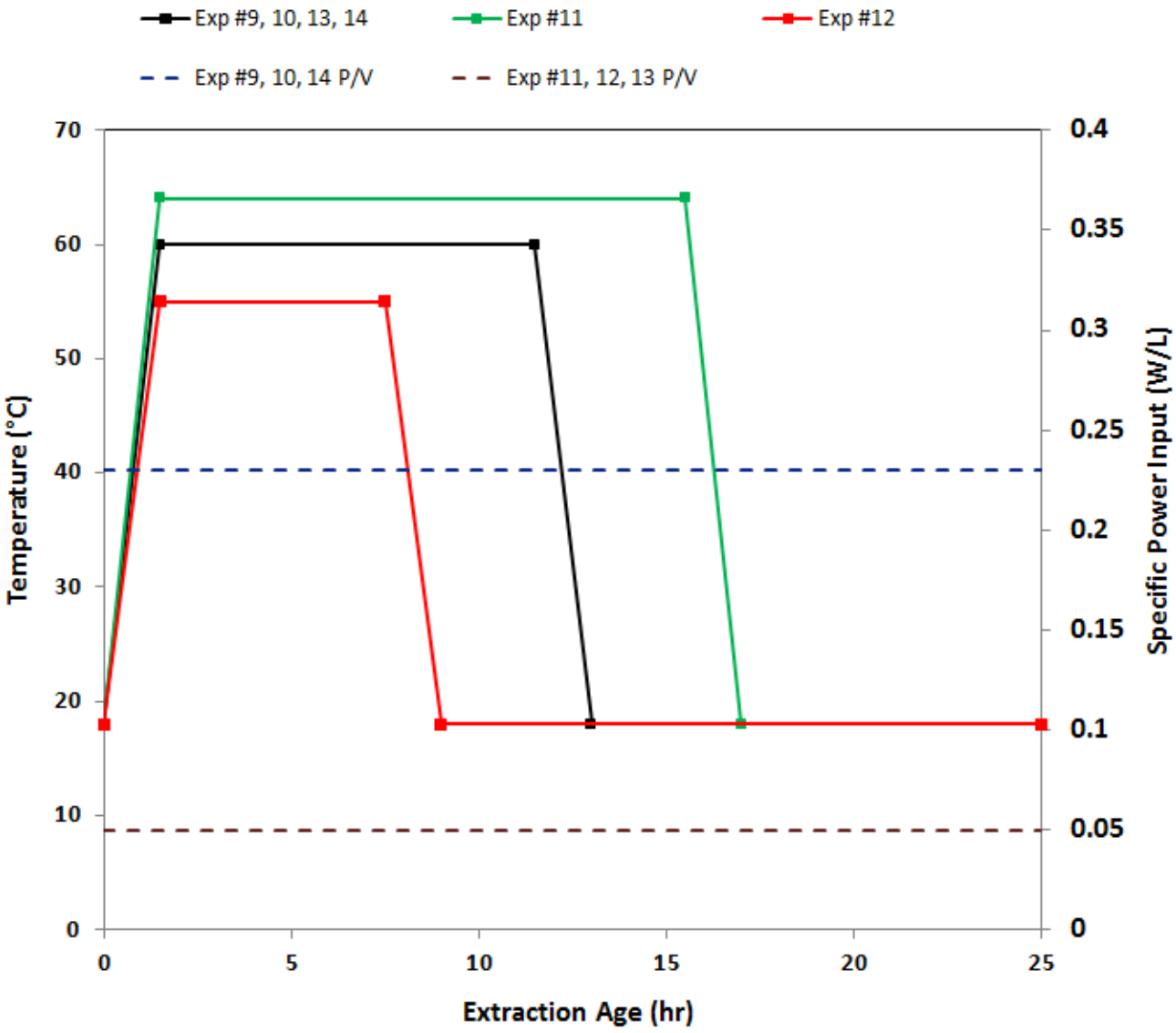

Temperature profiles are shown in solid lines and the specific power input profiles for the stirred tank vessels are shown in dashed lines.

Appendix 6B: Exp #9 temperature profile and acid addition volumes

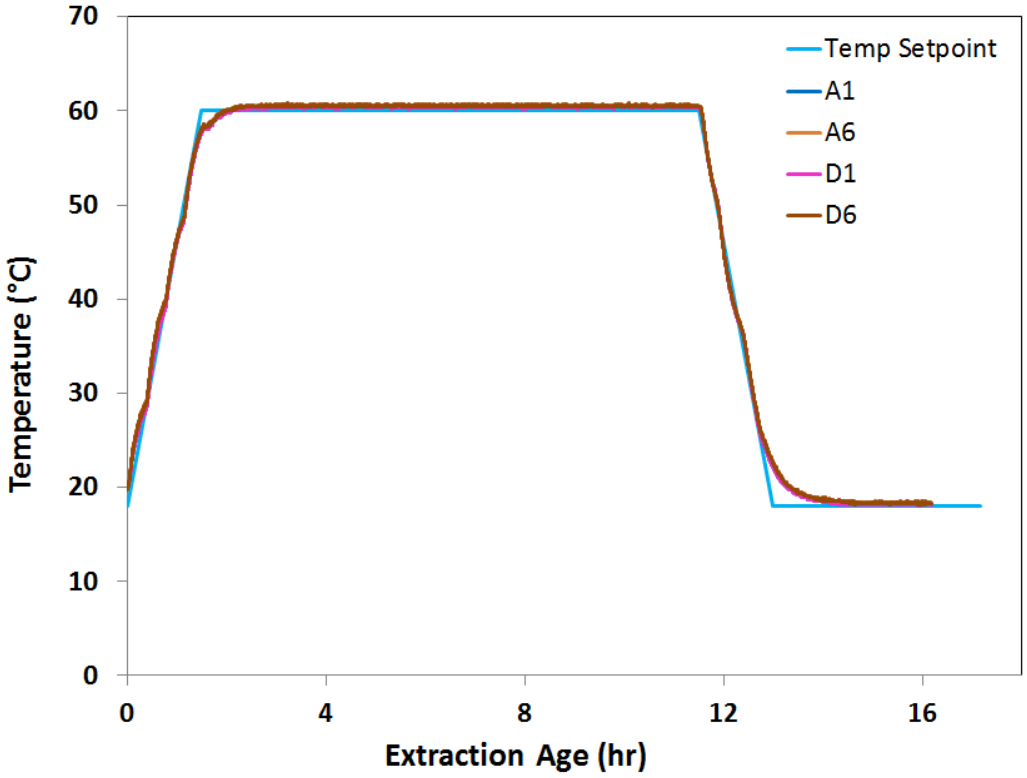

Example of a temperature profile in wells A1, A6, D1 and D6 in a 24-well DSW plate during heat extraction (Exp #9)

A2			
		B4	
	C3		
D2			D5

Well	Start pH	Acid added (µL)	End pH
A2	6.46	40	4.50
D2	6.37	35	4.52
C3	6.46	40	4.49
B4	6.47	40	4.48
D5	6.40	42	4.49

The starting pH, volume of acetic acid added and the final pH are shown for wells A2, D2, C3, B4 and D5 in Exp #9

References

1. Adrian RJ. 1991. Particle-imaging techniques for experimental fluid mechanics. *Annual review of fluid mechanics*, 23(1):261-304
2. Ali S, Perez-Pardo MA, Aucamp JP, Craig A, Bracewell DG, Baganz F. 2011. Characterization and feasibility of a miniaturized stirred tank bioreactor to perform *E. coli* high cell density fed-batch fermentations. *Biotechnology Progress*, 28(1):66–75.
3. Andersen DC, Reilly DE. 2004. Production technologies for monoclonal antibodies and their fragments. *Current Opinion in Biotechnology*, 15:456–62.
4. Andersson L, Strandberg L, Enfors S. 1996. Cell segregation and lysis have profound effects on the growth of *Escherichia coli* in high cell density fed batch cultures. *Biotechnology progress*, 12(2):190–195.
5. Ascanio G. 2015. Mixing time in stirred vessels: a review of experimental techniques. *Chinese Journal of Chemical Engineering*, 23:1065–1076.
6. Aucamp JP, Davies R, Hallet D, Weiss A, Titchener-Hooker NJ. 2014. Integration of host strain bioengineering and bioprocess development using ultra-scale down studies to select the optimum combination: an antibody fragment primary recovery case study. *Biotechnology and Bioengineering*, 9999:1–11.
7. Balasundaram B, Harrison S, Bracewell DG. 2009. Advances in product release strategies and impact on bioprocess design. *Trends in Biotechnology*, 27(8):477–485.
8. Baldi S, Hann D, Yianneskis M. 2002. On the measurement of turbulence energy dissipation in stirred vessels with PIV techniques. *Proc. 11th Int. Symposium on Applications of Laser Techniques to Fluid Mechanics, Instituto superior técnico, Center for innovation, technology, and policy research*, Lisbon, July 2002, 1 January.
9. Barata TS, Zhang C, Dalby PA, Brocchini S, Zloh M. 2016. Identification of protein – excipient interaction hotspots using computational approaches. *International Journal of Molecular Sciences*, 17(6):853.
10. Bareither R, Pollard D. 2011. A review of advanced small-scale parallel bioreactor technology for accelerated process development: current state and future need. *Biotechnology Progress*, 27(1):2–14.
11. Barrett TA, Wu A, Zhang H, Levy MS, Lye GJ. 2009. Microwell engineering characterization for mammalian cell culture process development. *Biotechnology and Bioengineering*, 105(2):260–275.

12. Baudou C, Xuereb C, Bertrand J. 1997. 3-D hydrodynamics generated in a stirred vessel by a multiple propeller system. *The Canadian Journal of Chemical Engineering,* 75:653–663.
13. Berlec A, Strukelj B. 2013. Current state and recent advances in biopharmaceutical production in *Escherichia coli*, yeasts and mammalian cells. *Journal of Industrial Microbiology and Biotechnology*, 40:257–274.
14. Betts JI, Doig SD, Baganz F. 2006. Characterization and application of a miniature 10 mL stirred-tank bioreactor, showing scale-down equivalence with a conventional 7 L reactor. *Biotechnology Progress*, 22(3):681–688.
15. Betts JI, Baganz F. 2006. Miniature bioreactors: current practices and future opportunities. *Microbial Cell Factories*, 5:1–14.
16. Bhambure R, Kumar K, Rathore AS. 2011. High-throughput process development for biopharmaceutical drug substances. *Trends in Biotechnology*, 29(3):127–135.
17. Birch JR, Onakunle Y. 2000. Biopharmaceutical proteins: opportunities and challenges. *Therapeutic proteins: Methods and protocols*, pg. 1–16.
18. Bouaifi M, Roustan M. 2001. Power consumption, mixing time and homogenisation energy in dual-impeller agitated gas–liquid reactors. *Chemical Engineering and Processing*, 40(2):87–95.
19. Büchs J, Maier U, Milbradt C, Zoels B. 2000. Power consumption in shaking flasks on rotary shaking machines: II nondimensional description of specific power consumption and flow regimes in unbaffled flasks at elevated liquid viscosity. *Biotechnology and Bioengineering*, 68(6):594–601.
20. Cabaret F, Bonnot S, Fradette L, Tanguy PA. 2007. Mixing time analysis using colorimetric methods and image processing. *Industrial and Engineering Chemistry Research*, 46:5032–5042.
21. Chapman AP, Antoniw P, Spitali M, West S, Stephens S, King DJ. 1999. Therapeutic antibody fragments with prolonged in vivo half-lives. *Nature Biotechnology*, 17(8):780–783.
22. Chan GHT. 2006. An ultra scale-down study to understand and predict *E.coli* cell recovery from high-speed discharge centrifuges. *PhD Thesis*. *University College London*, London.
23. Chen A, Chitta R, Chang D, Amanullah A. 2009. Twenty-four well plate miniature bioreactor system as a scale-down model for cell culture process development. *Biotechnology and Bioengineering*, 102(1):148–160.
24. Chunmei PAN, Jian MIN, Xinhong LIU, Zhengming GAO. 2008. Investigation of fluid flow in a dual Rushton impeller stirred tank using particle image velocimetry. *Chinese Journal of Chemical Engineering*, 16(5):693–699.

25. De Petris E. 1967. Ultrastructure of the cell wall of *Escherichia coli* and chemical nature of its constituent layers. *Journal Ultrastructure Research*, 83:45–83.
26. Doig SD, Pickering SCR, Lye GJ, Baganz F. 2005: Modelling surface aeration rates in shaken micro-titre plates using dimensionless groups. *Chemical Engineering Science*, 60:2741-2750.
27. Driss Z, Karray S, Chtouroou W, Kchaou H, Abid MS. 2012. A study of mixing structure in stirred tanks equipped with multiple four-blade Rushton impellers. *The Archive of Mechanical Engineering,* 59:53–72.
28. Duetz WA, Witholt B. 2004. Oxygen transfer by orbital shaking of square vessels and deepwell microtiter plates of various dimensions. *Biochemical Engineering Journal*, 17:181–185.
29. Dürauer A, Hobiger S, Walther C, Jungbauer A. 2016. Mixing at the microscale: power input in shaken microtiter plates. *Biotechnology Journal,* 11:1539–1549.
30. Einsele A. 1978. Scaling up bioreactors. *Process Biochemistry*, 13:13–14.
31. Ellert A and Vikström C. 2014. Design of experiments with small-scale bioreactor systems-efficient bioprocess development and optimization. *BioProcess International*, 12(5):10–13.
32. Ellis M, Humphreys DP. 2011. Bacterial host strain comprising a mutant SPR gene and a wild-type TSP gene. Patent: World Intellectual Property Organization, WO 2011/086138 A1.
33. Eriksson L, Johannson E, Kettaneh-Wold N, Wikström C, Wold S. 2008. Design of experiments: principles and applications. Third Edition.
34. European Commission. 2009. The financing of biopharmaceutical product development in Europe. The framework contract of sectoral competitiveness studies – *ENTR/06/054 Final Report*. Copenhagen/Brussels.
35. European Medicines Agency. 2009. Assessment report for Cimzia. Procedure No. EMEA/H/C/001037. Canary Wharf, London.
36. Fernandes P, Cabral JMS. 2006. Microlitre/millilitre shaken bioreactors in fermentative and biotransformation processes – a review. *Biocatalysis and Biotransformation*, 24(4):237–252.
37. Galaction AI, Lupăşteanu AM, Caşcaval D. 2008. Comparative evaluation of radial impellers efficiency for bioreactors with stirred bed of immobilized cells 3. Paddle with six blades and pitched bladed turbine. *Romanian Biotechnological Letters*, 14(5):4681–4693.
38. Gill NK, Appleton M, Baganz F, Lye GJ. 2008a. Design and characterisation of a miniature stirred bioreactor system for parallel microbial fermentations. *Biochemical Engineering Journal*, 39:164–176.

39. Gill NK, Appleton M, Baganz F, Lye GJ. 2008b. Quantification of power consumption and oxygen transfer characteristics of a stirred miniature bioreactor for predictive fermentation scale-up. *Biotechnology and Bioengineering*, 100(6):1144–1155
40. Goel N, Stephens S. 2010. Certolizumab pegol. *mAbs*, 2(2):137–147.
41. Gogate PR, Beenackers ACM, Pandit AB. 2000. Multiple-impeller systems with a special emphasis on bioreactors: a critical review. *Biochemical Engineering Journal,* 6:109–144.
42. Goldschmidt MC, Wyss O. 1967. The role of tris in EDTA toxicity and lysozyme lysis. *Journal of General Microbiology*, 47:421–431.
43. Grant Y, Dalby PA, Matejtschuk P. 2012. Use of design of experiment and microscale down strategies in formulation and cycle development for lyophilization. *American Pharmaceutical Review*, 15:2.
44. Hammad KJ, Papadopoulos G. 2000. Phase-resolved PIV measurements within a triple impeller stirred-tank. Paper presented at AIChE 2000, Nov. 12-17, 2000, Los Angeles, CA, USA.
45. Hartmann H, Derksen JJ, van den Akker HEA. 2006. Mixing times in a turbulent stirred tank by means of LES. *AICHe Journal*, 52(11):3696–3706.
46. Hartmann M, Berditsch M, Hawecker J, Ardakani MF, Gerthsen D, Ulrich AS. 2010. Damage of the bacterial cell envelope by antimicrobial peptides gramicidin S and PGLa as revealed by transmission and scanning electron microscopy. *Antimicrobial Agents and Chemotherapy*, 54(8):3132–3142.
47. Hermann R, Lehmann M, Büchs J. 2002. Characterization of gas–liquid mass transfer phenomena in microtiter plates. *Biotechnology and Bioengineering*, 81(2):179–186.
48. Hewitt CJ, Nienow AW. 2007. The scale-up of microbial batch and fed-batch fermentation processes. *Advances in Applied Microbiology*, 62:105–135.
49. Hsu CC. 2013. New approaches to the production and separation of recombinant proteins. *PhD Thesis*. *University of Birmingham*, Birmingham.
50. Huang CJ, Lin H, Yang X. 2012. Industrial production of recombinant therapeutics in *Escherichia coli* and its recent advancements. *Journal of Industrial Microbiology and Biotechnology*, 39(3):383-399.
51. Hudcova W, Machon W. 1989. Gas-liquid dispersion with dual Rushton turbine impellers. *Biotechnology and Bioengineering*, 34:617–628.
52. Humphreys DP, Weir N, Lawson A, Mountain A, Lund PA. 1996. Co-expression of human protein disulphide isomerase (PDI) can increase the yield of an antibody Fab' fragment expressed in *Escherichia coli*. *FEBS Letters*, 380:194–197.

53. Humphreys DP, Heywood SP, Henry A, Ait-Lhadj L, Antoniw P, Palframan R, Greenslade KJ, Carrington B, Reeks DG, Bowering LC, West S, Brand HA. 2007. Alternative antibody Fab' fragment PEGylation strategies: combination of strong reducing agents, disruption of the interchain disulphide bond and disulphide engineering. *Protein Engineering, Design and Selection*, 20(5):227–234.
54. Irvin RT, Macalistair TJ, Costerton JW. 1981. Tris(hydroxymethyl)aminomethane buffer modification of *Escherichia coli* outer membrane permeability. *Journal of Bacteriology*, 145(3):1397–1403.
55. Isett K, George H, Herber W, Amanullah A. 2007. Twenty-four-well plate miniature bioreactor high-throughput system: assessment for microbial cultivations. *Biotechnology and Bioengineering*, 98(5):1017–1028.
56. Islam RS, Tisi D, Levy MS, Lye GK. 2007. Framework for the rapid optimization of soluble protein expression in *Escherichia coli* combining microscale experiments and statistical experimental design. *Biotechnology Progress*, 23(4):785–793.
57. Jahanmiri M. 2011. Particle image velocimetry: Fundamentals and its applications. Chalmers University of Technology.
58. Jahoda M, Machoň V. 1994. Homogenization of liquids in tanks stirred by multiple impellers. *Chemical Engineering and Technology*, 17:95–101.
59. Kasat GR, Pandit AB. 2004. Mixing time studies in multiple impeller agitated reactors. *The Canadian Journal of Chemical Engineering*, 82:892–904.
60. Katsui N, Tsuchido T, Hiramatsu R, Fujikawa S, Shibasaki I. 1982. Heat-induced blebbing and vesiculation of the outer membrane of *Escherichia coli*. *Journal of Bacteriology*, 151(3):1523–1531.
61. Kuboi R, Nienow AW. 1986. Intervortex mixing rates in high-viscosity liquids agitated by high-speed dual impellers. *Chemical Engineering Science*, 41(1):123–134.
62. Kusterer A, Krause C, Kaufmann K, Arnold M, Weuster-Botz D. 2008. Fully automated single-use stirred-tank bioreactors for parallel microbial cultivations. *Bioprocess and Biosystems Engineering*, 31(3):207–215.
63. Lamping SR, Zhang H, Allen B, Ayazi Shamlou P. 2003. Design of a prototype miniature bioreactor for high throughput automated bioprocessing. *Chemical* Engineering Society, 58:747–758.
64. Lamberto DJ, Alvarez MM, Muzzio FJ. 1999. Experimental and computational investigation of the laminar flow structure in a stirred tank. *Chemical Engineering Science*, 54*:* 919–942.

65. Lee KC, Yianneskis M. 1997. A liquid crystal thermographic technique for the measurement of mixing characteristics in stirred vessels. *Chemical Engineering Research and Design*, 75(8):746–754.
66. Lee SY, Choi JH, Lee SJ. 2005. Secretory production of therapeutic proteins in *Escherichia coli*. In: *Methods in Molecular Biology, vol 308: therapeutic proteins: methods and protocols*, Totowa, NJ, Humana Press Inc., pg. 31–41.
67. Li F, Hashimura Y, Pendleton R, Harms J, Collins E, Lee B. 2006. A systematic approach for scale-down model development and characterization of commercial cell culture processes. *Biotechnology Progress*, 22(3):696–703.
68. Li Q, Aucamp JP, Tang A, Chatel A, Hoare M. 2012. Use of focused acoustics for cell disruption to provide ultra scale-down insights of microbial homogenization and its bioprocess impact- recovery of antibody fragments from rec *E.coli*. *Biotechnology and Bioengineering*, 109(8):2059–2069.
69. Li Q, Mannall G J, Ali S, Hoare M. 2013. An ultra scale-down approach to study the interaction of fermentation, homogenization, and centrifugation for antibody fragment recovery from rec *E. coli*. *Biotechnology and Bioengineering*, 110(8):2150–2160.
70. Liu H, May K. 2012. Disulphide bond structures of IgG molecules: structural variations, chemical modifications and possible impacts to stability and biological. *mAbs*, 4(1):17–23.
71. Lydersen BK, Brehm-gibson T. 1994. Acid precipitation of mammalian cell fermentation broth. *Annals of the New York Academy of Sciences*, *745*:222–231.
72. Mackey BM, Parsons SE, Miles CA, Owen RJ. 1988. The relationship between the base composition of bacterial DNA and its intracellular melting temperature as determined by differential scanning calorimetry. *Journal of General Microbiology*, 134:1185–1195.
73. Magelli F, Montante G, Pinelli D, Paglianti A. 2013. Mixing time in high aspect ratio vessels stirred with multiple impellers. *Chemical Engineering Science*, 101:712–720.
74. Mahmoudi SM, Yianneskis M. 1991. The variation of flow pattern and mixing time with impeller spacing in stirred vessels with two Rushton turbines. *Proc. of 7th European Conference on Mixing, Brugges, Belgium*, 18-20 September, pg. 17–24.
75. Mahmoudi SM, Yianneskis M. 1992. The variation of flow pattern and mixing time with impeller spacing in stirred vessels with two Rushton turbines. In *King R, editor. Fluid Mechanics and Its Applications*. Springer Science + Business Media, pg. 11–18.
76. Mahmoudi SMS. 1994. Velocity and mixing characteristics of stirred vessels with two Rushton impellers. *PhD Thesis*. *King' s College London,* London.

77. Marques MPC, Cabral JMS, Fernandes P. 2010. Bioprocess scale-up: quest for the parameters to be used as criterion to move from microreactors to lab-scale. *Journal of Chemical Technology and Biotechnology*, 85:1184–1198.
78. Mavros P. 2001. Flow visualization in stirred vessels- a review of experimental techniques. *Trans IChemE*, 79:113–127.
79. Melton LA, Lipp CW, Spradling RW, Paulson KA. 2002. Dismt - determination of mixing time through color changes. *Chemical Engineering Communications*, 189(3):322–338.
80. Middelberg APJ. 1995. Process-scale disruption of microorganisms. *Biotechnology Advances*, 13(3):491–551.
81. Millipore. 2015. Application note: benzonase endonuclease for improved primary recovery in an *E.coli* based process for Fab production. Germany.
82. Mishra VP, Joshi JB. 1994. Flow generated by a disc turbine Part IV: multiple-impellers, *Chemical Engineering Research and Design*, 72(5):657–668.
83. Molen KVD, Maanen HREV. 1978. Laser doppler measurements of the turbulent flow in stirred vessels to establish scaling rules*. Chemical Engineering Science*, 33:1161–1168.
84. Montante G, Lee K, Brucato A, Yianneskis M. 1999. An experimental study of double-to-single-loop- transition in stirred vessels. *The Canadian Journal of Chemical Engineering*, 77:649–659
85. Mununga L, Hourigan K, Thompson M. 2003. Numerical study of the effect of blade size on pumping effectiveness of a paddle impeller in an unbaffled mixing vessel. In: *Third International Conference on CFD in the Minerals and Process Industries CSIRO, Melbourne, Australia*, 299–304.
86. Nealon AJ, O'Kennedy RD, Titchener-Hooker NJ, Lye, G. J. 2006. Quantification and prediction of jet macro-mixing times in static microwell plates. *Chemical Engineering Science*, 61(15):4860–4870.
87. Nelson AL. 2010. Antibody fragments- hope and hype. *mAbs*, 2:77–83.
88. Newton JM, Schofield D, Vlahopoulou J, Zhou Y. 2016. Detecting cell lysis using viscosity monitoring in *E.coli* fermentation to prevent product loss. *Biotechnology Progress*, 32(4):1069–1076.
89. Odeleye AOO, Marsh DTJ, Osborne MD, Lye GJ, Micheletti M. 2014. On the fluid dynamics of a laboratory scale single-use stirred bioreactor. *Chemical Engineering Science*, 111:299–312.
90. Oosterhuis NMG. 1984. Scale up of bioreactors a scale down approach. *PhD Thesis, Delft University of Technology*, Netherlands.

91. Perez-Pardo MA, Ali S, Balasundaram B, Mannall GJ, Baganz F, Bracewell DG. 2011. Assessment of the manufacturability of *Escherichia coli* high cell density fermentations. *Biotechnology Progress*, 27(5):1488–1496.
92. Popplewell AG, Sehdev M, Spitali M, Weir ANC. 2005. Expression of antibody fragments by periplasmic secretion in *Escherichia coli*. Therapeutic Proteins: *Methods in Molecular Biology*, pg. 17–30.
93. Pouran B, Amoabediny G, Saghafinia MS, Abbas MPH. 2012. Characterization of interfacial hydrodynamics in a single cell of shaken microtiter plate bioreactors applying computational fluid dynamics technique. *Procedia Engineering*, 42:924–930.
94. Rayat ACME, Micheletti M, Lye GJ. 2010. Evaluation of cell disruption effects on primary recovery of antibody fragments using microscale bioprocessing techniques. *Biotechnology Progress*, 26(5):1312–1321.
95. Rayat ACME. 2011. Microscale bioprocessing platform for the evaluation of membrane filtration processes for primary recovery. *PhD Thesis. University College London*, London.
96. Rayat, ACME, Chatel A, Hoare M, Lye GJ. 2016. Ultra scale-down approaches to enhance the creation of bioprocesses at scale: impacts of process shear stress and early recovery stages. *Current Opinion in Chemical Engineering*, 14:150–157.
97. Reshes G, Vanounou S, Fishov I, Feingold M. 2008. Cell shape dynamics in *Escherichia coli*. *Biophysical journal*, 94(1):251–264.
98. Rodriguez G, Anderlei T, Micheletti M, Yianneskis M, Ducci A. 2014. On the measurement and scaling of mixing time in orbitally shaken bioreactors. *Biochemical Engineering Journal*, 82:10–21.
99. Rosenberg M. 2000. Proceedings of IBC's production and economics of biopharmaceuticals-transcending the limits of manufacturing medicines. La Jolla, CA, November 13–15
100. Rouet R, Lowe D, Dudgeon K, Roome B, Schofield P, Langley D, Andrews J, Whitfield P, Jermutus L, Christ D. 2012. Expression of high-affinity human antibody fragments in bacteria. *Nature Protocols*, 7(2):364–373.
101. Roush DJ, Lu Y. 2008. Advances in primary recovery: centrifugation and membrane technology. *Biotechnology Progress*, 24(3):488–495.
102. Rowland RT. 1992. Strain improvement and strain stability. In: *Finkelstein DB, Ball C. Biotechnology of Filamentous Fungi: Technology and Products*. Butterworth-Heinemann, pg. 41–64.
103. Rushton JH, Costich EW, Everett HJ. 1950. Power characteristics of mixing impellers. *Chemical Engineering Progress*, 46:395–404.

104. Rutherford K, Lee KC, Mahmoudi SMS, Yianneskis M. 1996a. Hydrodynamic characteristics of dual Rushton impeller stirred vessels. *AIChE Journal*, 42(2):332–346.

105. Rutherford K, Mahmoudi SMS, Lee KC, Yianneskis M. 1996b. The influence of Rushton impeller blade thickness on the mixing characteristics of stirred vessels. *Chemical Engineering Research and Design*, 74(3):369–378

106. Sano Y, Usui H. 1985. Interrelations among mixing time, power number and discharge flow rate number in baffled mixing vessels. *Journal of Chemical Engineering of Japan*, 18(1):47–52.

107. Saravanan K. 2009. Gas hold up in multiple impeller agitated vessels. *Modern Applied Science*, 3(2):49–59.

108. Sehdev M, Spitali M. 2006. Process for obtaining antibodies. *Patent: World Intellectual Property Organization,* WO2006/054063 A1.

109. Shahab N, Flett F, Oliver SG, Butler PR. 1996. Growth rate control of protein and nucleic acid content in Streptomyces coelicolor A3(2) and *Escherichia coli* B/r. *Microbiology*, 142:1927–1935.

110. Sharp KV, Adrian RJ. 2001. PIV study of small-scale flow structure around a Rushton turbine. *AIChE Journal*, 47(4):766–778.

111. Shekhar SM, Jayanti S. 2002. CFD study of power and mixing time for paddle mixing in unbaffled vessels. *Chemical Engineering Research and Design,* 80:482–498.

112. Shiue SJ, Wong CW. 1984. Studies on homogenization efficiency of various agitators in liquid blending. *The Canadian Journal of Chemical Engineering*, 62:602–609.

113. Singh N, Pizzelli K, Romero JK, Chrostowski J, Evangelist G, Hamzik J, Soice N, Cheng KS. 2013. Clarification of recombinant proteins from high cell density mammalian cell culture Systems using new improved depth filters. *Biotechnology and Bioengineering*, 110(7):1964–1972.

114. Tai M, Ly M, Leung I, Nayar G. 2014. Efficient high-throughput biological process characterization: definitive screening design with the Ambr250 bioreactor system. *Biotechnology Progress*, 31(5):1338–1395.

115.

116. Tanguy PA, Fradette L, Ascanio G, Yatomi R. 2015. Laminar mixing processes in stirred vessels. In: *Kresta SM, Etchells III AW, Dickey DS, Atiemo-Obeng VA. Advances in industrial mixing: a companion to the handbook of industrial mixing*. New Jersey: John Wiley & Sons Inc, pg. 261–357.

117. Therapeutic Goods Administration. 2010. Australian public assessment report for Certolizumab pegol: proprietary product name: Cimzia. Australia.

118. Tissot S, Farhat M, Hacker DL, Anderlei T, Kühner M, Comninellis C, Wurm F. 2010. Determination of a scale-up factor from mixing time studies in orbitally shaken bioreactors. *Biochemical Engineering Journal*, 52:181–186.

119. Tustian, AD, Salte H, Willoughby NA, Hassan I, Rose MH, Baganz F, Hoare M, Titchener-Hooker, NJ. 2007. Adapted ultra scale-down approach for predicting the centrifugal separation behavior of high cell density cultures. *Biotechnology Progress*, 23(6):1404–1410.

120. Tsuchido T, Katsui N, Takeuchi A, Takano M, Shibasaki I. 1985. Destruction of the outer membrane permeability barrier of *Escherichia coli* by heat treatment. *Applied and Environmental Microbiology*, 50(2):298–303.

121. Vaara M. 1992. Agents that increase the permeability of the outer membrane. *Microbiological Reviews*, 56(3):395–411.

122. Vasconcelos JMT, Orvalho SCP, Rodrigues AMAF. 2000. Effect of blade shape on the performance of six-bladed disk turbine impeller. *Industrial & Engineering Chemistry Research,* 39:203–213.

123. Voulgaris I, Chatel A, Hoare M, Finka G, Uden M. 2016. Evaluation of options for harvest of a recombinant *E.coli* fermentation producing a domain antibody using ultra scale-down techniques and pilot-scale verification. *Biotechnology Progress*, 32(2):1–11.

124. Voss JG. 1967. Effects of organic cations on the gram-negative cell wall and their bactericidal activity with ethylenediaminetetra-acetate and surface active agents. *Journal of General Microbiology*, 48(3):391–400.

125. Vallejos JR, Kostov Y, Ram A, French JA, Marten MR. 2005. Optical analysis of liquid mixing in a minibioreactor. *Biotechnology and Bioengineering*, 93(5):906-911.

126. Walsh G. 2000. Biopharmaceutical benchmarks. *Nature Biotechnology*, 28(9):917–924.

127. Walsh G. 2010. Biopharmaceutical benchmarks 2010. *Nature Biotechnology*, 28(9):917–924.

128. Walsh G. 2014. Biopharmaceutical benchmarks 2014. *Nature Biotechnology*, 32(10):992–1002.

129. Weheliye W, Yianneskis M, Ducci, A. 2012. On the fluid dynamics of shaken bioreactors - flow characterization and transition. *AICHe Journal*, 59(1):334–344.

130. Weir ANC, Bailey NA. 1997. Process for obtaining antibodies utilizing heat treatment. *Patent: United States Patent*, 5 665 866. 1997-9-9.

131. Weiss S, John GT, Klimant I, Heinzle E. 2002. Modeling of mixing in 96-well microplates observed with fluorescence indicators. *Biotechnology Progress*, 18:821–830.

132. Wenger MD, Dephillips P, Bracewell DG. 2008. A microscale yeast cell disruption technique for integrated process development strategies. *Biotechnology Progress*, 24(3):606–614.

133. Wernersson ES, Tragardh C. 1999. Scale-up of Rushton turbine-agitated tanks. *Chemical Engineering Science*, 54:4245-4256.

134. Westoby M, Chrostowski J, De Vilmorin P, Smelko JP, Romero JK, Carolina N. 2011. Effects of solution environment on mammalian cell fermentation broth properties: enhanced impurity removal and clarification performance. *Biotechnology and Bioengineering*, 108(1):50–58.

135. Weuster-botz D. 2005. Parallel reactor systems for bioprocess development. *Advances in Biochemical Engineering/Biotechnology*, 92:125–143.

136. Wu H, Patterson GK. 1989. Laser-doppler measurements of turbulent flow parameters in a stirred mixer. *Chemical Engineering Science*, 44(10):2207–2221.

137. Xinhong L, Yuyun B, Zhipeng L, Zhengming G. 2008. Particle image velocimetry study of turbulence characteristics in a vessel agitated by a dual Rushton impeller. *Chinese Journal of Chemical Engineering*, 16(5):700–708.

138. Xinhong L, Yuyun B, Zhipeng L, Zhengming G. 2010. Analysis of turbulence structure in the stirred tank with a deep hollow blade disc turbine by time-resolved PIV. *Chinese Journal of Chemical Engineering*, 18(4):588–599.

139. Yianneskis M, Popiolek Z, Whitelaw JH. 1986. An experimental study of the steady and unsteady flow characteristics of stirred reactors. *Journal of Fluid Mechanics*, 175:537–555.

140. Yoon S, Kim Y-S,Shim H, Chung J. 2012. Current perspectives on therapeutic antibodies. *Biotechnology and Bioprocess Engineering*, 15:709–715.

141. You ST, Raman AAA, Shah RSSRE, Nor MIM. 2014. Multiple-impeller stirred vessel studies. *Reviews in Chemical Engineering*, 30(3):323–336.

142. Zhang H, Lamping SR, Pickering SCR, Lye G. J, Shamlou PA. 2008. Engineering characterisation of a single well from 24-well and 96-well microtitre plates. *Biochemical Engineering Journal*, 40(1):138–149.